PMU-Based Applications for Improved Monitoring and Protection of Power Systems

Anamitra Pal

Dissertation submitted to the faculty of Virginia Polytechnic Institute and State University in partial fulfillment of the requirements for the degree of

Doctor of Philosophy
In
Electrical Engineering

James S. Thorp, Chair
Arun G. Phadke
Virgilio A. Centeno
Jaime De La Ree
Sandeep K. Shukla
Michael R. Taaffe

April 11, 2014
Blacksburg, Virginia

Keywords: Binary Integer Programming, Classification & Regression Tree (CART), Data Conditioning, Fisher's Linear Discriminant (FLD), Kalman Filter, Observability, Phasor Measurement Units (PMUs), Stress Assessment, Wide Area Measurement Systems (WAMS)

PMU-Based Applications for Improved Monitoring and Protection of Power Systems

Anamitra Pal

Abstract

Monitoring and protection of power systems is a task that has manifold objectives. Amongst others, it involves performing data mining, optimizing available resources, assessing system stresses, and doing data conditioning. The role of PMUs in fulfilling these four objectives forms the basis of this dissertation. Classification and regression tree (CART) built using phasor data has been extensively used in power systems. The splits in CART are based on a single attribute or a combination of variables chosen by CART itself rather than the user. But as PMU data consists of complex numbers, both the attributes, should be considered simultaneously for making critical decisions. An algorithm is proposed here that expresses high dimensional, multivariate data as a single attribute in order to successfully perform splits in CART.

In order to reap maximum benefits from placement of PMUs in the power grid, their locations must be selected judiciously. A gradual PMU placement scheme is developed here that ensures observability as well as protects critical parts of the system. In order to circumvent the computational burden of the optimization, this scheme is combined with a topology-based system partitioning technique to make it applicable to virtually any sized system.

A power system is a dynamic being, and its health needs to be monitored at all times. Two metrics are proposed here to monitor stress of a power system in real-time. Angle difference between buses located across the network and voltage sensitivity of buses lying in the middle are found to accurately reflect the static and dynamic stress of the system. The results indicate that by setting appropriate alerts/alarm limits based on these two metrics, a more secure power system operation can be realized.

A PMU-only linear state estimator is intrinsically superior to its predecessors with respect to performance and reliability. However, ensuring quality of the data stream that leaves this estimator is crucial. A methodology for performing synchrophasor data conditioning and validation that fits neatly into the existing linear state estimation formulation is developed here. The results indicate that the proposed methodology provides a computationally simple, elegant solution to the synchrophasor data quality problem.

To My Parents: Dipankar Pal and Lopamudra Pal

Acknowledgements

Pursuing a PhD degree has been a life-long dream for me and I am grateful to all the people who have supported and motivated me on this path to becoming a “Doctorate”.

I extend my sincerest gratitude to my advisor Dr. James S. Thorp for his help and guidance towards the work contained in this dissertation. His enthusiasm and passion for teaching is incredible and the fact that he leads by example, motivates one like nothing else. I have learned a tremendous amount through the discussions that we have had together. As a mentor and guide on both academic as well as non-academic topics, he is second to none. This dissertation would not have been what it is without him.

I am very grateful to Dr. Arun G. Phadke and Dr. Virgilio A. Centeno for their invaluable insights and constructive criticisms. Their contribution towards the betterment of my work is immense. I am indebted to Dr. Jaime De La Ree for providing me with a helping hand whenever I needed it. I am thankful to Dr. Sandeep K. Shukla and Dr. Michael R. Taaffe for their genuine interest in my work.

In summer of 2012 and 2013, I got the opportunity to work at Electric Power Group (EPG), LLC in Pasadena, California. The internship enabled me to apply my theoretical knowledge to solve real-world problems. I am grateful to EPG for allowing me to include a part of the work I did over there in my dissertation. I would like to especially thank my mentor at EPG, Mr. Bharat Bhargava, whose precious inputs were instrumental for the successful completion of that task.

My four years in the Power Lab at Virginia Tech has been a dream come true. The support and companionship that my fellow graduate students have given me is beyond belief. I am especially thankful to Gerardo Sanchez, Kate Vance, and Fenghua Gao for encouraging me to always persevere even when the chips were down.

Last, but in no way the least, I am thankful to God for giving me such wonderful parents and a loving and caring younger brother. My family has always been a constant source of motivation for me and I am eternally grateful to them for their unwavering faith in me. Their love and support has been critical for the successful completion of my degree.

April 11, 2014. Anamitra Pal

Publications

Journal Papers

- A. Pal, G. A. Sanchez-Ayala, V. A. Centeno, and J. S. Thorp, "A PMU placement scheme ensuring real-time monitoring of critical buses of the network," *IEEE Trans. Power Del*., vol. 29, no. 2, pp. 510-517, Apr. 2014.
- A. Pal, J. S. Thorp, T. Khan, and S. S. Young, "Classification trees for complex synchrophasor data," *Elect. Power Compon. Syst.*, vol. 41, no. 14, pp. 1381-1396, Sep. 2013.
- M. Li, A. Pal, A. G. Phadke, and J. S. Thorp, "Transient stability prediction based on apparent impedance trajectory recorded by PMUs," *Int. J. Elect. Power Energy Syst.*, vol. 54, pp. 498-504, Jul. 2013.
- A. Pal, J. S. Thorp, S. S. Veda, and V. A. Centeno, "Applying a robust control technique to damp low frequency oscillations in the WECC," *Int. J. Elect. Power Energy Syst.*, vol. 44, no. 1, pp. 638-645, Jan. 2013.

Conference Papers

- K. Vance, A. Pal, and J. S. Thorp, "A robust control technique for damping inter-area oscillations," in *Proc. IEEE Power and Energy Conference at Illinois (PECI)*, Champaign, IL, pp. 1-8, Feb. 2012.
- F. Gao, J. S. Thorp, A. Pal, and S. Gao, "Dynamic state prediction based on Auto-Regressive (AR) model using PMU data," in *Proc. IEEE Power and Energy Conference at Illinois (PECI)*, Champaign, IL, pp. 1-5, Feb. 2012.
- A. Pal, and J. S. Thorp, "Co-ordinated control of inter-area oscillations using SMA and LMI," in *Proc. IEEE Power Eng. Soc. Conf. Innovative Smart Grid Technol.*, Washington D.C., pp. 1-6, Jan. 2012.
- G. A. Sanchez, A. Pal, V. A. Centeno, and W. C. Flores, "PMU placement for the Central American power network and its possible impacts," in *Proc. IEEE Power Eng. Soc. Conf. Innovative Smart Grid Technol.*, Medellin, Colombia, pp. 1-7, Oct. 2011.

Books

- A. Pal, and J. S. Thorp, Coordinated Control of Inter-area Oscillations using SMA and LMI: A Robust Control Technique for Damping Low Frequency Oscillations, *Lambert Academic Publishing*, Oct. 2012.

Submitted Articles (under review)

- K. D. Jones, A. Pal, and J. S. Thorp, "Methodology for performing synchrophasor data conditioning and validation," submitted to *IEEE Trans. Power Syst.*
- F. Gao, J. S. Thorp, S. Gao, A. Pal, and K. A. Vance, "A voltage phasor based fault classification method for PMU only state estimator output," submitted to *Elect. Power Compon. Syst.*
- T. Wang, A. Pal, J. S. Thorp, Z. Wang, J. Liu, and Y. Yang, "Multi-polytope based adaptive robust damping control in power systems using CART," submitted to *IEEE Trans. Power Syst.*
- A. Pal, G. A. Sanchez-Ayala, J. S. Thorp, and V. A. Centeno, "A community-based partitioning approach for PMU placement in large systems," submitted to *IEEE Latin America Trans.*

Table of Contents

List of Figures

List of Tables

Chapter 1: Introduction

The invention of phasor measurement units (PMUs) has revolutionized the world of power systems. Also called synchrophasors, PMUs are devices that measure *phasors* that are *synchronized* in time. They have made possible the measurement of voltages and currents at diverse locations in the power grid at the same time. This provision of *time-stamping* has enabled system operators and planners to measure the state of the electrical system and manage power quality. This synchronization in time is facilitated through the use of global positioning system (GPS) satellites. As these measurements are truly synchronized, they can be used to assess system conditions in real-time. Fig. 1.1 shows the block diagram of a typical PMU whereas Fig. 1.2 shows how they are utilized in power systems.

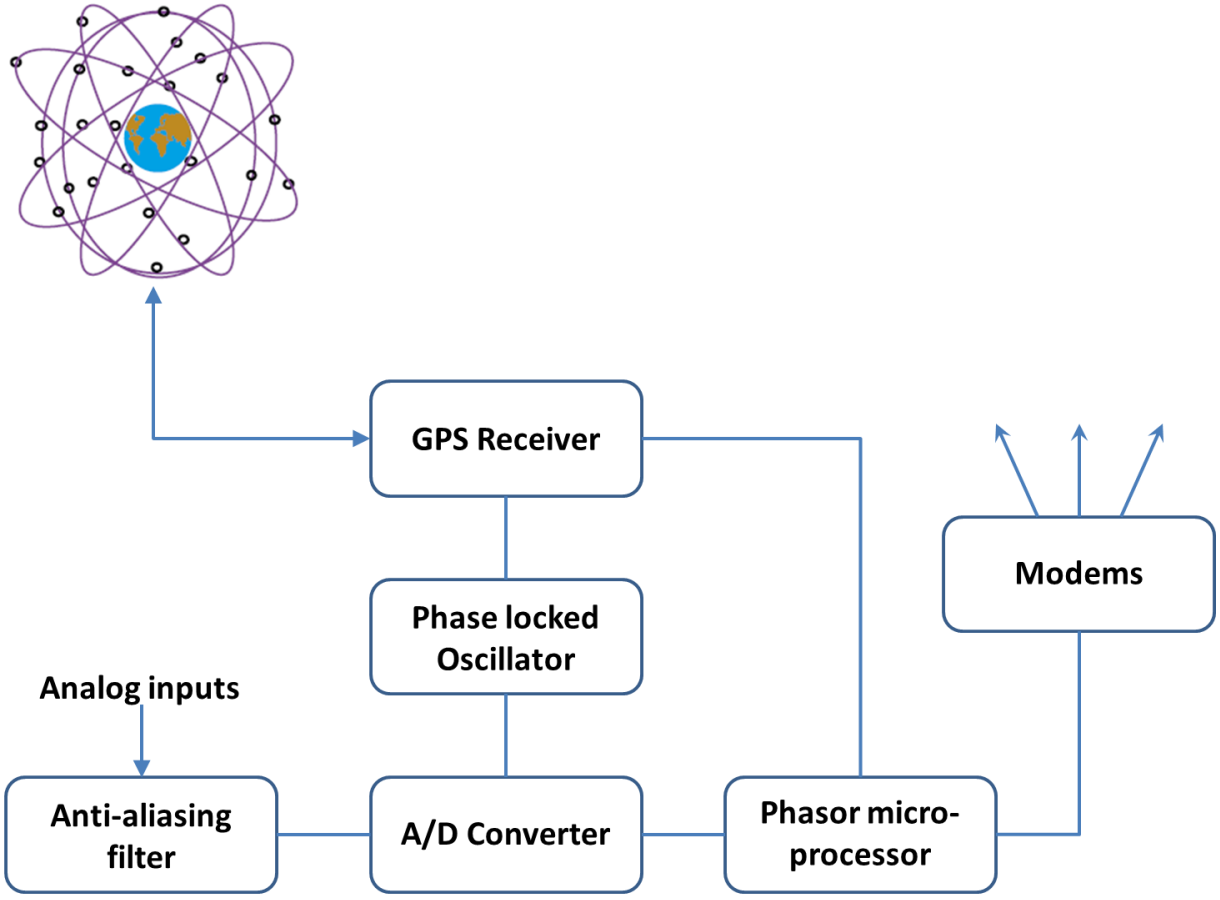

Fig. 1.1: Block Diagram of a phasor measurement unit (PMU)

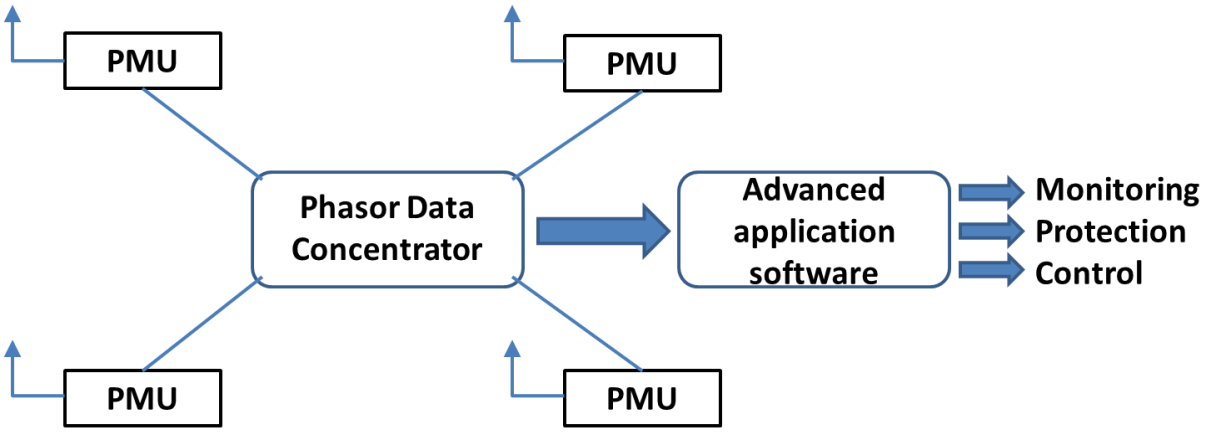

Fig. 1.2: PMU Utilization in a Power System

PMUs have been used for a variety of applications in power systems [1]. Collectively called wide area measurement system (WAMS)-based applications, these can be broadly classified into three categories (as shown in Fig. 1.2):

- Monitoring
- Protection
- Control

They are described in more details as follows.

Monitoring: Under the category of monitoring, PMUs have been primarily used in post-event analysis and state estimation. When the first commercial PMUs became available, because of their high cost, they were only used for post event monitoring. As more and more companies started manufacturing PMUs in accordance with the standards [2]-[4], the quality of the phasors produced by the PMUs improved significantly and so did their applicability. The monitoring capabilities of PMUs proved especially useful in performing quick and accurate post-mortem analysis of the 1996 U.S. West Coast blackout and the 2003 Northeastern U.S. blackout. Accordingly, one of the recommendations from the United States–Canada Task Force on the 14 August 2003 blackout was to "require use of time synchronized data recorders" to all utilities [5]. This and other recommendations led to the creation of the Eastern Interconnection Phasor Project (EIPP), now known as North American SynchroPhasor Initiative (NASPI). The use of PMUs for performing post-event analysis has increased considerably since then.

State Estimation of the power system from real-time measurements is one of the most important elements of modern energy management systems (EMSs). The state of the power system is defined as the collection of voltages of all the network buses obtained simultaneously. The technology of state estimation currently in use is primarily based on unsynchronized measurements obtained from the supervisory control and data acquisition (SCADA) system. This results in a nonlinear equation that must be solved iteratively to estimate the system state. Due to low scanning rates and relatively slow computations, present technology is incapable of providing information about the dynamic state of the power system. Synchronized phasor measurements enable a recast of the entire state estimation process. PMUs are capable of providing measurements as often as once per cycle of the power frequency. These measurements can become the basis for developing a coherent picture (state) of the network. Knowing the network state in turn makes stability and vulnerability assessments possible [6]. Thus, with the use of this technology, much of the delay inherent in the present state estimation systems can be removed, and the utilities can move on to advanced static and dynamic contingency analyses of their network in real-time.

Protection: Synchronized phasor measurements enhance the effectiveness of power system protection by offering solutions to a number of complex protection problems. This involves equipment and system protection, as well as remedial action schemes. For example, the status of certain circuit-breakers and switches, power flows in key transmission lines, voltages at critical buses, power output of key generators, etc., measured by PMUs, could be used to formulate a strategy of responses if these parameters should fall within 'dangerous' patterns [7]. In this way, PMU measurements have the potential to limit the damage that can be caused to the power system by catastrophic events [8].

In general, phasor measurements are particularly effective in improving protection functions which have relatively slow response times. For such protection functions, the latency of communicating information from remote sites is not a significant issue. A few examples of protection systems that could benefit from remote phasor measurements information include control of backup-protection of distance relays; protection functions concerned with angular voltage stability of networks; security-dependability based adaptive voting schemes, etc. [9]-[12]. A number of other WAMS-based protection improvements can be found in [13].

Control: The traditional controllers used in power systems like power system stabilizers (PSSs), High Voltage DC (HVDC) links, and Flexible AC Transmission Systems (FACTS) were designed to act so that the defined control objective functions are optimized. However, prior to the introduction of synchronized

phasor measurements, these types of controls were essentially local. Therefore, because of the "local" nature of the control, in its efforts to damp a local mode of oscillation, a controller could negatively damp an inter-area mode of oscillation and vice-versa [14]. The introduction of PMUs prevents these kinds of occurrences as they offer the possibility of a control based on measurements obtained from remote areas (WAMS-based control).

A WAMS-based control brings in the remote measurements of the system state vector to the controller, and thus removes from the control loop, the uncertainty associated with the mathematical model. As a result, in its implementation the controller becomes primarily feedback-based rather than model-based. Latency of the phasor measurements is an issue, but as many of the processes (like inter-area oscillations) are in the low frequency range, the effect of latency-related problems is less. Moreover, since the phasor data is time-tagged, the control is based on the actual state of the system, albeit, a short time in the past (quasi-real time). Thus, these measurements can effectively integrate control actions of different controllers present in the system. Such a coordinated control scheme for damping inter-area oscillations has been developed in [15] and applied to a 4000+ bus Enhanced California model of the Western Electricity Coordinating Council (WECC) in [16], [17].

Thus, the use of PMUs has elevated the standards of power system monitoring, protection, and control. They have facilitated innovative solutions to traditional utility problems and have offered power system engineers a whole range of potential benefits like –

- Improved post-disturbance analyses because of precise snapshots of the system states obtained through GPS synchronization
- Precise estimates of the power system state obtained at frequent intervals, enabling dynamic phenomena to be observed from a central location
- Implementation of advanced protection schemes based upon synchronized phasor measurements for improving overall system response to catastrophic events
- Improving controller performance through advanced control using remote feedback

PMU-based applications for the improved monitoring and protection of power systems forms the basis of the work contained herein. In the course of this dissertation, the four objectives of performing more accurate data mining, optimizing PMU locations to reap maximum benefits out of their placement, assessing static and dynamic stress of a power system in real-time, and doing conditioning and validation of PMU data, will be met.

1.1 Decision making using PMU data

PMUs, when placed at a bus, provide time synchronized measurements of the voltage phasor and the branch current phasors of all the branches emerging from that bus. Therefore, the "phasors" that a traditional PMU measures are:

- Voltage magnitude and angles/real and imaginary components of voltages
- Current magnitude and angles/real and imaginary components of currents

Complex voltages and/or currents being the primary entities based on which decisions are made in a power system, the ability of PMUs to directly measure them, gives PMUs an enormous edge over other telemetry devices. As the power system has evolved, it has been observed that a combination of these phasors makes better "sense" for decision-making than an individual phasor. For instance, in [12] voltage angles were combined with real and imaginary currents to classify the system as safe or stressed. Similarly, a trajectory of an individual phasor measured over a period of time can be more reliable for decision-making than its value at a particular instant. Furthermore, the decisions being made may not always be "binary" – like classifying the system as "safe" or "stressed" or "stable" or "unstable". PMU data can also be used to identify events, like the type of fault that has taken place. Thus, PMU data, in general, will be high dimensional (complex numbers/trajectory of complex numbers) and can be used for making multi-class decisions. An algorithm is proposed in this dissertation that uses Fisher's Linear Discriminant (FLD) to make *multi-class* splits involving *high-dimensional* synchrophasor data.

1.2 Optimal PMU Placement

Before benefits can be reaped from the placement of PMUs in the power grid, the criterion of "site selection" with respect to their placement must be addressed. The placement sites are restricted by the available communication facilities, the costs of which are often higher than that of the PMUs themselves. To optimize cost and intended applications, it is necessary to choose PMU locations judiciously. Therefore, the path to be followed is to progressively deploy PMUs at select locations within the network to eventually observe the whole system [18]-[20]. The concept of optimal PMU placement has been a highly researched topic since PMUs came to be used commercially [21], [22]. Primarily, there have been two methods followed by power engineers for addressing this issue [18]:

- Development of a prioritized list of placement sites based essentially on observability, and
- Placement of PMUs to correctly represent critical dynamics of the system

However, the first approach does not take into account the transient and dynamic stability of the system, whereas the second approach does not consider complete observability as one of its priorities. The net outcome is that for the same system different "optimal" PMU placement sets are created depending on the methodology followed. As it is not possible for any utility to implement all the schemes that are proposed, either transient/dynamic stability, observability, or often both are compromised. In this dissertation, a PMU placement scheme is presented that combines both the methodologies. Binary integer programming and "depth of unobservability" [19] are used to find the relevant PMU placement set. The computational burden of the optimization appeared to be a limitation for applying this scheme to big systems (> 500 buses). In order to circumvent this problem, the proposed scheme was combined with a topology-based system partitioning technique to make it applicable to virtually any sized system.

1.3 Phasor Measurement based Stress Assessment Metrics

Courtesy the deregulation of power systems many tie-lines between control areas have come to operate near their maximum capacity, especially the ones serving heavy load centers. Such stressed operating conditions have increased inter-area oscillations between different control areas and even led to major disturbances [23]-[26]. In this chapter, two metrics are proposed for assessing static and dynamic stresses present in a power system. The base loading of the system constitutes static stress. It refers to the normal/pre-contingency state of the system. Dynamic stress refers to the event/contingency that the system is subjected to. Angle difference between buses located across the network and voltage sensitivity of buses lying in the middle were two metrics that were found to accurately reflect the static and dynamic stress of the system. The results indicate that with the aid of PMUs and modern software tools, it is now possible to assess metrics like these for large systems (10,000+ buses) in real-time.

1.4 Synchrophasor Data Conditioning and Validation and Possible Applications

A three-phase PMU-only (linear) state estimator has been created for Dominion Virginia Power's (DVP's) 500kV network as part of a DOE (Department Of Energy) Demonstration Project. The estimator will update every $1/30^{th}$ of a second with time-tagged measurements of high voltage buses as its outputs. However, the raw data obtained from these PMUs is not suitable for many of the applications for which they are expected to be used. As such, there is an imminent need to "clean" the raw synchrophasor data so that correct decisions can be made using these measurements.

A technique to predict the next voltage measurement from a history of previous estimates was developed in [27]. Using this technique, a methodology to "clean" raw synchrophasor data is proposed here. This process can be used to detect bad data by using an observation residual as well as to smooth data by using subsequent measurements to obtain a better estimate (a technique for supplying missing data). In this work, the data conditioning and validation process has been integrated with the linear state estimator (LSE) developed for DVP [28]. However, even if a state estimator is not desired, the proposed data conditioning algorithm can be used as a stand-alone tool for detecting bad data, finding the best estimate, and increasing the observability of the network. The use of conditioned and validated data in calibrating positive sequence instrument transformers is also touched upon.

1.5 Overview of the Dissertation

This dissertation is organized as follows:

Chapter 1 gives a brief overview of the different applications of synchrophasor measurements in the domain of power systems. It explains the decision making process involving complex synchrophasor data. It presents a PMU placement scheme that ensures real-time monitoring of important buses of the network while gradually enhancing system observability. It also shows how the proposed PMU placement scheme can be combined with a partitioning scheme to further increase its applicability to large systems. Then, it proposes two metrics for assessing stress in a modern power system network. Finally, it describes a methodology to clean raw synchrophasor data in real-time and suggests possible applications of the conditioned data. The chapter concludes by outlining the contents of the following chapters.

Chapter 2 begins with an overview of classification and regression tree (CART), a decision tree algorithm that is commonly used in power system applications. Next, it outlines some of the problems faced by the traditional CART logic with regards to synchrophasor data, thereby highlighting the potential applications of the proposed technique – Fisher's Linear Discriminant applied to Synchrophasor Data (FLDSD). The chapter concludes with simple examples to demonstrate the superiority of the proposed approach to other techniques that have been developed previously to address this problem.

Chapter 3 illustrates the application of the FLDSD technique to solve power system problems. In the first problem, it is applied to a detailed model of the California power system, where it is used for developing an adaptive protection scheme. This example illustrates the ability of the FLDSD technique to efficiently handle large data sets. In the second problem, it is applied to the IEEE 118-bus system, where it is used

to classify dynamic events based on trajectories of voltage measurements obtained from PMUs. This example highlights the technique's ability to make decisions involving high-dimensional, multi-class synchrophasor data.

Chapter 4 presents a PMU placement scheme called critical bus based binary integer optimization (CBBBIO) that provides real-time monitoring of key buses of the network. High voltage lines, substations relevant for transient and dynamic stability of the network, and buses with high connectivity are given maximum priority while placing the PMUs. Binary integer programming and "depth of unobservability" are combined to find the relevant PMU placement set. The placement scheme is tested on the IEEE 118-bus system, IEEE 300-bus system, a 283-bus model of the Central American Power Transmission System, and a complex 996-bus network describing the Northern and the Eastern power grids of India. The results indicate that the CBBBIO technique will be useful to utilities that want to initially protect the most important buses of their system on their way to attaining complete observability.

Chapter 5 extends the CBBBIO technique developed in the previous chapter by combining it with a community-based partitioning approach for computing PMU placement schemes in very large power system models. A bound is also developed to compute for the maximum error from an optimal solution. The technique developed here is applied to standard IEEE systems as well as on more realistic power system networks. The partitioning logic appears to provide a considerable reduction in computational burden of the optimization without significantly changing the system structure/topology.

Chapter 6 introduces two metrics for static and dynamic stress assessment in a modern power system. The base loading of the system constitutes static stress. It refers to the normal/pre-contingency state of the system. Dynamic stress refers to the event/contingency that the system is subjected to. Angle difference between buses located across the network and voltage sensitivity of buses lying in the middle were found to accurately reflect the static and dynamic stress of the system. A 10,000+ bus model of the WECC system is used as a test system for this analysis. The results indicate that by doing data mining on these two parameters and setting appropriate alerts/alarm limits, a more secure power system operation can be realized.

Chapter 7 delves upon a methodology to perform data conditioning and validation of phasor data obtained from a PMU-only state estimator. A PMU only state estimator is intrinsically superior to its SCADA analogue with respect to performance and reliability. However, ensuring the quality of the data stream which leaves the linear estimator is crucial before establishing it as the front end of an EMS. This

can be done by pre-processing the phasor data before it arrives at the linear estimator and by using the estimator itself as a means to clean the data. This chapter presents an algorithm for synchrophasor data conditioning and validation that fits neatly into the existing linear state estimation formulation. The results indicate that the proposed technique provides a computationally simple, elegant solution to the synchrophasor data quality problem. Its use in the calibration of positive sequence instrument transformers is also discussed.

Chapter 8 summarizes the dissertation and suggests possible topics that can be explored in the future. The references and appendices are provided in Chapter 9 and Chapter 10, respectively.

Chapter 2: Decision Trees for Complex Synchrophasor Data

Wide area measurement system (WAMS) using synchronized phasor measurement units (PMUs) have been extensively used in power system networks all over the world. PMU-based measurements provide new methods for achieving real-time control, stability enhancement, and transfer capacity improvement of the power network. Especially, in the developed nations, these measurements have been widely used for state estimation, protection, and control based on situational awareness for operational decision making. Various data mining techniques have been employed by power engineers to make decisions based on this information [29]-[33], with decision trees (DTs) being the most popular approach [34].

Decision trees (DTs) extract information from large sets of data and intuitively represent the gained knowledge through a series of if-else statements. And because DTs use if-else logic, they can be programmed and implemented very easily in the field. Decision trees have been used extensively in power systems for performing different types of analysis. A security-dependability based adaptive protection scheme separately using voltage angles and current magnitudes is developed in [12]. In [35], a real-time transient stability prediction scheme using voltage angles and decision trees is investigated. Voltage angles are again used in decision tree processing for response-based discrete event control [36]. A fast online voltage security monitoring scheme using PMU measurements with decision trees built using voltage angles is developed in [37]. Phasor magnitude and angle have (separately) been used for real-time transient instability detection [38]. In [39], power system security assessment is done using decision trees built from voltage angles obtained from PMUs. A wide-area response-based control using phasor measurements and decision trees based on voltage angles is developed in [40]. Splitting of decision trees on a single attribute is done in [41]-[43]. Voltage angles have again been used for power system transient stability forecasting in [44].

Classification and regression tree (CART) is a binary decision tree that is constructed by splitting the parent node and subsequent nodes into two child nodes repeatedly, beginning with the root node that contains the whole learning sample. The logic is based on choosing the best split among all possible splits at each parent node so that the child nodes are purest. The CART algorithm initially grows a decision tree as large as possible and then selectively prunes it upwards. Cost complexity criterion is used in the pruning process. The objective is to attain a minimum sized tree with minimized cost complexity. Cost complexity criterion and number of branches vary depending on the application. More details about the computational aspects of the CART methodology – splitting criteria, structural

complexity, etc. can be found in [45]. A commercial implementation of this technique (CART®) has also been developed by Salford Systems [46].

Being a non-parametric decision tree learning technique, CART is especially suited to power systems because of the latter's complex, and non-linear behavior [47], [48]. A typical classification and regression tree is trained by a large number of cases called the "Learning Set" (LS) which is a sample of pre-classified states and a list of attributes. The tree splits the data into two subsets at each node so as to get maximum purity in the generated subsets. The tree not only finds the optimal attribute required for partitioning, but also computes the optimal value of that attribute. The tree will stop growing when either of the two terminal criteria is met:

- The class of a terminal node is "sufficiently" pure, or
- The accuracy cannot be improved by further partitioning

A set of "Testing Set" (TS) is then used to test the accuracy of the tree that has been built. To get a reliable and unbiased estimate, the test data set needs to be large. The CART logic explores the underlying mechanism based on which the data was created and uses binary recursive splitting to partition the sample space. Classification is used to analyze categorical type data while regression is used to analyze continuous type data [45].

The popularity of CART is because of its apparent robustness and efficiency of use. It requires little data for its preparation, works well even if some of the assumptions made during data generation are violated and performs very well with large data in a comparatively short time [49]. Moreover, the resulting model is easy to understand and implement. The advantages of CART over other data mining techniques like Automatic Interaction Detection (AID), Chi-square Automatic Interaction Detection (CHAID), and C5.0 (a commercial decision-tree and rule-learning package developed by RuleQuest Research) are briefly summarized below [46]:

- Optimal tree creation due to superior predictive accuracy
- Assessing goodness of fit of solution via cross-validation
- Ability to use same variable in different parts of the tree
- Resistance to presence of outliers

2.1 Illustration of the problem

CART data is in the form of an array with rows being the events/outcomes and columns being the measurements. In its simplest form, CART picks one measurement at a time for performing the splits. While this is very effective in handling data having univariate attributes, difficulties are observed where the predictors are multivariate. Multi-modal classification problems involve pattern recognition from disjoint regions in feature space. Synchrophasor data are an example of a multi-modal classification problem in the domain of power systems.

PMU measurements are generally complex. When CART picks one column, it uses either the real or the imaginary part of the measurement, but not both. Thus, it is not able to address the complete phasor in a single split. This also creates problems when there is a change of reference [50]. Moreover, although CART allows splitting on Linear Combinations (LCs) involving as many as 6 attributes, these are chosen as "p chooses d" [51]. Hence, for performing the split, CART is not particularly likely to select a linear combination that includes both the real and the imaginary part of the same complex number.

This drawback of CART (inability to perform an optimum split at a single node when applied on data having many attributes) limits its applicability to solve power system problems to a great extent. In most of the applications mentioned previously, decisions were being made based on one measurement obtained from a PMU. As such, CART was making decisions based on a single attribute. However, a PMU placed on a bus records the complete voltage phasor (magnitude and angle) and the complete branch current phasor (real and imaginary components) of all the branches emerging from that bus. Although using one attribute (for instance, voltage angle) works at times, it is not *always* a good strategy. As will be illustrated in this dissertation, on many occasions, it is more appropriate to use all the data that is made available through the placement of the PMU for making decisions, rather than just one attribute. Moreover, since the complex number (synchrophasor data) is a single entity (voltage, current, apparent impedance, etc.), it should be treated as such. Splitting only on the real or only on the imaginary component of a PMU measurement does not address the complete phasor.

Similarly, a linear combination involving the real part of one variable and the imaginary part of another variable is not physically meaningful and is inefficient for placing PMUs. For instance, if complex currents are considered separately then CART might choose to do a split based on the real current flowing through one line and the imaginary current flowing through a different line, in which case at least two PMUs would be needed for measuring the currents. However, if the complex currents are treated as a

single entity, then CART will decide based on the real and imaginary components of the current simultaneously and so even a single PMU might suffice. Thus, it can be inferred that there is a need to examine in greater detail the splits made by decision trees that use complex synchrophasor data.

2.2 Previous Approach – Rotation along a reference

The challenge that is encountered in making a split involving complex data is that two or more groups of high-dimensional quantities have to be separated by a single entity. This means that the multi-dimensional data has to be represented in a manner that a single dimensional variable is able to distinguish patterns present in that data. In the domain of power systems, [50] describes a way to make decisions concerning complex synchrophasor data by rotating along a reference. Their approach is described as follows.

In [50], Garlapati and Thorp studied the problem of splitting on the real or imaginary part of a complex quantity for a decision tree built using real-time data. Their logic is based on the fact that complex synchrophasor measurements have a reference angle associated with them. For instance, if a load flow is used to generate the data, the angle of the swing bus can be used as the reference. However, the actual application requires a physical reference as the measured angles would have the reference angle subtracted from them. That becomes a problem when the reference is changed. Typically this occurs when the PMU on the reference bus fails or when the utility decides to install the needed PMU elsewhere. Performing the split on the real or the imaginary part of a complex measurement would then result in the performance of the tree to degrade significantly.

This being the motivation for their work, Garlapati and Thorp proposed rotating along a reference as a potential solution to the problem. To illustrate their logic, let us assume a variety of load flow simulations have been performed for a system of N buses. For the load flow data that is generated, the utility swing bus, say bus n, is the reference. Therefore, the angle of bus n will be zero for all the cases. Now, if the utility places a PMU at bus n, then its angle will be used as the reference for all synchrophasor measurements and no change has to be made to the load flow data. However, if the utility decides to place the PMU at some other bus, say bus b, where $b \in N$ and $b \neq n$, then in order to use the new bus b as the reference, the angle of bus b has to be subtracted from all the other angles of the data set. Thus, bus b will now be at an angle of zero and all the angles will be referenced to it (instead of bus n). Graphically, this can be thought of as rotating all the data points by the angle difference between bus n and bus b. The following example illustrates this concept.

Fig. 2.1 denotes a randomly generated set of 40 data points. Without any loss of generality, it can be assumed that the X-axis depicts the real voltages in p.u. whereas the Y-axis depicts the imaginary component of the voltages also in p.u., when referenced to the swing bus of an arbitrary system for some simulated experiment. The blue circles can then correspond to the stable voltages while the red circles will denote the unstable voltages. The dotted line shows the single column splitter obtained when this set of complex voltage measurements is fed into CART. However, from the figure it becomes clear that by splitting in this way, two blue points which are supposed to be above the line are below it resulting in a misclassification of 5%.

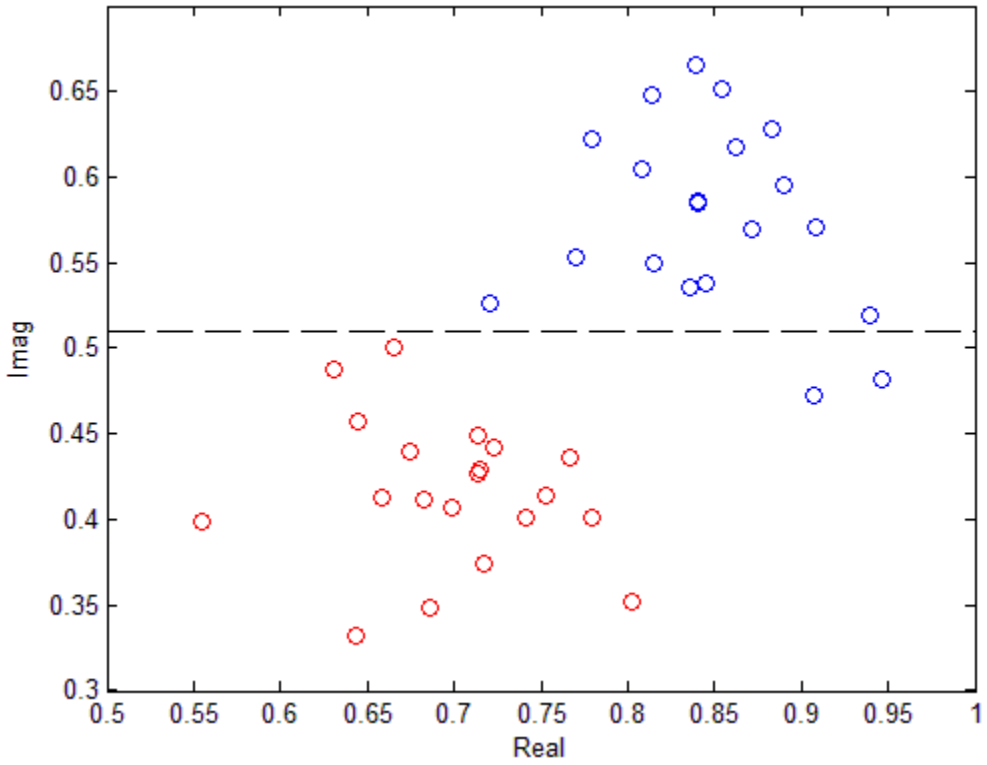

Fig. 2.1: Best split obtained by using the swing bus as reference

Now based on the logic developed in [50], one can shift the reference from the swing bus to other buses of this arbitrary system to get different splits. By successively making three other buses say bus a, bus b and bus c as the reference (where buses a, b and c are not the initial swing bus) one can obtain plots such as the ones shown in Figs. 2.2-2.4. From these figures it becomes clear that the reference used in Fig. 2.3 i.e. bus b is the best reference for performing the split for the said experiment.

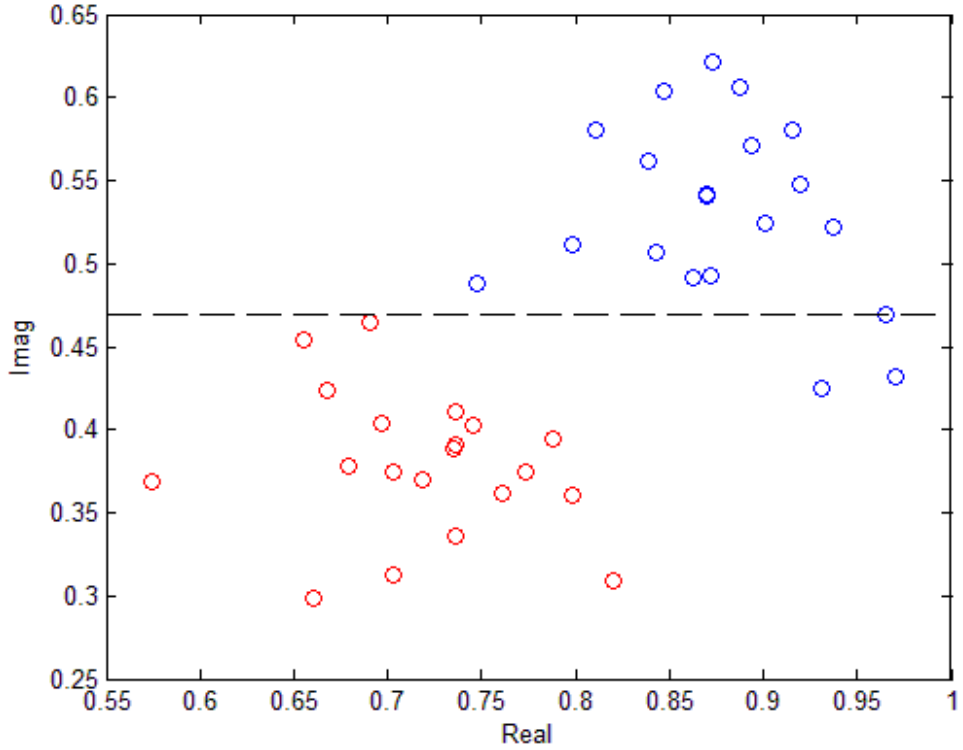

Fig. 2.2: Best split obtained by using bus a as reference

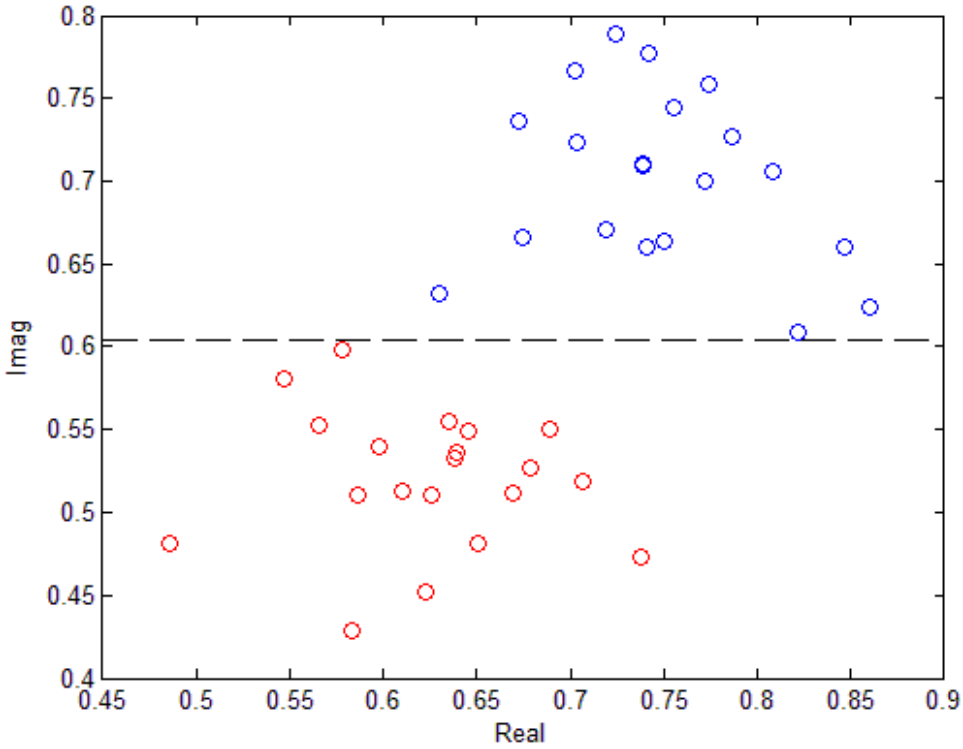

Fig. 2.3: Best split obtained by using bus b as reference

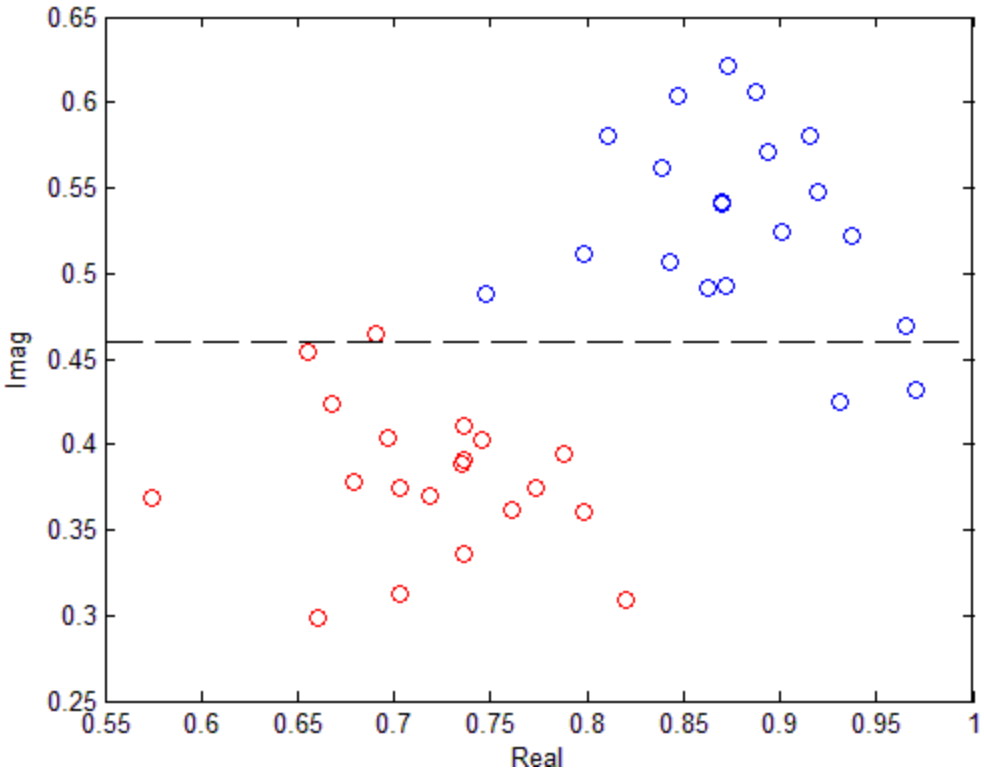

Fig. 2.4: Best split obtained by using bus *c* as reference

The approach proposed in [50] is impressive because it not only provides a possible solution to the problem of using complex measurements for decision making, but also can be used to find out the most suitable reference bus for a given application. Out of the buses selected by the decision tree, the bus that results in the least number of misclassifications will be the best bus to be used as a reference. The only thing that needs to be done is to try different buses as the reference to see which bus best suits the need.

2.3 Proposed Algorithm – Fisher's Linear Discriminant applied to Synchrophasor Data (FLDSD)

The technique that is presented in [50] is one way in which splits can be performed for decision making using complex synchrophasor data. However, it is not the most optimal way of addressing this issue. The drawbacks of the approach developed in [50] are identified as follows:

- It does not necessarily produce the best possible results
- It's a very "manual process" and cannot be easily applied to large and complex power system problems
- It cannot be extended to data having more than two-dimensions

- It cannot make multi-class distinctions

In order to implement the logic developed in [50] the reference has to be moved from one bus to the other in order to find the reference that is best suited for the given application. But there is no guarantee that there "will" be a reference bus that will give the optimum split in all situations. Similarly, the transfer of the reference from one bus to the other is a very "manual process" because it requires "checking" for the bus that gives the least number of misclassifications and then "choosing" that bus for decision making. Therefore it becomes very difficult to apply this logic directly to large and complex power system problems. Finally, the logic developed in [50] cannot be extended to data having more than two attributes, nor can it make distinctions between multiple classes. The technique developed in this chapter called Fisher's Linear Discriminant applied to Synchrophasor Data (FLDSD) overcomes all the aforesaid drawbacks.

2.3.1 Strategy for making two-class classification of high dimensional data

Consider a set of observations $\vec{\boldsymbol{p}}$ for each sample of an event with known classes q_b and q_r; the subscripts b and r denoting the "blue" and "red" data sets which are to be separated. The objective of the classification problem is to then find a good predictor for the class q of any sample given only an observation $\vec{\boldsymbol{p}}$. By performing simulations and analyzing the results, it was realized that for similar distributions (skewed or otherwise), a simple and efficient way of doing the split was by making the two distributions spherical. This is based on the logic of linear discriminant analysis (LDA) which is a simplification of Fisher's Linear Discriminant (FLD) [52]. This is done by multiplying the individual distributions with the Cholesky-Decomposition [53] of the inverse of its covariance matrix. This results in the new distributions becoming spherical with an identity covariance matrix. The advantage is that the perpendicular bisector of the line joining the two centroids of the new (spherical) distributions then becomes the optimum split between the two data sets.

Let the two classes of observations have centroids $\vec{\boldsymbol{\mu}}_{\boldsymbol{q_b}}$ and $\vec{\boldsymbol{\mu}}_{\boldsymbol{q_r}}$ and covariance $\boldsymbol{C_q}$. Then the optimum split for this new distribution is obtained by solving for $\vec{w}_{\mathrm{new}}$ such that,

$$\boldsymbol{S}\left(\vec{\boldsymbol{\mu}}_{\boldsymbol{q_b}} - \vec{\boldsymbol{\mu}}_{\boldsymbol{q_r}}\right)^T . \left(\vec{\boldsymbol{w}}_{\mathbf{new}} - \frac{\left(\vec{\boldsymbol{\mu}}_{\boldsymbol{q_{b_{\mathbf{new}}}}} + \vec{\boldsymbol{\mu}}_{\boldsymbol{q_{r_{\mathbf{new}}}}}\right)}{2} \right) = 0 \tag{2.1}$$

Where,

$$\vec{\boldsymbol{\mu}}_{q_{b_{\mathbf{new}}}} = \boldsymbol{S}\vec{\boldsymbol{\mu}}_{q_b}$$
$$\vec{\boldsymbol{\mu}}_{q_{r_{\mathbf{new}}}} = \boldsymbol{S}\vec{\boldsymbol{\mu}}_{q_r} \quad (2.2)$$
$$\boldsymbol{S}^T\boldsymbol{S} = \boldsymbol{C_q}^{-1}$$

It is to be noted here that $\vec{\boldsymbol{w}}_{\mathbf{new}}$ defines the hyper-plane which perpendicularly bisects the line joining the two new centroids. Therefore, (2.1) holds true in the new co-ordinate system where the two distributions are spherical with identity covariance matrices. The data points to be segregated are now projected onto $\vec{\boldsymbol{w}}_{\mathbf{new}}$. For example, let $\vec{\boldsymbol{w}}_{\mathbf{new}}$ be parameterized by a linear equation in 3-d space as shown in (2.3),

$$\vec{\boldsymbol{w}}_{\mathbf{new}}: ax + by + cz + d = 0 \quad (2.3)$$

Then, if $\vec{\boldsymbol{p_i}} = (x_i, y_i, z_i)$ be the i^{th} data point belonging to the set of observations $\vec{\boldsymbol{p}}$, then the shortest distance from $\vec{\boldsymbol{p_i}}$ to the hyperplane defined by $ax + by + cz + d = 0$ is given by,

$$D(i) = \frac{ax_i + by_i + cz_i + d}{\sqrt{a^2 + b^2 + c^2}} \quad (2.4)$$

The split can now be performed on the following basis –

$$D(i) \leq 0: \text{Red}$$
$$D(i) > 0: \text{Blue} \quad (2.5)$$

From (2.3)-(2.5) it becomes clear that, since the distance vector will be a one-dimensional quantity irrespective of the number of dimensions the hyperplane has, this logic can be extended to address high dimensional data with ease.

When the two distributions are very different, an optimum split can be performed by adding the covariances of the two data sets and using it on both the data (based on traditional FLD). Let the two classes of observations have centroids $\vec{\boldsymbol{\mu}}_{q_b}$ and $\vec{\boldsymbol{\mu}}_{q_r}$ and experimental covariances $\boldsymbol{C}_{q_b}$ and $\boldsymbol{C}_{q_r}$. Then, FLD defines a performance index ρ which maximizes the projected class differences relative to the sum of the projected within-class variability [52], [54]. Mathematically, this is stated as –

$$\text{Maximize } \rho: \rho = \frac{\left(\vec{\boldsymbol{m}}^T\left(\vec{\boldsymbol{\mu}}_{q_b} - \vec{\boldsymbol{\mu}}_{q_r}\right)\right)^2}{\vec{\boldsymbol{m}}^T\left(\boldsymbol{C}_{q_b} + \boldsymbol{C}_{q_r}\right)\vec{\boldsymbol{m}}} \quad (2.6)$$

Where the vector $\vec{\boldsymbol{m}}$ is the normal to the discriminant hyper-plane

On solving (2.6), it is realized that the maximum separation occurs when,

$$\vec{\boldsymbol{m}} = \left(\boldsymbol{C}_{q_b} + \boldsymbol{C}_{q_r}\right)^{-1}\left(\vec{\boldsymbol{\mu}}_{q_b} - \vec{\boldsymbol{\mu}}_{q_r}\right) \tag{2.7}$$

If $\vec{\boldsymbol{\mu}}_{q_{b_n}} = \left(\boldsymbol{C}_{q_b} + \boldsymbol{C}_{q_r}\right)^{-1}\vec{\boldsymbol{\mu}}_{q_b}$ and $\vec{\boldsymbol{\mu}}_{q_{r_n}} = \left(\boldsymbol{C}_{q_b} + \boldsymbol{C}_{q_r}\right)^{-1}\vec{\boldsymbol{\mu}}_{q_r}$, then any vector perpendicular to $\vec{\boldsymbol{m}}$ and passing through its mid-point is given by,

$$\frac{1}{2}\left(\vec{\boldsymbol{\mu}}_{q_{b_n}} - \vec{\boldsymbol{\mu}}_{q_{r_n}}\right) + \vec{\boldsymbol{w}}\alpha \tag{2.8}$$

In (2.8) α is the optimizing variable. In order to find the optimum hyper-plane, we have to minimize:

$$\left\|\vec{\boldsymbol{p}} - \frac{1}{2}\left(\vec{\boldsymbol{\mu}}_{q_{b_n}} - \vec{\boldsymbol{\mu}}_{q_{r_n}}\right) - \vec{\boldsymbol{w}}\alpha\right\|^2 \tag{2.9}$$

On solving (2.9) using weighted least squares (WLS) algorithm, we get the expected value of α as,

$$\hat{\alpha} = (\vec{\boldsymbol{w}}^T\vec{\boldsymbol{w}})^{-1}(\vec{\boldsymbol{w}}^T)\left(\vec{\boldsymbol{p}} - \frac{1}{2}\left(\vec{\boldsymbol{\mu}}_{q_{b_n}} - \vec{\boldsymbol{\mu}}_{q_{r_n}}\right)\right) \tag{2.10}$$

Using this value of $\hat{\alpha}$, we obtain the splitting variable D as:

$$D = [I - \vec{\boldsymbol{w}}(\vec{\boldsymbol{w}}^T\vec{\boldsymbol{w}})^{-1}\vec{\boldsymbol{w}}^T]\left(\vec{\boldsymbol{p}} - \frac{1}{2}\left(\vec{\boldsymbol{\mu}}_{q_{b_n}} - \vec{\boldsymbol{\mu}}_{q_{r_n}}\right)\right) \tag{2.11}$$

From (2.11), it can be inferred that the original multivariate data can be replaced in CART by the single variable D. It is also easy to show that the hyperplane perpendicularly bisecting the line joining the two centroids in the new co-ordinate system is equivalent to a rotation of the hyperplane perpendicularly bisecting the line joining the two centroids in the original co-ordinate system, thereby making it no longer perpendicular. This is the geometric interpretation of Fisher's algorithm. Therefore, for any unknown distribution a direct application of FLD is sufficient for performing an optimum split. As such, a suitable name for this method is Fisher's Linear Discriminant applied to Synchrophasor Data (FLDSD).

2.3.2 Strategy for making multi-class classification of high dimensional data

In the previous sub-section, it was proved that the proposed approach is able to perform binary splits on high-dimensional data. However, this method could also be used to separate multiple classes, by taking two classes at a time. In order to do so, distances of the data points from all the hyperplanes must be

initially computed. Taking two classes at a time, (2.11) is used to compute for the distances. For n-class distribution, we have,

$$Number\ of\ Hyperplanes = \frac{n \times (n-1)}{2} \tag{2.12}$$

The distances to the hyperplanes must then be fed into CART for selecting the optimum distance variable for performing the split. Since all the input variables have single attributes, CART can directly select the distance variable that will result in the best possible split. By selecting two classes at a time, and proceeding until all the class combinations have been covered, even a tree of depth $\mathrm{n}-1$ can successfully separate n data classes. The flowchart of the proposed algorithm is shown in Fig. 2.5, while the pseudo-code describing its application to an example problem is given in Appendix A. The next sub-section demonstrates the application of this logic to typical synchrophasor data.

2.4 Illustrating application of FLDSD to synchrophasor data

Since PMU data are usually complex numbers, the goal is to express such multivariate data by a single entity. This single entity/variable would be used for performing the split in CART. But real-time PMU measurements offer some challenges of their own. It was observed that data sets often had very skewed distributions (as seen in Fig. 2.6). The reason for this was that voltage magnitudes and steady state currents expressed in "per unit" were near unity, but the angles expressed in degrees and transient current values were not so. Thus, when such diverse measurements were combined together to make decisions, the resulting cloud became ellipsoidal in shape. This issue was addressed by transforming the ellipsoid into a sphere using the proposed algorithm as shown in Fig. 2.7. It becomes obvious from Fig. 2.7 that this technique has resulted in the two distributions becoming circular (spherical, for higher dimensions) from their earlier elliptical (ellipsoidal, for higher dimensions) shapes. This was further verified by computing the covariances of the new distributions, both of which were found to be identity.

Another problem was the apparent randomness in some of the distributions when, for example, a fault occurred in the system. Similar to what is seen in Fig. 2.8; it was observed that such distributions followed no set pattern. The application of the proposed approach to the example in Fig. 2.8 is shown in Fig. 2.9. It becomes obvious from Fig. 2.9 that using this method a perfect split between the data points has been obtained. The next sub-section illustrates how a split performed using FLDSD compares with that performed using the traditional CART algorithm.

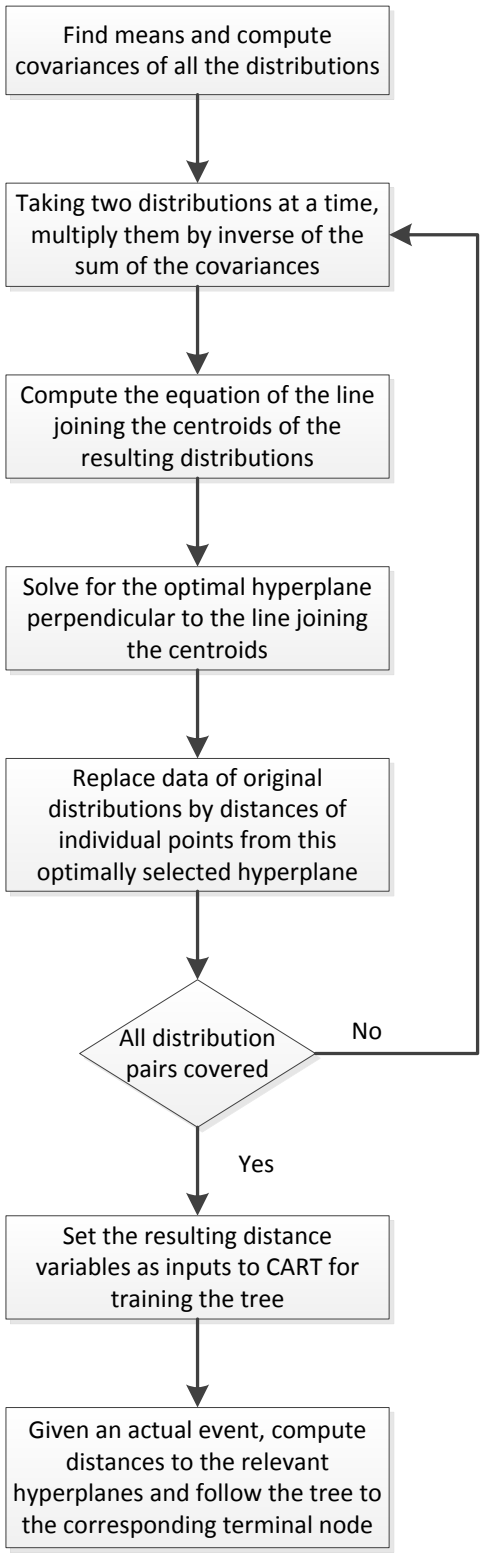

Fig. 2.5: Flowchart of Proposed Algorithm

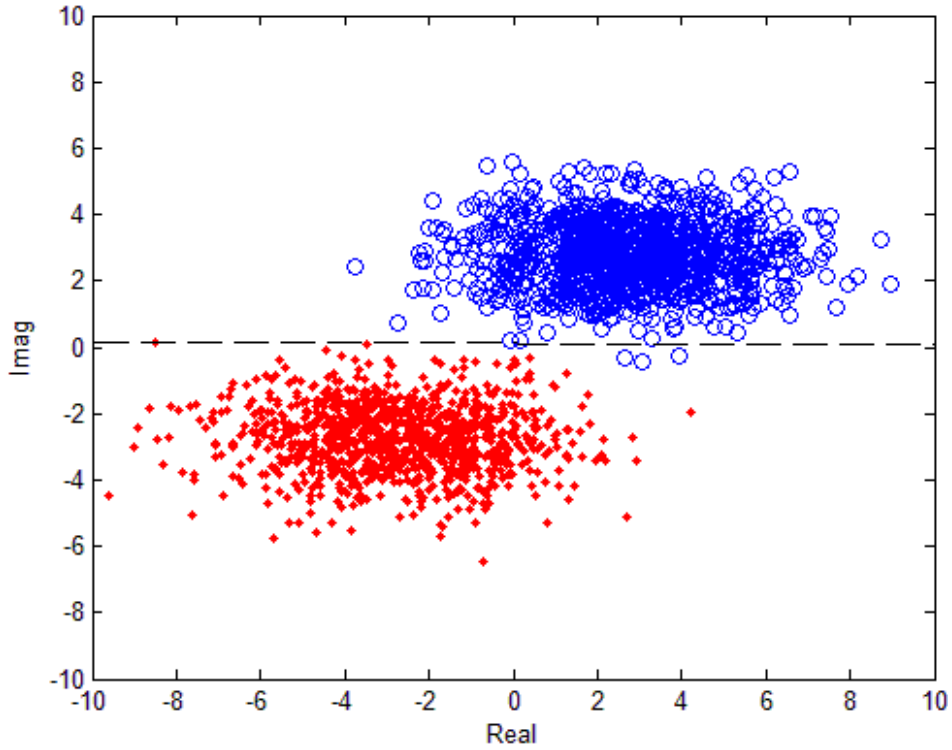

Fig. 2.6: Dotted line shows best first single column split

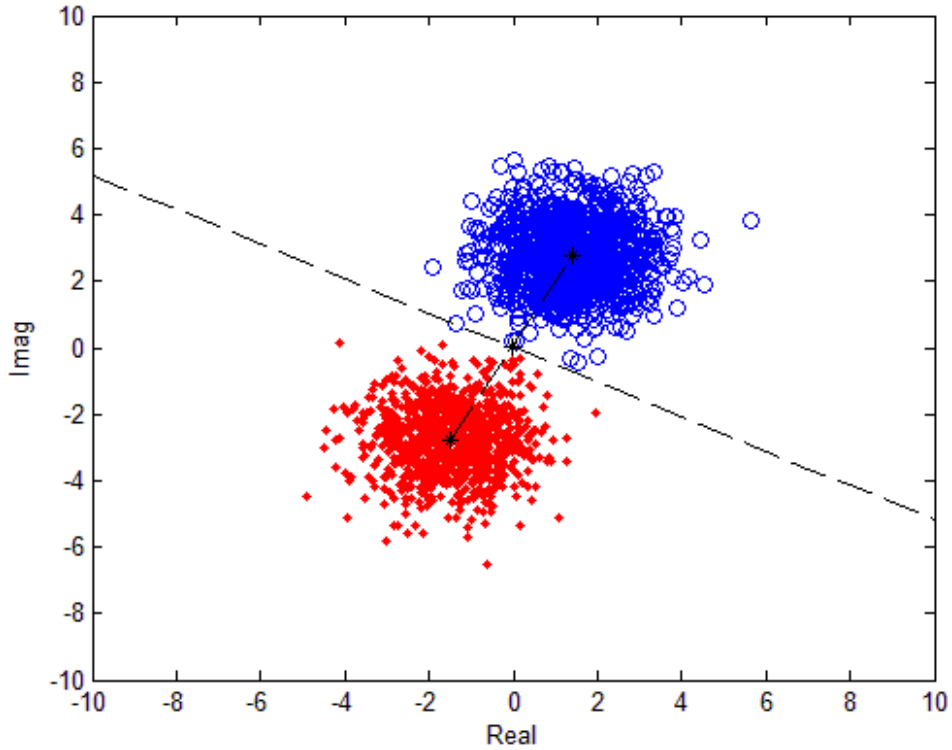

Fig. 2.7: Dotted Line shows the optimal first split

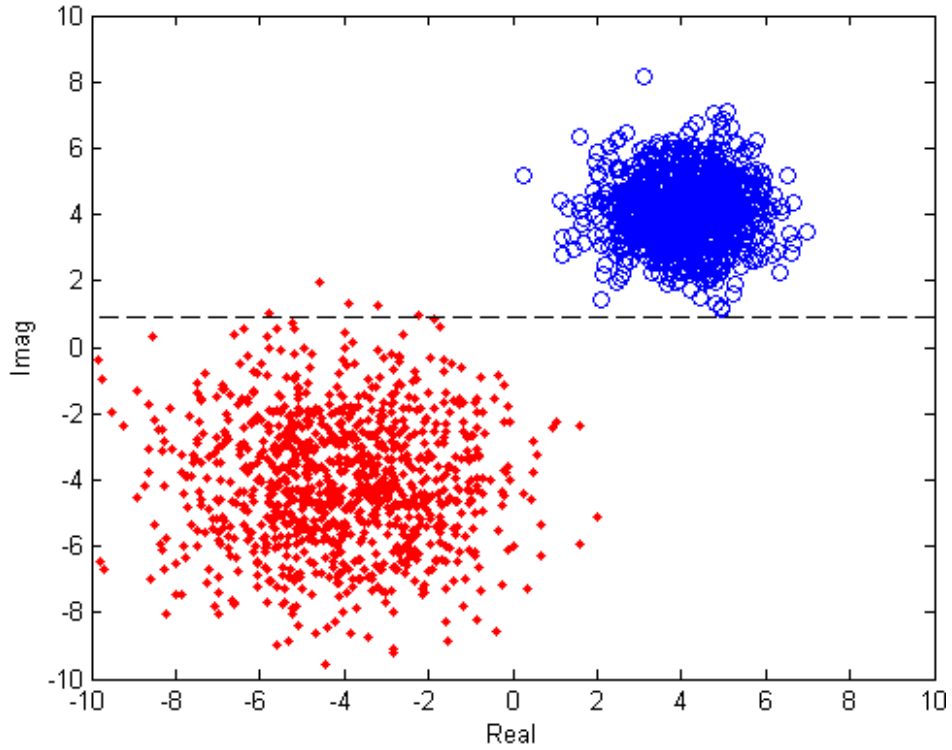

Fig. 2.8: Dotted line shows best first single column split

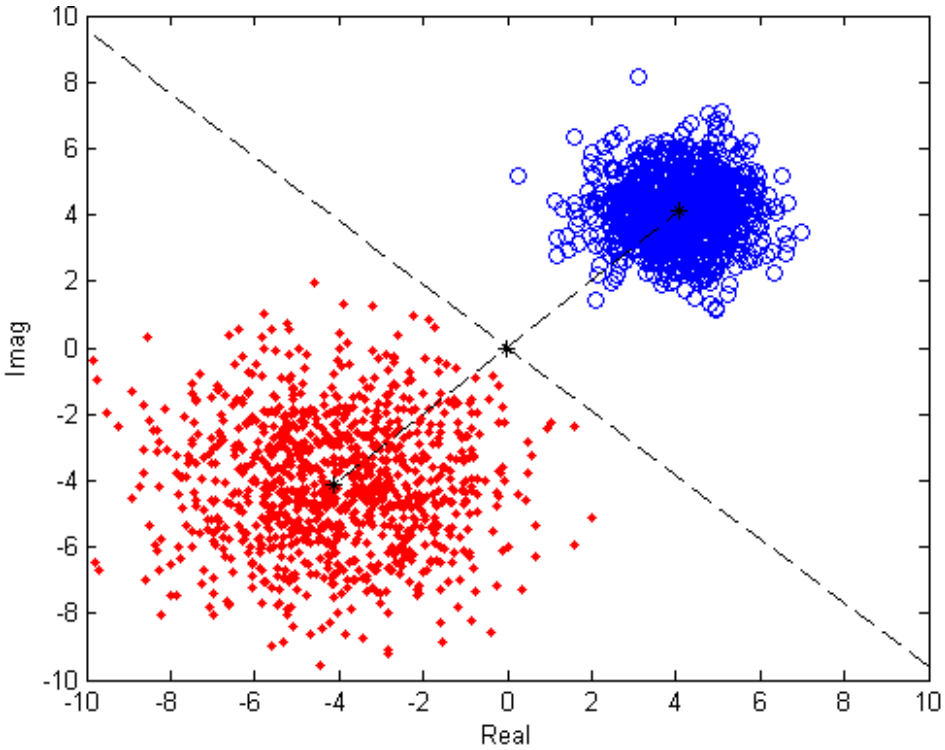

Fig. 2.9: Dotted Line shows the optimal first split

2.5 Comparison of FLDSD with the traditional CART algorithm

In the previous sub-section, the application of FLDSD to split randomly generated synchrophasor data was demonstrated. From the results, it was clear that the proposed logic is able to perform a better split than the one obtained using data from a single column. In this sub-section, a direct comparison of this algorithm (used as a preprocessing step) is made with the traditional CART algorithm to show its ability to solve general power system problems.

Let there be a hypothetical 3-bus system as shown in Fig. 2.10. The three buses (A, B, and C) are connected to each other by three transmission lines (1, 2, and 3). Six transient stability simulations were run on this system with the first three resulting in a stable system whereas the remaining three resulting in the system losing stability. The current (real and imaginary) flowing in the three lines for the six cases is as shown in Table 2.1. In the table, the rows denote the event (stable/unstable) while the columns denote the corresponding measurements (real and imaginary currents).

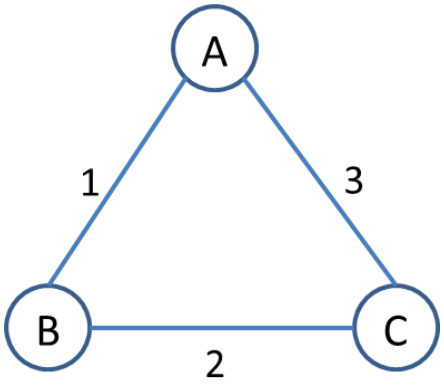

Fig. 2.10: A generic 3-bus system

Table 2.1: Original currents flowing in the lines to be fed as inputs to CART

Data / Event	I_R1	I_I1	I_R2	I_I2	I_R3	I_I3
Stable	3.45	0.46	1.15	0.05	2.65	0.45
Stable	3.40	0.35	1.20	0.02	2.55	0.42
Stable	3.52	0.57	1.11	0.10	2.80	0.46
Unstable	4.00	0.50	1.10	0.15	2.85	0.60
Unstable	3.53	0.30	1.00	0.05	2.60	0.47
Unstable	3.75	0.45	1.05	0.06	2.75	0.50

Since CART can pick only one measurement at a time for performing binary splits, it will choose either the real or the imaginary part of the complex current measurement for performing the split. In agreement with this logic, when the data shown in Table 2.1 was fed into CART, it generated a decision tree as shown in Fig. 2.11. From the figure, it becomes clear that the real current in line 1, the imaginary current in line 3 and the real current in line 2 are needed by the decision tree to make a successful prediction. Correspondingly, it can be inferred that PMUs must be placed on all the three lines. Therefore, three PMUs will be needed for making real-time transient stability predictions for this system. By treating the complex number as a single entity using FLDSD, it will be shown that a better result can be obtained both in terms of accuracy and speed of prediction.

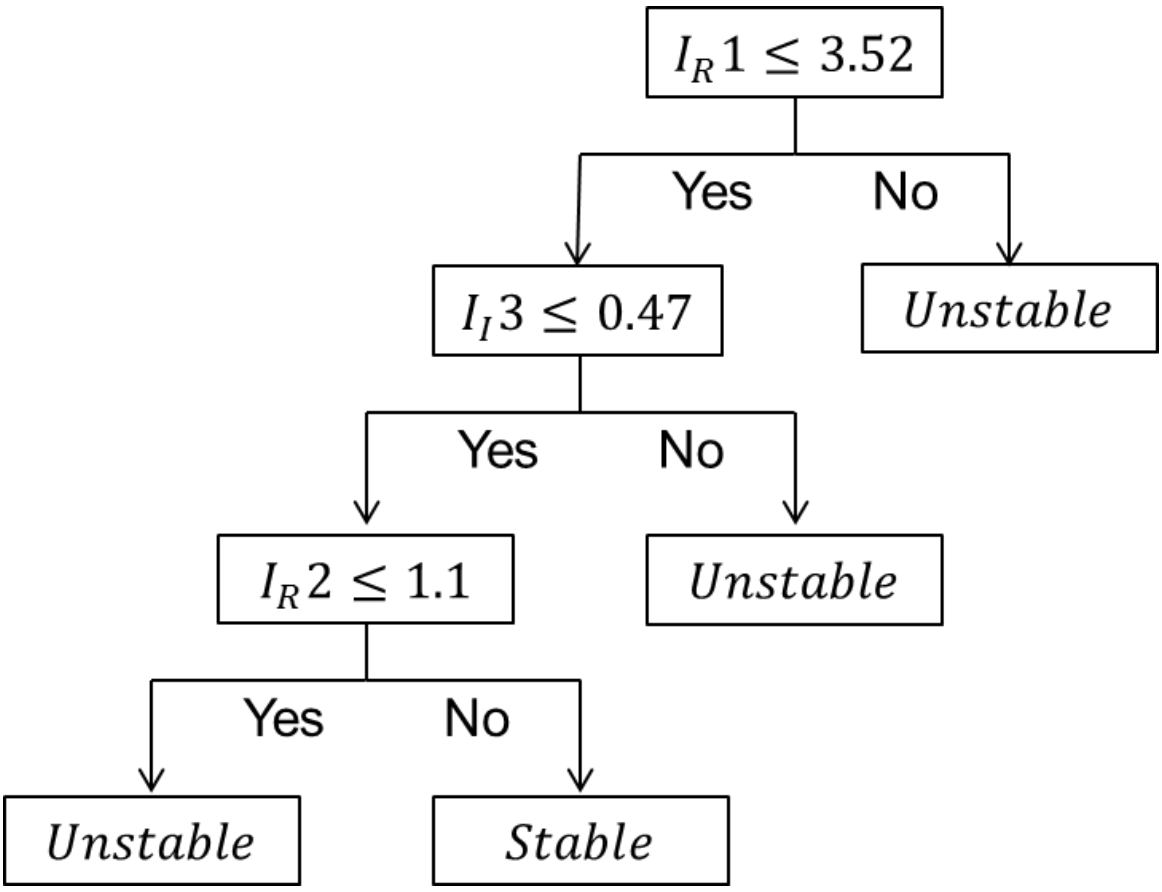

Fig. 2.11: Decision Tree created by CART when the original currents were fed as inputs

According to the proposed algorithm (FLDSD), the complex currents have to be represented by a single entity. In order to do so, the means and covariances of the three currents were initially computed. The mean of the currents for the stable and unstable cases were found as follows:

$$
\begin{aligned}
M_{Line1_{stable}} &= (3.4567, 0.4600) \\
M_{Line1_{unstable}} &= (3.7600, 0.4167) \\
M_{Line2_{stable}} &= (1.1533, 0.0567) \\
M_{Line2_{unstable}} &= (1.0500, 0.0867) \\
M_{Line3_{stable}} &= (2.6667, 0.4433) \\
M_{Line3_{unstable}} &= (2.7333, 0.5233)
\end{aligned} \tag{2.13}
$$

It is to be noted here that in (2.13), the abscissa denotes the real part of the complex current whereas the ordinate denotes the imaginary part. Similarly the covariances of the three currents for the stable and unstable cases were found to be:

$$
\begin{aligned}
\boldsymbol{S_{Line1_{stable}}} &= \begin{bmatrix} 0.0036 & 0.0066 \\ 0.0066 & 0.0121 \end{bmatrix} \\
\boldsymbol{S_{Line1_{unstable}}} &= \begin{bmatrix} 0.0553 & 0.0233 \\ 0.0233 & 0.0108 \end{bmatrix} \\
\boldsymbol{S_{Line2_{stable}}} &= \begin{bmatrix} 0.0020 & -0.0018 \\ -0.0018 & 0.0016 \end{bmatrix} \\
\boldsymbol{S_{Line2_{unstable}}} &= \begin{bmatrix} 0.0025 & 0.0025 \\ 0.0025 & 0.0030 \end{bmatrix} \\
\boldsymbol{S_{Line3_{stable}}} &= \begin{bmatrix} 0.0158 & 0.0024 \\ 0.0024 & 0.0004 \end{bmatrix} \\
\boldsymbol{S_{Line3_{unstable}}} &= \begin{bmatrix} 0.0158 & 0.0078 \\ 0.0078 & 0.0046 \end{bmatrix}
\end{aligned} \tag{2.14}
$$

Then, for the three currents, the equation of the straight line joining the means and passing through the mid-point of the means was computed using the formula:

$$
y - y_{mid_i} = \left(\frac{y_{2_i} - y_{1_i}}{x_{2_i} - x_{1_i}}\right)\left(x - x_{mid_i}\right) ;\ i = 1{:}3 \tag{2.15}
$$

In (2.15), (x_{1_i}, y_{1_i}), and (x_{2_i}, y_{2_i}) are the means for the stable and unstable current values of the i^{th} line, while (x_{mid_i}, y_{mid_i}) were computed as shown below:

$$
\begin{aligned}
x_{mid_i} &= \frac{x_{1_i} + x_{2_i}}{2} \\
y_{mid_i} &= \frac{y_{1_i} + y_{2_i}}{2}
\end{aligned} \tag{2.16}
$$

The three lines obtained as outcomes of (2.15) were rotated by the sum of the covariances of the respective lines; the covariances having been obtained as shown in (2.14). Then, if m_{1_i} denotes the slope of the i^{th} line, then the slope of the hyperplane perpendicular to that line (denoted by m_{2_i}) will be given by,

$$m_{2_i} = -\frac{1}{m_{1_i}} \tag{2.17}$$

Therefore, the equation of the hyperplane for the current distribution of the i^{th} line passing through the point $\left(x_{mid_i}, y_{mid_i}\right)$ and having a slope m_{2_i} will be given by,

$$y - y_{mid_i} = m_{2_i}\left(x - x_{mid_i}\right) \tag{2.18}$$

On computing the distances of the respective data points from their corresponding hyperplane, we get the new splitting variables as seen in Table 2.2. The distance variable D_1 corresponds to the complex currents of the first line, the distance variable D_2 for the second line, and the distance variable D_3 for the third line. When these new variables were fed as inputs to CART, it generated a decision tree as shown in Fig. 2.12.

Table 2.2: Distances to the hyperplanes obtained by applying FLDSD technique

Data / Event	D_1	D_2	D_3
Stable	0.063	-0.049	-0.005
Stable	0.028	-0.102	-0.006
Stable	0.092	0.003	-0.012
Unstable	-0.102	0.029	0.019
Unstable	-0.039	0.079	0.003
Unstable	-0.042	0.040	0.001

By comparing Fig. 2.12 with Fig. 2.11, it can be realized that by using the proposed approach (FLDSD), a smaller decision tree is able to perform the split perfectly. The advantages of a smaller decision tree are numerous. In terms of placement of PMUs, instead of monitoring real current in line 1, imaginary current in line 3, and real current in line 2, we only need to measure the complex currents in lines 1 and 3. Since when a PMU placed on a line automatically measures the real and imaginary currents flowing in that line, for the given system, two PMUs (instead of three as computed previously) are sufficient for making a successful decision regarding transient stability. Therefore, by using the proposed technique, the installation and maintenance cost of one PMU device has been recovered. Furthermore, since the decision tree shown in Fig. 2.12 is smaller than the one shown in Fig. 2.11, in terms of real-time implementation, it is implied that the tree obtained using FLDSD will give results more quickly than the one created without it. Although some amount of "time" will be consumed in computing the distance variable from the measured currents, it is hypothesized that the reduction in "time" occurring due to the

smaller tree size will more than compensate for the “time consumed in pre-processing”. All things considered, it can be implied that the proposed approach is an efficient technique for decision making involving complex synchrophasor data.

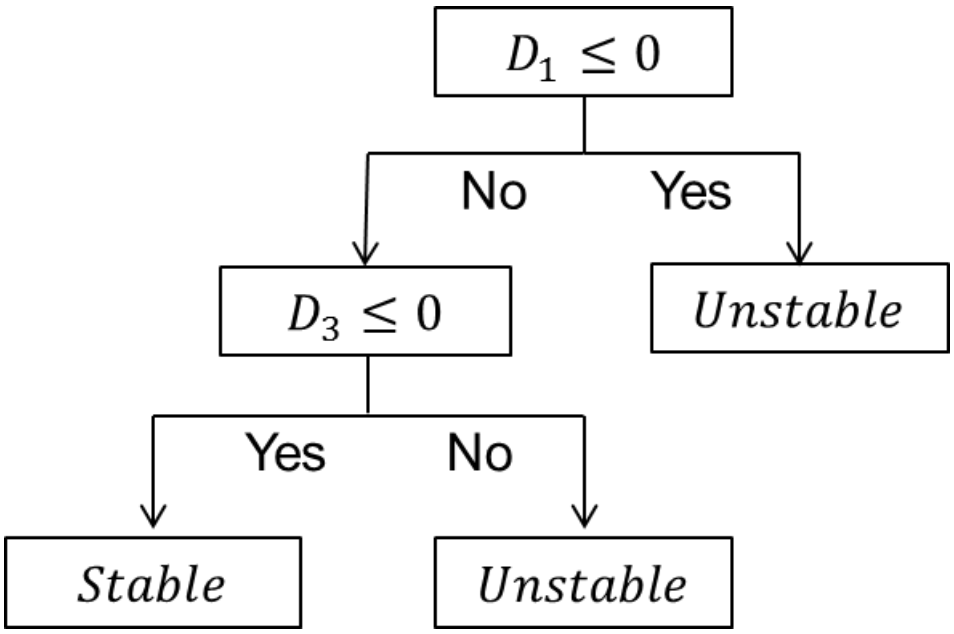

Fig. 2.12: Decision Tree created by CART after incorporating FLDSD

2.6 Conclusion

An algorithm titled “Fisher’s Linear Discriminant applied to Synchrophasor Data” (FLDSD) is developed in this chapter to make decisions involving complex PMU data. When only the real or the imaginary attribute of the phasor is used for making the split, the result is not optimal as the complete phasor is not considered. Others who have tried to solve this problem have done so by rotating the axes along a reference, but that approach does not provide a guarantee for a successful result in all situations. In the proposed algorithm, by using FLD, complex numbers are represented by a single variable which is then used for performing the splits. The simulations performed indicate that the technique developed here is simple, fast, and robust. Its applicability to solve problems occurring in large and complex power system networks is studied in the next chapter.

Chapter 3: Application of FLDSD in Power Systems

With the advent of phasor measurement units (PMUs) in power systems, it is now possible to monitor behavior of the system in real-time. A variety of techniques make use of this real-time PMU data for operational decision making. These techniques include fuzzy-logic based approaches, artificial neural network (ANN) based approaches, support vector machine (SVM) based approaches [55]-[58], etc. However, in recent years, decision trees (DTs) has emerged as the most popular data mining technique in power systems [34]. In the previous chapter, an algorithm was developed that makes decision involving complex synchrophasor data. CART (Classification and regression tree), which is a non-parametric decision tree learning technique, was used in the development of this algorithm. The results indicated that the proposed algorithm (FLDSD) had potential for solving large-scale and complex power system problems. This "indication" is explored in more details in this chapter.

Fisher's Linear Discriminant applied to Synchrophasor Data (FLDSD), illustrated in the previous chapter, showed how the CART algorithm can be used to make decisions while considering measurements having multiple attributes in a single split without needing a reference. Since it is only the inputs to CART which were modified, and not the algorithm on which CART operates, this technique can be readily applied to any engineering problem which involves decision making based on multivariate data. As such, the proposed method is expected to find use in the areas of –

- Adaptive Protection Schemes
- Event Classification
- Real-time power system transient stability/instability predictions
- Development of Islanding schemes
- Online voltage security monitoring
- Online dynamic security assessment
- Response based control using phasor measurements
- Optimal PMU placement, etc.

In this chapter, the proposed methodology is implemented on two systems – a detailed model of the California power system where it is used for developing an adaptive protection scheme, and the IEEE 118-bus system where it is used to classify dynamic events based on trajectories of voltage measurements obtained from PMUs. The MATLAB implementation of CART (classregtree.m) has been used for performing both the analysis. Studies employing the proposed technique for transient stability

predictions [59], [60] and islanding detection and classification [61] have been done. But those studies are not included in the present scope of work.

3.1 An adaptive protection scheme for the California power system

In [12], an algorithm was developed which used CART to categorize a system as “safe” or “stressed” based on data collected from PMUs. Two scenarios of the California power system, heavy winter (HW) and heavy summer (HS) were used for the study. The main goal of that algorithm was to partition the power system state space intelligently in order to develop decision rules to adjust security/dependability balance of relay protection schemes. It was argued that the likelihood of hidden failures and potential cascading events could be significantly reduced by adjusting the security/dependability balance of protection systems to better suit prevailing system conditions. In [12], Emanuel et al. used decision trees to classify the power system state and to predict the optimal security/dependability bias of a critical protection scheme. Using [12] as a case study, classifications based on measurements having two attributes is discussed here.

3.1.1 Security/Dependability based adaptive protection scheme

The adaptive protection scheme that Emanuel et al. proposed works as follows. PMUs placed at critical locations in the network provide information regarding the “state” of the power system. Using that information, the system is classified as “safe” or “stressed”. A “safe” system is biased towards dependability whereas a “stressed” system is biased towards security. As defined by IEEE [62], dependability is “the degree of certainty that a relay or relay system will operate correctly”, i.e., it is a measure of the certainty that the relays will operate correctly for all the faults for which they are designed to operate [63]. On the other hand, security “relates to the degree of certainty that a relay or relay system will not operate incorrectly”. Although, traditionally, protection systems were biased towards dependability, it was demonstrated in [12] that under stressed system conditions, a favorable bias towards security is more beneficial.

As shown in Fig. 3.1, in [12], Emanuel et al. proposed an adaptive voting scheme to alter the security-dependability balance in accordance with the “current” system state. The voting scheme consists of a set of three independent and redundant relays. Based on PMU measurements, if the system state is found to be “safe”, then in the case of a fault, voting is disabled and any of the three relays can trip the line (biased towards dependability). However, if the PMU measurements indicate that the system is in a “stressed” condition, then the voting scheme is enabled and the line will trip only if two or more relays

see the fault (biased towards security). Emanuel et al. also identified the critical locations where the PMUs should be placed (nodes of the decision trees), as well as the attributes that the PMUs should monitor (bus voltage angles and line currents). Figs. 3.2a and 3.2b show the decision trees that they obtained for the HW and HS scenarios, respectively [12], [64].

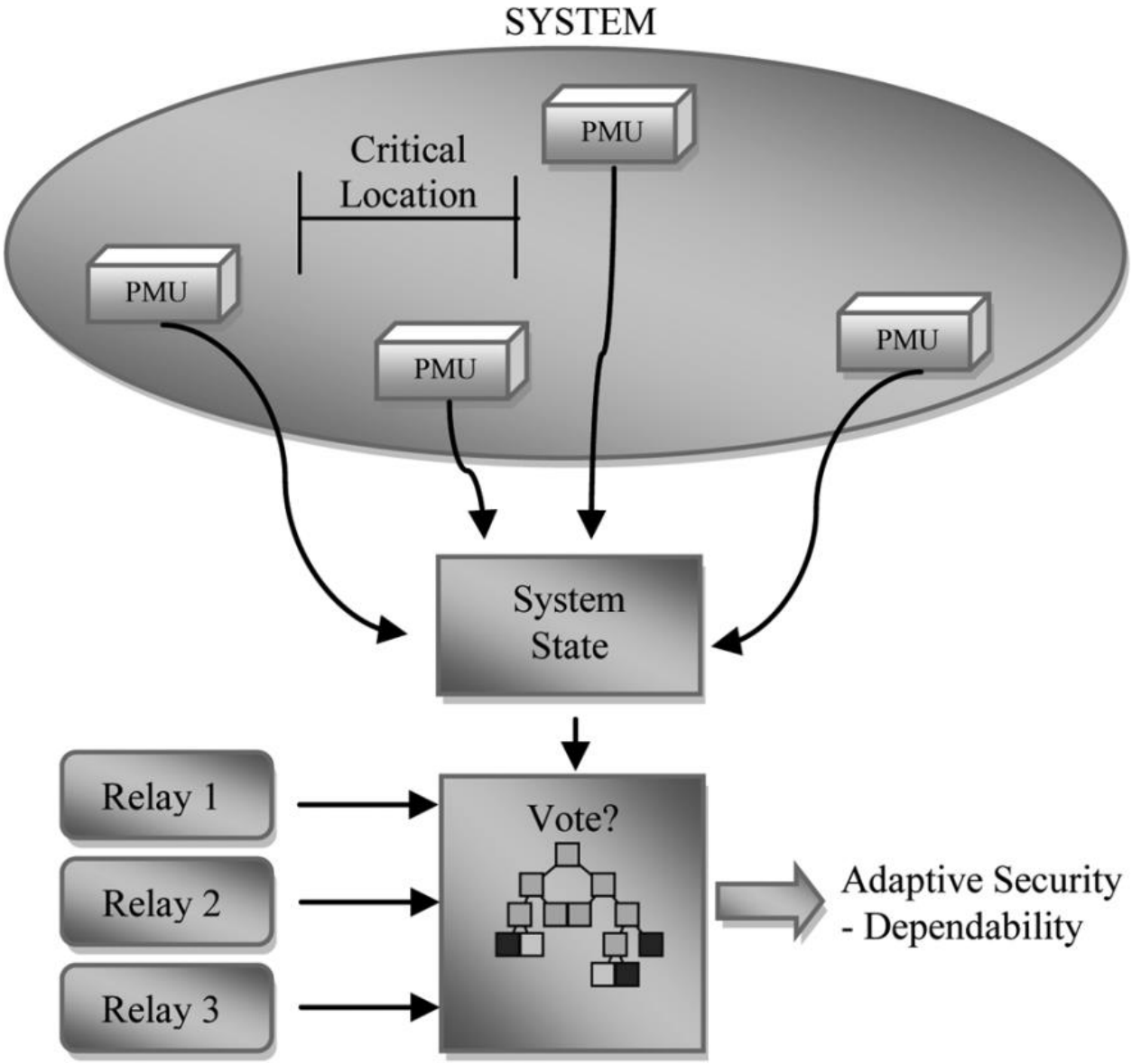

Fig. 3.1: Security/Dependability based adaptive protection scheme

(Courtesy of Dr. Emanuel E. Bernabeu) [64]

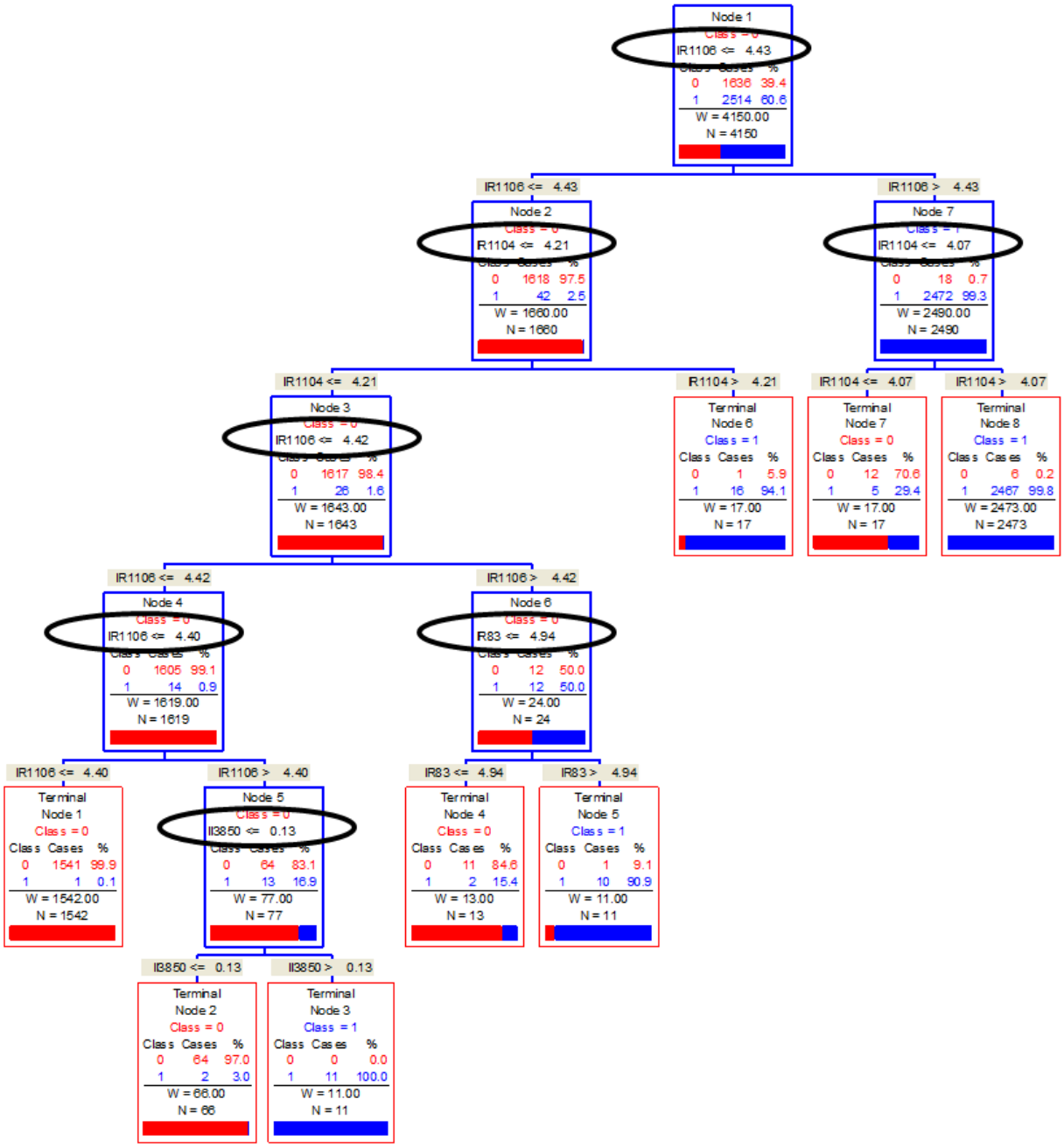

Fig. 3.2a: Decision tree for heavy winter (HW) case as obtained by Emanuel

(Courtesy of Dr. Emanuel E. Bernabeu) [64]

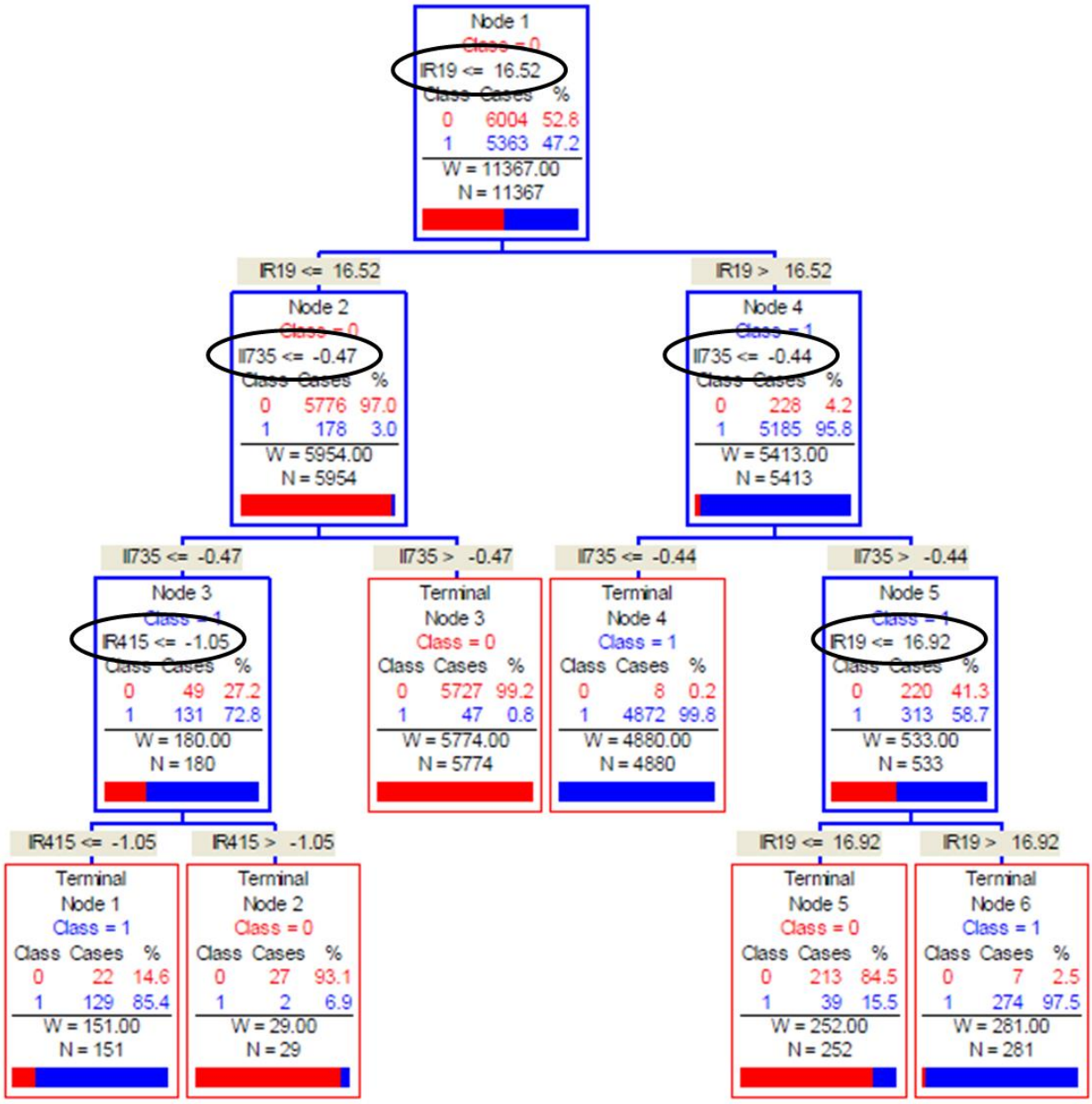

Fig. 3.2b: Decision tree for heavy summer (HS) case as obtained by Emanuel

(Courtesy of Dr. Emanuel E. Bernabeu) [64]

3.1.2 Using FLDSD technique for classifying system state

The adaptive voting scheme developed in [12] required the system to be classified as “safe” or “stressed” based on measurements obtained from PMUs. However, as highlighted in black ovals in Fig. 3.2, in their analysis Emanuel et al. considered the complex quantities separately. The splits in Fig. 3.2 were based on either the real or the imaginary component of the complex currents. Since it was proved

in the previous chapter that such a partitioning does not yield optimal results, their study became a suitable choice for the application of the proposed algorithm. FLDSD technique was applied on both the heavy winter (HW) as well as the heavy summer (HS) scenarios. The total number of training cases in the HW case was 4150, whereas in the HS case it was 11367. The total number of "out-of-sample" cases was 660 for the HW case and 1155 for the HS case.

The data presented to the CART implementation program in MATLAB (classregtree.m) were all the 500kV voltage angles and currents present in the system – a total of 42 voltage angle and 90 complex current measurements. Every 500kV current was measured as a complex number and each complex number was treated as a single entity. Ten-fold cross-validation was done to improve the accuracy of the prediction. In selecting the splitting nodes CART picked the substations where PMUs would be placed. Thus, it was the CART algorithm which chose the nodes that would result in an optimum split as seen in Figs. 3.3 and 3.4. Fig. 3.3 depicts the decision tree obtained for the HW case. An overall accuracy of 99.46% was obtained for this case with $x65, x83$, and $x18$ denoting currents and/or voltage angles of specific lines and buses. Fig. 3.4 depicts the decision tree for the HS case. It had an overall accuracy of 99.38%. The results indicate that PMUs placed on lines and buses selected by the tree can classify the system as "safe" (blue) or "stressed" (reds) with very high accuracy.

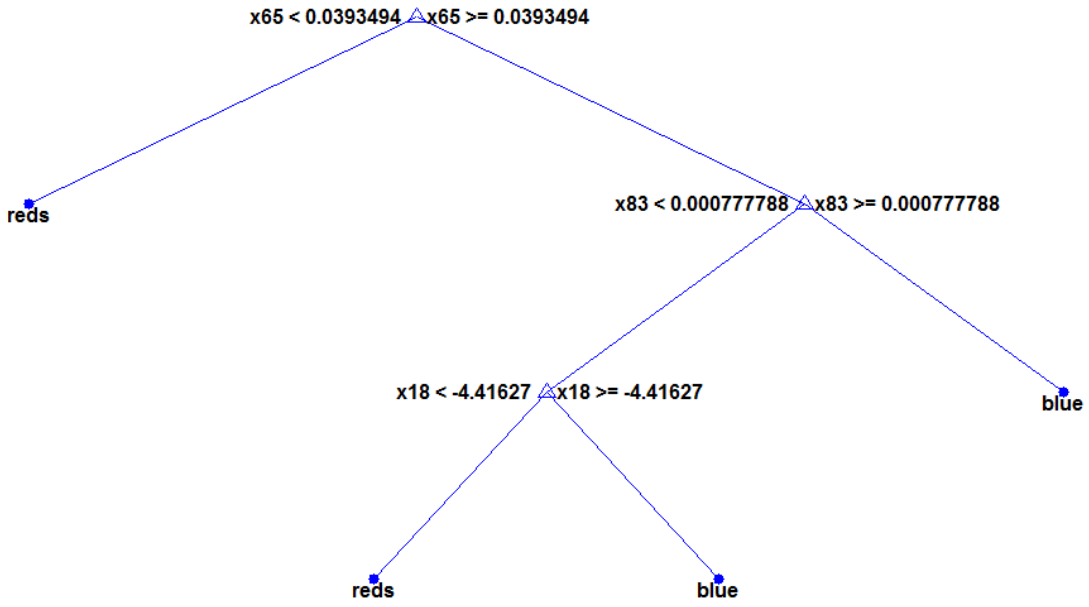

Fig. 3.3: Decision tree for heavy winter (HW) case using FLDSD technique

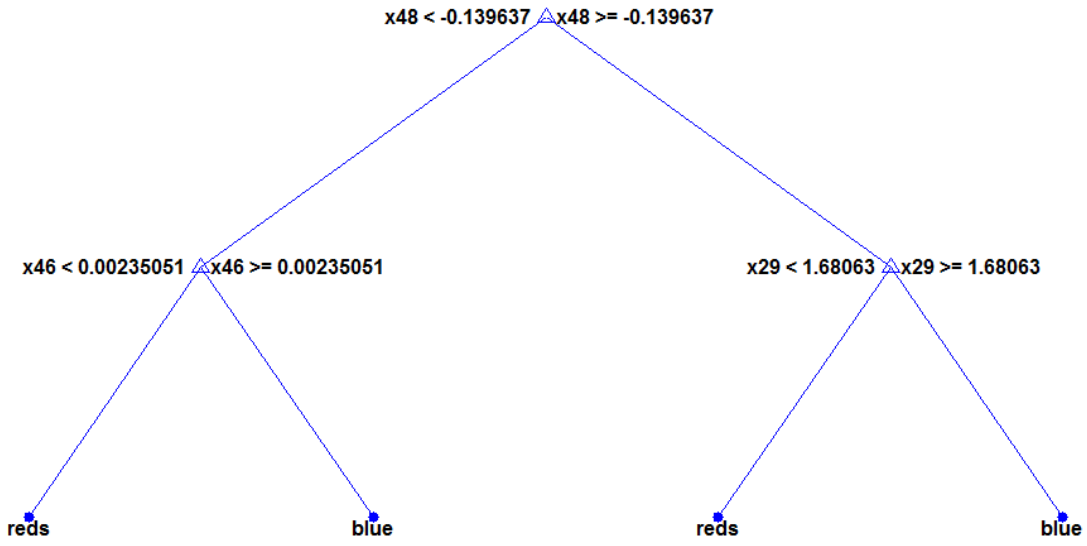

Fig. 3.4: Decision tree for heavy summer (HS) case using FLDSD technique

In Figs. 3.5-3.8, real buses and lines are denoted as Bus X and Line Y respectively, where X and Y are natural numbers. This is done in accordance with the restrictions imposed by FERC: CEII (Federal Energy Regulatory Commission: Critical Energy Infrastructure Information). Fig. 3.5 shows the first splitting node ($x65$) chosen by CART for the HW case. The blue circles denote a "safe" system whereas the red dots denote a "stressed" system. In the actual system, node $x65$ corresponds to the total current flowing in line 1104. Accordingly, Fig. 3.5 shows the plot of the real vs. imaginary current components of line 1104. The plot denoting the distance variable D for this distribution is given in Fig. 3.6. Similarly, Fig. 3.7 shows the first splitting node ($x48$) chosen by CART for the HS case. In the actual system, node $x48$ corresponds to the total current flowing in line 735, whose real and imaginary components are depicted in Fig. 3.7. The corresponding plot of D is shown in Fig. 3.8. From the plots shown in Figs. 3.5 and 3.7 respectively, it becomes clear that a single line parallel to the X-axis or the Y-axis will not be able to provide an optimum split. However, by using the proposed technique, it is observed in Figs. 3.6 and 3.8 respectively that the new distance variable D is able to easily differentiate between the two classes.

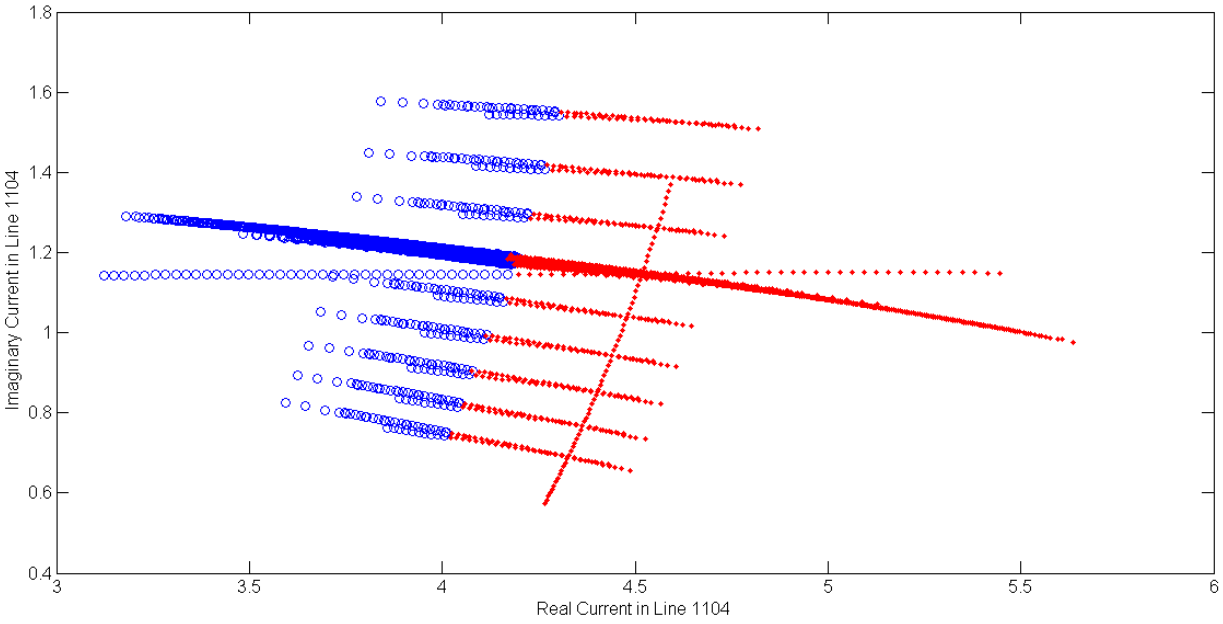

Fig. 3.5: First splitting node for heavy winter (HW) case

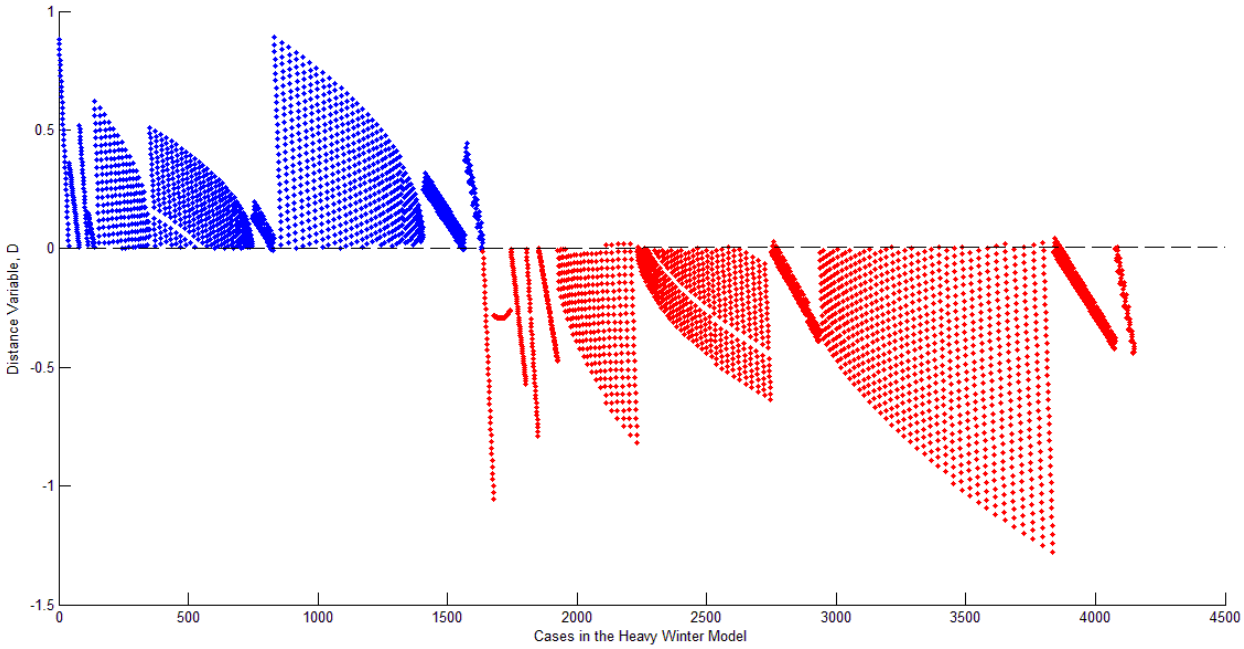

Fig. 3.6: Distance D for the first splitting node of the heavy winter (HW) case

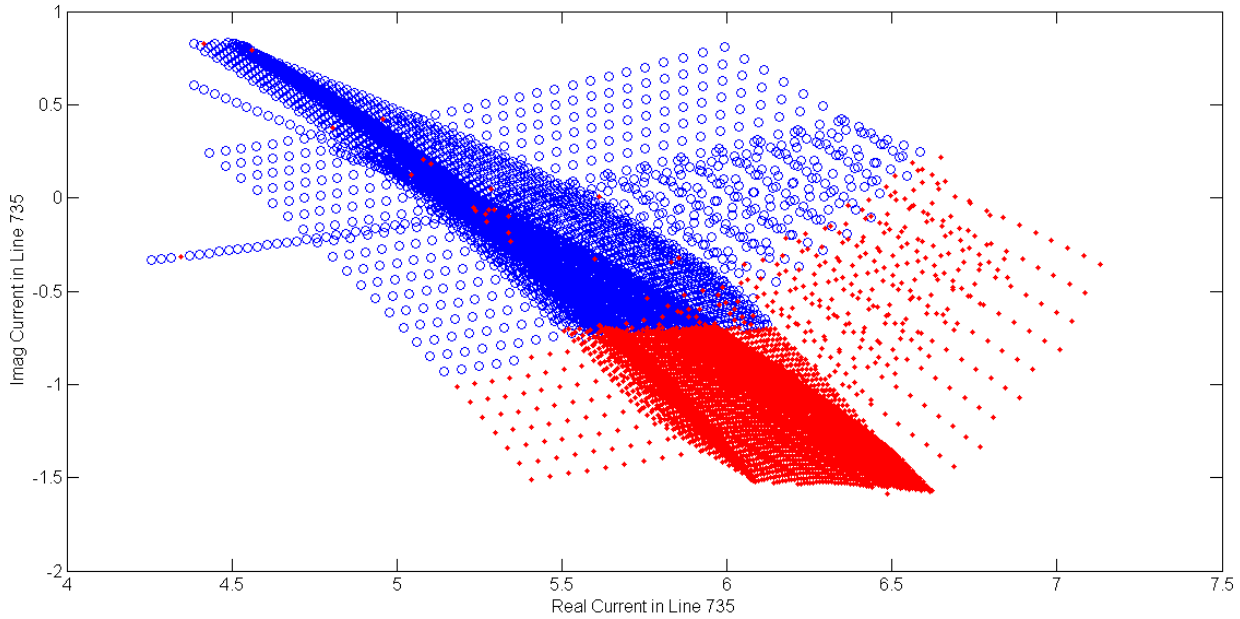

Fig. 3.7: First splitting node for heavy summer (HS) case

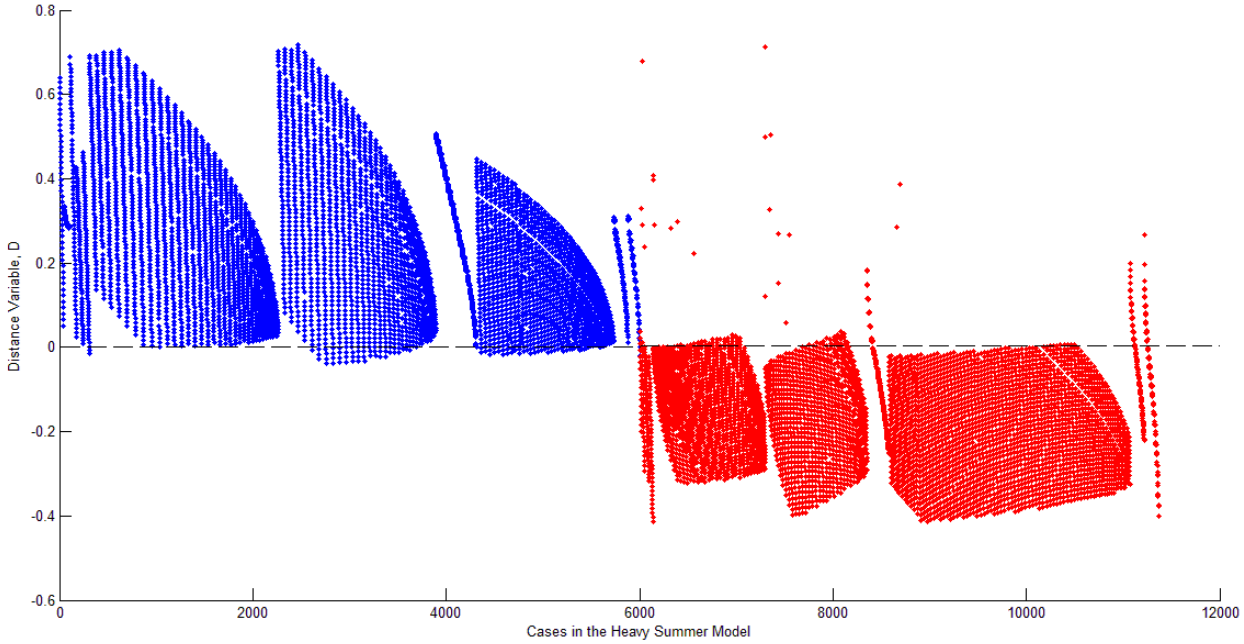

Fig. 3.8: Distance D for the first splitting node of the heavy summer (HS) case

Table 3.1 compares the results obtained here with those obtained in [12]. From the table, it is realized that by using FLDSD, a smaller tree (faster decision with lesser number of PMUs) is able to provide

higher classification accuracy. Table 3.2 compares the performance of the decision trees obtained using this technique with that obtained by rotating along a reference as was done in [50]. From Tables 3.1 and 3.2, it becomes clear that the proposed methodology is more accurate in making decisions involving complex synchrophasor data. There are applications where only the voltage angle, for example, is relevant for making decisions. However, relaying in particular deals with complex quantities and the technique developed here is necessary for making an optimal split. Simulation cases developed in [12] were used here because it provided a real system that was big enough to test the robustness of this technique. In this analysis, FLDSD was used to perform splits on high-dimensional, two-class data. In the next example, application of this technique to high-dimensional, multi-class data is illustrated.

Table 3.1: Comparing size of decision trees (for training purposes)

Scenario	Using algorithm developed in [12]		Using Proposed Algorithm	
	Number of Nodes	Misclassification Rate (%)	Number of Nodes	Misclassification Rate (%)
Heavy Winter	6	1.00	3	0.14
Heavy Summer	6	1.00	3	0.20

Table 3.2: Comparing overall (training and testing) performance of decision trees

Scenario	Number of Cases	Using a Reference for Rotation [50]		Using Proposed Algorithm	
		Number of Errors	Accuracy (%)	Number of Errors	Accuracy (%)
Heavy Winter	4810	48	99.00	*26*	99.46
Heavy Summer	12522	172	98.63	78	99.38

3.2 Dynamic power system state estimation using synchrophasor measurements

One of the conclusions of the report on the 1965 Northeast blackout was that, at that point, power system operators had insufficient information about the system they were controlling. State estimation and the modern EMS were created to deal with these problems. The state of the power system is the collection of all of the complex bus voltages. The calculation of the state in conventional estimators involved iteratively solving large numbers of nonlinear equations. The computational complexity

combined with the data scan across the system made the process slow and new estimates could only be obtained every few minutes [65], [66]. The result was that the picture that was provided to the operators about the state of their system was delayed both in time as well as in space. Faster computers and improved communication have reduced minutes to seconds over the decades but even with a 4 sec. interval the static assumption is still a poor approximation.

From the beginning of synchronized phasor measurements it was clear that PMU measurements would be an important addition to state estimation. Today, many commercial state estimators have PMU inputs. However, since these mixed estimators still "poll" SCADA measurements, they are non-linear and iterative [67]. A three phase PMU only estimator has already been developed for Dominion Virginia Power's (DVP's) 500kV network. This linear state estimator updates every 1/30 of a second. Only complex voltages are measured and time tagged (IEEE C37.118), and so the calculation is the solution of a set of over-defined (more measurements than states) linear equations. Moreover, no iterations are involved. Assuming the system topology remains unchanged, the column of time-tagged data is multiplied by a pre-computed matrix to compute the estimate of the states. A topology processor developed as part of the estimator accounts for system changes. Time tagged breaker statuses and measured voltages sense changes in network topology and the pre-computed matrix is altered accordingly [28].

This linear estimator being built for Dominion's 500kV network is the world's first three-phase PMU-only state estimator. Since the events captured by this estimator will have never been seen previously (relaying action, remote backup, transient swings, etc.), there is an imminent need to understand its outputs. Similar to a conventional estimator, the PMU-only state estimator not only detects bad/missing data, but also identifies the exogenous events that it has captured. Detection of discrepancies in the data is done through an Auto-Regressive (AR) model [27] that is described in sub-section 3.2.1, while the identification of dynamic events is done using the FLDSD technique which is illustrated in sub-section 3.2.2.

3.2.1 Dynamic state prediction based on an Auto-Regressive (AR) model

The idea of a three phase linear state estimator using only synchrophasor data that is being implemented in DVP's 500kV network was originally proposed in [28]. However, this model of the state estimator was not a *tracking* state estimator as it considered each new frame as a separate problem. Therefore, it was impossible to detect/identify bad data using that model. The idea of tracking the state

of the power system is not new. Even before the introduction of phasor measurements, a Kalman filter like process for tracking the system state was suggested in [68]. The difficulty then and now is that the number of measurements is inadequate to produce a successful estimate. Dominion has approximately 4,000 buses but only about 30 EHV (500kV) buses. As such, the Kalman filter based technique would need to solve a state equation based on all the states of the 4000 bus network which would not be a practical approach. Since it is believed that in the foreseeable future PMUs will only be placed at the high voltage and extra-high voltage buses of the network, there is a need to develop a mechanism to predict the next measurement for this small section of buses using their previous measurements. A method to do so was developed in [27] and is briefly summarized below.

Auto-Regressive (AR) modeling [69] is a time-series analysis widely applied to forecasting areas, such as signal processing, state estimation, control, pattern recognition, etc. A general AR model of the order m is denoted by $AR(m)$ and is defined in 3.1.

$$y_t = \alpha_1 y_{t-1} + \alpha_2 y_{t-2} + \cdots + \alpha_m y_{t-m} + \omega_t, \qquad t = m+1, \ldots, n \tag{3.1}$$

In (3.1), $y_1, y_2, \ldots, y_n$ are the time-series data, m is the order of the AR model, $\alpha_1, \alpha_2, \ldots, \alpha_m$ are the corresponding coefficients of the AR model, and ω_t is white noise. When the load is increased linearly at constant power factor, the behavior of the power system can be illustrated as shown in Fig. 3.9.

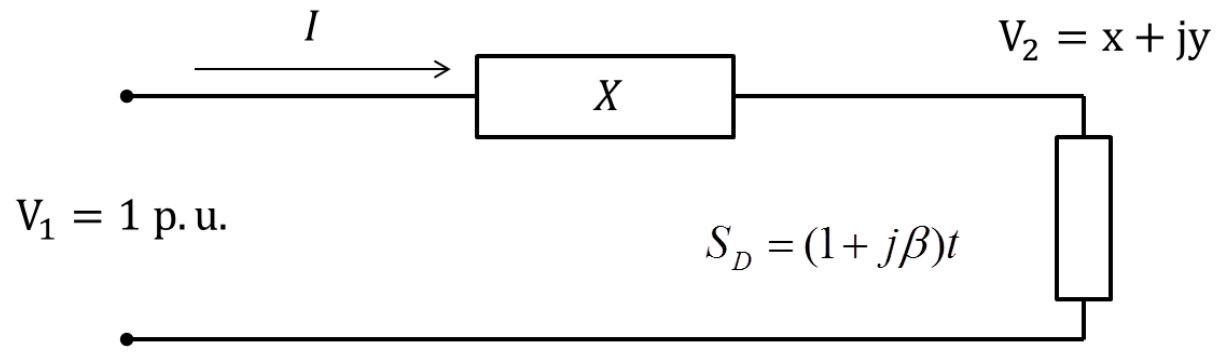

Fig. 3.9: One-line diagram of a model power system

In Fig. 3.9, X is the transmission line reactance, and $\boldsymbol{S_D}$ is the load increased linearly with time t at constant power factor. Now, $\boldsymbol{S_D}$ is also given by,

$$\boldsymbol{S_D} = \boldsymbol{V_2 I^*} \tag{3.2}$$

From Fig. 3.8 and (3.2), we have,

$$(x+jy)\left(\frac{1-x+jy}{-jX}\right)=(1+j\beta)t \tag{3.3}$$

Equating real and imaginary components of (3.3), we get (3.4) and (3.5),

$$x^2-x+X^2t^2+X\beta t=0 \tag{3.4}$$

$$y=-Xt \tag{3.5}$$

In (3.4) and (3.5), X and β are constant real numbers. The solution of (3.4) is,

$$x=\frac{1\pm\sqrt[2]{1-4X^2t^2-4X\beta t}}{2} \tag{3.6}$$

On writing a Taylor series expansion for (3.6) it is realized that for the linear load increase, the voltages follow an approximately quadratic trajectory as shown in (3.7), where a_k, b_k, c_k are complex numbers. If more precision is needed the order of the polynomial can be further increased.

$$v_k(t)=a_k+b_kt+c_kt^2 \tag{3.7}$$

Equation (3.7) is a polynomial of degree $m-1$ as seen in (3.8a), and which can be interpolated [70] and expressed in the form shown in (3.8b).

$$y(t)=\ a_{m-1}t^{m-1}+a_{m-2}t^{m-2}+a_{m-3}t^{m-3}+\ \ldots+a_1t+a_0 \tag{3.8a}$$

$$\begin{bmatrix} y(1)\\ y(2)\\ \vdots\\ y(m-1)\\ y(m)\end{bmatrix}=\begin{bmatrix}1 & 1 & 1^2 & \ldots & 1^{m-1}\\ 1 & 2 & 2^2 & \ldots & 2^{m-1}\\ 1 & \vdots & \vdots & \ddots & \vdots\\ 1 & (m-1) & (m-1)^2 & \ldots & (m-1)^{m-1}\\ 1 & m & m^2 & \ldots & m^{m-1}\end{bmatrix}\begin{bmatrix} a_0\\ a_1\\ \vdots\\ a_{m-1}\\ a_m\end{bmatrix} \tag{3.8b}$$

In (3.8a) and (3.8b), $a_0, a_1, \ldots, a_{m-1}$ are constant coefficients. Equation (3.8b) can be re-written as

$$y=Va \tag{3.9}$$

In (3.9), V is the well-known Vandermonde matrix [71]. Now, if $b=[b_1 \quad b_2 \quad \ldots \quad b_{m-1} \quad b_m]$ denotes the first row of V^{-1}, then on pre-multiplying both sides of $y=Va$ with b, we get (3.10a) in which $y(0)$ equals a_0, in accordance with (3.8a).

$$b_1y(1)+b_2y(2)+\cdots+b_{m-1}y(m-1)+b_my(m)=y(0) \tag{3.10a}$$

Finally (3.10a) can be rearranged and written as (3.10b).

$$y(m) = -\frac{b_{m-1}}{b_m}y(m-1) - \frac{b_{m-2}}{b_m}y(m-2) - \cdots - \frac{b_1}{b_m}y(1) + y(0) \qquad (3.10b)$$

Pascal's triangle [72] is a two-dimensional triangular array representing the coefficients of the binomial expansion, $(x+y)^n$ where n varies from zero to positive-infinity. Pascal's triangle shown in Fig. 3.10 actually indicates the magnitudes of the coefficients of the AR model that is obtained from the inversion of the Vandermonde matrix.

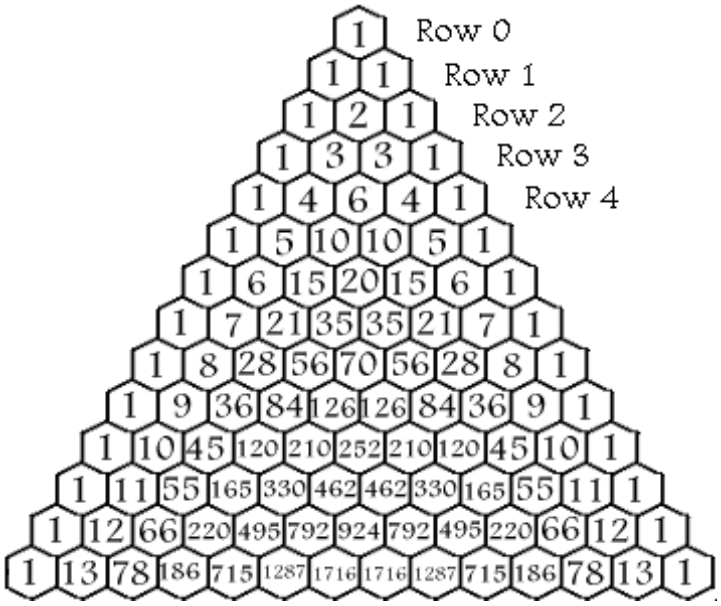

Fig. 3.10: Pascal's Triangle

Since for a linear increase in load, the voltages follow a quadratic trajectory, corresponding to the third row of the Pascal's triangle. Thus, the quadratic AR model for predicting the next set of voltage measurements will be based on three prior estimates as shown in (3.11), where $y(n), y(n-1), y(n-2), y(n-3)$ are complex bus voltages.

$$y(n) = 3y(n-1) - 3y(n-2) + y(n-3) \qquad (3.11)$$

Now, when this logic is integrated with the fact that the measurements will be made at a very high speed (for example, 30 times a second), the limitation of the applicability of (3.11) on only quadratic trajectories can be removed. The reason for this is that the data taken at such high speeds will satisfy the locally quadratic behaviors even without the assumption that the load is changing linearly. This is because in the extremely small time increment, the load is seen as linear because the system loads do not change that quickly. Equation (3.11) can be expressed in the Kalman filter notation as,

$$\hat{y}(k+1|k) = 3\hat{y}(k|k) - 3\hat{y}(k-1|k-1) + \hat{y}(k-2|k-2) \quad (3.12)$$

In (3.12), $\hat{y}$ (read as y-hat) denotes the estimated value of the state y, while the symbol | is the "given" operator. Thus, $\hat{y}(k|j)$ reads as y-hat of k given j and is the expected value of $y(k)$ given that $y(j)$ is known. The discovery of this "quadratic" dependence of the estimate of the future state on the estimates of the three previous states gives one the ability to detect data inconsistencies. By using the three prior estimates of a particular measurement, its future measurement can be predicted. Next, by comparing this estimate with the actual measurement, an observation residual can be computed. Finally, by comparing the observation residual with a pre-defined threshold, discrepancies in the incoming data can be detected. More details about this prediction model can be found in [27].

3.2.2 Classification of dynamic events based on voltage measurements obtained from PMUs

In the previous sub-section, a quadratic model was developed to predict the next measurement and thereby detect anomalies in the data. However, the quadratic model is not able to identify the event that has caused the anomaly. The FLDSD technique developed in the previous chapter appears to alleviate this concern. By treating trajectories of complex voltages as a single entity, classification of dynamic events is illustrated as follows. Since FERC: CEII regulations makes it difficult to do thesis work and publish results on real systems, the IEEE 118-bus system is used here as the test system. This system was chosen amongst others because it was similar in structure to the DVP system. The IEEE 118 bus system [73] is shown in Fig. 3.11 with its 345kV network highlighted in red. The system has 118 buses, 186 branches, and 11 345kV buses. In order to make the analysis more realistic, it is assumed that PMUs are installed on the eleven 345kV buses, and voltage magnitude and angle measurements are obtained at 30 times a second. By doing so, a direct comparison of the results obtained from the two systems (IEEE 118-bus system and DVP system) can be made.

The typical output of the PMU only state estimator for the IEEE 118-bus system for a dynamic event (a three-phase fault on line 26-30 followed by an unsuccessful high speed reclose) is shown in Fig. 3.12. The figure shows the trajectories of the eleven complex voltages (positive sequence), for one second. The display has been split into four windows for clarity. From Fig. 3.12 it can be realized that unless a label is provided to the plots that the estimator generates, it will be very difficult to identify, just by looking at the plots, the event that has occurred. The FLDSD algorithm provides a solution to this problem by treating the trajectory of complex numbers as a single attribute which is then used for classifying different dynamic events.

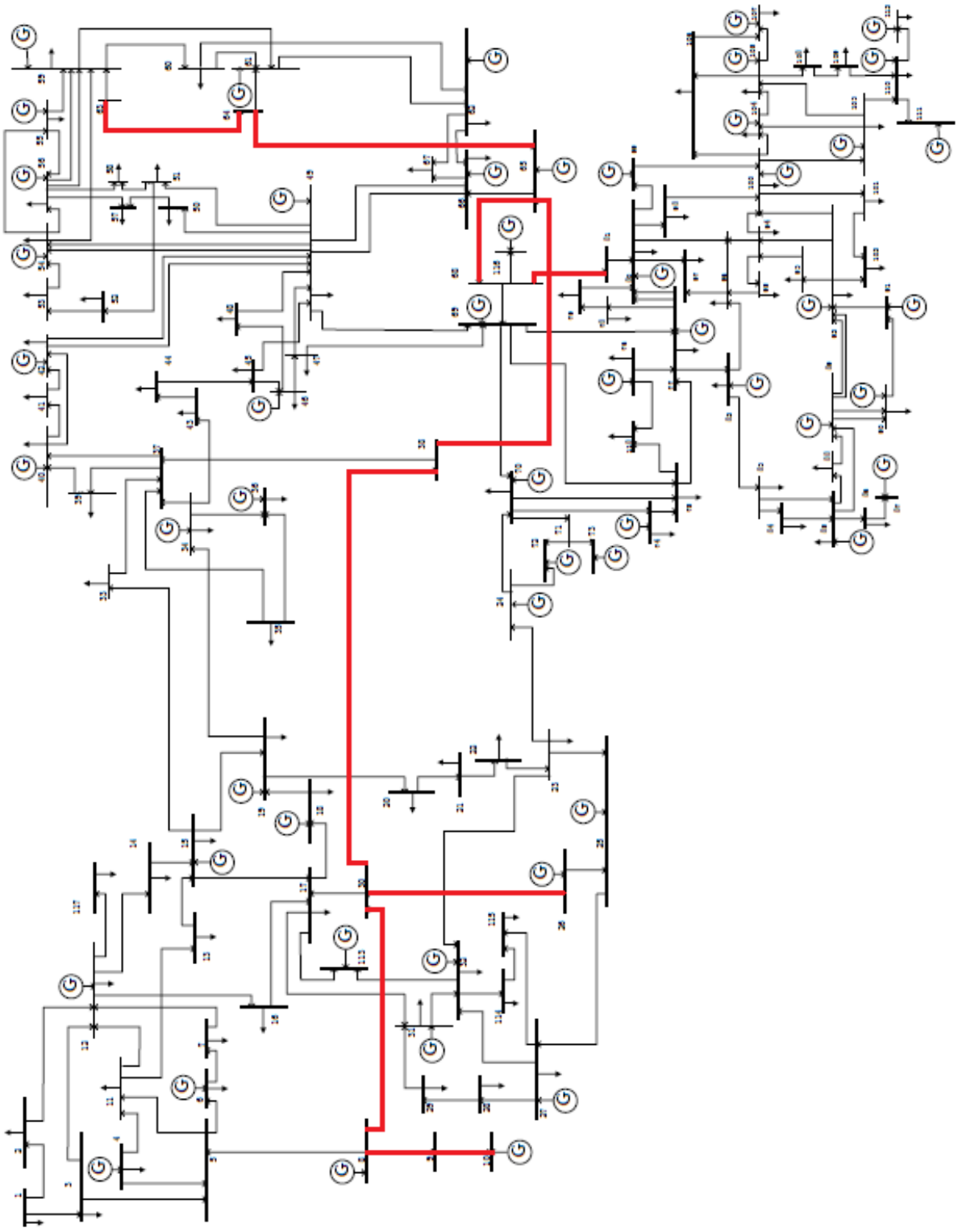

Fig. 3.11: IEEE 118-bus system with 345 kV lines highlighted in red

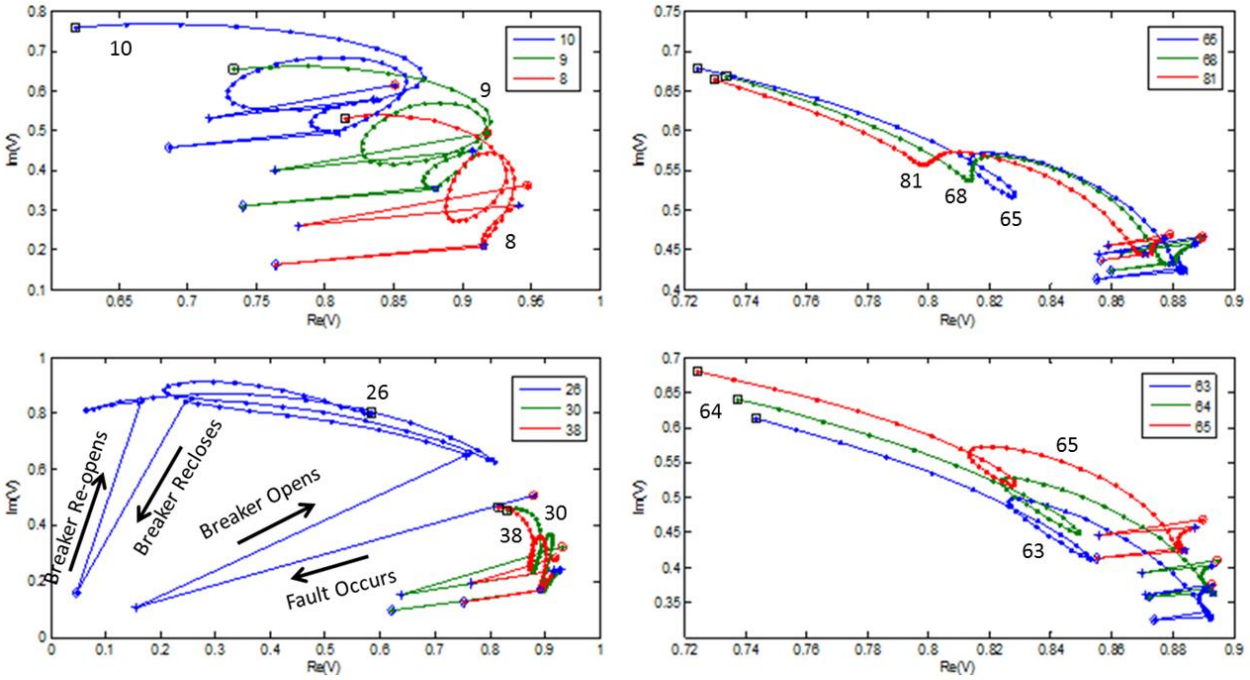

Fig. 3.12: Typical 345 kV bus voltage trajectories of IEEE 118-bus system after a fault

The primary difference between the simulations done in this example in comparison to the one analyzed previously (adaptive protection scheme) with respect to the application of the FLDSD technique, lies in the dimension of the data that is being handled as well as the number of classes in which the partitioning is being done. For the California power system, although the system was fairly large and complex, the analysis was relatively simple. The system had to be classified into two states ("safe" or "stressed") by analyzing voltage angles and complex currents for different system conditions. Hence, it was a two-class classification (safe or stressed) of three-dimensional data (one dimension for the voltage angle, one for the real component of current, and one for the imaginary component of current). However, in this example, where classification of dynamic events is done on the basis of voltage trajectories, the dimension of the data and the number of class partitions depend on the topology of the network. Hence, for this case, although the system is relatively simple (IEEE 118-bus system), the analysis is fairly complex and therefore, should be explored in greater detail.

3.2.2.1 Topology dependent dimension of the data

Depending on the topology of the network, for a one second complex voltage trajectory at a data rate of 30 samples per second, the dimension of the data can be computed as shown in Fig. 3.13. Fig. 3.13 is partitioned into four segments. In all four segments,

- The line marked in “red” (between bus 1 and 2) is the line-under-focus
- The high-voltage buses (where PMUs are assumed to have been placed) are filled in blue, whereas the low-voltage/other buses are left unfilled
- The lines joining two high-voltage buses are solid, whereas the line joining a high-voltage bus to a low-voltage bus are dashed

In segment (a), bus 1 is at the terminal end of a radial line. Since the line-under-focus (1-2) is only connected to bus 3 on bus 2 side, and as all three buses are high-voltage buses, buses 1, 2 and 3 are the buses to be considered for event classification. Now, for a data rate of 30 samples per second, a one-second trajectory would have 30 complex voltage measurements. Then, since every complex voltage measurement consists of two components, the dimension of the data for an individual bus is $30 \times 2 = 60$. Thus, for segment (a), the dimension of the data will be $60 \times 3 = 180$.

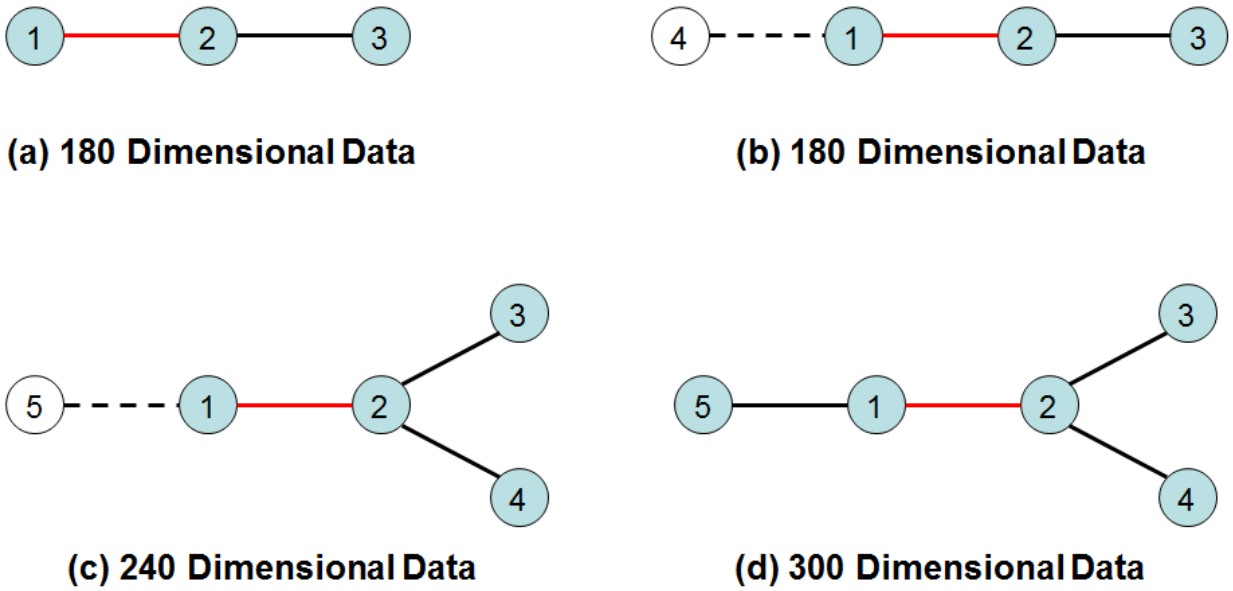

Fig. 3.13: Topology dependent dimension of the data

In segment (b), bus 1 is connected to a low-voltage bus (bus 4), whereas bus 2 is connected to a high-voltage bus (bus 3). In this case also, since there are only three high-voltage buses in the vicinity of the line-under-focus (1-2), the dimension of the data will be $60 \times 3 = 180$. The reason why bus 4 was not considered for analysis is that although it is connected to a high-voltage bus (bus 1), no PMUs are placed on bus 4 and so, complex voltage measurements at 30 times a second from bus 4 would not be available. Segment (c) is similar to segment (b), except that bus 2 is connected to two high-voltage buses

(bus 3 and bus 4) whereas bus 1 is connected to one low-voltage bus (bus 5). In this case, since there are four high-voltage buses in the vicinity of the line-under-focus (1-2), the dimension of the data will be $60 \times 4 = 240$. In segment (d), both bus 1 and bus 2 are connected to high-voltage buses (via bus 5, and bus 3 and bus 4, respectively) and so the dimension of the data will be $60 \times 5 = 300$. On the basis of this analysis, the formula to be used for computing the dimension of the data for any network topology is given in (3.13).

$$Dimension\ of\ Data\ =\ N_{HV} \times (2n) \tag{3.13}$$

In (3.13), N_{HV} denotes the number of high-voltage buses that are one bus away from the terminal buses of the line-under-focus, and n is the data rate which is equal to 30. It should be noted here that (3.13) implies that if the data rate is changed from 30 samples per second to (say,) 60 samples per second, then the only difference that will occur will be that the dimension of the data will be doubled.

3.2.2.2 Topology dependent classification of the data

The dynamic events used for classification were single line-to-ground (SLG) fault, three phase-to-ground (TPG) fault and Zone II operation. The possible classes under line-to-ground faults and three phase-to-ground faults are no-reclose (NR), successful high speed reclose (SHSR), and unsuccessful high speed reclose (USHSR). Zone II operation with an over-reach of up to 150% is assumed to occur because of a stuck breaker following a single sine-to-ground fault or a three phase-to-ground fault. As such, the possible classes under Zone II operation are single line-to-ground-Zone II (SLGZ2) and three phase-to-ground-Zone II (TPGZ2). On the basis of the dynamic events that are selected for classification and using the topology of the network, the number of classes in which the data is to be partitioned is analyzed next.

Similar to Fig. 3.13 which depicted the topology dependent dimensions of the data, Fig. 3.14 shows the topology dependent classifications of the data. In segment (a), since the line-under-focus (1-2) is only connected to bus 3 on bus 2 side, a Zone II operation for this topology is not meaningful. The reason for this being that the system will separate the instant a Zone II operation occurs and the voltages would drop down to zero. Therefore, for the topology shown in segment (a), there can be single line-to-ground with no-reclose (SLGNR), single line-to-ground with successful high speed reclose (SLGSHSR), single line-to-ground with unsuccessful high speed reclose (SLGUSHSR), three phase-to-ground with no-reclose (TPGNR), three phase-to-ground with successful high speed reclose (TPGSHSR), and three phase-to-ground with unsuccessful high speed reclose (TPGUSHSR) resulting in a 6-class classification.

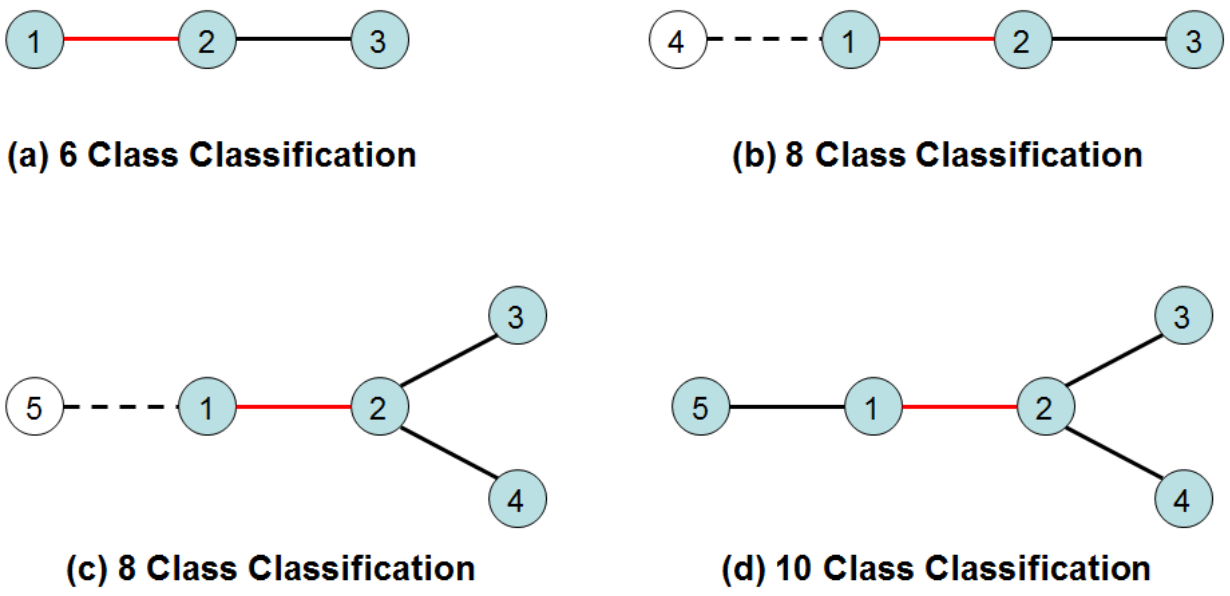

Fig. 3.14: Topology dependent classification of the data

In segment (b), contrary to segment (a), when a Zone II operation takes place, the system does not separate. However, since bus 1 is connected to a low voltage bus (bus 4), Zone II operation on 50% of line 1-4 is not detectable. Hence, Zone II operation is only possible on the bus 2 side (which is connected to a high voltage bus – bus 3). Therefore, for this topology, along with the three types of single line-to-ground and three phase-to-ground faults, two types of Zone II operations are also possible – single line-to-ground-Zone II at bus 2 end (SLGZ2_2) and three phase-to-ground-Zone II at bus 2 end (TPGZ2_2) resulting in an 8-class classification. Similar to segment (b), in segment (c) also, Zone II operation is only detectable on bus 2 side and so, for the topology described in segment (c), an 8-class classification of the data will take place.

For the topology shown in segment (d), Zone II operation is detectable on both bus 1 as well as bus 2 side. Hence for this segment the number of classifications of the data will be: single line-to-ground with no-reclose (SLGNR), single line-to-ground with successful high speed reclose (SLGSHSR), single line-to-ground with unsuccessful high speed reclose (SLGUSHSR), three phase-to-ground with no-reclose (TPGNR), three phase-to-ground with successful high speed reclose (TPGSHSR), three phase-to-ground with unsuccessful high speed reclose (TPGUSHSR), single line-to-ground-Zone II at bus 1 end (SLGZ2_1), three phase-to-ground-zone II at bus 1 end (TPGZ2_1), single line-to-ground-Zone II at bus 2 end (SLGZ2_2), and three phase-to-ground-Zone II at bus 2 end (TPGZ2_2). Thus, for segment (d), the number of classifications in which the data can be partitioned is 10.

3.2.2.3 Simulation set-up and Results

DSA Tools® [74] was used for generating the data to train the trees. Since there were ten 345kV lines present in the IEEE 118-bus system, ten parallel decision trees were created (one tree for each line), with the time-tagged breaker statuses used to identify the relevant tree in the case of an event. For line-to-ground faults and three-phase-to-ground faults, 270 cases were created for all the ten lines. The number of cases for Zone II operation varied from line to line (depending on how the line-under-test was connected to the rest of the system). A total of 6674 cases were created. Taking 345kV line between buses 38 and 65 as an example, the complex voltages (real and imaginary) of the two buses were obtained for different classes. Since both buses 38 and 65 were connected to other 345kV buses, Zone II operation could be detected on either end. A total of 722 cases were identified for this line which fell under 10 classes – three classes for line-to-ground fault, three classes for three phase-to-ground fault, two classes for Zone II operation on bus 38 end, and two classes for Zone II operation on bus 65 end. A second's worth of data starting from the time of the fault was used for classification purposes. This resulted in a 10-class classification of 300-dimensional data for each of the 722 cases. The dimension of the data is based upon 30 complex (real and imaginary) voltages for five 345kV buses – 38, 65, 30 (which is connected to 38), 64 and 68 (which are connected to 65).

The proposed algorithm was applied to this data to calculate the distances to the 45 $\left(=\frac{10\times(10-1)}{2}\right)$ possible hyperplanes. These distances were fed into the CART implementation program in MATLAB (classregtree.m) for selecting the optimal distance variables for performing the splits. Ten-fold cross-validation was done to improve the accuracy of the prediction. The resulting decision tree is shown in Fig. 3.15, where "$di-j$" denotes the distance of the individual points from the hyperplane separating classes i and j. From the figure, it is observed that for line 38-65, CART chose the distances $d1-2, d1-3, d2-8, and\ d9-10$ as the optimal variables for performing the splits. Given an actual event, the distances from each data point to the five hyper-planes need to be computed and the tree followed to the respective terminal node to identify the event that has been captured. Fig. 3.16 shows the percentage accuracy plot as a function of the cost vs. tree size for line 38-65. From this figure it becomes clear that with ten terminal nodes 100% accuracy (0% Cost) was realized for this line.

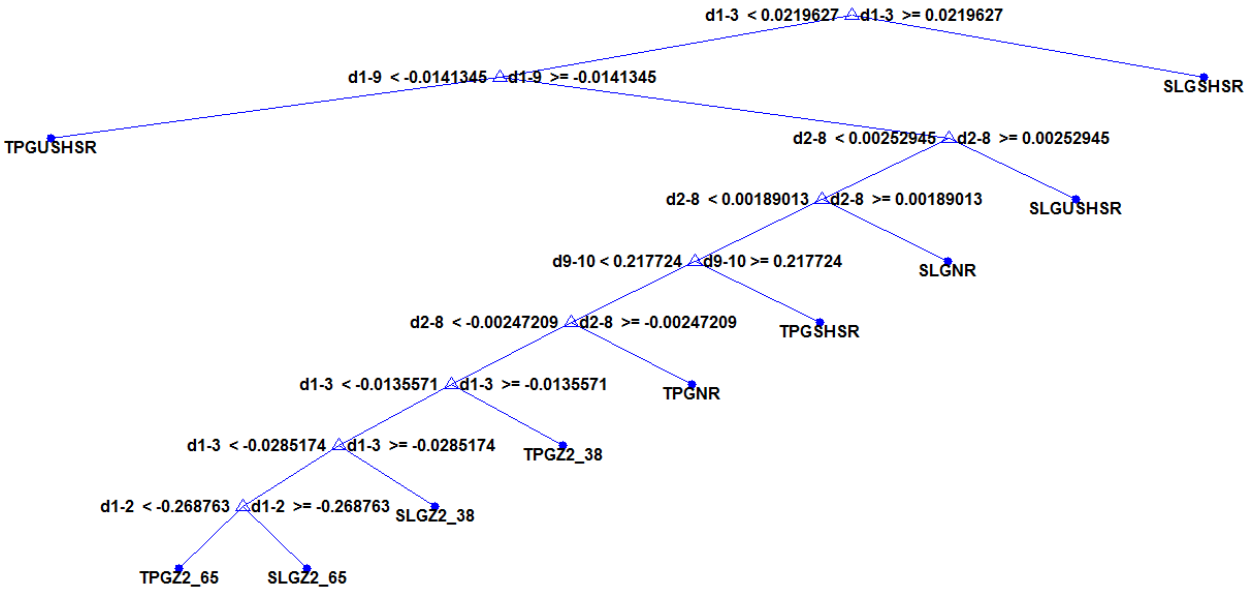

Fig. 3.15: Decision tree generated for a fault on line 38-65 using FLDSD

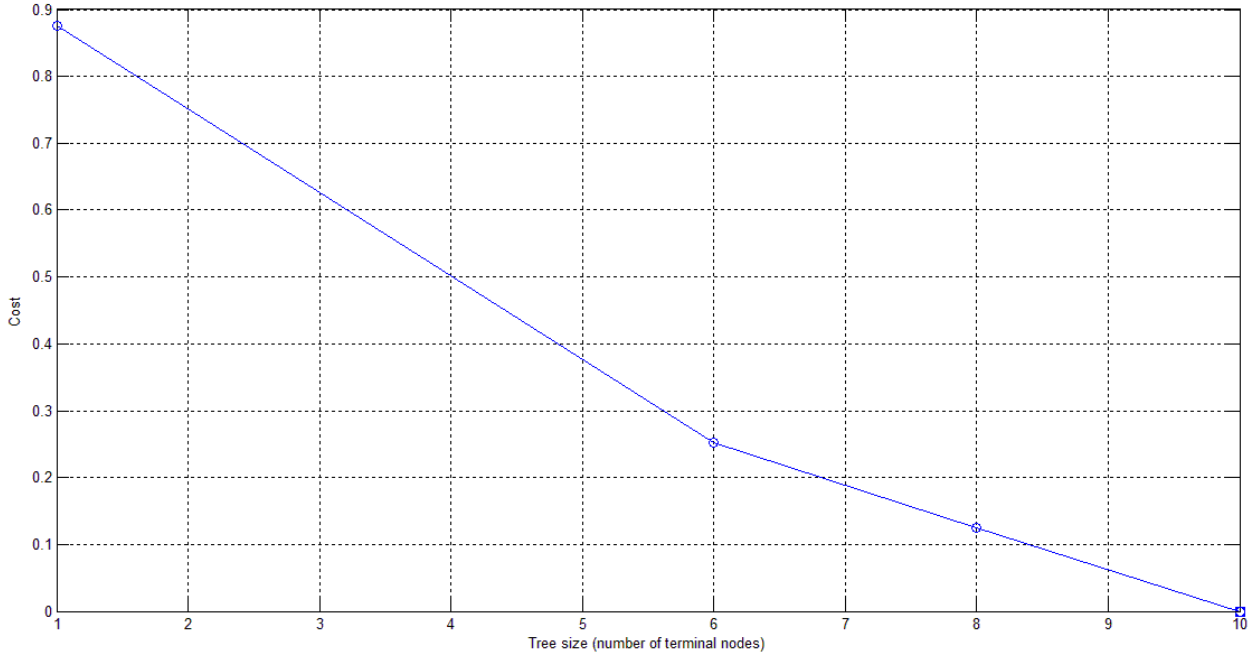

Fig. 3.16: Plot of cost vs. tree size for faults on line 38-65

Similar decision trees were obtained for the other nine lines. The decision trees for the other lines as well as the corresponding cost vs. tree size plots are shown in Figs. 3.17-3.34. The percentage accuracy obtained for classifying the data into n classes (where n is the number of classes into which data of that line is partitioned) by a tree of n terminal nodes for all the lines of the IEEE 118-bus system is given in

Table 3.3. From the plots and the table, it can be inferred that by using this technique events captured by the dynamic state estimator can be identified quickly and accurately.

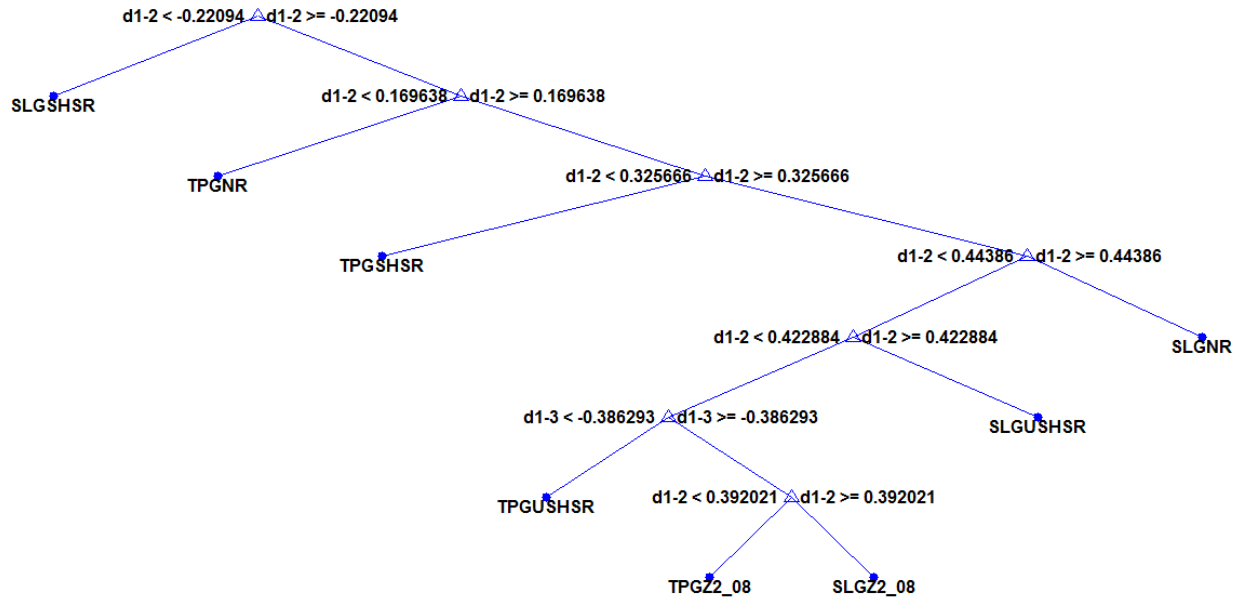

Fig. 3.17: Decision tree generated for a fault on line 8-9 using FLDSD

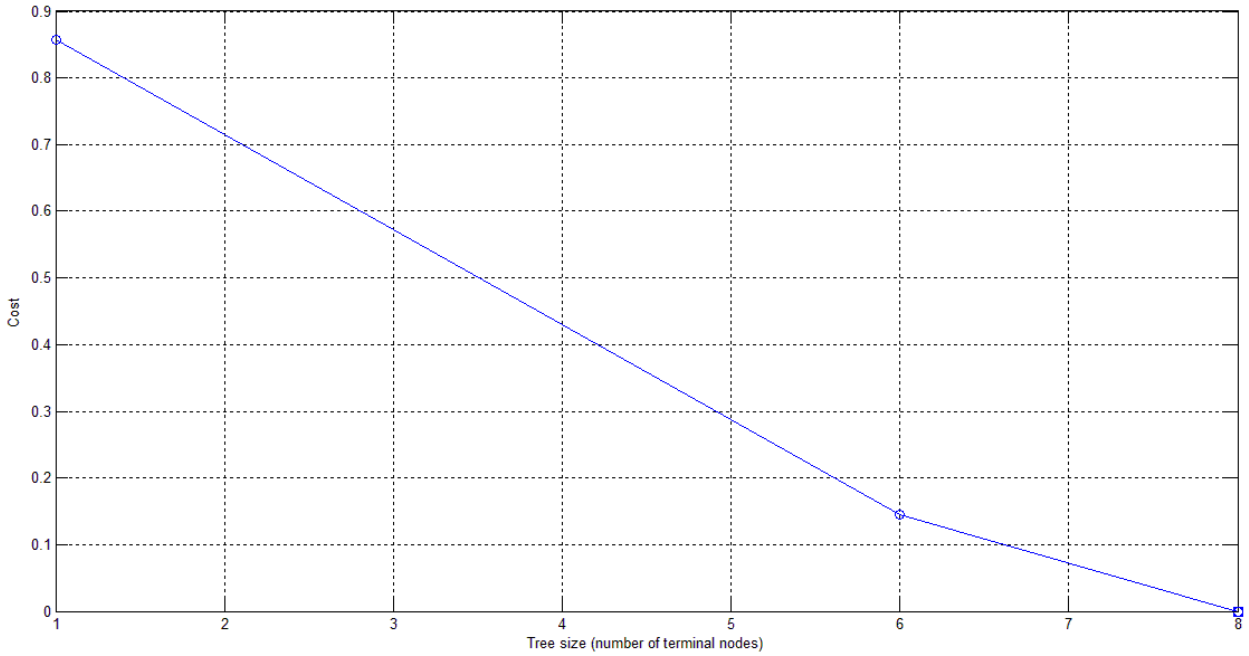

Fig. 3.18: Plot of cost vs. tree size for faults on line 8-9 using FLDSD

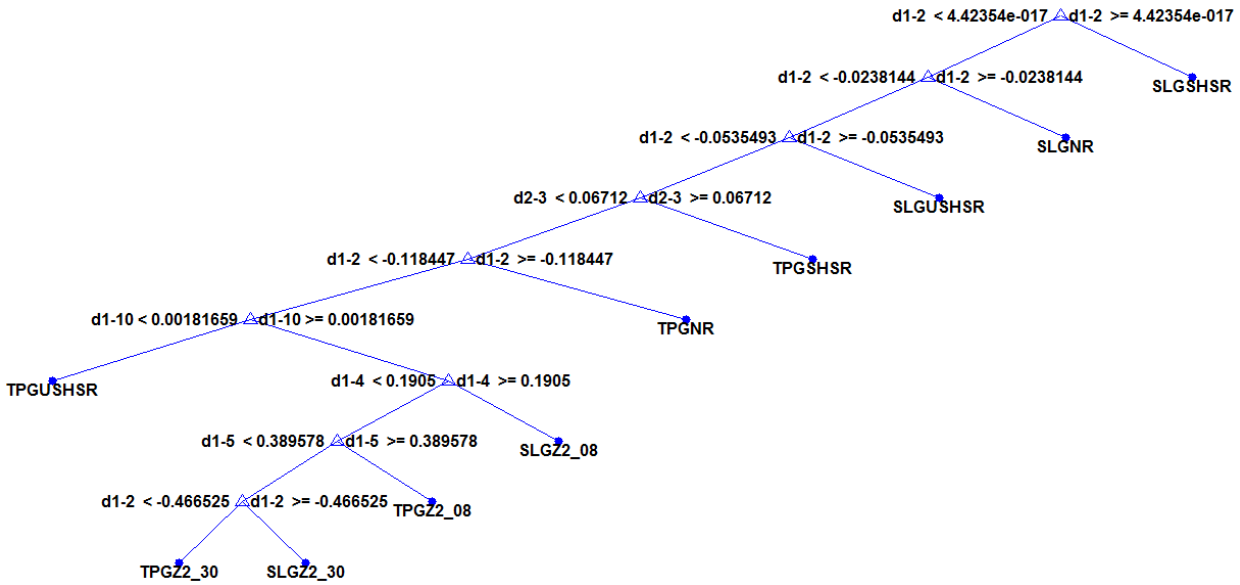

Fig. 3.19: Decision tree generated for a fault on line 8-30 using FLDSD

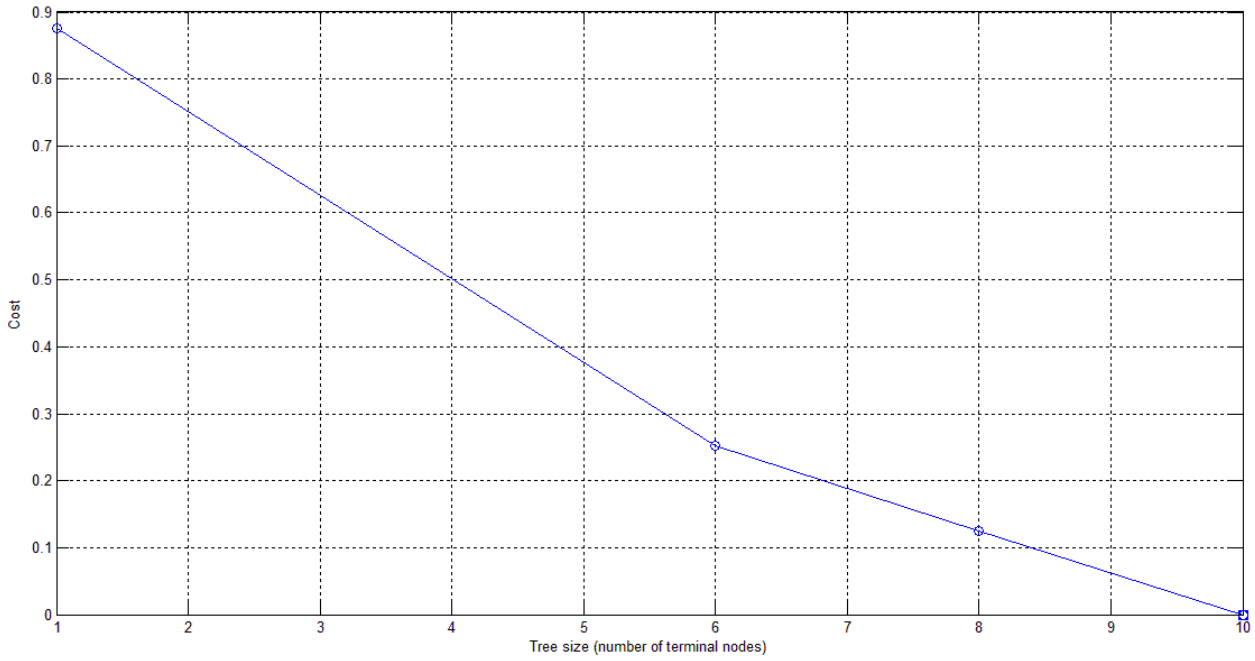

Fig. 3.20: Plot of cost vs. tree size for faults on line 8-30 using FLDSD

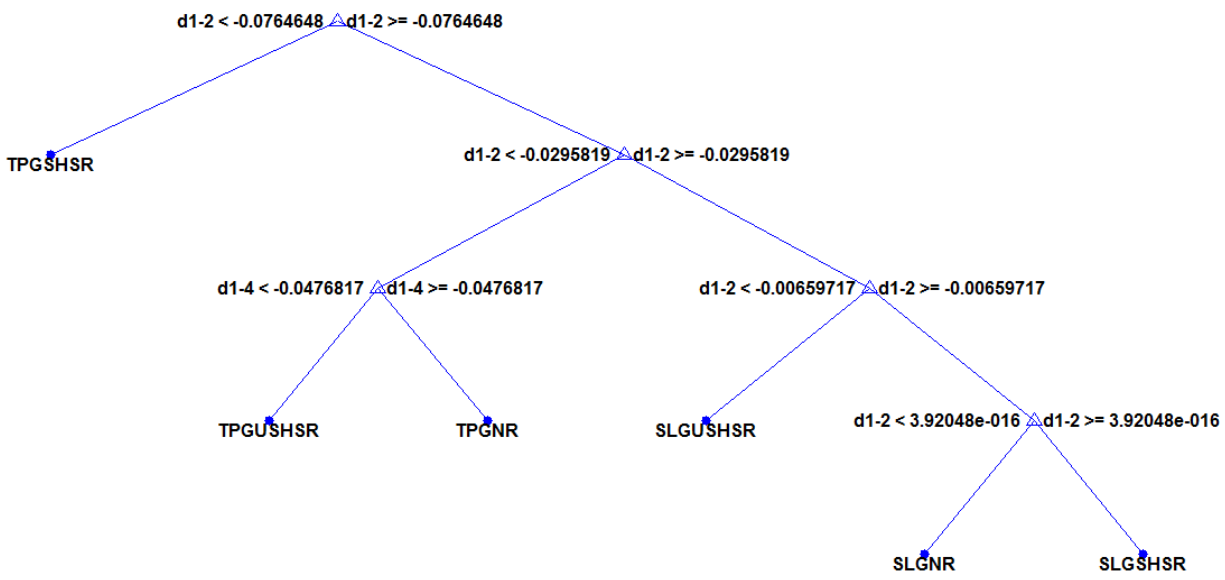

Fig. 3.21: Decision tree generated for a fault on line 9-10 using FLDSD

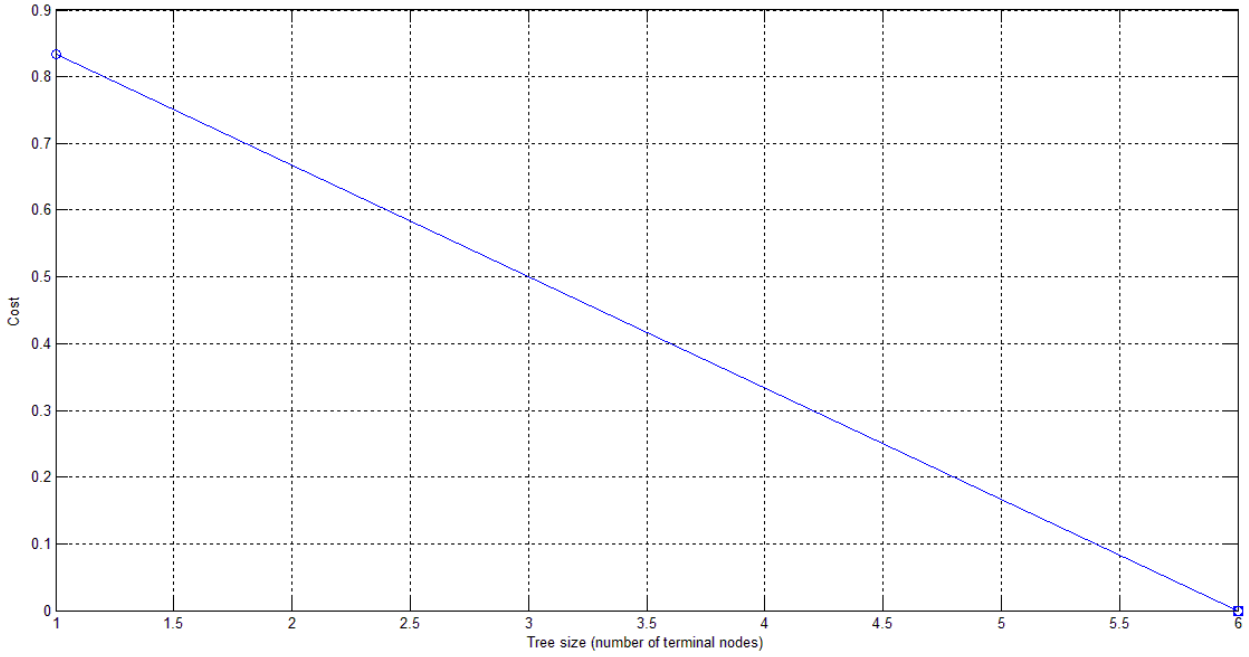

Fig. 3.22: Plot of cost vs. tree size for faults on line 9-10 using FLDSD

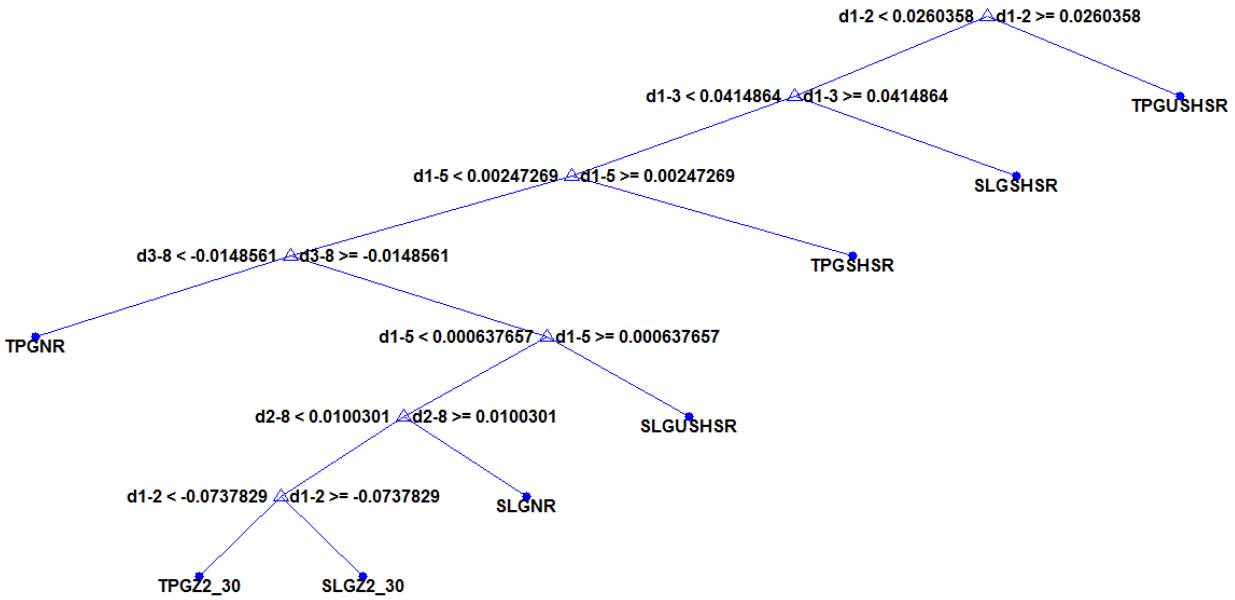

Fig. 3.23: Decision tree generated for a fault on line 26-30 using FLDSD

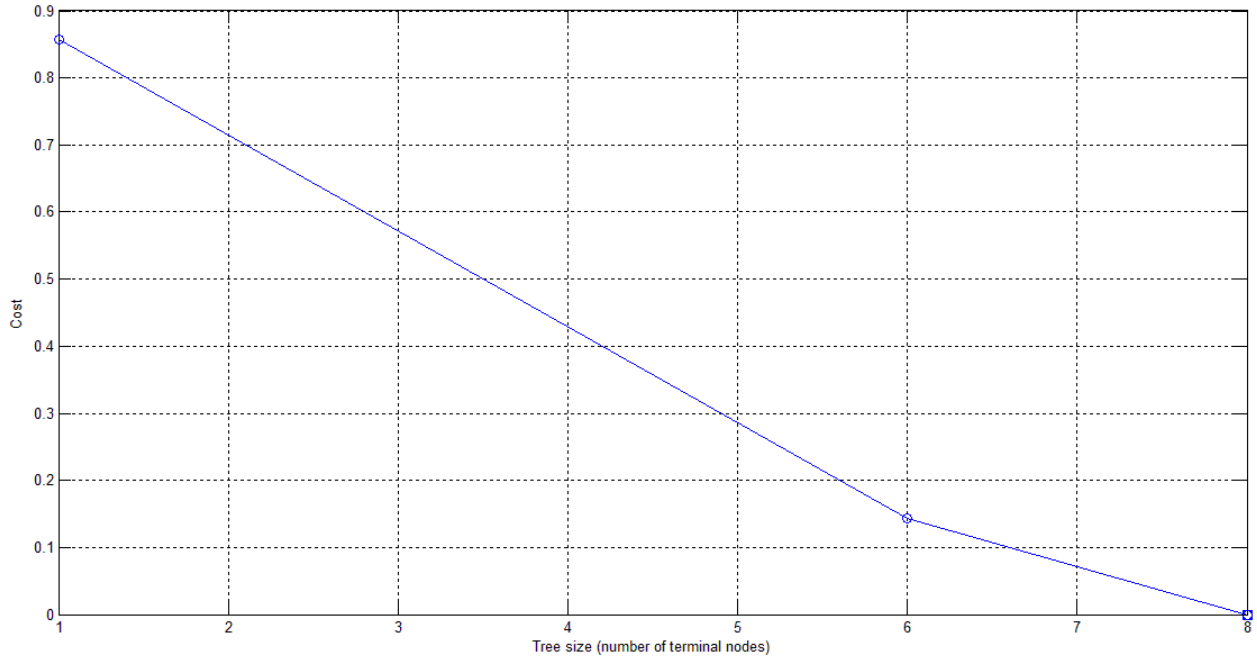

Fig. 3.24: Plot of cost vs. tree size for faults on line 26-30 using FLDSD

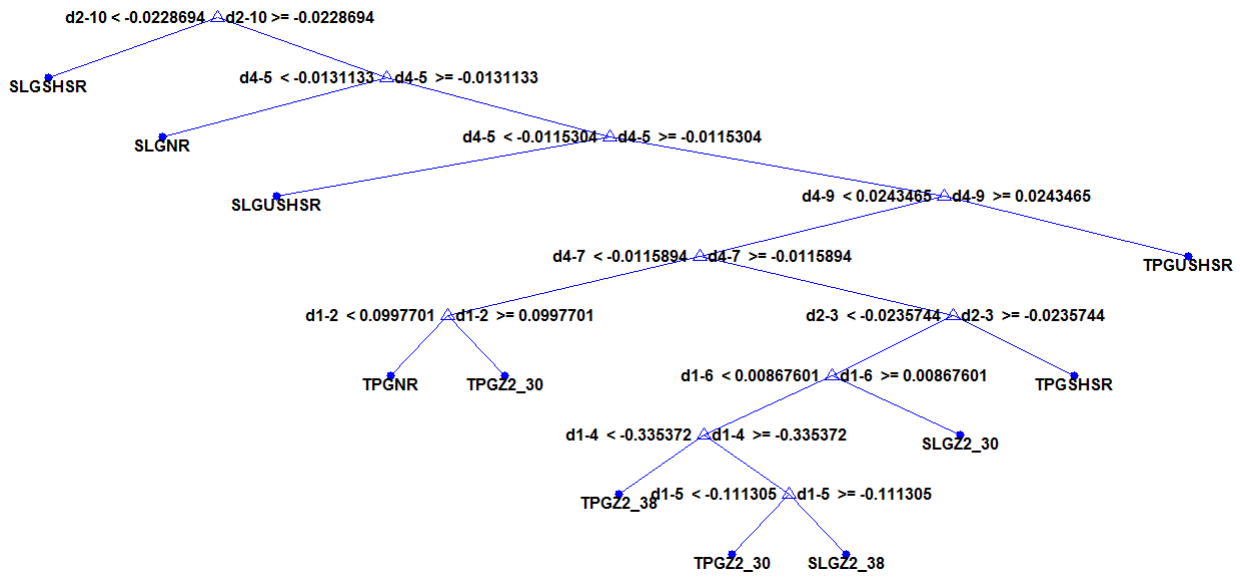

Fig. 3.25: Decision tree generated for a fault on line 30-38 using FLDSD

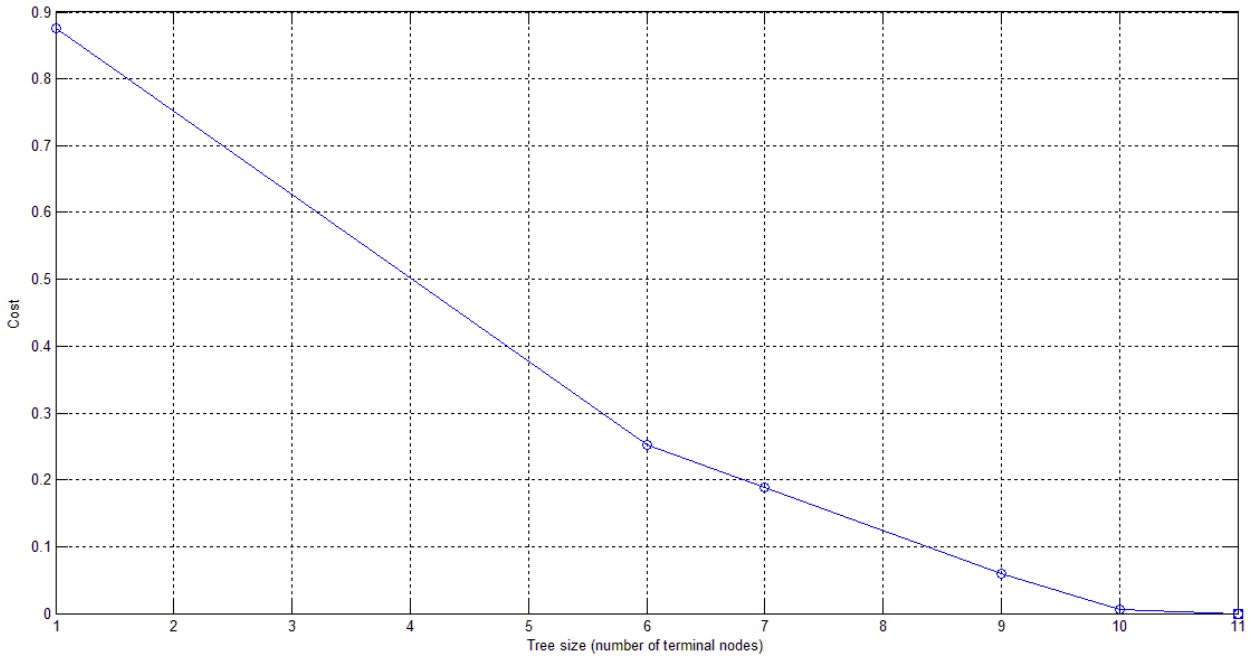

Fig. 3.26: Plot of cost vs. tree size for faults on line 30-38 using FLDSD

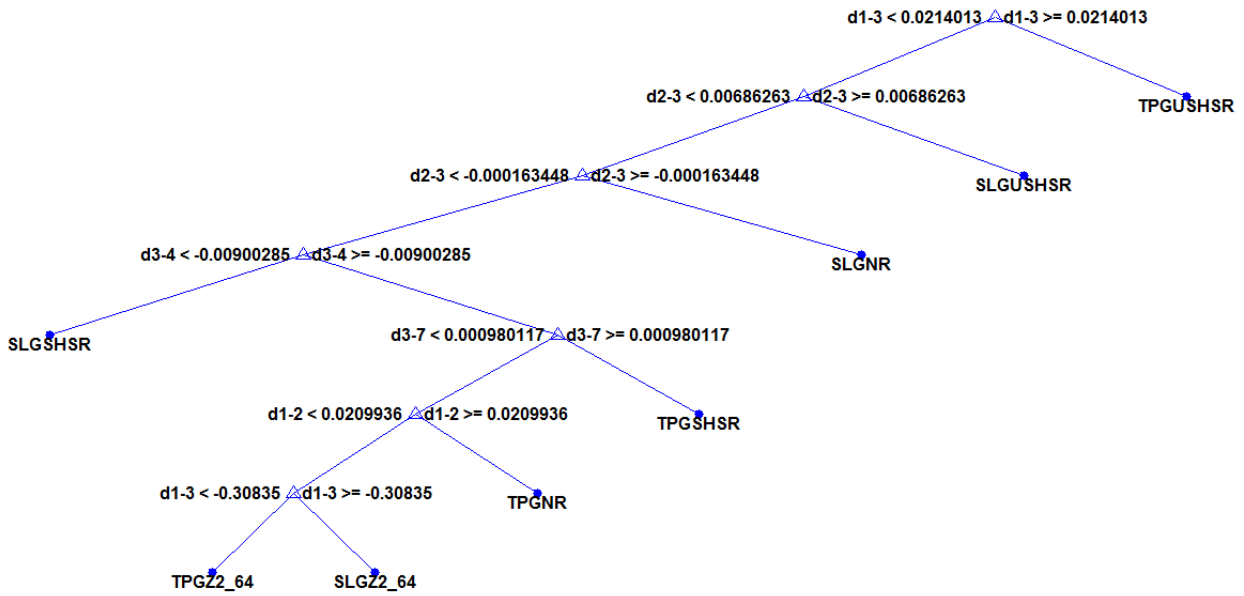

Fig. 3.27: Decision tree generated for a fault on line 63-64 using FLDSD

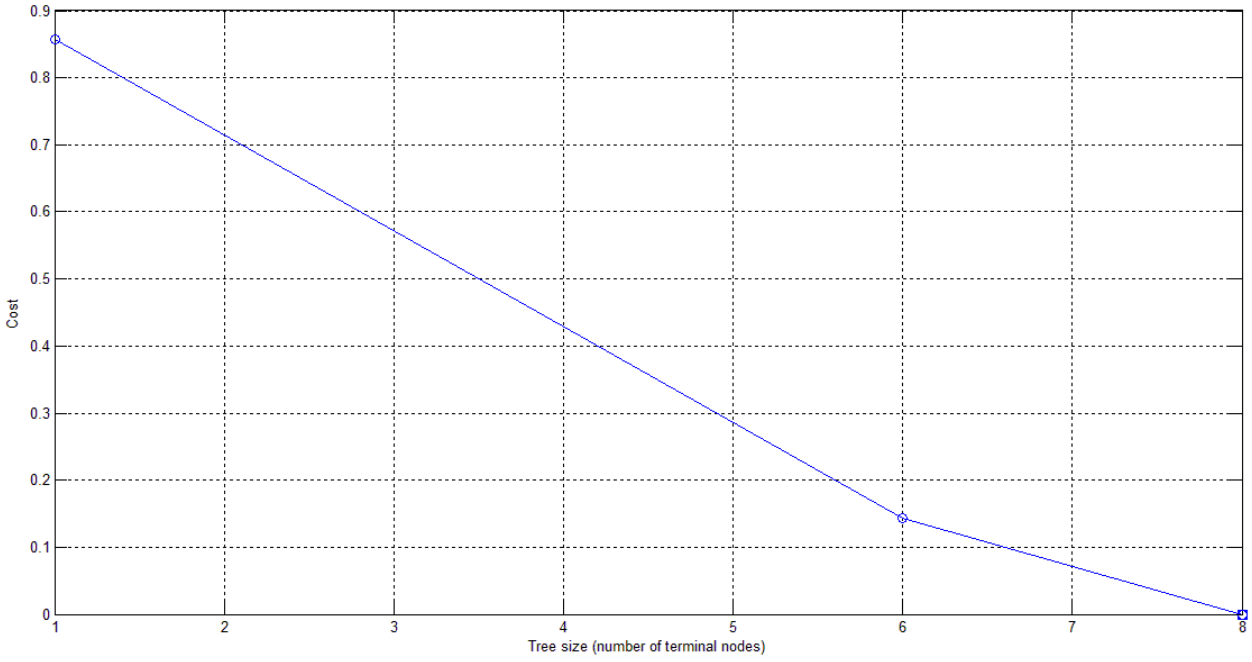

Fig. 3.28: Plot of cost vs. tree size for faults on line 63-64 using FLDSD

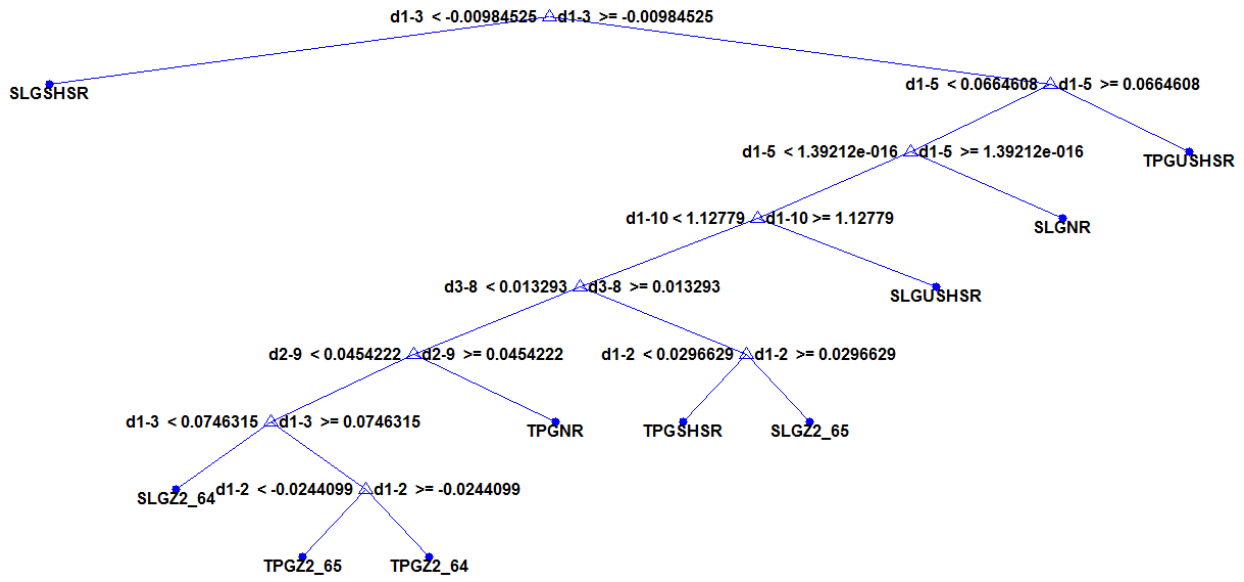

Fig. 3.29: Decision tree generated for a fault on line 64-65 using FLDSD

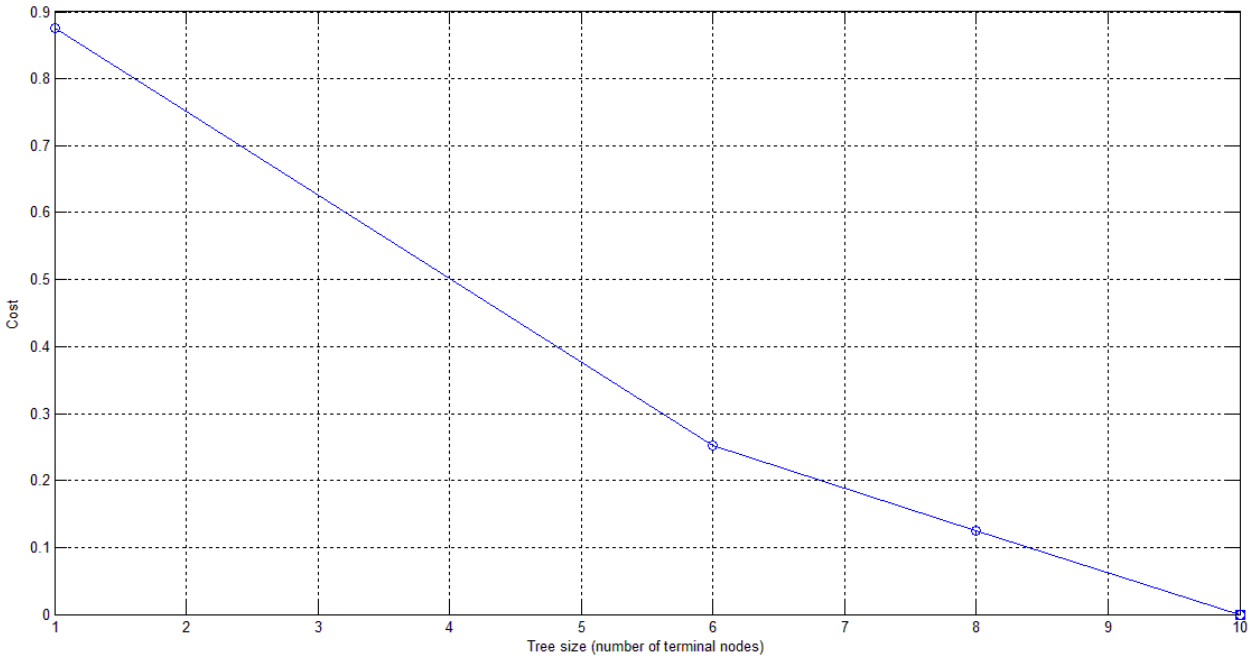

Fig. 3.30: Plot of cost vs. tree size for faults on line 64-65 using FLDSD

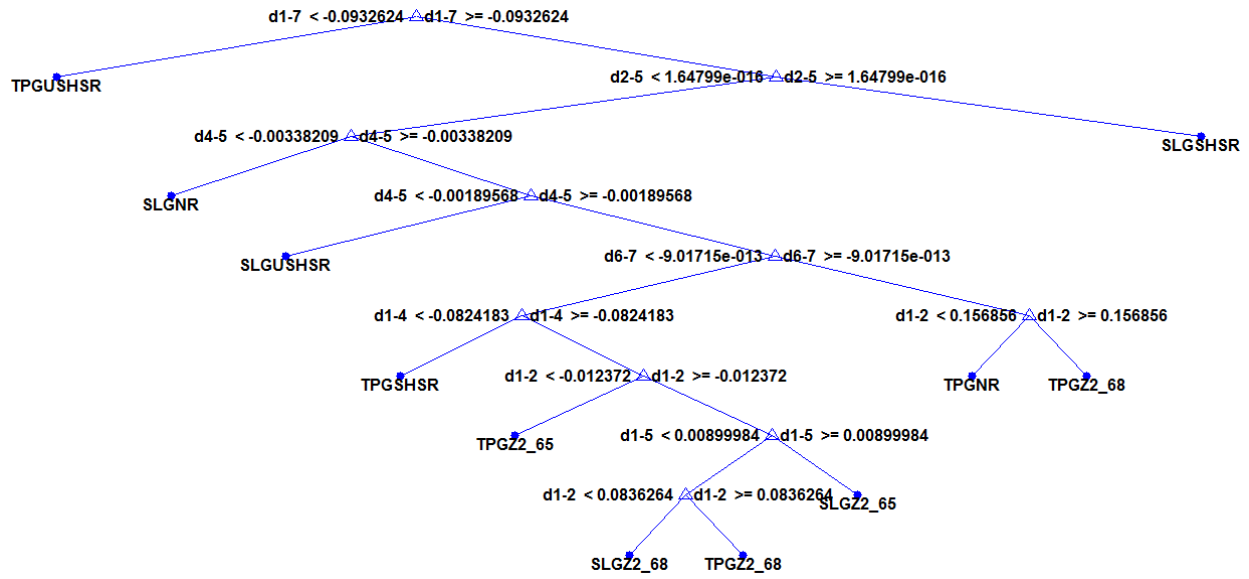

Fig. 3.31: Decision tree generated for a fault on line 65-68 using FLDSD

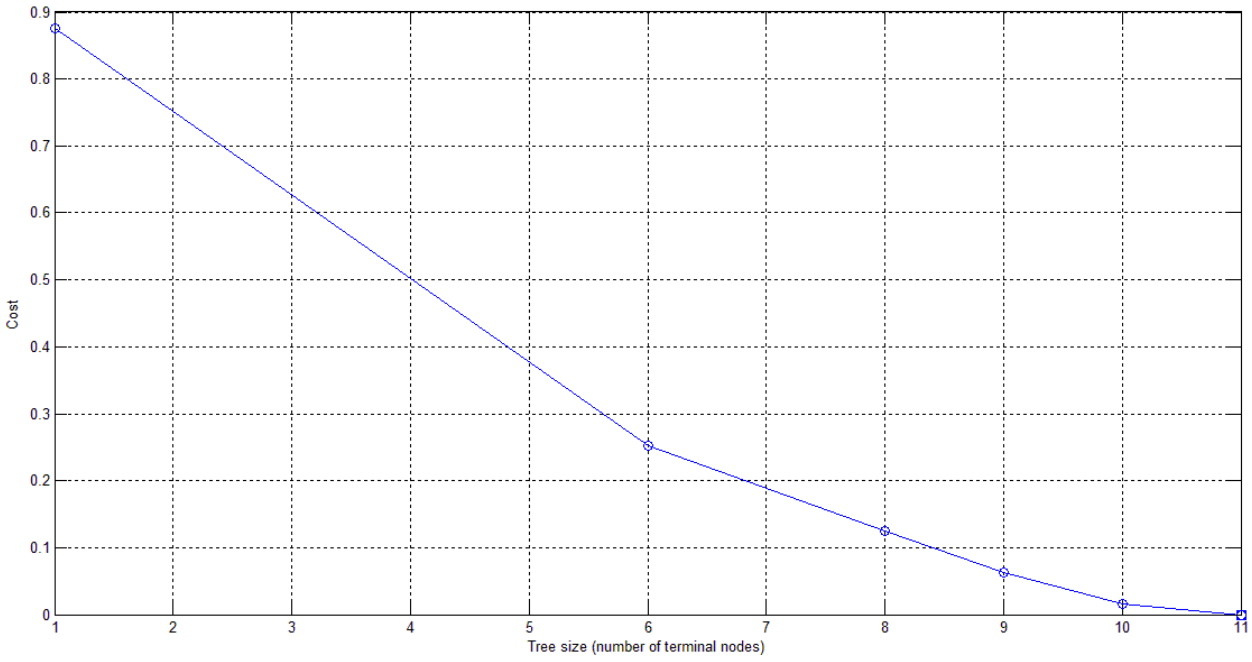

Fig. 3.32: Plot of cost vs. tree size for faults on line 65-68 using FLDSD

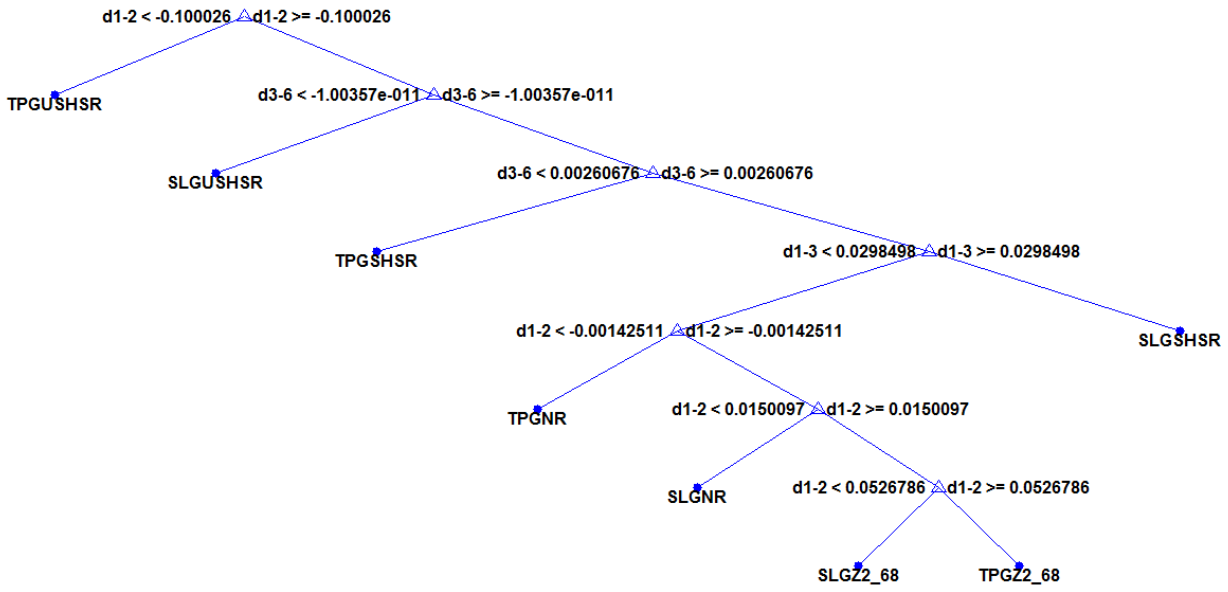

Fig. 3.33: Decision tree generated for a fault on line 68-81 using FLDSD

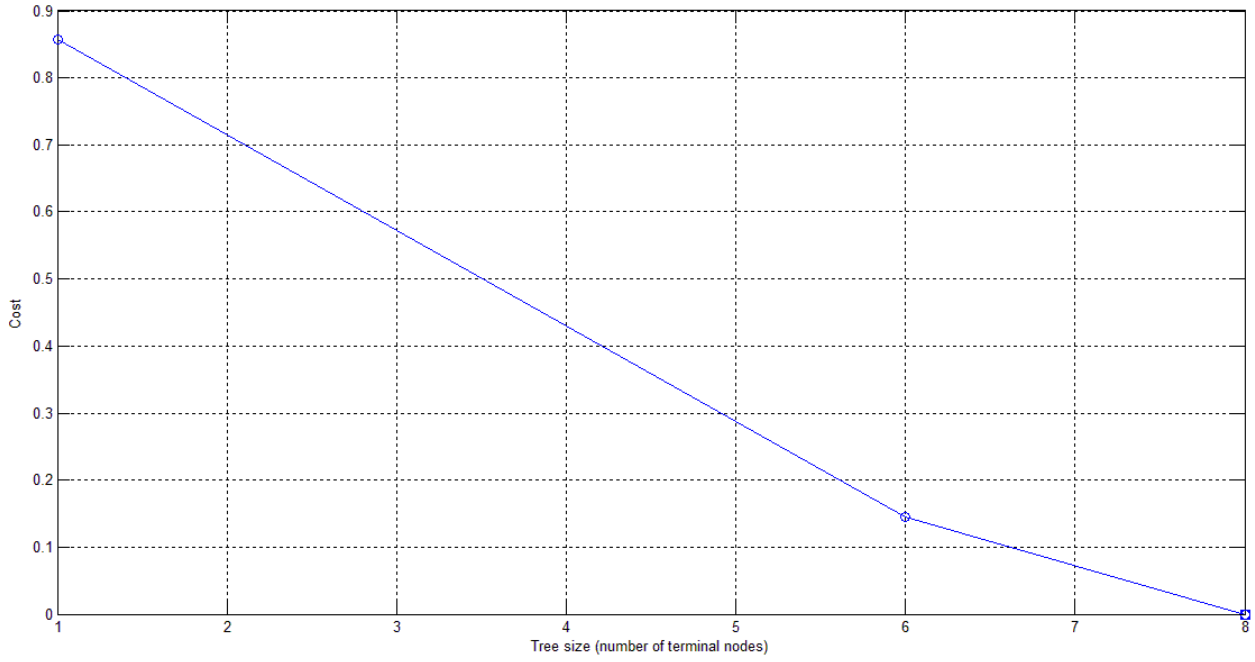

Fig. 3.34: Plot of cost vs. tree size for faults on line 68-81 using FLDSD

Table 3.3: Performance of the FLDSD algorithm for multi-class classification of dynamic events in the IEEE 118-bus system

Line	Number of Cases	Number of dimensions in the data	Number of classes in which data is to be partitioned (n)	Accuracy of a tree of n terminal nodes	Number of terminal nodes needed for 100% accuracy
8-9	632	240	8	100%	8
8-30	722	300	10	100%	10
9-10	540	180	6	100%	6
26-30	630	240	8	100%	8
30-38	722	300	10	99.58%	11
38-65	722	300	10	100%	10
63-64	630	180	8	100%	8
64-65	722	300	10	100%	10
65-68	722	300	10	98.48%	11
68-81	632	180	8	100%	8

3.3 Conclusion

PMU data have been used for making critical decisions for quite some time now, but the true potential of these devices has not yet been realized. When placed at a bus, they provide real-time measurements of voltages and currents connecting that bus with the rest of the system. But, being complex quantities, these measurements have not been addressed completely until the development of the FLDSD technique. In this chapter, using the FLDSD technique complex numbers/trajectory of complex numbers is represented by a single variable which is then used to perform optimal splits in CART.

Two power system applications have been considered in this chapter. The first application is directed towards two scenarios of the California power system where it is used to classify the system as “safe” or “stressed” based on measurements obtained from PMUs. The results indicate that by using this approach, a smaller sized decision tree is able to do the classification more accurately. The second application is directed towards classification of events captured by a dynamic state estimator. The traditional static state estimator is able to detect and identify bad data and topology changes, and it is imperative that the dynamic state estimator is able to do that as well. A quadratic prediction model

based on three prior estimates is shown to be able to detect discrepancies in the data, while the proposed FLDSD technique is shown to be able to successfully identify the captured events. From these two studies it is realized that the proposed methodology of using the distance variable for separating high-dimensional, multi-class data is a logical approach that yields good solutions. By utilizing both the real and the imaginary components of the phasor data, a new understanding of PMU data is obtained. This approach will not only be useful for solving synchrophasor based problems, but it will also be useful in other engineering applications that involve decision making based on multivariate data.

Chapter 4: An Integrated PMU Placement Scheme

Phasor measurement units (PMUs) provide synchronized measurements of real-time voltage and current phasors. The synchronization is done through simultaneous sampling of voltage and current waveforms using timing signals obtained from global positioning system (GPS) satellites. PMUs are capable of providing measurements as often as once per cycle of the power frequency. These measurements become the basis for developing a coherent picture (state) of the network. Knowing the network state in turn makes stability and vulnerability assessments possible. The use of PMUs has thus elevated the standards of power system protection, monitoring and control [6]. However, the criterion of *site selection* with respect to PMU placement needs to be addressed before its benefits can be reaped [75]. The placement sites are restricted by the available communication facilities, the costs of which are often higher than the PMUs themselves. To optimize cost and intended applications, it is necessary to choose PMU locations judiciously. Therefore, the path to be followed is to progressively deploy PMUs at select locations within the network to eventually observe the whole system [18]-[20].

The concept of optimal PMU placement has been a highly researched topic ever since PMUs came to be used commercially [21], [22]. Primarily, there have been two methods followed by power engineers for addressing this issue [18]:

- Development of a prioritized list of placement sites based essentially on observability,
- Placement of PMUs to correctly represent critical dynamics of the system

References [76]-[83] have used the former method whereas [12], [37], [84], [85] have followed the latter approach. References [76]-[79] used Integer Linear Programming (ILP) techniques based on binary search algorithms for finding the optimal locations for placement of PMUs to ensure complete network observability. Reference [80] proposed a two indices approach involving the bus observability index and the system observability redundancy index. References [81], [82] used Integer Quadratic Programming and Genetic Algorithms, respectively, to achieve the twin objectives of minimizing the required number of PMUs and maximizing the measurement redundancy. Reference [83] developed a unified approach of preserving system observability, and lowest system metering economy. The second method has been extensively used for adaptive protection schemes [12], voltage security assessment [37], [84], and voltage stability analysis [85].

Inspite of all the analysis that has been done with regards to PMU placement, the implementation of these ideas has been far from satisfactory. The 2012 blackout in India is the latest in a long list of power system failures that could have been averted, or its effects minimized, had proper measures been taken in time. The primary reason behind this inadequacy in implementation is attributed to the differences in the two methods described above. The first method does not take into account the transient and dynamic stability of the system, whereas the second approach does not consider complete observability as one of its priorities. The net outcome is that for the same system different "optimal" PMU placement sets are created depending on the methodology followed. As it is not possible for any utility to implement all the schemes that are proposed, either transient/dynamic stability, observability, or often both are compromised.

This chapter addresses the topic of PMU placement for generic systems by combining both the aforementioned methodologies – ensuring observability as well as protecting critical parts of the system. As such, the proposed algorithm is expected to be useful to utilities that want to initially protect the most important buses of their system on their way to attaining complete observability. In order to integrate the two methodologies, a modified version of the concept of depth of unobservability originally introduced in [86] is combined with the binary integer programming technique, along with some more constraints. The next section describes the depth of unobservability idea that has been used in this work as well as the incidence matrix based binary integer programming method that was developed in [13].

4.1 Theoretical Background

The traditional depth of unobservability concept was a systematic step-by-step approach that was proposed in [86] and later expanded in [19] for attaining complete observability through improved monitoring of the network at each stage of implementation. Unobservability level ends at depth 0 which represents complete observability. A depth of one unobservability placement refers to the process of placing PMUs that strives to create depth of one unobservable bus in the system. Similarly, a depth of two unobservability condition exists when two observed buses bound two adjoining unobserved buses, and so on. Figs. 4.1 and 4.2 show how the traditional definition of depth of unobservability of a system varies with the placement of PMUs. The arrows indicate power injections. Comparing Fig. 4.1 with Fig. 4.2, it is realized that for the same system, by moving the PMUs from bus 2 to bus 1, the depth of unobservability of the system changed from 1 to 2.

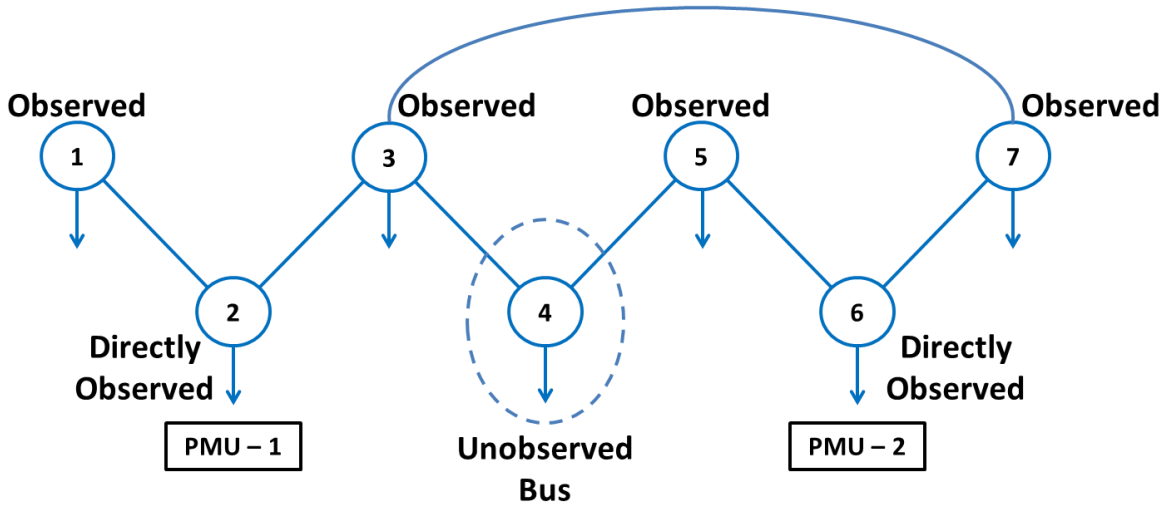

Fig. 4.1: Example illustrating traditional depth of unobservability equal to 1

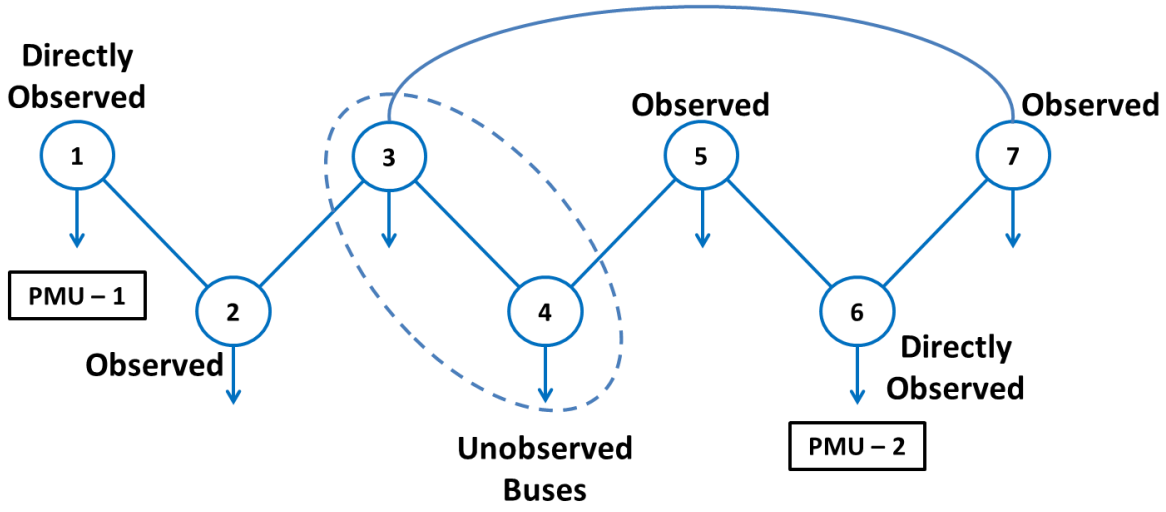

Fig. 4.2: Example illustrating traditional concept of depth of unobservability equal to 2

4.1.1 Modified depth of unobservability concept

The concept of depth of unobservability can be interpreted in a number of ways. The traditional definition of depth of unobservability was developed for computing incomplete observability using spanning trees. It worked well for radial systems but its use for handling more complex, inter-connected networks was limited due to the complexity of its definition. This was highlighted in [87]. In [87], Altman proposed an alternate definition for the depth of unobservability. He defined it as the addition of the minimum distances of any two differently observable buses from the furthest unobserved bus. This

meant computing the shortest path going through each unobserved bus that is bounded by two PMUs for every bus, and then choosing the longest of these shortest paths as the depth of unobservability of the system. Mathematically, this is defined as,

$$DOU_{bus_n} = \min_{\mathrm{i}}{}^{\mathrm{X}}(Dist_{ni}) + \min_{\mathrm{j}}{}^{\mathrm{X}}\left(Dist_{nj}\right) - 1 \tag{4.1}$$

$$DOU_{system} = \max_{\mathrm{n}}{}^{\mathrm{N}}\left(DOU_{bus_n}\right) \tag{4.2}$$

In (4.1) and (4.2), DOU_{bus_n} is the depth of unobservability of the n^{th} bus, X is the set of observable buses, i and j are different observable buses, N is the set of all buses present in the system, and DOU_{system} is the depth of unobservability of the whole system. A closer look at Altman's formulation reveals that for developing a simple yet robust definition for the concept of depth of unobservability, there is no need to compute the "sum of path lengths" of an unobservable bus from two different observable buses. A simpler definition would be to express depth of unobservability as *only* the "path length" rather than the "sum of path lengths". Thus, the modified definition of depth of unobservability that has been used in this work is that *it is the highest distance that an unobserved bus has from an observed bus when all unobserved buses are considered*. Mathematically, this means,

$$DOU_{system} = \max_{\mathrm{n}}{}^{\mathrm{N}}\left(\left(\min_{\mathrm{i}\neq\mathrm{n}}{}^{\mathrm{X}}(Dist_{ni})\right) - 1\right) \tag{4.3}$$

In (4.3), N is the set of all buses present in the system, n is a bus belonging to the set N, X is the set of directly observable buses, i is a bus belonging to the set X, and DOU_{system} is the depth of unobservability of the whole system. The path length is an attractive definition for depth of unobservability because by this definition, the depth of unobservability would never exceed the "maximum number of unknowns for a given set". In order to illustrate the proposed definition, the system depicted in Figs. 4.1 and 4.2 is shown again in Figs. 4.3 and 4.4. In Fig. 4.3, the PMU is placed only at bus 1. In such a scenario, buses 5 and 6 are at a distance of three paths (5-4-3-2 and 6-7-3-2, respectively) from the observed bus (bus 2) and so for a PMU placed at bus 1, the depth of unobservability of the system would be three. This is equal to the "maximum number of unknowns for each set" which must be "known" (in this case, three unknowns for the two sets – voltages at 5, 4, 3 and 6, 7, 3, respectively) so as to make the system completely observable. In Fig. 4.4, the PMU is moved to bus 3. In such a scenario, buses 1, 5 and 6 are at a distance of one path (1-2, 5-4 and 6-7, respectively) from the observed buses (bus 2, bus 4, bus 7) and so for a PMU placed at bus 3, the

depth of unobservability of the system would be one. This is again equal to the "maximum number of unknowns for each set" which must be "known" (in this case, one unknown for the three sets – voltages at 1, 5 and 6, respectively) so as to make the system completely observable. It should also be noted here that the proposed concept of depth of unobservability gives the same results when applied to the PMU placement configurations shown in Figs. 4.1 and 4.2. However, the proposed definition is easier to implement as will be shown in the next sub-section.

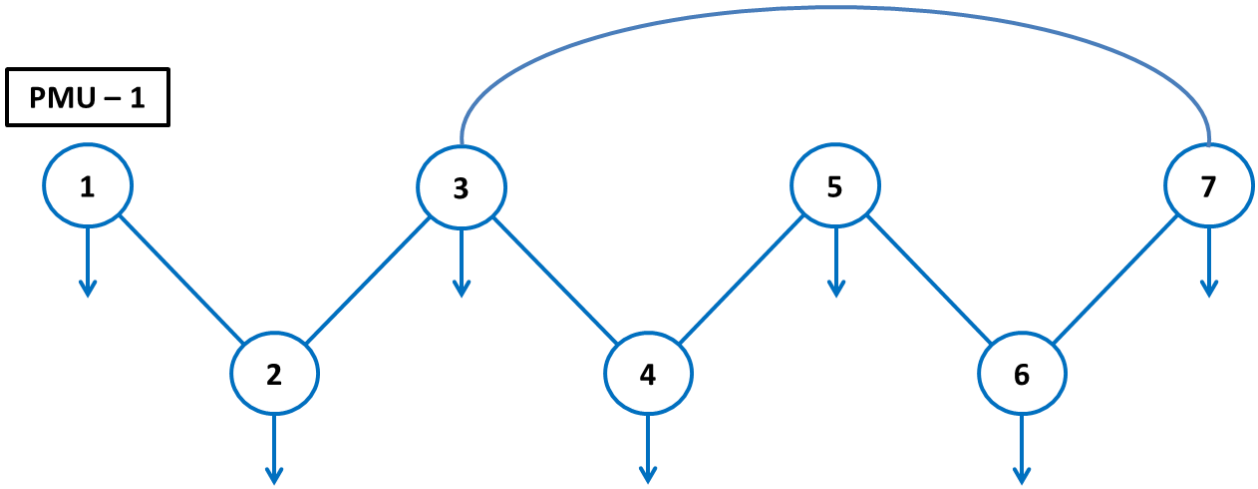

Fig. 4.3: Example illustrating proposed concept of depth of unobservability equal to 3

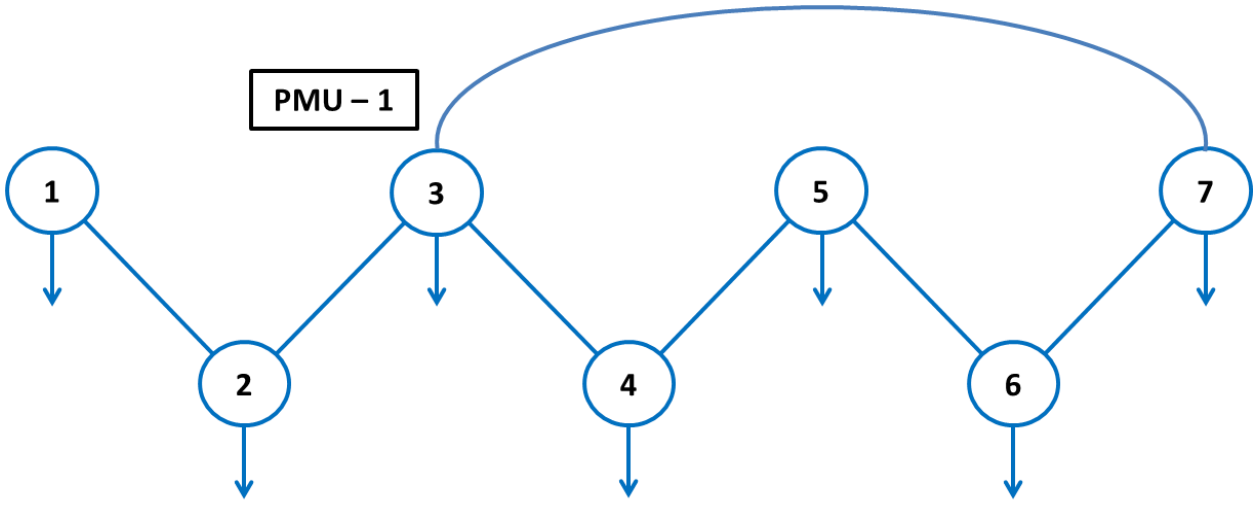

Fig. 4.4: Example illustrating proposed concept of depth of unobservability equal to 1

4.1.2 Incidence matrix based binary integer programming

As was in the case with the traditional definition of depth of unobservability, for the proposed definition also, the objective is to reduce the depth of unobservability to zero. A further constraint which must be imposed on this minimization is the fact that once a PMU is placed at a bus at a higher depth of unobservability, in subsequent depths, that PMU cannot be removed from that bus. Thus, the two objectives of the optimization are:

- Minimize depth of unobservability with every step
- PMUs once placed at a bus cannot be removed in subsequent steps

A simple way to perform this optimization is described in this sub-section.

In [19], [86], the authors had used simulated annealing for computing the (traditional) different depths of unobservability. Enumerating trees for a large system can become a computationally over-whelming problem. In his work, Altman had proposed an alternate definition for the depth of unobservability concept [87]. In the course of the work done here, it was realized that an even simpler approach (simpler than Altman's) could be developed by defining the depth of unobservability as a measure based on the "path lengths" and not "sum of path lengths". This "path lengths" based depth of unobservability concept can be implemented using incidence matrix based binary integer programming as done in [13]. A brief overview of that methodology is presented below.

The problem of computing the minimum number of PMUs required for complete observability (depth zero) of a network is stated as an integer programming problem [88] of the form,

$$\min_{\boldsymbol{X}}(\boldsymbol{f}^T.\boldsymbol{X}) \tag{4.4}$$

$$\text{Subject to: } \boldsymbol{AX} > \boldsymbol{0} \tag{4.5}$$

In (4.4) and (4.5), $\boldsymbol{A}$ is the $N \times N$ incidence matrix of a N bus system, $\boldsymbol{X}$ is a $N \times 1$ matrix composed of ones and zeroes with ones depicting the buses where PMUs must be placed for complete observability, and $\boldsymbol{f}$ is a $N \times 1$ matrix of ones. In order to compute higher depths of unobservability, the matrix $\boldsymbol{A}$ has to be replaced by sign of the higher powers of $\boldsymbol{A}$. This is in accordance with the following Theorem [89]:

***Theorem**: The ij entry in the n^{th} power of the incidence matrix for any graph or diagraph is exactly equal to the number of different paths of length n, beginning at vertex i and ending at vertex j.*

This theorem implies that, for instance, if the incidence matrix is raised to the power two and its sign taken, then every bus of this new network (whose incidence matrix is sign of $\boldsymbol{A}^2$) will be *directly* connected to one bus away of the original network, and so on. In order to illustrate this with an example, let us again consider the 7-bus system given in Figs. 4.1-4.4 which is re-drawn for convenience in Fig. 4.5. The incidence matrix of this system is,

$$\boldsymbol{A} = \begin{bmatrix} 1 & 1 & 0 & 0 & 0 & 0 & 0 \\ 1 & 1 & 1 & 0 & 0 & 0 & 0 \\ 0 & 1 & 1 & 1 & 0 & 0 & 1 \\ 0 & 0 & 1 & 1 & 1 & 0 & 0 \\ 0 & 0 & 0 & 1 & 1 & 1 & 0 \\ 0 & 0 & 0 & 0 & 1 & 1 & 1 \\ 0 & 0 & 1 & 0 & 0 & 1 & 1 \end{bmatrix} \tag{4.6}$$

The sign of the square of the incidence matrix given in (4.6) is,

$$\boldsymbol{A}_1 = signum(\boldsymbol{A}^2) = \begin{bmatrix} 1 & 1 & 1 & 0 & 0 & 0 & 0 \\ 1 & 1 & 1 & 1 & 0 & 0 & 1 \\ 1 & 1 & 1 & 1 & 1 & 1 & 1 \\ 0 & 1 & 1 & 1 & 1 & 1 & 1 \\ 0 & 0 & 1 & 1 & 1 & 1 & 1 \\ 0 & 0 & 1 & 1 & 1 & 1 & 1 \\ 0 & 1 & 1 & 1 & 1 & 1 & 1 \end{bmatrix} \tag{4.7}$$

The system whose incidence matrix is given by (4.7) is shown in Fig. 4.6 with the dotted lines indicating the new branches formed. On comparing Figs. 4.5 and 4.6, it becomes clear that the new branches that were created in Fig. 4.6 corresponded to the joining of buses that were previously one-bus-away from each other. This, then, fits in directly with our definition for the concept of depth of unobservability because the power to which the incidence matrix is raised in order to change the ij entry from 0 to 1 corresponds to the number of "path lengths" between i and j. Thus, to compute for the n^{th} depth of unobservability, the integer problem formulation becomes [13],

$$\min(\boldsymbol{f}^T.\boldsymbol{X}_n) \tag{4.8}$$

$$\text{Subject to: } \text{signum}(\boldsymbol{A}^{n+1})\boldsymbol{X}_n > \boldsymbol{0} \tag{4.9}$$

$$(\boldsymbol{f} - \boldsymbol{X}_{n-1})^T\boldsymbol{X}_n = 0 \tag{4.10}$$

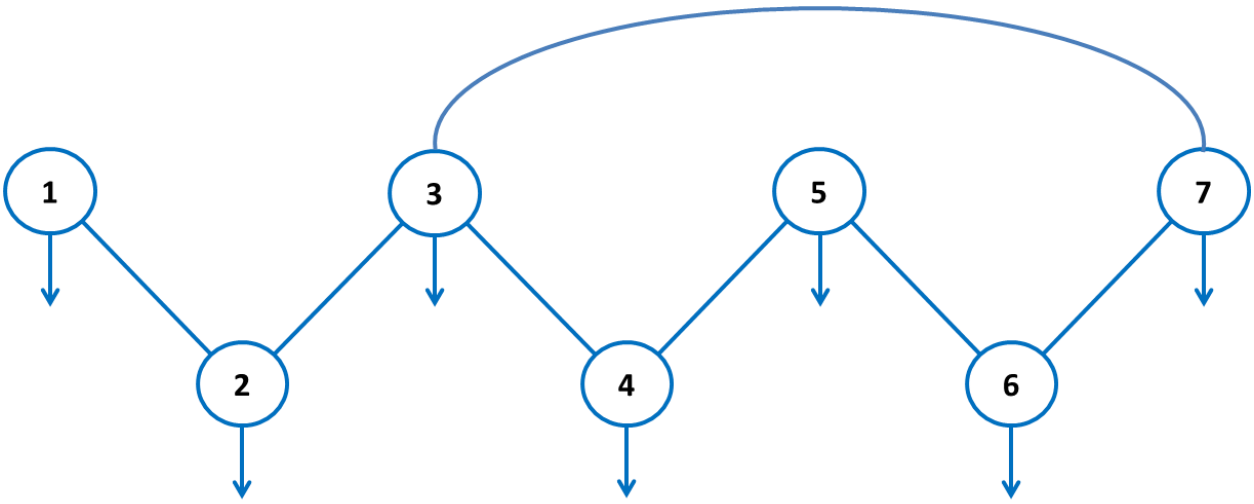

Fig. 4.5: The 7-bus system whose incidence matrix is $\boldsymbol{A}$ as given in (4.6)

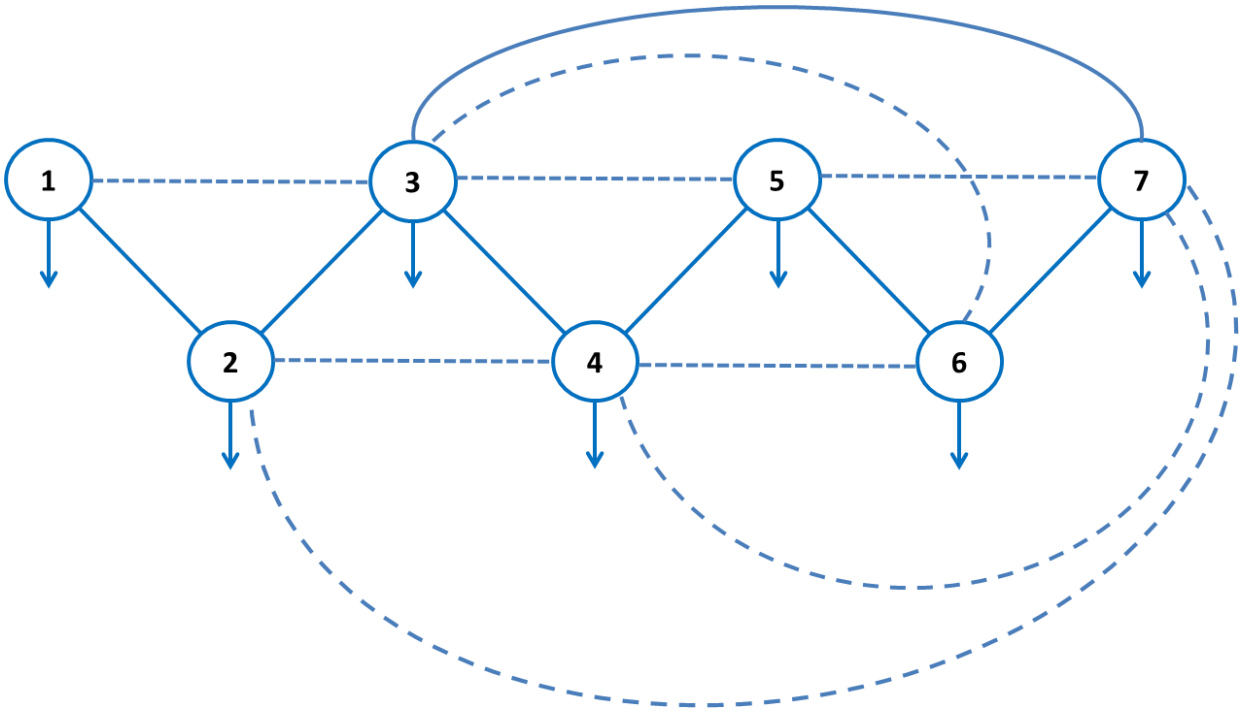

Fig. 4.6: The 7-bus system whose incidence matrix is $\boldsymbol{A}_1$ as given in (4.7)

The signum function used in (4.9) is defined as follows: Let $\boldsymbol{B}$ be a real matrix of order $m \times p$ where the element in the i^{th} row and j^{th} column is denoted by $\boldsymbol{B}(i,j)$. Then $\boldsymbol{S} = \text{signum}(\boldsymbol{B})$ is a real matrix of order $m \times p$ whose element in the i^{th} row and j^{th} column, denoted by $\boldsymbol{S}(i,j)$, is

$$\boldsymbol{S}(i,j) = \begin{cases} 1 & if\ \boldsymbol{B}(i,j) > 0 \\ -1 & if\ \boldsymbol{B}(i,j) < 0 \\ 0 & if\ \boldsymbol{B}(i,j) = 0 \end{cases} \quad (4.11)$$

The PMU placement algorithm described in this section only improves the observability of the network. It is not concerned with the other benefits (improving transient/dynamic stability and better control) that placing a PMU on specific buses will deliver. It also does not provide redundancy to any of the measurements. An algorithm is developed in the next section, based on the modified concept of depth of unobservability described and binary integer programming that has been described in this section, to ensure protection of relevant portions of the system while moving towards complete observability without exorbitantly increasing the total number of PMUs required.

4.2 A PMU placement scheme ensuring real-time monitoring of critical buses of the network

One way to ensure that the critical dynamics of the system is addressed is by adding more importance to the relevant buses. This can be done by designating those buses as more "critical" than other buses. The "critical" buses can be chosen based on the topology of the network, as well as on the basis of transient and dynamic stability studies that have been performed on the system. An alternate way to select "critical nodes" based only on transient stability studies was developed in [90]. However, a much more comprehensive methodology for selecting "critical" buses is developed here. The buses identified as critical form the *starting* set. The concept of depth of unobservability described in Section 4.1.1 is then used to determine the final PMU placement set. The next sub-section defines the term critical as is used in this context, and describes the process for selecting such buses.

4.2.1 The concept of Criticality

PMUs when placed at a bus provide time synchronized measurements of the voltage phasor and the branch current phasors of all the branches emerging from that bus. This information can be used for making a variety of decisions. Power engineers all over the world have used PMUs for dynamic security assessment, transient stability/instability predictions, adaptive protection schemes, etc. Under such circumstances, defining an optimal PMU placement scheme for a general network becomes subject to the required needs and the available facilities. One important factor which contributes towards PMU placement but is very different from its other applications is the concept of observability. A power system is called completely observable when all of its states can be uniquely determined [91], [92]. This is also an essential criterion for performing accurate state estimation. Therefore, along with catering to

the relevant system dynamics, an optimal PMU placement scheme must also satisfy the observability constraint. In such a scenario, traditional methods based only on transient/dynamic stability study or topological observability, are not sufficient. The concept of "criticality" developed in this sub-section helps in coming up with a PMU placement set that integrates both the requirements. In the proposed scheme, buses are defined to be "critical" if they satisfy one or more of the following conditions:

- High voltage buses
- High connectivity buses
- Buses relevant to transient/dynamic stability
- Potential small signal control buses

From the utility point of view, the high voltage network is the backbone of the system. For measurement and protection purposes it is necessary to monitor this network continuously. Therefore, it is practical to have the high voltage buses in the list of critical buses. Buses with high connectivity not only allow monitoring of a large number of lines from one location, but they are also the substations which have good communication facilities and are typically located in areas where expansions/installations can be easily carried out. Since the associated costs for placing a PMU at a substation may exceed the cost of the PMU itself, it is logical to place them at substations where these costs can be kept to a minimum. However, the criteria for selecting high connectivity is very subjective and system specific. The buses relevant to the transient/dynamic stability of the system are selected based on their significance in preventing voltage collapses; minimizing impacts of faults; and/or for their participation towards damping inter area oscillations. Potential small signal control buses are the buses where controllers are placed. They include locations of Flexible AC Transmission Systems (FACTS) devices, energy storage devices (ESDs), HVDC terminals, etc. The definition of criticality can also be extended to include pricing and utility preferences. However, care must be taken to ensure that too many buses are not selected as critical as doing so will dilute the very definition of "criticality".

Another issue which needs to be addressed when computing for the optimal placement of PMUs in a network is the question of redundancy. The norm in the industry is to have a $N-1$ contingency criterion in the system. A $N-1$ contingency means that even if one PMU or transmission line goes down, the system remains observable. Different techniques have been employed by researchers to provide redundancy in measurement under the $N-1$ contingency criterion. Some of the most popular ones like Primary and Back-up Method [79], Integer Linear Programming-based method [80], Local

Redundancy Method [83] have been cited in the literature. But from the studies performed, it has been realized that for a system to have complete PMU-based observability and redundancy of all the buses present under the $N-1$ contingency criterion, a very large number of PMUs will be required. In the absence of conventional measurements, the number of PMUs required could well be higher than half the total number of buses present. It is obvious that no utility will place that many PMUs in their system. However, by using the concept of criticality developed here, it can be argued that in practice, it is sufficient to provide redundancy in measurement to *only* the critical buses of the network. If the critical buses are selected carefully, then by providing redundancy to their measurements alone, the system can be made sufficiently secure with much less PMUs. The algorithm developed for doing this is described in the next sub-section.

4.2.2 Proposed Algorithm – Critical Bus Based Binary Integer Optimization (CBBBIO)

The technique developed in this section uses the concept of "criticality" described in the previous sub-section with the depth of unobservability technique to determine the optimal scheme for PMU placement using binary integer programming. However, neither the traditional concept of depth of unobservability, nor the modified version that has been used in this work, "directly" take into account the redundancy in measurement of specific buses. This has to be done by modifying the constraints of the optimization. The number of PMUs needed for observing as well as providing redundancy in measurements of the critical buses, constitutes the *starting* set. That is, the number of PMUs in the starting set constitutes the highest depth of unobservability. To illustrate, if the number of PMUs in the starting set is n, then the proposed algorithm finds the depth of the bus that is farthest from the n buses where PMUs have been placed and assigns that depth to be the highest depth of unobservability. In subsequent steps, more PMUs are added to attain lower depths of unobservability until complete observability is eventually achieved.

The methodology proposed for determining the optimal PMU set is based on the extension of the binary integer optimization technique developed in [20]. For a system represented by its $N \times N$ incidence matrix $\boldsymbol{A}$, the 1–norm of a $N \times 1$ length binary integer matrix $\boldsymbol{X}$ must be minimized, where the nonzero elements of $\boldsymbol{X}$ denote the PMU locations. Two $N \times 1$ matrices are also defined: the initialization matrix $\boldsymbol{X}_{init}$ having only zero and unity as its elements of which the unity elements correspond to those buses where PMUs must be placed even at the highest depth of unobservability (that is, the *starting* set), and a matrix $\boldsymbol{f}$ all of whose elements are unity.

The *starting* set is created by following these steps:

1. Identify the critical buses of the network based on the logic developed in Section 4.2.1 and set the corresponding elements $\boldsymbol{X}_{init}$ of to one
2. Check if the first critical bus is connected to at least one other critical bus
3. If the critical bus is not connected to at least one other critical bus, then place a PMU at an adjoining bus and set the corresponding element of $\boldsymbol{X}_{init}$ to one
4. Repeat Steps 2 and 3 until all critical buses are connected to at least one other bus that has a PMU on it, thereby making the other bus critical as well
5. If all critical buses are connected to at least one other bus with a PMU on it, then the number of buses thus selected constitutes the starting set; terminate the process

Next, a matrix $\boldsymbol{f}_i$ is defined such that,

$$\boldsymbol{f}_i = \boldsymbol{f} - w\boldsymbol{X}_{init} \tag{4.12}$$

In (4.12), the scalar weight w has the function of guaranteeing priority in placement of PMUs on the critical buses. Any integer value of w greater than one will ensure priority to the critical buses. That is, as long as $w > 1$, the final solution will not be sensitive to the numerical value selected for w. The minimization criterion is now specified as:

$$\min_{\boldsymbol{X}} \left(\boldsymbol{f}_i{}^T . \boldsymbol{X} \right) \tag{4.13}$$

Equation (4.13) utilizes the scalar product to ensure that all the critical bus locations are preserved in the final solution as they have higher contribution towards the minimization. The constraints further imposed on (4.13) are:

$$\boldsymbol{M}\,\boldsymbol{X} \leq \boldsymbol{b} \tag{4.14}$$

$$\boldsymbol{M}_{eq} . \boldsymbol{X} = b_{eq} \tag{4.15}$$

In (4.14) and (4.15),

$$\begin{aligned} \boldsymbol{M} &= -\boldsymbol{A} \\ \boldsymbol{M}_{eq} &= \boldsymbol{X}_{init}^T \\ \boldsymbol{b} &= -\boldsymbol{f} \\ b_{eq} &= \text{Number of nonzero elements in } \boldsymbol{X}_{init} \end{aligned} \tag{4.16}$$

Equation (4.14) implies that each bus is observed by atleast one PMU [1], while (4.15) ensures that each critical bus will be assigned a PMU. Equations (4.13)-(4.16) are used to find the number of PMUs required for complete observability. In order to compute the number of PMUs required for higher depths of unobservability, (4.13)-(4.16) is used again, but with the following modifications,

$$\begin{aligned} \boldsymbol{M} &= -\text{signum}(\boldsymbol{A}^{n+1}) \\ \boldsymbol{M}_{eq} &= (\boldsymbol{f} - \boldsymbol{X}_{n-1})^T \\ b_{eq} &= 0 \end{aligned} \tag{4.17}$$

In (4.17), $\boldsymbol{X}_{n-1}$ is the optimal allocation matrix found for the $(n-1)^{th}$ depth of unobservability. Finally, the total number of PMUs required for an unobservability of depth n is given by,

$$\text{Number of PMUs at depth } n = \boldsymbol{f}^T.\boldsymbol{X}_n \tag{4.18}$$

The numerical value of the elements in $\boldsymbol{A}^{n+1}$ denotes the number of trajectories that link pairs of buses. However, for the placement of PMUs, this multiplicity is irrelevant [13]. As stated previously, the signum function eliminates path multiplicities and generates an equivalent incidence matrix valid for subsequent depths of unobservability [89]. This reduction in path multiplicity greatly reduces the inherent computational complexity of the optimization. Also, in (4.17), $\boldsymbol{M}_{eq}$ and b_{eq} are updated so that the equality constraint warrants no additional PMUs than those determined from previous depths of unobservability. Fig. 4.7 shows the flowchart of the proposed algorithm while the pseudo-code for performing the optimization is explained with an example in Appendix B. PMU allocation using this technique is found to provide real-time monitoring of the critical buses of the network with redundancy, as well as ensure complete system observability with reduced computational complexity. Since this methodology integrates the idea of critical buses with the binary integer programming logic, a suitable name for this technique was found to be Critical Bus Based Binary Integer Optimization (CBBBIO).

4.3 Simulations Performed

For testing the performance of the CBBBIO technique proposed in this chapter, a variety of power system networks were selected for analysis. The first set of simulations was performed on standard IEEE systems like the IEEE 118-bus system and the IEEE 300-bus system. A 283-bus model of the Central American Power Transmission System was analyzed next. The final simulation was performed on a 1196-bus network describing the Northern and the Eastern power grids of India. The results obtained on applying the proposed approach on these systems form the basis of this sub-section.

Fig. 4.7: Flowchart for the CBBBIO Technique

4.3.1 Standard IEEE Systems

The proposed algorithm was applied to the IEEE 118-bus and the IEEE 300-bus systems. For the first illustration, only the highest voltage buses were considered critical. By expressing the voltages in kV rather than in p.u., the highest voltage buses were identified directly from the system data. As these buses were connected to one another, redundancy under the $N-1$ contingency criterion was automatically ensured. In both systems, 345kV is found to be the highest voltage level present. The IEEE 118-bus system has eleven 345kV buses (8, 9, 10, 26, 30, 38, 63, 64, 65, 68, and 81), while the IEEE 300-bus system has fourteen 345kV buses (4, 16, 28, 33, 36, 40, 68, 169, 173, 174, 198, 210, 216, and 242). Therefore, the minimum number of PMUs required for complete observability of the two systems was 11 and 14 respectively. This became the starting set for the proposed PMU placement technique.

Table 4.1 gives a comparison of the number of PMUs required at different depths of unobservability without and with the consideration of critical buses. In Table 4.1, the traditional method used for computing the number of buses on which PMUs must be placed for different depths of unobservability is based on the algorithm developed in [13]. The computations were performed on an Intel (R) Core™ i5 Processor having a speed of 2.40 GHz and an installed memory (RAM) of 5.86 GB. The advantage of using the signum function in the proposed algorithm was also realized during this simulation. It was observed that when the signum function was removed from (4.6), the time required for computing the sixteen depths of unobservability for the IEEE 118-bus system (given in Table 4.1) was 23.29 seconds instead of the 0.73 seconds that the same machine took when the signum function was in place. Thus, it was confirmed that by removing the path multiplicities using the signum function, the inherent computational complexity of the optimization is greatly reduced.

For the second illustration, along with the highest voltage buses, the buses having high connectivity were also considered critical. As stated in Section 4.2.1, the criteria for selecting high connectivity buses is subjective and system specific. It can include buses which are connected to many other buses, substations where communication related expansions can be easily carried out, as well as buses that cater to utility preferences. For these two systems, it was assumed that the cost for developing communication facilities was equal for all the buses and that there were no utility specific preferences. Therefore, the high connectivity buses were selected purely on the basis of the number of connections that the buses had.

Table 4.1: Comparison of proposed algorithm with the traditional method when only high voltage buses are considered critical

Depths of Unobservability	IEEE 118-Bus System		IEEE 300-Bus System	
	Not Considering any bus as Critical [13]	Considering highest voltage buses as critical	Not Considering any bus as Critical [13]	Considering highest voltage buses as critical
0	32	39	87	96
1	16	23	47	55
2	8	17	34	41
3	7	13	19	29
4	4	13	14	24
5	3	12	9	20
6	2	11	8	18
7	2		7	16
8	2		5	15
9	2		3	15
10	1		3	15
11			3	14
12			2	
13			2	
14			2	
15			2	
16			1	
CPU Time (in seconds)	0.73	0.40	4.04	4.42

From a study of the incidence matrix for the IEEE 118-bus system, it was observed that ten buses had six or more connections; whereas, only four buses had seven or more connections. Therefore, it was logical to define the number of buses having seven or more connections as the critical high connectivity buses. Thus, 12, 49, 80 and 100 were identified as high connectivity buses resulting in the total number of

critical buses for this system becoming 15. In order to provide redundancy in measurements to these high connectivity buses, PMUs were added to buses 11, 66 and 92. Although other buses would have sufficed, these three were chosen because they had high connectivity (like bus 11), they were connected to two different critical buses (like bus 66), they had generators on them (which was important from control perspectives), or a combination of the above (like bus 92). It is to be noted here that the criterion of "best" adjoining bus to place a PMU has been intentionally kept flexible so as to incorporate a wide variety of practical constraints. Thus, the minimum number of PMUs for the starting set for the IEEE 118-bus system was 18.

On doing a similar analysis for the IEEE 300-bus system, nine buses were found to have seven or more connections; whereas, only four buses had eight or more connections. Thus, the four buses which had eight or more connections (31, 109, 190 and 268) were considered critical high connectivity buses with 15, 147, 177 and 272 acting as the buses providing redundancy to those measurements. Thus, the minimum number of PMUs for the starting set for the IEEE 300-bus system became 22. Table 4.2 shows the number of PMUs required at different depths of unobservability for the two systems in accordance with the proposed scheme.

Table 4.2: Number of PMUs at different depths of unobservability when high voltage and high connectivity buses are considered critical

Depths of Unobservability	IEEE 118-Bus System	IEEE 300-Bus System
0	41	97
1	26	59
2	22	43
3	18	34
4		30
5		25
6		24
7		22

CPU Time (in seconds)	0.29	2.36

From Tables 4.1 and 4.2, it can be inferred that an increase in the number of PMUs required for complete observability corresponding to an increase in the number of critical buses, is an almost linear relationship. That is, a small increase in the number of critical buses *does not* result in a large increase in the number of PMUs required for complete observability. This is a very important observation because it ensures that even if the number of critical buses is increased, the minimum number of PMUs required would not increase exponentially.

Table 4.3 compares the total number of PMUs required for complete observability of the IEEE 118-bus system in absence of conventional measurements using the proposed methodology and other similar algorithms. For the comparison done in Table 4.3, Zero Injection (ZI) buses were considered for PMU placement. ZI buses are those buses that are present in the system, but from which no power is injected into the system. In the proposed approach, unless the ZI bus was a critical bus, it was removed from the system and the incidence matrix was updated accordingly. The ZI buses for the IEEE 118-bus system are: 5, 9, 30, 37, 38, 63, 64, 68, 71, and 81. Out of these ten buses, as buses 5, 37 and 71 do not fall in the list of critical buses identified previously, in the proposed approach, these three buses were removed from the system.

Table 4.3: Minimum number of PMUs for complete observability under $N-1$ criterion, in absence of conventional measurements for IEEE 118-bus system

	Primary and Back-up Method [79]	Integer Linear Programming [80]	Local Redundancy Method [83]	CBBBIO Technique
Number of PMUs	65	64	61	39

In the proposed approach, redundancy is provided to the measurements of *only* the critical buses (high voltage and high connectivity buses). This is the reason for the significant difference in the total number of PMUs required. Thus, from Table 4.3 it becomes clear that by using the proposed approach, an intelligent choice of critical buses can provide an optimal cost-benefit ratio with respect to PMU placement. In the next sections, more diverse methods for selecting the critical buses are explored. Two real-life models – a reduced order model of the Central American power transmission system and a 1196-bus model of the North and East Indian power transmission network are used for the analysis.

4.3.2 Central American Power Transmission Network

The Central American region has an inter-connected transmission system that links the electrical power systems of six countries, namely, Guatemala, El Salvador, Honduras, Nicaragua, Costa Rica and Panama. This transmission corridor is presently operating at a voltage level of 230kV. Recently, a transmission line at 400 kV has been established between Guatemala and Mexico, and another high voltage line between Panama and Colombia is under study [93]. Fig. 4.8 shows the 230kV transmission system which is the backbone of the Central American Power System (CAPS) [94]. This network consists of 1,588 nodes, and handles around 6,400 MW in a deregulated regional energy market, coordinated by the Regional Operating Entity (EOR). The geography of the Central American isthmus forces the regional transmission grid to have an inherently radial topology, comprising approximately 1,900 km in a single transmission line trajectory from the North to the South [20].

This system had several outages in the past decade mainly due to loss of generation blocks and from tripping of critical tie-lines. The loss of a 200 MW generator block in Honduras on June 13, 2010 resulted in a multi-national blackout [95]. The loss of two 230 kV lines due to a lightning-strike on September 9, 2010 caused a severe power outage in Honduras, Nicaragua and El Salvador [96]. Currently the CAPS has no PMUs installed at any of its buses. This lack of synchronized measurements makes it very difficult for the system to cope with such contingencies. The implementation of PMUs can solve many of the problems that the CAPS currently suffers from. Small signal, inter-area oscillations can be better damped by re-tuning the PSSs using remote measurements. Voltage collapses in non-metered radial substations can be prevented by intelligent load shedding schemes. Accurate transmission line models using synchronized measurements of strategic buses can give rise to correct state estimations. Bottlenecks can be monitored to ensure optimal use of the transmission capabilities, and the settings for protection and control systems can be precisely determined based on realistic system models. This role that PMUs can play in solving and/or mitigating different exigencies of the CAPS is described below.

- Erroneous Tripping: It is expected that in the event of a sudden loss of a block of generation or load in a particular country, the tie-lines that connect the affected system to the neighboring systems will become stressed. This will result in an increase in power flow through some of the lines which will cause them to be over-charged for certain periods of time. If this over-charge is below the threshold limit of the lines, it should be endured under the existing contingency conditions to prevent cascade tripping and subsequent outage of larger portions of the system.

In such a situation, PMU measurements can be used to develop an adaptive protection scheme aimed at reducing the likelihood of manifestation of hidden failures and potential cascading events by adjusting the security/dependability balance of protection systems [12].

- Voltage Collapse: Although the tie to Mexico has helped in stabilizing the system, under critical conditions like the ones described in [95], [96], it has been observed that the increased power flow coming from Mexico, while crossing a country to supply the load unbalance of another country, has caused an increased consumption of reactive power in the country that is being crossed over. This causes a dramatic voltage drop of the country in the transfer path which forces that country to trip the tie-lines, in order to avoid its own voltage collapse. These circumstances can be prevented by applying intelligent load shedding schemes based on synchronized measurements obtained from PMUs.
- Transient Instability: In Central America an important amount of generation comes from bunker plants. These machines usually possess low inertia constants, making them prone to loss-in-synchronism under sudden losses of generation blocks. This out-of-step condition can be detected promptly by PMUs, which can then be used for generating appropriate actions so as to isolate the load-generation imbalances. Once stabilized, PMUs can help in bringing the isolated sections back to the system.
- Small Signal Oscillations: The radial topology of the CAPS is prone to inadequate damping or negative damping of small signal, inter-area oscillations. In the past these kinds of oscillations have occurred between hydroelectric machines in Panama, Honduras and Guatemala, forcing the installation of PSSs in the participating generators. After the inter-connection with Mexico, new inter-area oscillations have emerged in the system. For handling such cases, PMUs can provide remote measurements which can be used for re-tuning the PSSs so as to improve their effectiveness. In future, WAMS can also be used for developing a coordinated type of control using PSSs, SVCs etc. to damp all low frequency oscillations as developed in [14]-[17], [97].

From the above description, it becomes clear that the computation of an optimal PMU placement scheme for CAPS is a multi-objective optimization function. This can be accomplished using the CBBBIO technique very effectively as shown below. In this system, the two highest voltage levels are 230kV and 138kV. The transmission network also comprises of few 69kV elements, culminating in a total of 283 buses and 365 links. The determination of critical buses for this system can be done based on the criteria outlined in Section 4.2.1.

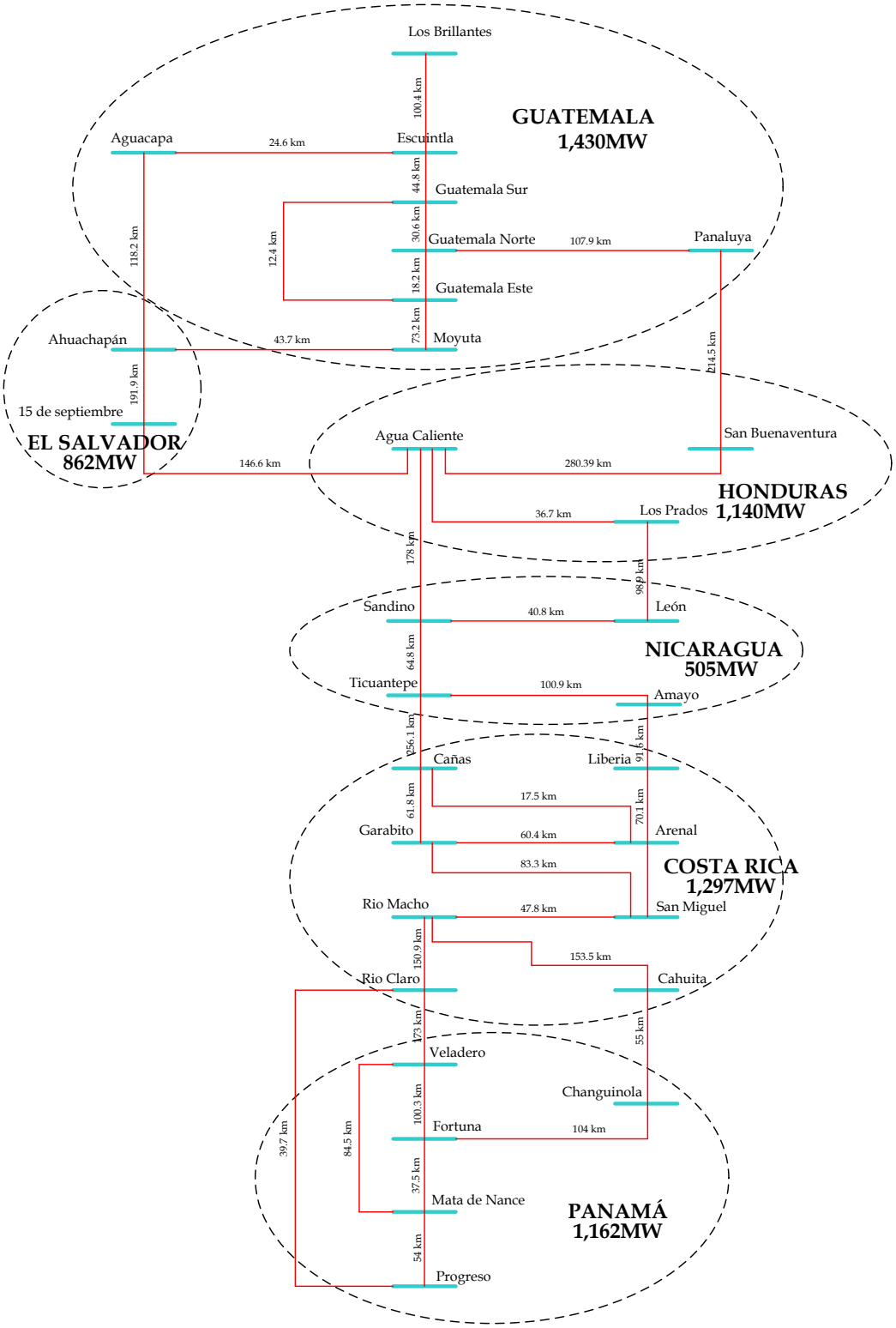

Fig. 4.8: Backbone transmission links of the CAPS

The critical buses of the Central American Power System (CAPS) are:

- High connectivity buses: Eight buses were labeled as critical buses for having the highest connectivity (comprising of 6 or more links to other buses). These buses were also found to have good communication facilities and high energy concentrations.
- Buses relevant for transient stability: From a transient analysis point of view, those buses which were electrically closest to generation units and which lost synchronism when a three phase fault lasting for less than six cycles took place in any element of the network were considered critical. Three phase faults were simulated as they were the most severe of all transient events. A critical time of 100ms (six cycles) was assumed to be the typical time period needed to isolate the fault. Based on the list of contingencies provided in [98], it was found that only one contingency had a critical time of less than 6 cycles, which resulted in two generators being selected.
- Buses relevant for small signal stability: After performing small signal analysis on this network, ten generators were found to have high participation factors and low damping ratios for the inter area modes of oscillation present in this system. The corresponding transmission buses were identified to be critical to facilitate PMU-based control applications.
- Buses relevant for preventing voltage collapse: Four transmission buses having operational voltages below 0.95 p.u. were identified as critical buses for their facility to monitor potential voltage instability in radial areas.

The total number of critical buses identified for the Central American system was 24. By initially placing PMUs on these 24 buses, it was observed that 19 critical buses already had redundancy in their measurements. PMUs were placed on five other buses to provide redundancy to the remaining critical buses resulting in a total of 29 critical or redundancy exclusive buses. Applying the algorithm developed in Section 4.1.2, and taking into consideration those 29 critical buses, 101 PMUs were found to be required for complete network observability with $N-1$ redundancy of the critical buses. Table 4.4 illustrates the number of PMUs required at different depths of unobservability for this network. From Table 4.4, it becomes clear that although 87 PMUs provide complete observability to the Central American Transmission System, they do not guarantee an optimal PMU placement as far as dynamics and practical constraints are concerned. However, by following the proposed approach and adding PMUs in select locations, one can make the Central American system much more robust.

Table 4.4: Number of PMUs required at different depths of unobservability when redundancy of critical buses is considered for the Central American Power Transmission Network

Depths of Unobservability	Central American Power System (283 buses)	
	Not Considering any buses as Critical	Considering critical buses with redundancy
0	87	101
1	61	67
2	37	47
3	24	37
4	13	33
5	11	32
6	9	30
7	8	30
8	6	29
9	5	
10	5	
11	5	
12	5	
13	4	
14	1	

CPU Time (seconds)	3.07	2.27

4.3.3 North and East Indian Power Transmission Network

The map of the complete power transmission system of India is shown in Fig. 4.9 [99]. It is composed of five regional grids – the Northern region (NR) grid, the Eastern region (ER) grid, the North-Eastern region (NE) grid, the Western region (WR) grid, and the Southern region (SR) grid. In this study, PMU placement was analyzed for the power system networks of the Northern and the Eastern region grids (henceforth, called North and East Indian power system network). This system comprises of the power system networks located in the North and East of India and contains 1196 buses.

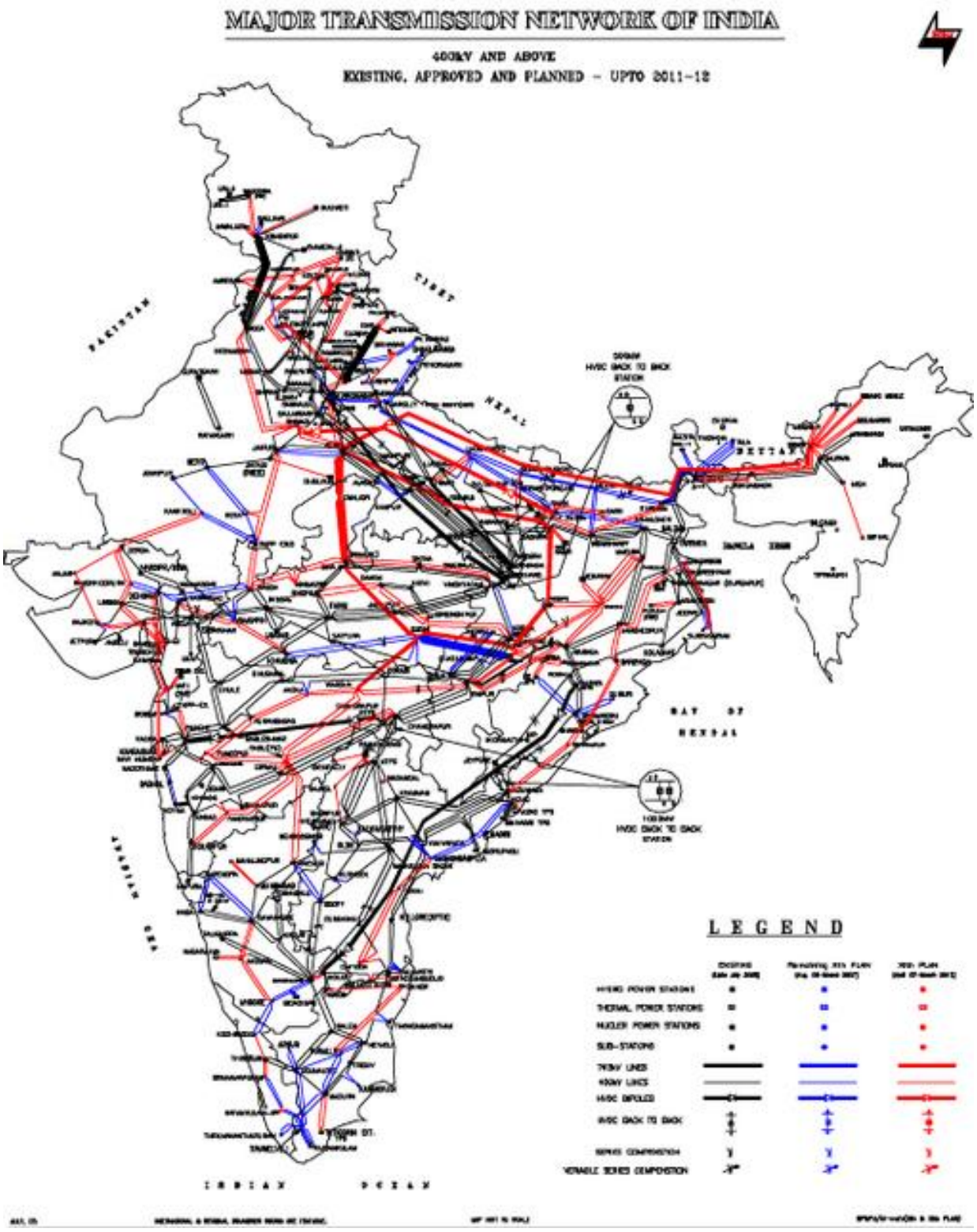

Fig. 4.9: Indian Power Transmission Network

Information about this system was made available in the form of PSS/E models [100]. As is typical of system information obtained from commercial packages, they include “virtual/dummy buses” that do not physically exist and/or are not practical locations to install metering devices [100]. Typical examples of such buses are tapped line buses, series capacitor nodes, disconnected buses, etc. Before performing any PMU placement study, such virtual/dummy buses must be removed from the available system models. The methodology followed for eliminating virtual buses from the model of the North and East Indian power transmission system is based on the logic developed in [102]. It is briefly described as follows –

- Tapped lines: Tapped lines create a bus in the middle of a branch where there are no measurement facilities to monitor the signals. For a virtual bus at a tapped line, the bus created by the tapped line and the branches connecting the tap to rest of the system are removed and equivalent injections are added on the adjoining buses.
- Virtual generators: These are equivalent generators connected to the system by a virtual (non-existing) bus. Such virtual buses connecting equivalent generators to the rest of the system are removed and replaced by equivalent injections.
- Shunt elements: For convenience of analysis, shunt circuits are often modeled as virtual buses. But since physically they are present on the actual bus, if a virtual bus connects to a shunt element, the virtual bus and the shunt element are removed and the combination is replaced by a corresponding injection on the actual bus.
- Series capacitors: Series capacitors are modeled with virtual buses, which physically do not exist. Hence, if a virtual bus connects to a series capacitor (regardless of the capacitor line location) the bus and the two connecting branches are removed and the combination is replaced by an equivalent branch.
- Distinction between bus and substation: During model-based analysis of a system, transformers separating different voltage levels are treated as separate buses. However, when placing PMUs, it is assumed that a PMU placed at a substation will monitor all the transformers at that substation. Therefore, at a given substation it is presumed that multiple-voltage levels/lines are monitored by a single PMU. This assumption is not a good assumption for practical installations and needs to be analyzed in greater depth. However, the study that needs to be done to *better* this assumption is beyond the scope of this work.

- Three winding transformers: Three winding transformers are typically modeled as three 2-winding transformers with one side in common. In per unit, the three buses represent the same voltage and so could be monitored by a single PMU. Thus, if a virtual bus is the middle point of a three winding transformer, then the corresponding three winding transformer is replaced by a single bus. This bus is then connected to the buses originally connecting the middle and high voltage windings.
- Disconnected buses: Some buses in the model are not connected to any other bus of the system. Such stand-alone buses are removed without making any other change in the network.

On applying the above-mentioned virtual/dummy bus elimination logic to the North and East Indian Power Transmission Network, the total number of buses was reduced from 1196 to 996. The critical buses of this network were then found out based on the criteria outlined in Section 4.2.1 with the details highlighted as shown below –

- Highest voltage buses: As 765kV was the highest voltage present in this network; all active buses having this voltage were selected as the relevant high voltage buses of the system. The total number of these buses was 19.
- High connectivity buses: Buses having ten or more connections were identified as high connectivity buses. The total number of these buses was 16.
- Buses relevant for small signal stability: Buses having high participation towards the control of the low frequency inter area modes of oscillation were considered critical for small signal stability analysis. The total number of these buses was 12.
- Low voltage load buses: Load buses having voltages of less than 0.90 p.u. were identified as critical buses. The total number of these buses was 10.
- Buses connected to DC lines: AC Buses connected to either ends of the DC lines were identified as important from control perspectives and were therefore considered to be critical buses for this analysis. The total number of these buses was 8.

Once the critical buses of the system were identified, the size of the system was reduced further by eliminating the ZI buses present in the system. Similar to what was done for the IEEE 118-bus system in Table 4.3, unless the ZI bus of the North and East Indian system was a critical bus, it was removed from the system. The number of critical ZI buses was 27, while the number of ZI buses eliminated from the system was 246. Consequently, the system was reduced from a 996-Bus model to a 750-Bus model with

a total of 65 buses recognized as critical buses. 56 of these 65 critical buses were observed to be connected to atleast one other critical bus. PMUs were then placed on nine more buses to provide redundancy to the remaining critical buses resulting in a total of 74 critical buses. A total of 208 PMUs were found to be needed for this system to ensure complete observability with redundancy in measurement of the critical buses. Table 4.5 summarizes the placement of PMUs at different depths of unobservability for this system.

Table 4.5: Number of PMUs required at different depths of unobservability when redundancy of critical buses is considered for the North and East Indian Power System

Depths of Unobservability	North and East Indian Transmission System (750 buses)	
	Not Considering any buses as Critical	Considering critical buses with redundancy
0	161	208
1	80	131
2	41	92
3	20	77
4	9	74
5	7	
6	3	
7	3	
8	2	
9	1	

CPU Time (seconds)	3674.98	3675.58

From Table 4.5 it can be realized that for the North and East Indian system, by adding 47 PMUs more than the ones needed for basic observability, one can ensure an optimum balance between cost and intended PMU applications. Moreover, from the results, it is also implied that by placing PMUs at 208 locations of this system, one can effectively monitor and control the reduced 750-Bus system and through it, the entire 996-Bus network. Thus, by placing PMUs on less than one-third of the buses for the reduced system and approximately one-fifth of the buses of the full system, an excellent knowledge

of the state of the complete network can be obtained. The results obtained in this section indicate that irrespective of the way in which the critical buses are chosen, they can be incorporated into the proposed methodology to find an optimal PMU placement scheme that will ensure real-time monitoring of the key regions of any system.

4.4 The 2012 Blackout in India

In one of the worst blackouts in power system history, two separate events on 30 and 31 July, 2012 resulted in over 620 million people of India losing power. The outages were spread across 22 states in Northern, Eastern, and North-Eastern regions with an estimated 48 GW of load being affected in its wake. The Northern Region (NR) grid was affected by the blackout on 30 July; whereas the Northern Region (NR) grid, Eastern Region (ER) grid, and the North-Eastern Region (NER) grid were affected by the blackout that occurred on 31 July. A map of the affected regions is provided in Fig. 4.10 [103].

The initiating event on both occasions was the tripping of the 400kV Bina-Gwalior line on zone 3 protection of distance relays. The corresponding rerouting of power resulted in cascade tripping of the tie-lines along the interfaces of the different regions. The eventual collapse of the grids in the individual regions due to multiple tripping was attributed to internal power swings, under frequency and overvoltage at different places [103]. Thus, the factors leading to the grid disturbance on both occasions can be grouped under:

- Loss of balance between security and dependability [62]
- Absence of real-time system visibility
- Inadequate contingency analysis

A brief sequence of events following the initiating event for both the days is provided as follows [103]. On 30th July, 2012, after the NR got separated from the WR due to tripping of the 400kV Bina-Gwalior line, the NR loads were met through WR-ER-NR route, which caused power swing in the system. Since the center of swing was in the NR-ER interface, the corresponding tie-lines tripped, isolating the NR system from the rest of the NEW grid system. The NR grid system collapsed due to under-frequency and further power swing within the region.

On 31st July, 2012, after NR got separated from the WR due to tripping of 400kV Bina-Gwalior line, the NR loads were met through WR-ER-NR route, which caused power swing in the system. On this day the center of swing was in the ER, near ER-WR interface, and, hence, after tripping of lines in the ER itself, a

small part of ER (Ranchi and Rourkela), along with WR, got isolated from the rest of the NEW grid. This caused power swing in the NR-ER interface and resulted in further separation of the NR from the ER-NER system. Subsequently, all the three grids (NR, ER, and NER) collapsed due to multiple tripping attributed to the internal power swings, under-frequency and over-voltage at different places.

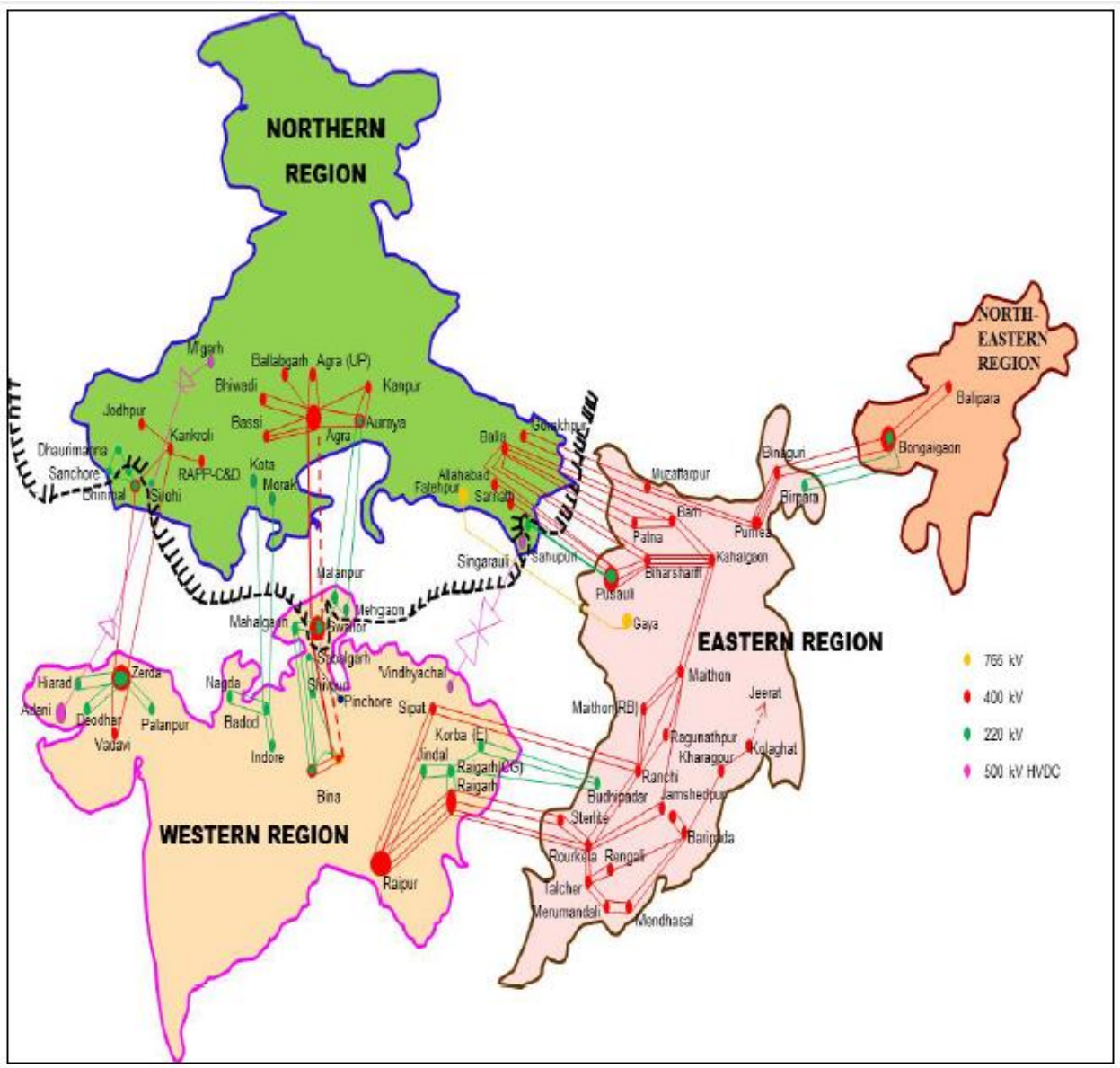

Fig. 4.10: Map indicating the inter-regional links

A PMU-based wide areas measurement system (WAMS) will play a key role in making the Indian grid smarter. It will improve visibility and provide real time monitoring, protection, and control of the system [104]. Intelligent load shedding schemes, modern dynamic security assessment techniques, and

security/dependability based adaptive protection schemes are some of the ways in which PMUs can improve the reliability of the Indian grid. Some of the PMU-based applications that could have saved the system from the July 2012 collapse are summarized below:

- Measures to avoid misoperation/maloperation of protective relays: The blackouts followed immediately after a zone 3 operation on the Bina-Gwalior line. The implementation of a PMU-based security/dependability adaptive protection scheme [12] would have prevented that from occurring.
- Faster dynamic security assessment: The lack of proper frequency control processes was responsible for both the blackouts. An efficient deployment of PMUs could track frequency accurately across the network and generate alarms when the system starts becoming unstable. A variety of Remedial Action Schemes (RAS) based on PMU measurements can also be implemented.
- Intelligent load shedding schemes: The implementation of frequency and df/dt based load shedding schemes can be easily done using WAMS [105].
- Accurate state estimation: Imprecise state estimation played a central role in the blackouts. This can be greatly improved through the proposed PMU placement scheme using which measurements obtained from optimally located PMUs can be combined with traditional state estimators [67].
- Faster Island detection: The cascade tripping following outage of the Bina-Gwalior line resulted in the different regional grids separating from each other. Faster island detection schemes using PMUs [106] would allow for prompt island identification, stabilization of the islands formed and a more efficient system restoration.

As [103] states, an appropriate deployment of PMUs is highly recommended to prevent events similar to the July 2012 India blackouts. This chapter provides guidelines for creating an effective and efficient PMU deployment strategy. By placing PMUs on generators which are more vulnerable to frequency swings and selecting locations which will quickly pick up on growing instabilities (when they occur), a set of critical buses can be identified. With these critical buses forming the starting set, the proposed methodology can be used to find an optimized PMU placement set that will prevent/minimize the effects of such events.

4.5 Conclusion

A PMU placement scheme has been developed in this chapter which takes into account the monitoring and protection of important buses of the system while moving towards complete observability of the network. When applying analytical or graphical methods to determine the optimal number of PMUs for complete observability of a system, it is realized that not all buses possess the same degree of preference from the techno-economic perspective. In this sense, priority should be given to high voltage buses, high connectivity buses, buses with good communication facilities etc. Similarly, buses more relevant to the transient and dynamic stability of the system have higher priority than those with less relevance. This chapter uses this logic to create a set of critical buses where PMUs must be installed first before going for complete observability. The proposed scheme also provides redundancy in measurement of these selected buses under the $N-1$ criterion.

The proposed algorithm has been applied to two standard test systems as well as two real power system networks. The ways in which the proposed methodology might have avoided/ minimized the impact of a real-life blackout is also described. The buses identified as critical to the system are observed even at the highest depth of unobservability. The increased number of PMUs required for complete observability is more than compensated by the added benefit of providing redundancy in measurement to the critical buses of the system. The technique is simple, efficient and easily applicable to large power system problems. The methodology developed here is expected to provide flexibility to utilities in the implementation of their PMU placement scheme. The locations where PMUs have already been placed in the system based on previous studies and utility needs can be integrated into the proposed scheme under the definition of critical buses. Finally, the utilities are provided with the option that if they wish to remain at a certain depth of unobservability and not go for complete observability or delay their plans for it due to practical constraints; they are atleast assured that the vital segments of their system are protected.

Chapter 5: A Community-Based Partitioning Approach for PMU Placement in Large Systems

In the previous chapter, a PMU placement methodology was developed for generic systems. It involved combining the "critical" bus concept with "depth of unobservability" and "binary integer programming" to compute for an optimal PMU placement scheme. The results indicated that using the CBBBIO technique a utility would be able to deploy PMUs at select locations within the network over some period of time so as to eventually observe the whole system. However, in the course of that analysis, it was also observed that the computational complexity of the optimization limits the applicability of such techniques to large power system networks.

In this chapter, a PMU placement scheme is presented that ensures complete observability of large systems while reducing the computational burden of the optimization. The proposed methodology also provides redundancy in measurement of the critical buses of the network that are identified based on system studies/topologies. The community-based islanding approach used here initially partitions the system into smaller islands. Placement of PMUs in these islands is then computed using binary integer programming. A bound is also developed to compute for the maximum error from an optimal solution. The proposed technique has been applied to standard IEEE systems as well as on more realistic power system network models. The results show that the community-based partitioning approach enables the CBBBIO technique to be applied to any sized system.

5.1 PMU placement in large systems

Now that a synchrophasor-only state estimator is becoming a reality [28], it is clear that more and more PMUs will be installed in the power grid. It is believed that PMUs/dual purpose line relays in the order of thousands will be introduced in the US power system in the next few years [107]. China plans to have PMUs installed on all of its high voltage substations. The six countries in Central America are also installing PMUs in their inter-connected networks [20]. India plans to add many more PMUs to its national grids in the near future. With this over-abundance of PMUs in the network, it is essential to develop a technique that can efficiently compute PMU placements in large systems.

As stated previously, a variety of mathematical tools have been proposed by researchers to perform the optimizations for computing an optimal PMU placement scheme for generic systems [76]-[86]. However,

the two primary problems which have led to the downfall of most of these techniques as far as implementation in large systems is concerned are:

1. The diversity of applications, and
2. The computational burden of the optimization

Reference [18] states that on the basis of applications there are two methods followed by power engineers for placing PMUs in a system:

a) Development of a prioritized list of placement sites based on observability, and
b) Measurements are placed to correctly represent critical dynamics of the system

However, as stated in the previous chapter, the first method is concerned with state estimation and so does not take into account transient and dynamic stability of the system, while the second approach does not consider complete observability as one of its priorities. The CBBBIO technique developed in the previous chapter reconciled these two approaches by initially placing PMUs on the critical buses of the network identified on the basis of system studies/topologies and then computing for the optimal number of PMUs required for complete system observability. However, the problem of heavy computational burden was still found to persist. This is particularly relevant for large power system networks (> 500 buses), because in such networks it's computationally cumbersome to *directly* compute for an optimal PMU placement scheme using traditional methods. Moreover, if the locations are not chosen judiciously, then the large amounts of data that will be collected will cause network congestion in downstream applications [108].

This chapter tries to address the issue of PMU placement in large systems by introducing a community-based islanding approach [109] that partitions the system into smaller islands. The concept of "critical buses" proposed in the previous chapter is then used to find the optimal PMU placement scheme in the resulting islands. A bound is also developed to compute the maximum error from an optimal solution. The proposed technique is initially applied to standard IEEE systems and then tested on larger and more realistic power system networks, such as a 283-bus model of the Central American system, a 1064-bus model of the Dominion Virginia Power (DVP) system, a 1133-bus model of the Indian system, and a 1443-bus model of the Brazilian Power System. The results indicate that the methodology developed here is a logical approach that yields good solutions for large systems.

5.2 Community-based islanding

An interesting analysis was done in [109] for finding and evaluating community structure in general networks. The dictionary definition of a "community" is a group of individuals living in a particular area and having a common interest [110]. In the world of graphs, this translates to a group of nodes inside a network within which the network connections are high, but between which, they are low. Examples of this in the power system will be different utilities operating under an independent system operator (ISO) or, regional grids belonging to distant geographic regions that are connected by tie-lines. Fig. 5.1 shows communities that can be present in a graph. In Fig. 5.1, the thicker black lines denote edges that connect different communities. The goal is to identify these inter-community edges so that by eliminating them, the network can be partitioned into islands. In this chapter it is shown how the methodology developed in [109] can be used to address the PMU placement problem.

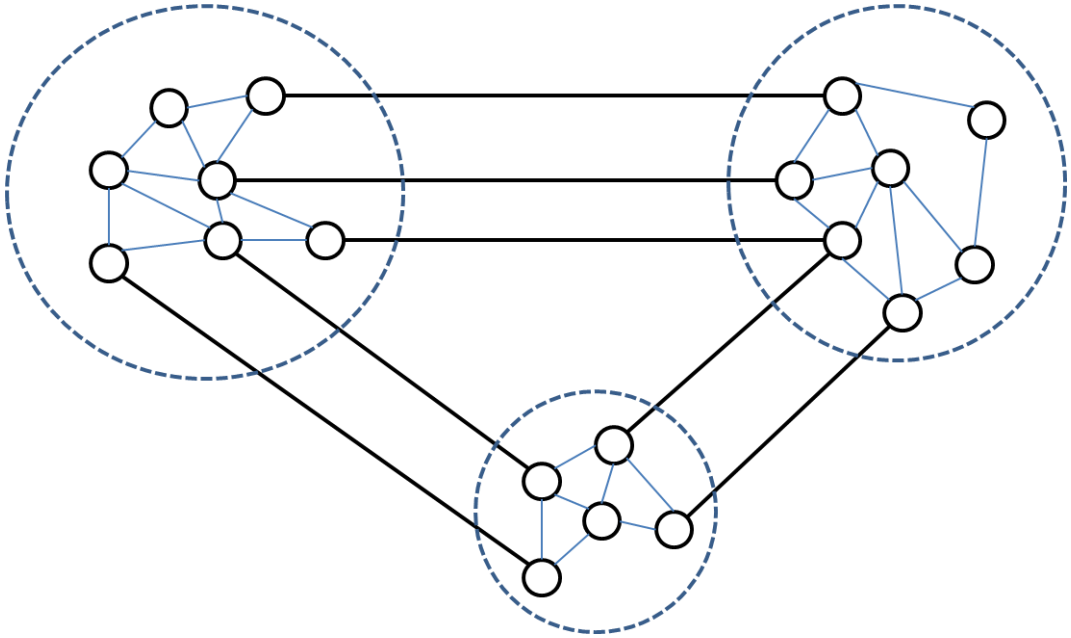

Fig. 5.1: Communities in a graph

Developing an optimal PMU placement scheme in a large power system network is a computationally intensive task. Fig. 5.2 shows an example of how the computational burden can increase as the size of the system increases. In Fig. 5.2, X-axis denotes the number of buses present while the Y-axis depicts the time required (in seconds) for computing the optimization using the Integer Programming algorithm developed in [1]. The computations were performed on an Intel (R) Core™ i5 Processor having a speed of 2.40 GHz and an installed memory (RAM) of 5.86 GB. Power system networks ranging from 14 buses

to more than 1400 buses were analyzed to create the plot. It is believed that although other techniques used for computing optimal PMU placement will give different values, the general trend with respect to system size will remain the same for all of them.

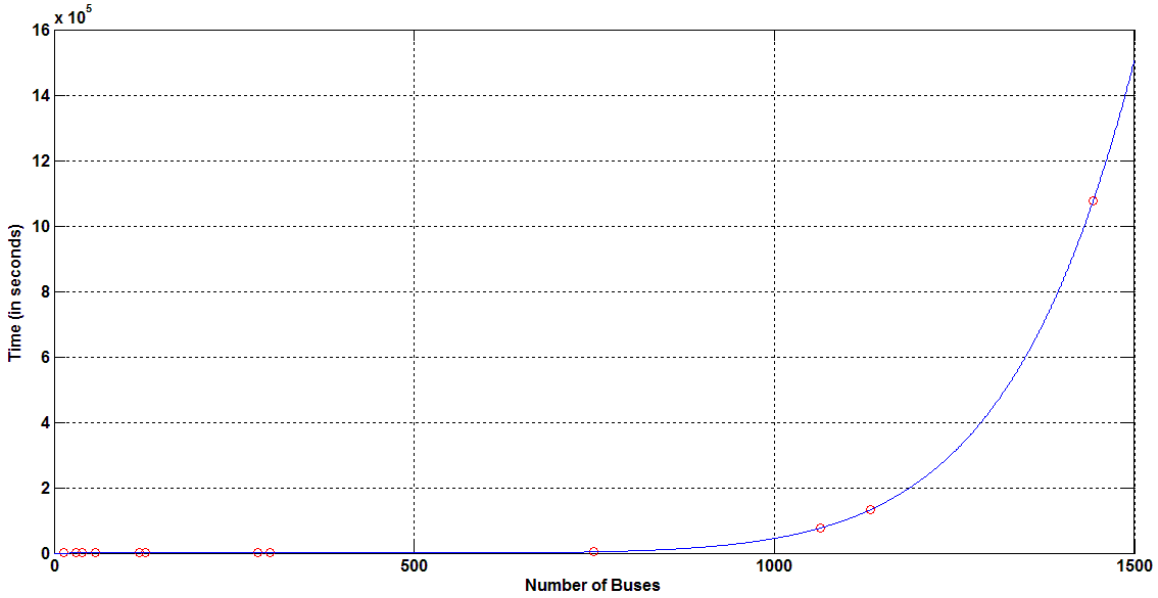

Fig. 5.2: Indication of the computational burden of the optimization

The reason for the time vs. number of buses plot being an exponential one (as seen in Fig. 5.2) is that the algorithms tend to solve the problem by searching through all possible solutions for a given system model in order to find the optimal solution. For a n bus system such a brute force approach would require a worst-case time of $O(2^n)$. The reason being that for every new node that is added, there will be two possibilities-whether it will have a PMU on it, or whether it will not. Moreover, since for both the possibilities, the rest of the nodes also need to be analyzed, the total worst-case time will become $O(2^n)$. Therefore, as the size of the system increases, the required computational effort increases exponentially. A pre-processing method for effective PMU placement studies was developed in [111]. However, that approach resulted in the system losing its initial structure/topology to such an extent that it became almost impossible to accurately retrace the results back to the original system [13]. The technique developed in this chapter shows how PMU placement can be done in large systems without significantly affecting the system's basic structure/topology.

The idea of partitioning a system into smaller sub-systems provides an elegant solution to the PMU placement problem. The locations where PMUs must be placed are usually computed in the planning stages. But, for large systems, it is not practically feasible to directly compute for an optimal PMU

placement scheme. In order to circumvent this problem, engineers create reduced-order models of their networks (by making various assumptions), and then perform the optimization. However, by partitioning a large system into islands, PMUs can be placed at the desired locations without any pre/post-processing or making any assumptions. Apart from facilitating placement of PMUs, another use of the community-based islanding approach could be in the placement of phasor data concentrators (PDCs). Since PDCs compile signals from several PMUs, by using the partitioning logic, a cluster of PMUs can be identified such that over-all latency and/or other communications issues are minimized.

The community based partitioning logic is illustrated as follows. Let us have a network of n nodes. We now break this network into k sub-networks having at most m nodes each by removing a certain number of edges. Once we do that, we have k islands each having m nodes or less in them. Then, the optimization problem for the individual islands will have a worst-case time of $O(2^m)$. Similarly, the worst-case time for computing the optimization for all the islands would be $O(k \times 2^m)$. Now, as m can be made a lot smaller than n (by increasing the number of partitions k), the worst-case time can be reduced by a significant amount. An example of this is provided in Fig. 5.3. In Fig. 5.3, $m = n/k$ and so the worst-case time for computing for the optimal PMU placement in the created islands will be,

$$\mathrm{T}_{\mathrm{worst-case}} = \mathrm{k} \times 2^{\left(\frac{\mathrm{n}}{\mathrm{k}}\right)} \tag{5.1}$$

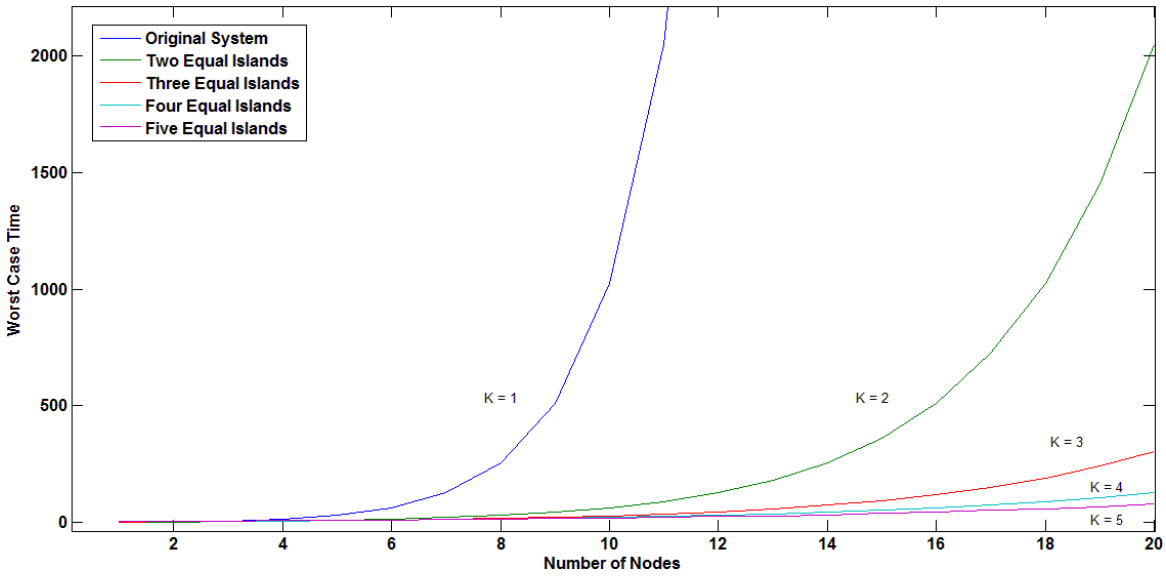

Fig. 5.3: Variation of worst-case time with number of nodes for different values of k

In accordance with (5.1), Fig. 5.3 shows that while the original system takes more than 1000 seconds for a 10-node system, the same system when partitioned into five equal islands takes less than 100 seconds. Thus, by partitioning the system into islands ($k > 1$), the computation times can be greatly reduced. Another inference that is drawn from this analysis is that by partitioning the system into smaller islands, the increase in computational burden with increase in number of nodes is almost linear (and not exponential). This is realized from a study of the slopes for $k = 1$ (blue line) and $k = 5$ (magenta line). Thus, by partitioning the system into independent islands, computational advantage is attained without significant alteration of the structure of the original system.

5.3 Computation of bound

The community-based islanding approach provides a "shortcut" to the PMU placement problem. However, the cost of using this shortcut is the "distance" from an optimal PMU placement solution. When a system is partitioned into islands, it is done so by removing edges from the network. Removing an edge results in loss of "visibility" of the nodes between which the edge initially lay. Now, as more and more edges are removed to form islands, it is likely that nodes which might have been optimal locations for placing PMUs in the original network would no longer be optimal locations in the created islands. Therefore, it is possible that the total number of PMUs required for complete observability of the individual islands is more than the number of PMUs required for complete observability of the original system. This increase in the number of PMUs required is defined as the "distance" from an optimal solution. Under such circumstances, it becomes necessary to compute for a "bound" on the furthest "distance" from an optimal solution that will be achieved by partitioning the system. This is developed as follows.

In order to find the reason behind the need for more PMUs in the created islands, the optimal PMU placement locations of the original system needs to be analyzed. In order to do that, let us start with a network of n nodes that needs the removal of an edge between node i and node j to form islands. Then, based on the optimal PMU placement scheme of the original system, the following four situations may arise –

- Neither node i nor node j have PMUs on them
- Both node i and node j have PMUs on them
- One of the nodes (say node i) has a PMU on it, but that PMU is not the only way in which the other node (node j) is observed

- One of the nodes (say node i) has a PMU on it, and that PMU is the only way in which the other node (node j) can be observed

For the first situation, since neither node i nor node j has PMUs on them, it can be inferred that both the nodes are observed by PMUs placed on neighboring nodes. In such a scenario, the edge between nodes i and j is a redundant one (as far as observability is concerned) and can be removed to create islands without increasing the total number of PMUs required. For the second situation, since both the nodes already have PMUs on them, even if the edge between them is removed, the observability of the system will not be affected in any way. Therefore, for this scenario also, the edge between nodes i and j can be removed without causing any increment in the total number of PMUs required. For the third situation, since one node has a PMU on it but it is not needed for observing the other node, it can be inferred that the other node is observed by a neighboring PMU. So, in this scenario also, no extra PMUs will be required when the edge between nodes i and j is eliminated. Figs. 5.4-5.6 depict the first three scenarios for a 4-bus radial network ($n = 4$). In each of the figures, the nodes where PMUs have been placed for complete observability of the system are marked by $\mathbf{X}$. In all three figures, the line between buses 2 and 3 is considered to be the edge that must be removed to partition the system into two islands (comprising of buses 1 and 2 and buses 3 and 4, respectively). As can be seen from the figures, the numbers of PMUs remain the same before and after partitioning. Moreover, there is no need to even rearrange the locations of the PMUs in the created islands in comparison to the original system.

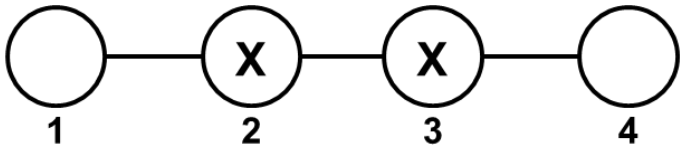

(a)

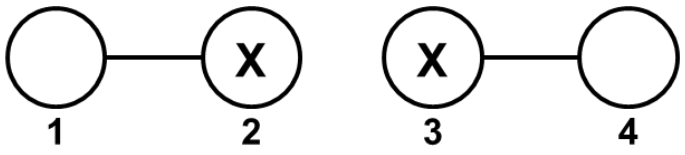

(b)

Fig. 5.4: Four-node network depicting the first scenario

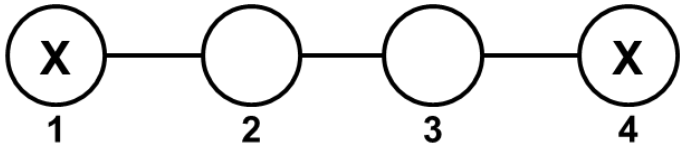

(a)

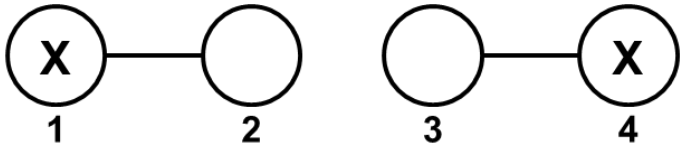

(b)

Fig. 5.5: Four-node network depicting the second scenario

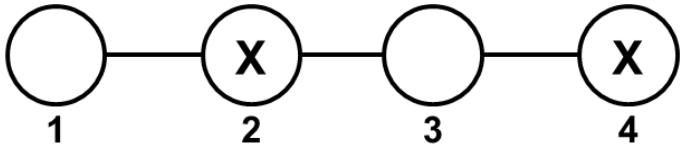

(a)

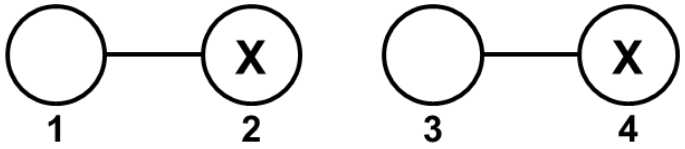

(b)

Fig. 5.6: Four-node network depicting the third scenario

In the fourth situation, since the only way to observe node j is by the PMU placed on node i, when the edge between nodes i and j is removed, a rearrangement of the placed PMUs needs to be done in order to observe the now "unobservable" node j. In such a scenario, there *might* be an increase in the total number of PMUs required. Thus, the fourth situation needs to be analyzed in more details and this is done so in the form of two illustrative examples as shown below.

In Fig. 5.7a, $n = 7$ and the nodes where PMUs have been placed for complete observability of the system (nodes 2, 5 and 7) are marked by $\mathbf{X}$. Next, the edge between nodes 4 and 5 is removed to create

two islands as shown in Fig. 5.7b. Since in the original system, the only way in which node 4 could have been observed is by the PMU on node 5 this scenario is an example of the fourth situation. Now that the edge between nodes 4 and 5 is absent, node 4 can no longer be observed by the PMU at node 5. Therefore a rearrangement of the placed PMUs needs to be done in the created islands. On doing that, the new locations for PMUs are found to be nodes 2, 4 and 6 as seen in Fig. 5.7c. Thus, in this case, although a rearrangement of the PMUs was done to observe all the nodes, the total number of PMUs required remained the same.

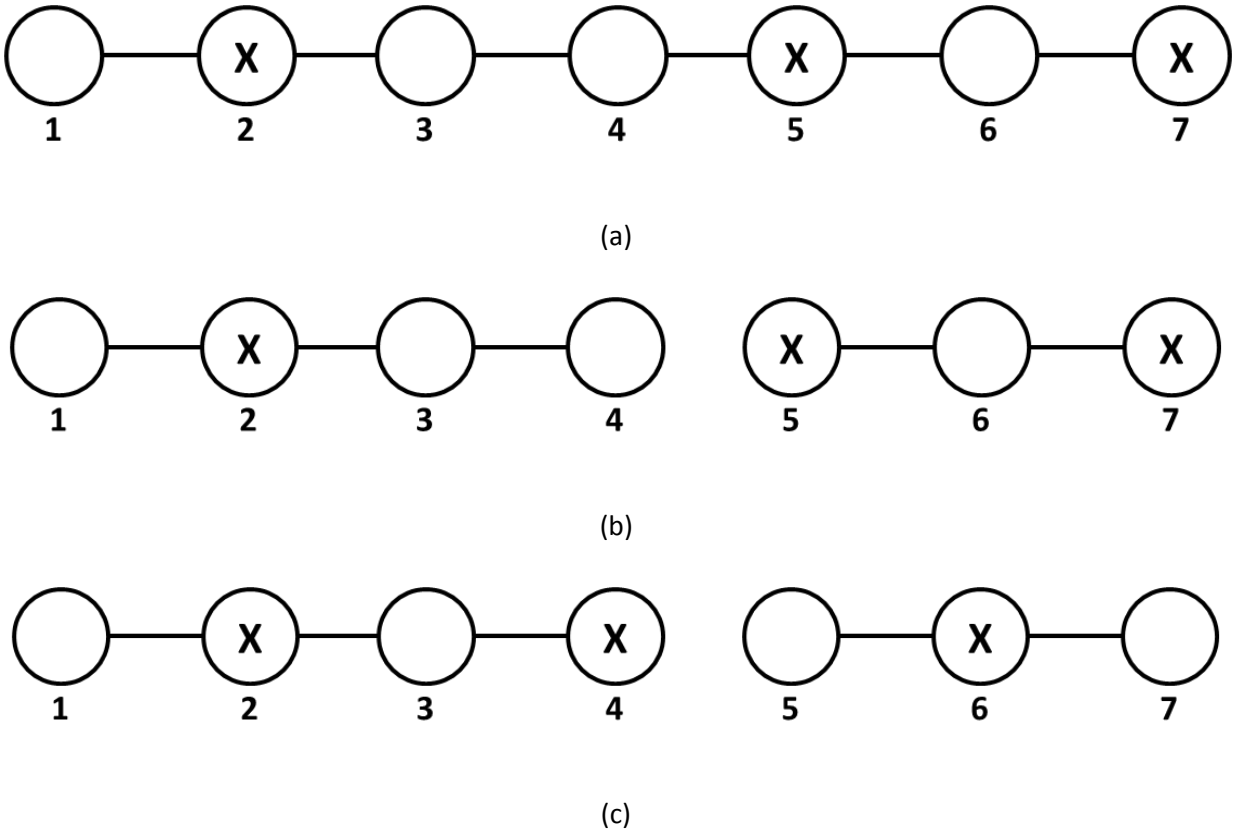

Fig. 5.7: Seven-node network depicting the fourth scenario

In Fig. 5.8a, another example is considered in which $n = 8$ and the nodes on which PMUs have been placed for complete observability of the original system are 2, 5 and 8. Similar to the previous example, the edge between nodes 4 and 5 is removed to create two islands having four nodes each as shown in Fig. 5.8b. Since the removal of the edge results in node 4 becoming unobservable, a rearrangement of the placed PMUs is done to make it observable again. On doing so, it is realized that one more PMU is needed for complete observability of the individual islands as shown in Fig. 5.8c. Thus, in this case, the removal of the edge has caused an increment by one in the total number of PMUs required.

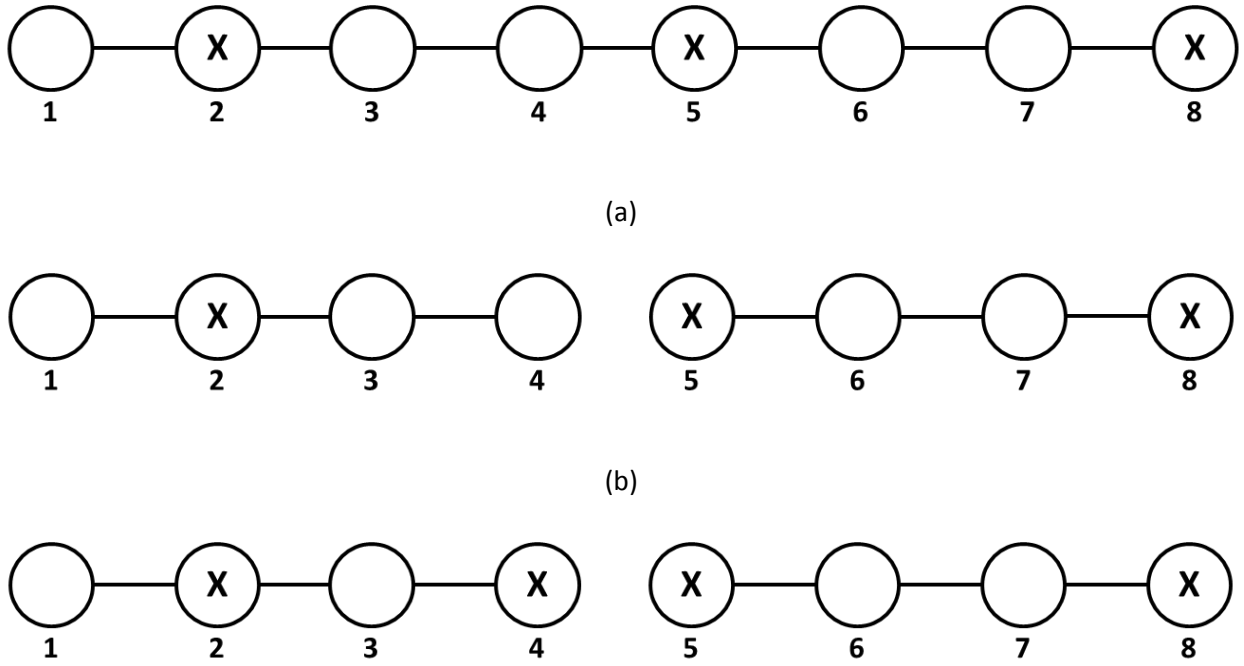

Fig. 5.8: Eight-node network depicting the fourth scenario

Based on this analysis done here, a relationship can be defined between the number of edges removed to create the sub-networks and the number of extra PMUs required for complete observability of the created sub-networks. The relation can be expressed in the form of a Lemma as shown below:

Lemma: *If one edge is removed to create two sub-networks, then, irrespective of the structure/topology of the original network or the created sub-networks, at most only one more PMU will be needed for complete observability of the two sub-networks.*

In the above-mentioned lemma, "one more PMU" means that in the worst case-scenario, the total number of PMUs required for the complete observability of the two sub-networks will be one more than the optimal number of PMUs required for the complete observability of the original network. Therefore, if b branches are removed to create k islands, then the *largest factor* by which the number of PMUs required for complete observability of the created islands will exceed the optimal number of PMUs needed is limited by b. From the above analysis it can also be inferred that if equal likelihood for all the scenarios is assumed, then one extra PMU will be needed for every five branches that are removed. The reason for this is that only in one of the situations listed above is there a possibility of an extra PMU being needed. Thus, as long as the number of branches removed to create the islands is kept to a

minimum, the proposed approach is guaranteed to give near-optimal results. In accordance with this realization, an algorithm is developed in the next section that creates islands by eliminating least number of branches.

5.4 Branch Elimination and PMU Placement (BEPP) scheme

In the previous section, a bound was developed on the maximum error from an optimal PMU placement solution. However, in order for this bound to be effective, an algorithm is needed which can identify the minimum number of branches that must be removed for creating the desired number of islands. Based on the logic given in [109], an algorithm is developed here that not only creates islands by removing minimum number of branches but also computes for the optimal placement of PMUs in the created islands under different system constraints.

The proposed Branch Elimination and PMU Placement (BEPP) scheme comprises of three stages. The first stage involves assigning weights to the different edges of the network. The logic followed for doing so is that branches that have the highest probability of connecting nodes from two different communities should have the highest weights. Although a variety of ways are possible for assigning weights to the edges the one used in [109] was used here because of its ability to create evenly-sized partitions while removing minimal number of edges. Once the branch with the highest weight is identified and removed, a clustering algorithm is used to check for presence of islands. The clustering algorithm identifies nodes that belong to the same community and groups them together. If all the nodes can be clustered under the same group, then it means that no island has been formed by the removal of the highest weight branch and the weighting scheme needs to be repeated to identify the next branch with the highest weight. Once the desired number of islands has been formed, the third stage involves using binary integer programming to compute for an optimal PMU placement in the created islands. Constraints like redundancy in measurement of the critical buses of the network are imposed at this stage. A flowchart of the BEPP scheme is provided in Fig. 5.9 while the pseudo-code for performing the optimization is illustrated with an example in Appendix C. The three stages are described in more details in the following sub-sections.

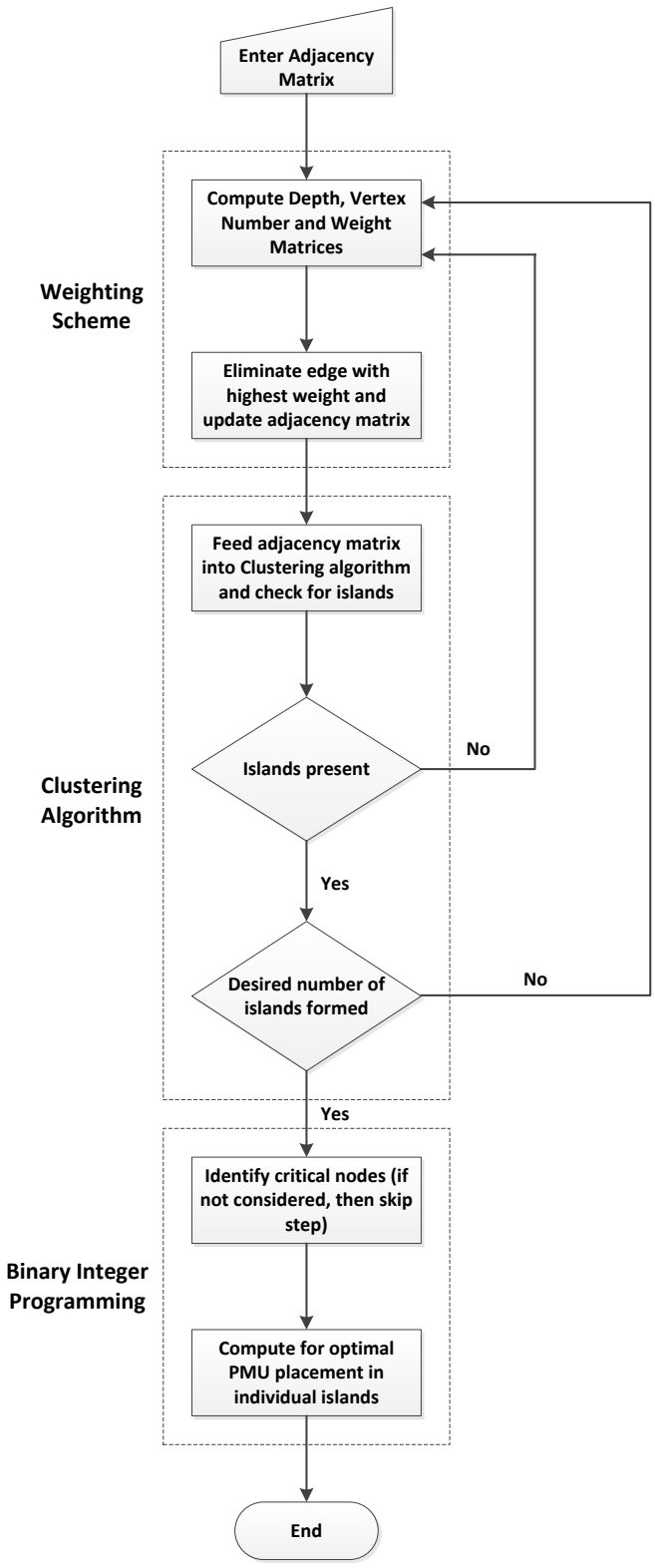

Fig. 5.9: Flowchart of the BEPP Scheme

5.4.1 Weighting scheme

The first stage of the proposed BEPP scheme involves identifying and eliminating least number of branches to create desired number of partitions. Since the partitioning of a network into islands requires the removal of the inter-community edges, for their successful identification and elimination, these edges must have the highest weights. One way to ensure that is by defining a measure for the number of times an edge is traversed when going by the shortest path from node i to node j for all i and j. On doing so, the following two cases arise:

- Nodes i and j are in the same community
- Nodes i and j are in different communities

In the first case, for most networks, the inter-community edges will not be traversed. The reason being that inside a community it is more likely that the shortest path between two nodes will be through edges that lie in the community itself. However, for the second case, it is a *must* that the inter-community edges are traversed. Now, as this process is repeated for all the nodes in the network, it can be surmised that the inter-community edges will be travelled more number of times than the intra-community edges. The reason for this is that whenever nodes from two different communities would need to be connected, they would be done so by travelling through the inter-community edges. Therefore, by definition, the measure that is developed based on the number of times an edge is traversed will be highest for the inter-community edges.

The above-mentioned concept is implemented in a three step process. In the first step, a symmetric matrix called the "Depth" matrix D is created whose element $D(i,j)$ denotes the "distance" of node j from node i. This "distance" is the minimum number of branches that have to be traversed to reach node j starting from node i. If node j cannot be reached from node i, then $D(i,j)$ is equal to zero. Similarly, the distance of node i from itself is also zero. After the computation of the Depth matrix, the next step is to define a "Vertex Number" matrix V whose element $V(i,j)$ denotes the number of shortest paths that have to be traversed to reach node j from node i. The Vertex Number matrix is also a symmetric matrix and can be computed from the Depth matrix. The third step is the creation of the "Weight" matrix. This is the most crucial step because it provides a measure for comparing one branch to another. With the aid of Depth and Vertex Number matrices, the Weight matrix is created using the script given in Fig. 5.10. In Fig. 5.10, A denotes the n-dimensional adjacency matrix of the network, i denotes the source node, j denotes the destination node, and k denotes a node which lies in between i

and j. The ratio $V(k,i)/V(j,i)$ is the index that measures the number of times an edge has been traversed. The variable $counter$ ensures that the weight of the node furthest from i is the least and it increases progressively as we move closer towards i. The gradual increase is quantified by the sum of all the weights of the downstream edges plus one to account for the decreasing depth, whole multiplied by the ratio of the vertex numbers. Once the Weight matrix is computed, the edge having the highest weight is removed from the network and the resulting adjacency matrix is set as an input to the clustering algorithm described next.

For $\mathrm{i, j, k} \in \mathrm{n}$
  if $\mathrm{D(j,i)} == \max\big(\mathrm{D(:,i)}\big)$
    if $\mathrm{A(j,k)} \neq 0$
      $$\mathrm{W(k,j)} = \frac{\mathrm{V(k,i)}}{\mathrm{V(j,i)}}$$
    endif
  endif
  $\mathrm{counter} = 1$
  if $\mathrm{counter} \leq \max(\mathrm{D(:,i)})$)
    if $\big(\mathrm{D(j,i)} == \max\big(\mathrm{D(:,i)}\big) - \mathrm{counter}\big)$
      if $\mathrm{A(j,k)} \neq 0$
        if $\big(\mathrm{D(j,i)} > \mathrm{D(k,i)}\big)$
          $$\mathrm{W(k,j)} = \big(\mathrm{sum(W(j,:)} + 1\big) \times \frac{\mathrm{V(k,i)}}{\mathrm{V(j,i)}}$$
        endif
      endif
    endif
  $\mathrm{counter} = \mathrm{counter} + 1$
  endif
endfor

Fig. 5.10: Script for computing the Weight matrix

5.4.2 Clustering algorithm

The second stage of the BEPP scheme is the clustering algorithm. Its function is to detect and identify created islands. It starts with the first element of the adjacency matrix and identifies the non-zero elements present in the first row (or column). A non-zero entry in the (i,j) position of the adjacency matrix implies that there is a direct path from i to j and so both i and j belong to the same island. Once it comes across a non-zero entry, it travels along the corresponding column (or row) to search for other non-zero entries. In this way, if all the nodes can be reached from the first node, it means that no islands have been formed by the removal of the branch identified in the previous sub-section and that the weighting scheme has to be repeated to identify the next branch to be eliminated.

However, if there are nodes that cannot be reached from the first node by following the above-mentioned process, then it means that an island is present. Then, in order to identify the nodes present in the island, the smallest numbered node which could not be reached by the first node is set as the first node of the new island and the clustering approach is repeated to identify other nodes which can be reached from this new "first" node. This process is repeated until all the islands have been identified. If the number of islands formed is less than the number of islands desired, then the weighting scheme is run again to identify more edges that have to be removed. However, if the desired number of islands has been formed, then the created islands along with the nodes present in each of them are set as inputs to the binary integer optimization technique described next.

5.4.3 Binary integer programming

A methodology was developed in the previous chapter that ensured observability of the most important buses of the network under $N-1$ contingency criterion. This was achieved by providing more "weights" to the nodes that were "critical". High voltage buses, high connectivity buses, buses relevant to transient/dynamic stability, and/or potential small signal control buses were recognized as "critical" nodes for this study. Since the "weighting scheme" described in section 5.4.1 does not affect the relative importance of the nodes of the system, the CBBBIO technique can be smoothly integrated with the proposed scheme. This is done by following a five-step process as shown below:

Step 1: Identify critical nodes of the original system.

Step 2: For the i^{th} island, identify the critical nodes present in it. Define a null vector $\boldsymbol{X}_{init_i}$ having the same length as the number of nodes in the i^{th} island. Set the locations of the critical buses as one in $\boldsymbol{X}_{init_i}$.

Step 3: Define a vector $\mathbf{g}_{\mathrm{i}}$ such that,

$$\mathbf{g}_{\mathrm{i}} = \mathbf{f}_{\mathrm{i}} - \mathrm{w}\mathbf{X}_{\mathrm{init_i}} \tag{5.2}$$

In (5.2), $\mathbf{f}_{\mathrm{i}}$ is a vector of ones having the same length as $\boldsymbol{X}_{init_i}$ and w is a scalar having any value greater than one. The scalar weight w ensures priority in placement of PMUs on the critical nodes.

Step 4: The optimization criteria is defined as,

$$\min_{\mathbf{X_i}} \left(\mathbf{g}_{\mathrm{i}}^{\mathrm{T}}.\mathbf{X}_{\mathrm{i}}\right) \tag{5.3}$$

The constraints imposed on (5.3) are

$$\begin{aligned} &\mathbf{A}_{\mathrm{i}}\mathbf{X}_{\mathrm{i}} \geq \mathbf{f}_{\mathrm{i}} \\ &{\mathbf{X}_{\mathrm{init}_{\mathrm{i}}}}^{\mathrm{T}}.\mathbf{X}_{\mathrm{i}} = \mathrm{nnz}\left(\mathbf{X}_{\mathrm{init}_{\mathrm{i}}}\right) \end{aligned} \tag{5.4}$$

In (5.4), $\boldsymbol{A}_i$ is the incidence matrix of the i^{th} island and $nnz(\boldsymbol{y})$ is the number of non-zero elements in vector $\boldsymbol{y}$. The incidence matrix is the same as the adjacency matrix except that its diagonal elements are unity instead of zeroes.

Step 5: If a critical node is not connected to any other node that has PMU on it, then define the node immediately next to that critical node as a critical node and repeat Steps 2 to 4.

By following these five steps for each of the created islands, an optimal PMU placement scheme can be realized that guarantees redundancy in measurement of all the critical buses of the network. It is to be noted here that the BEPP scheme developed in this chapter focuses only on complete observability (depth zero) whereas the CBBBIO technique described in the previous chapter also computed higher depths of unobservability. If need be, the higher depths of unobservability can be computed by using (4.17) on the individual islands.

Since the community-based partitioning technique has a worst-case time of $O(n^3)$ for sparse graphs [109], the maximum worst-case time for partitioning a system into k islands is $O\left(n^3 + k \times 2^{\left(\frac{n}{k}\right)}\right)$, which is considerably less than $O(2^n)$ for all $n > 10$ and $k \geq 2$. Thus, by combining binary integer optimization with the community-based islanding approach, a simple PMU allocation technique is developed that provides real-time monitoring of critical buses of the network as well as ensures complete system observability with reduced computational burden. A variety of power system networks were analyzed to assess the utility of this scheme. Its application to the IEEE 14-bus system is described in great details in the next section, while the results obtained on applying the BEPP scheme to larger and more complicated power systems are summarized in Section 5.6.

5.5 Illustration of BEPP scheme

In this section, the application of the BEPP scheme is demonstrated on the IEEE 14-bus system. It consists of 14 buses and 20 lines as shown in the equivalent graph in Fig. 5.11. The objective here is to create two islands in this network based on the proposed scheme. The adjacency matrix of the original network is shown in Fig. 5.12. The elements of the adjacency matrix indicate which buses are adjacent

to one another. For instance, since bus 1 is only connected to buses 2 and 5, only (1, 2), (2, 1), (1, 5), and (5, 1) elements of the first row and first column of the adjacency matrix are unity (rest of the entries in the first row and first column are zeroes). A similar logic is followed for obtaining the entries of the remaining rows and columns.

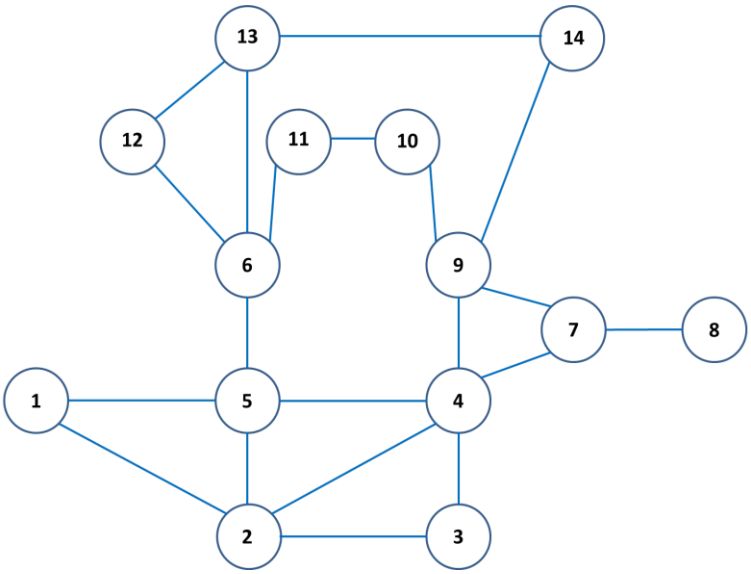

Fig. 5.11: Graph of the IEEE 14-bus system

Bus Numbers	1	2	3	4	5	6	7	8	9	10	11	12	13	14
1	0	1	0	0	1	0	0	0	0	0	0	0	0	0
2	1	0	1	1	1	0	0	0	0	0	0	0	0	0
3	0	1	0	1	0	0	0	0	0	0	0	0	0	0
4	0	1	1	0	1	0	1	0	1	0	0	0	0	0
5	1	1	0	1	0	1	0	0	0	0	0	0	0	0
6	0	0	0	0	1	0	0	0	0	0	1	1	1	0
7	0	0	0	1	0	0	0	1	1	0	0	0	0	0
8	0	0	0	0	0	0	1	0	0	0	0	0	0	0
9	0	0	0	1	0	0	1	0	0	1	0	0	0	1
10	0	0	0	0	0	0	0	0	1	0	1	0	0	0
11	0	0	0	0	0	1	0	0	0	1	0	0	0	0
12	0	0	0	0	0	1	0	0	0	0	0	0	1	0
13	0	0	0	0	0	1	0	0	0	0	0	1	0	1
14	0	0	0	0	0	0	0	0	1	0	0	0	1	0

Fig. 5.12: Original Adjacency matrix of the IEEE 14-bus system

When this matrix is fed into the weighting scheme, the Depth, the Vertex Number and the Weight matrices obtained as outputs are shown in Figs. 5.13-5.15. The elements of the Depth matrix indicate the minimum number of branches that must be traversed to reach one bus from another. For instance, bus 2 is directly connected to bus 1 and so the elements (1, 2) and (2, 1) of the Depth matrix are equal to one, while bus 3 is connected to bus 1 via bus 2 and so the elements (1, 3) and (3, 1) of the Depth matrix are equal to two. It is to be noted here that the Depth matrix gives an indication of the depth of unobservability of a network as defined in Chapter 4, Section 4.1.1. This is based on the fact that the largest entry in a particular row (or column) of the Depth matrix indicates the depth of unobservability of the system if a PMU is placed on that row (or column) number. That is, if a PMU is placed at bus 2 (or 4, or 5, or 9) in the original network of the IEEE 14-bus system, the depth of unobservability of the system will be three.

Bus Numbers	1	2	3	4	5	6	7	8	9	10	11	12	13	14
1	0	1	2	2	1	2	3	4	3	4	3	3	3	4
2	1	0	1	1	1	2	2	3	2	3	3	3	3	3
3	2	1	0	1	2	3	2	3	2	3	4	4	4	3
4	2	1	1	0	1	2	1	2	1	2	3	3	3	2
5	1	1	2	1	0	1	2	3	2	3	2	2	2	3
6	2	2	3	2	1	0	3	4	3	2	1	1	1	2
7	3	2	2	1	2	3	0	1	1	2	3	4	3	2
8	4	3	3	2	3	4	1	0	2	3	4	5	4	3
9	3	2	2	1	2	3	1	2	0	1	2	3	2	1
10	4	3	3	2	3	2	2	3	1	0	1	3	3	2
11	3	3	4	3	2	1	3	4	2	1	0	2	2	3
12	3	3	4	3	2	1	4	5	3	3	2	0	1	2
13	3	3	4	3	2	1	3	4	2	3	2	1	0	1
14	4	3	3	2	3	2	2	3	1	2	3	2	1	0

Fig. 5.13: Original Depth matrix of the IEEE 14-bus system

Bus Numbers	1	2	3	4	5	6	7	8	9	10	11	12	13	14
1	1	1	1	2	1	1	2	2	2	3	1	1	1	3
2	1	1	1	1	1	1	1	1	1	1	1	1	1	1
3	1	1	1	1	2	2	1	1	1	1	3	2	3	1
4	2	1	1	1	1	1	1	1	1	1	2	1	2	1
5	1	1	2	1	1	1	1	1	1	2	1	1	1	2
6	1	1	2	1	1	1	1	1	3	1	1	1	1	1
7	2	1	1	1	1	1	1	1	1	1	1	2	1	1
8	2	1	1	1	1	1	1	1	1	1	1	2	1	1
9	2	1	1	1	1	3	1	1	1	1	1	1	1	1
10	3	1	1	1	2	1	1	1	1	1	1	1	2	1
11	1	1	3	2	1	1	1	1	1	1	1	1	1	2
12	1	1	2	1	1	1	2	2	1	1	1	1	1	1
13	1	1	3	2	1	1	1	1	1	2	1	1	1	1
14	3	1	1	1	2	1	1	1	1	1	2	1	1	1

Fig. 5.14: Original Vertex Number matrix of the IEEE 14-bus system

Bus Numbers	1	2	3	4	5	6	7	8	9	10	11	12	13	14
1	0	9.33	0	0	16.67	0	0	0	0	0	0	0	0	0
2	9.33	0	8.33	17.33	14.33	0	0	0	0	0	0	0	0	0
3	0	8.33	0	17.67	0	0	0	0	0	0	0	0	0	0
4	0	17.33	17.67	0	32.33	0	26	0	30.67	0	0	0	0	0
5	16.67	14.33	0	32.33	0	**46.67**	0	0	0	0	0	0	0	0
6	0	0	0	0	**46.67**	0	0	0	0	0	22.67	18	18.67	0
7	0	0	0	26	0	0	0	26	22	0	0	0	0	0
8	0	0	0	0	0	0	26	0	0	0	0	0	0	0
9	0	0	0	30.67	0	0	22	0	0	26.67	0	0	0	30.67
10	0	0	0	0	0	0	0	0	26.67	0	18	0	0	0
11	0	0	0	0	0	22.67	0	0	0	18	0	0	0	0
12	0	0	0	0	0	18	0	0	0	0	0	0	8	0
13	0	0	0	0	0	18.67	0	0	0	0	0	8	0	22
14	0	0	0	0	0	0	0	0	30.67	0	0	0	22	0

Fig. 5.15: Original Weight matrix of the IEEE 14-bus system

The elements of the Vertex Number matrix denote the number of shortest path that must be traversed to reach one bus from another. For instance, there is only one shortest path between buses 1 and 3 (3-2-1) and so the elements (1, 3) and (3, 1) of the Vertex Number matrix are equal to one, while there are two shortest paths between buses 1 and 4 (4-2-1 and 4-5-1) and so the elements (1, 4) and (4, 1) of the Vertex Number matrix are equal to two. Next, the Weight matrix is created by following the logic outlined in Fig. 5.7. The elements of the Weight matrix are a measure of the frequency that a particular path has been traversed when travelling from one node to another node for all the nodes present in the system. From the Weight matrix obtained (Fig. 5.15), it is realized that branch 5-6 has the highest weight (highlighted in red), and that it should be the first branch that must be removed. After removing this branch from the adjacency matrix, the modified adjacency matrix is fed into the clustering algorithm. On checking for islands, it is realized that no islands have been formed by the removal of branch 5-6. Therefore, the modified adjacency matrix is fed back into the weighting scheme for identifying new branches that must be eliminated in order to create the desired number of islands (in this case, two).

On repeating this process two more times, branches 4-9 and 7-9 are identified as the branches with successively highest weights as shown in Figs. 5.16 and 5.17 (highlighted in red, along with the zero weights of the eliminated lines), and are subsequently removed. The new adjacency matrix obtained is shown in Fig. 5.18 (with the changes from the original adjacency matrix highlighted in red). When this adjacency matrix is fed into the clustering algorithm, it identifies two islands. The first island consists of buses 1, 2, 3, 4, 5, 7, and 8 while the second island consists of buses 6, 9, 10, 11, 12, 13, and 14. From this result it is realized that by using the community-based islanding approach, the IEEE 14-bus system has been successfully partitioned into two equal-sized partitions. Next, the two adjacency matrices are set as inputs to the binary integer programming section of the BEPP scheme (which is based on the CBBBIO technique described in the previous chapter). When none of the buses are considered critical, the numbers and locations obtained for placement of PMUs are shown in Table 5.1 (first row). Next, when bus 4 is considered to be a critical bus (with bus 2 identified to be the bus providing redundancy to the measurement of the critical bus), the new numbers and locations are again found out (as seen in second row of Table 5.1).

Bus Numbers	1	2	3	4	5	6	7	8	9	10	11	12	13	14
1	0	14	0	0	12	0	0	0	0	0	0	0	0	0
2	14	0	5	30	3	0	0	0	0	0	0	0	0	0
3	0	5	0	21	0	0	0	0	0	0	0	0	0	0
4	0	30	21	0	31	0	20	0	**70**	0	0	0	0	0
5	12	3	0	31	0	**0**	0	0	0	0	0	0	0	0
6	0	0	0	0	**0**	0	0	0	0	0	20	6	16	0
7	0	0	0	20	0	0	0	26	28	0	0	0	0	0
8	0	0	0	0	0	0	26	0	0	0	0	0	0	0
9	0	0	0	**70**	0	0	28	0	0	44	0	0	0	60
10	0	0	0	0	0	0	0	0	44	0	32	0	0	0
11	0	0	0	0	0	20	0	0	0	32	0	0	0	0
12	0	0	0	0	0	6	0	0	0	0	0	0	20	0
13	0	0	0	0	0	16	0	0	0	0	0	20	0	48
14	0	0	0	0	0	0	0	0	60	0	0	0	48	0

Fig. 5.16: Weight matrix of the IEEE 14-bus system after line 5-6 is removed

Bus Numbers	1	2	3	4	5	6	7	8	9	10	11	12	13	14
1	0	14	0	0	12	0	0	0	0	0	0	0	0	0
2	14	0	5	30	3	0	0	0	0	0	0	0	0	0
3	0	5	0	21	0	0	0	0	0	0	0	0	0	0
4	0	30	21	0	31	0	90	0	**0**	0	0	0	0	0
5	12	3	0	31	0	**0**	0	0	0	0	0	0	0	0
6	0	0	0	0	**0**	0	0	0	0	0	20	6	16	0
7	0	0	0	90	0	0	0	26	**98**	0	0	0	0	0
8	0	0	0	0	0	0	26	0	0	0	0	0	0	0
9	0	0	0	**0**	0	0	**98**	0	0	44	0	0	0	60
10	0	0	0	0	0	0	0	0	44	0	32	0	0	0
11	0	0	0	0	0	20	0	0	0	32	0	0	0	0
12	0	0	0	0	0	6	0	0	0	0	0	0	20	0
13	0	0	0	0	0	16	0	0	0	0	0	20	0	48
14	0	0	0	0	0	0	0	0	60	0	0	0	48	0

Fig. 5.17: Weight matrix of the IEEE 14-bus system after line 5-6 and line 4-9 are removed

Bus Numbers	1	2	3	4	5	6	7	8	9	10	11	12	13	14
1	1	1	0	0	1	0	0	0	0	0	0	0	0	0
2	1	1	1	1	1	0	0	0	0	0	0	0	0	0
3	0	1	1	1	0	0	0	0	0	0	0	0	0	0
4	0	1	1	1	1	0	1	0	**0**	0	0	0	0	0
5	1	1	0	1	1	**0**	0	0	0	0	0	0	0	0
6	0	0	0	0	**0**	1	0	0	0	0	1	1	1	0
7	0	0	0	1	0	0	1	1	**0**	0	0	0	0	0
8	0	0	0	0	0	0	1	1	0	0	0	0	0	0
9	0	0	0	**0**	0	0	**0**	0	1	1	0	0	0	1
10	0	0	0	0	0	0	0	0	1	1	1	0	0	0
11	0	0	0	0	0	1	0	0	0	1	1	0	0	0
12	0	0	0	0	0	1	0	0	0	0	0	1	1	0
13	0	0	0	0	0	1	0	0	0	0	0	1	1	1
14	0	0	0	0	0	0	0	0	1	0	0	0	1	1

Fig. 5.18: Adjacency matrix of the IEEE 14-bus system after removal of branches 5-6, 4-9, and 7-9

Table 5.1: Illustration of BEPP Scheme for computing PMU placements by partitioning IEEE 14-bus system into two islands

	Using CBBBIO Technique		Using BEPP Scheme	
	Number of PMUs	Location of PMUs	Number of PMUs	Location of PMUs
When no bus is considered critical	4	2, 6, 7, 9	4	2, 7, 10, 13
When bus 4 is considered critical	5	2, 4, 7, 10, 13	5	2, 4, 7, 10, 13

In Table 5.1, the results obtained using the proposed scheme is compared with the optimal results obtained through a direct application of the CBBBIO technique. The comparison indicates that when no buses are identified to be critical, the numbers of PMUs required remain the same for the two approaches, but the locations differ slightly. This is because in this case when the BEPP scheme is used to create the two islands, the fourth situation has occurred (as outlined in Section 5.3). Therefore, a rearrangement of the PMUs is needed for complete observability of the individual islands. However, from the table it is observed that even though a rearrangement of the PMUs had to be done and three

branches eliminated to create the two islands, no extra PMUs were required. In the second case, when bus 4 is identified to be a critical bus, it was observed that the numbers and locations of PMUs required remain the same for both the approaches. Thus, this illustration indicates that the proposed BEPP scheme is a good choice for reaching a near-optimal (if not *the* optimal) solution for PMU placement in power system networks, especially when used in conjunction with the concept of "critical" buses. This "indication" is tested on a variety of large networks in the following section.

5.6 Simulation Results

This section summarizes the results obtained when the BEPP scheme is applied to a variety of power system networks. The range of the systems tested varied from 14 buses to more than 1400 buses. For the study done here, zero injection (ZI) buses had not been removed from the test systems. Thus, the PMU placements computed could be directly applied on the actual systems.

In the first set of simulations, the effect of the proposed partitioning scheme on the ratio of the branches removed to the total branches present is analyzed. The systems selected for this study are the IEEE 14-bus system, the IEEE 30-bus system, the IEEE 57-bus system, the IEEE 118-bus system, a 127-bus model of the WECC system, a 283-bus model of the Central American system, the IEEE 300-bus system, a 750-bus model of the Indian system, a 1064-bus model of the Dominion Virginia Power (DVP) system, a 1133-bus model of the Indian system, and a 1443-bus model of the Brazilian system. No buses were defined to be critical for this analysis. The results obtained are shown in Fig. 5.19. From the plots it can be realized that as the size of the networks increase there is a decrease in the fraction of branches removed to create the islands. This indicates that the BEPP scheme will become more and more effective as the systems get bigger and bigger. The 750-bus and the 1133-bus were found to have slightly higher ratios than expected because they were more meshed than usual power system networks.

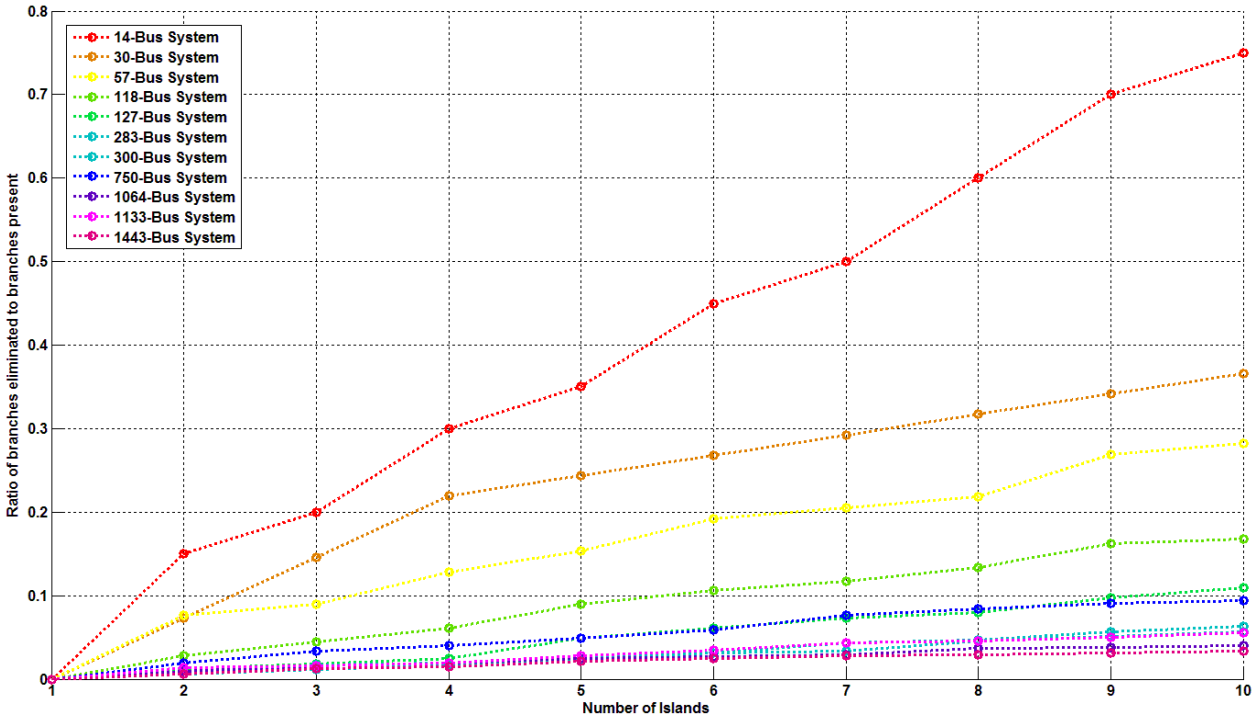

Fig. 5.19: Ratio of Branches eliminated to Branches present as number of islands is increased

In the next set of simulations, the effect of partitioning on the number of extra PMUs needed is analyzed. Since this chapter focuses more on large systems, the systems having more than 100 buses were selected for this study. In this simulation also, no buses were identified to be critical. The results obtained are shown in Fig. 5.20. From the figure it becomes clear that the number of extra PMUs needed, as more and more partitions are made, is much less. The reason for this observation is that of the four possibilities identified in Section 5.3, only one has the potential of adding more PMUs. Therefore, although a large number of branches may have been removed to create the islands, its net effect on the total number of PMUs required for observability is very small.

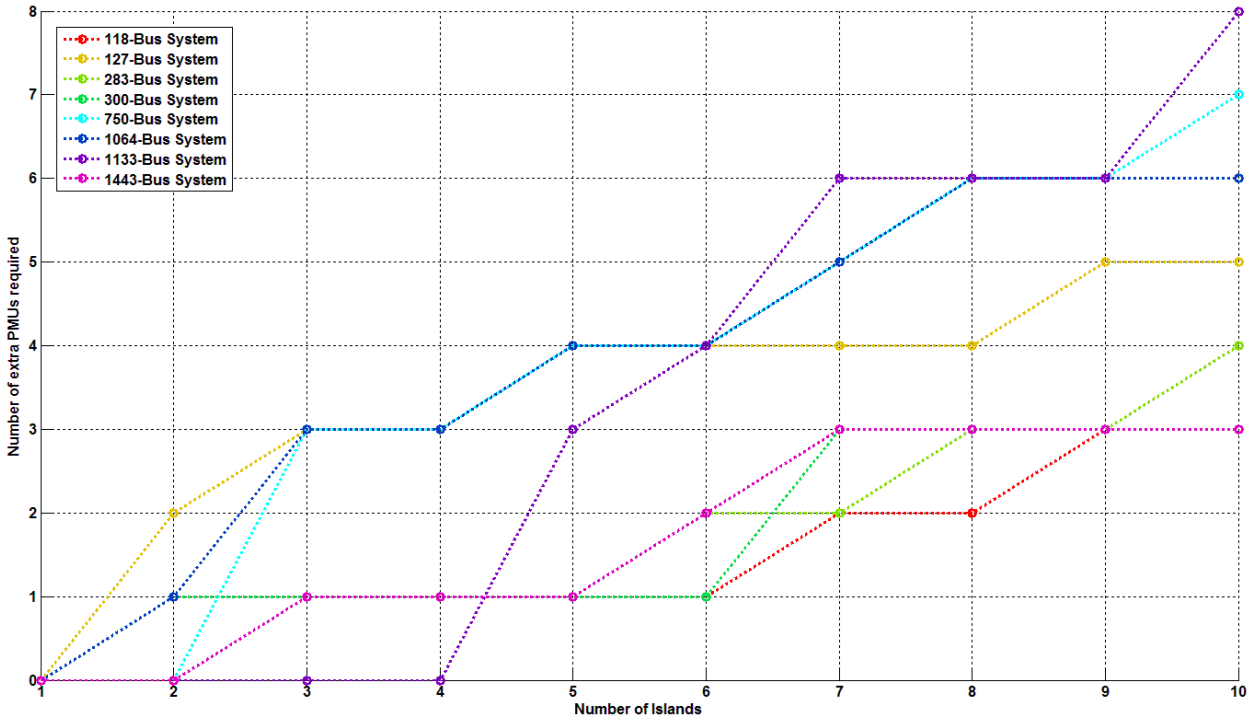

Fig. 5.20: Number of extra PMUs required as number of islands is increased

In the third set of simulations, the computation times required for performing the optimization using the BEPP scheme is compared with the integer programming technique developed in [1]. The power systems used for this study are the IEEE 14-bus system, the IEEE 30-bus system, the IEEE 57-bus system, the IEEE 118-bus system, the 127-bus WECC system, the 283-bus Central American system, the IEEE 300-bus system, the 750-bus Indian system, the 1133-bus Indian system, and the 1443-bus Brazilian system. None of the buses were considered critical for this analysis. For the BEPP scheme, the test systems were partitioned into minimum number of islands greater than or equal to two, such that the size of the individual islands was less than 500 buses. The simulations were performed on an Intel (R) Core™ i5 Processor having a speed of 2.40 GHz and an installed memory (RAM) of 5.86 GB. The results are provided in Table 5.2. From Table 5.2, it becomes clear that for systems with more than 500 buses, the computation times using the BEPP scheme is significantly less in comparison to the computation times using the integer programming technique developed in [1]. Of special emphasis are the computation times for the 1133-bus Indian system and the 1443-bus Brazilian system, for which optimal PMU placements could not be computed using the integer programming technique by the original computer even after letting it run for 150,000 seconds. A much more powerful computer (Intel (R) Core™ i7 Processor having a speed of 3.40 GHz and an installed memory (RAM) of 64 GB) was used to compute

for the optimal number of PMUs for those two systems. However, using the BEPP scheme, the original computer was able to come up with a near-optimal solution at a fraction of the time.

Table 5.2: Comparison of the proposed BEPP Scheme with the traditional Integer programming based PMU placement algorithm

System	Using Integer Programming [1]		Using BEPP Scheme			
	Number of PMUs	Time (in seconds)	Island Details		Number of PMUs	Time (in seconds)
			Number	Size		
IEEE 14-bus system	4	0.13	2	7+7	4	0.02
IEEE 30-bus system	10	0.04	2	7+23	10	0.03
IEEE 57-bus system	17	0.18	2	27+30	18	0.08
IEEE 118-bus system	32	0.73	2	38+80	32	0.12
127-bus WECC system	39	0.90	2	52+75	41	0.13
283-bus Central American system	87	3.07	2	119+164	87	0.36
IEEE 300-bus system	87	4.04	2	87+213	88	0.79
750-bus Indian system	161	3674.98	3	161+222+367	164	92.10
1133-bus Indian system	305	>150,000	3	310+363+460	305	146.61
1443-bus Brazilian system	443	>150,000	5	66+243+289+ 409+436	444	150.51

In the last set of simulations, the critical buses are identified and redundancy under the proposed scheme is provided to them. The test systems used for this study are the IEEE 118-bus system, the 283-

bus system, the IEEE 300-bus system, the 750-bus system, and the 1133-bus system. The critical buses were chosen based on their voltage levels and connectivity, as well as on the basis of the transient and dynamic stability studies that were performed on the systems. The number of partitions made was based on system topology and/or computational ease. The IEEE 118-bus and the IEEE 300-bus systems were split into three islands. Since the 283-bus system represented the Central American Power Transmission Network comprising of six countries (Guatemala, Nicaragua, Honduras, El Salvador, Costa Rica, and Panama), it was split into six islands. The 750 and the 1133-bus systems represented the Northern-and-Eastern Power Grids of India and were partitioned such that each of the islands formed had less than 500 buses. The results obtained for the test systems are shown in Table 5.3. From Table 5.3 it becomes clear that a near-optimal solution can be obtained using the BEPP scheme even after considering critical buses based on the CBBBIO technique.

Table 5.3: Number of PMUs required for different systems after considering critical buses

System	Number of islands created	Number of critical buses	Optimal number of PMUs using CBBBIO Technique	Number of PMUs using BEPP scheme
118-bus system	3	18	41	43
283-bus system	6	29	101	103
300-bus system	3	22	97	98
750-bus system	3	68	202	203
1133-bus system	3	74	344	344

Another observation that can be made from Table 5.3 is that the BEPP scheme provides a different approach towards PMU placement in real systems. The CBBBIO technique described in the previous chapter ensured that the depth of unobservability of the complete system decreased with every stage of PMU addition. The BEPP scheme ensures that selective regions of the original system can become completely observable independent of the observability of the whole system. This is especially

important for systems like the Central American system which is composed of the electrical transmission systems of different countries. In practice, it might be possible that one of the six countries in Central America (courtesy of some help from the World Bank, etc.), would like to place PMUs for complete observability of their own transmission system, while still being connected with the rest of the network. Under such circumstances, the BEPP scheme can be used to ensure that PMUs are placed optimally for the individual country (after islanding it from the rest of the system) while simultaneously keeping track of the observability of the complete Central American network in mind. Thus, based on the simulations performed in this section, it is realized that using the technique proposed here, a flexible PMU placement scheme can be developed that optimizes the benefits of having PMUs at strategic locations of a large power system network without the associated computational burdens.

5.7 Conclusion

This chapter introduces a partitioning logic that will create small networks from an initial large network, with the smaller networks retaining the original structure/topology and which can be studied individually, so as to get a coherent picture of the large network. Its use in dividing a large power system network into small islands for facilitating PMU placement is illustrated here. The partitioning scheme identifies communities in the system by analyzing the connections between nodes/buses. After splitting the network into islands, a critical bus based PMU allocation technique (CBBBIO technique) is used to compute for the optimal locations in the individual islands. The main advantage of the proposed approach is that PMU locations can be computed for large networks without performing any type of topology modification/reduction. Thus, the results produced would be more accurate even with models having low voltage inter-connections. To summarize, the proposed method is found to provide genuinely good results for computing PMU placements in large systems at reduced computational effort.

Chapter 6: Phasor Measurement Based Stress Assessment Metrics

In order to successfully monitor the health of a power system, it is necessary to constantly evaluate the stresses that develop within it due to different operating conditions. Correct estimation of the system's proximity to an insecure operation can go a long way in preventing that "insecure operation" from materializing into reality. In this chapter, two synchrophasor based metrics – angle difference and voltage sensitivity are proposed for measurement and real-time monitoring of system stresses in interconnected power grids. The simulations show that by monitoring these metrics in real-time, the system's ability to withstand a variety of contingencies can be found out with great accuracy. A way in which these metrics can be monitored through analytic and visualization platforms – such as Real Time Dynamics Monitoring System[1] (RTDMS), a synchrophasor based software application [112] is also shown. The proposed metrics are found to be very effective for real-time static and dynamic stress monitoring as well as for operator training.

6.1 Stresses in a power system

Modern power system has evolved from a local control area to a regional market. This evolution has brought new problems related to wide area grid stresses that have to be dealt with in real-time. Similarly, the decentralized mode of operation of power systems as well as the exponential increase in regional power transfers has resulted in the system facing levels of stress over large areas that it has never experienced before. Under such circumstances for a reliable operation it is important that static and dynamic stresses of the system over a wide area be monitored in real-time. The base loading of the system constitutes static stress. It refers to the normal/pre-contingency state of the system. Dynamic stress refers to the event/contingency that the system is subjected to. With the aid of PMUs [6], it is now possible to assess phenomena like these in real-time.

PMUs placed at strategic locations in the power system provide magnitude and angle measurements of voltages and currents. By using these measurements, different metrics can be developed for evaluating the state of the system as well as for estimating its "proximity" to an insecure operation. In this chapter, it will be shown how angle differences and voltage sensitivities can be used as effective indicators of system stress. The full model of WECC is used as the test system for this analysis. Two types of stressed conditions are simulated. In the first case, a large amount of generation is dropped in the South and the

[1] Built upon GRID-3P® platform. US Patent 7,233,843, US Patent 8,060,259, and US Patent 8,401,710.

resulting effect on the angle differences between two buses located across the network is examined. The second case is composed of two parts: in the first part, a small amount of load is increased in the South for different base loading conditions and its effect analyzed through a study of the voltage sensitivity. In the second part, a significant portion of the load is dropped in the North for different base loading conditions and its effect on the resulting oscillations is investigated. It is to be noted here that in the simulations performed, South and North refer to the Southern and Northern halves of the WECC.

6.2 Two metrics for assessing system stress

In order to analyze stresses in a typical power system, two metrics are proposed here. The first metric – angle difference between two buses, is relevant for buses that lie on opposite ends of the network. For this metric, the large generators and load buses are potential candidates. The reason being that since those buses act as "sources" and "sinks", respectively, the angle difference across them is a good measure of the stress lying in the system-in-between. The second metric – voltage sensitivity of a bus, is relevant for buses that lie in the middle. This metric is especially useful for buses that have been (historically) found to be prone to voltage collapse. More details about these two metrics are provided along with simple illustrations in the following sub-sections.

6.2.1 Angle difference as a measure of system stress

System operators use power/currents as indicators of system stress. A variety of alert/alarm limits established from base-lining studies are based on the power flowing in the lines. Similarly, relay trip settings are usually set based on current values. However, study of recent power system outages has shown that monitoring the power/current alone is not a reliable measure of system stability. For instance, in the September 8, 2011 San Diego Blackout, the situation worsened over 6 phases (11 minutes) because the breaker across the 500kV line between Hassyampa and North Gila could not be reclosed [113]. The reason why the breaker could not be closed was due to the "high" angle difference present across it.

Using voltage angles obtained from PMUs for decision making has already been suggested in literature [35]-[44]. In this chapter the importance of monitoring angle difference between certain buses of the network in real-time will be demonstrated. Figs. 6.1 and 6.2 depict two scenarios of a two-bus power system model. Bus 1 is a generator bus while Bus 2 is a load bus. For simplicity, it is assumed that the system is lossless. As such, the generator bus generates 2400 MW of power which is transferred via two identical transmission lines (1200 MW each) and is consumed by the 2400 MW load. Let us also assume

that the individual lines have a rating of 2500 MW, so that even when only one of the two lines is in-service, it is possible to successfully transfer the full power to the load.

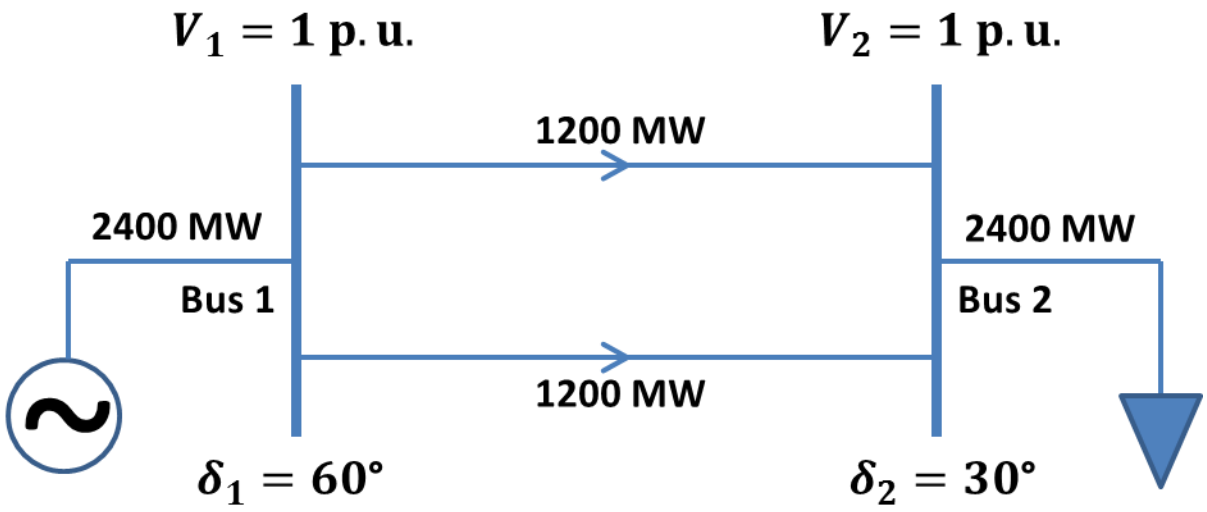

Fig. 6.1: Two-bus system with both transmission lines in service

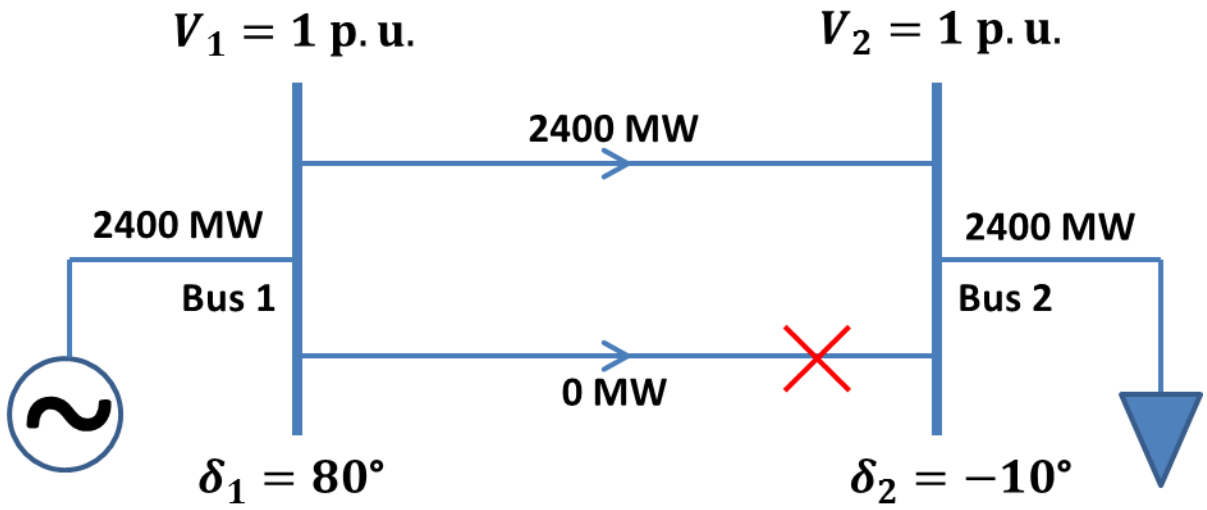

Fig. 6.2: Two-bus system with only one transmission line in service

In the first scenario (Fig. 6.1), both lines are in-service and for a given value of line reactance, the voltage angles of the two buses are 60° and 30°, respectively. Therefore, the angle difference between the two buses of the system under normal conditions is 30°. In the second scenario (Fig. 6.2), the second line is tripped due to an unforeseen event. Now, since the first line is capable of transferring the full power, a study of *only* the power flow would indicate that the system is in a relatively stable condition. However,

the instant the second line goes out, in order to transfer the same amount of power to the load, the angles of the two buses will change from 60° and 30° to 80° and -10°, respectively (Fig. 6.2). Hence, an angle difference of 90° will now exist across the two buses. Since usual relay-settings don't allow closure of a line when the angle differences are in excess of 60°, it can be surmised that the "second" line will not come back into service unless the loading is reduced. But since monitoring the power alone would not indicate this stressed condition, it is possible that the loading would not be reduced in time to allow the line reclosure to take place and that further damage will occur. Thus, from this example it can be concluded that real-time monitoring of angle differences is a better indicator of the actual stress on the system in comparison to *just* the power flows.

6.2.2 Voltage sensitivity as a measure of system stress

Voltage sensitivity is defined as the ratio of the change in voltage magnitude of a bus with respect to the change in power flowing in a line [114]. Usually measured in $kV/100\ MW$, it can give early warnings about deteriorating voltage conditions. For the two-bus system shown in Fig. 6.1, the voltage sensitivity of bus 1 with respect to the power flowing between buses 1 and 2 will be,

$$V_{sensitivity_1} = \frac{\Delta V_1}{\Delta P_{12}} \tag{6.1}$$

Thus, by definition, the voltage sensitivity is the slope of the PV-curve (nose curve). Similar to angle differences across two buses in a network, voltage sensitivity of key buses can also indicate (in real-time), the proximity of a system to an unstable operation (voltage collapse). However, unlike angle differences which are most relevant when the two buses lie on different ends of a network, voltage sensitivity of buses lying in the middle are most significant.

Figs. 6.3 and 6.4 use the example of a beam-balance to explain this concept. A general power system network can be thought of as a combination of different beam-balance systems with sufficient supports provided at either ends of the beam. In electrical terms, the support refers to the injected Volt-Ampere-Reactives (VARs) at the sending and receiving ends. Fig. 6.3 shows the state of the beam under normal conditions. A dynamic event (such as a contingency or an outage) can be represented by a downward arrow on the beam such as that shown in Fig. 6.4. Since the deformation of the beam will be most severe at the point of impact, it can be realized that the most vulnerable region with respect to voltage collapse will be the mid-portion of the system. Thus, voltage sensitivity of buses which lie in the middle of the network should be monitored in real-time.

Fig. 6.3: Normal operating condition

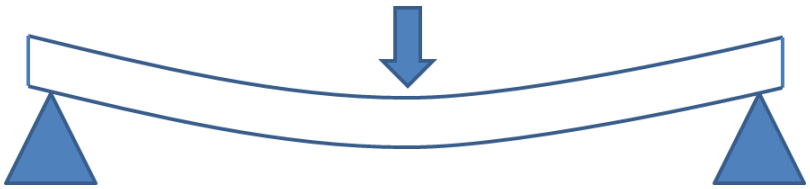

Fig. 6.4: Stressed operating condition

A recommended safe interval for voltage sensitivity of a 500kV bus under normal conditions is,

$$-4\ kV/100\ MW < V_{sensitivity} < -0.05\ kV/100\ MW \tag{6.2}$$

If the value goes below -4, it is an indication that the voltage is nearing the tip of the nose curve, whereas, if it becomes more than -0.05, it indicates that the voltage is overly-compensated. An over-compensated voltage is not good because it means that the voltage profile would be flat even when the power flow is increased making the system vulnerable to sudden voltage collapse. Thus, monitoring voltage sensitivity with change in power flow in real-time will also aid in efficient deployment of VAR supports. The next section summarizes the simulations that were performed to illustrate the use of these two metrics for analyzing different system events.

6.3 Simulations performed using the WECC system

WECC is the regional entity responsible for coordinating and managing bulk electric system reliability in the Western Interconnection. It covers a region extending from Canada to Mexico, including provinces of Alberta and British Columbia, northern portion of Baja California, Mexico, and all or portions of the fourteen states located West of the Rockies. Due to the wide area covered and diverse characteristics of the region, it faces unique challenges in coordinating the day-to-day interconnected system operations and the long range planning needed to provide reliable electric service across nearly 1.8 million square miles [115]. A 10,000+ bus model of the WECC system was used for the analysis done here.

In this chapter, two types of stressed conditions are investigated to assess the performance of angle difference and voltage sensitivity as measures of stress on this system. In the first set of simulations,

corresponding to different levels of static stress, dynamic stress in the form of outage of generating unit/s is explored. In the second set of simulations, the California-Oregon Intertie (COI) is stressed by increasing generation in the north and loads in the south. Then, two load changes are simulated (one in the South and the other in the North) for different levels of COI stress and its effects are analyzed using angle difference and voltage sensitivity plots. The results obtained are summarized below.

6.3.1 Generation drop in the South

In this simulation, three scenarios were created for the WECC system corresponding to three different levels of static stress. The three levels were:

- Lightly loaded system
- Medium loaded system
- Heavily loaded system

The angle difference between Grand Coulee in the North and Devers in the South was used for quantifying system stress. If the WECC system was a mass-spring system with the large loads/generators being the masses and the transmission lines being the springs, then the center of mass for the northern half would be located around Grand Coulee whereas the center of mass for the southern half would be located around Devers. It is because of this reason that the angle difference between these two buses would give an accurate estimate of the wide area system stress. As such critical node pairs can be identified in different power system networks; the measure developed based on this concept will be applicable to other networks as well.

For a lightly loaded system, the pre-contingency angle difference threshold between Grand Coulee and Devers was set at 65°. For a medium loaded system, the angle difference threshold was between 65° and 90°; while an angle difference of above 90° was considered a heavily loaded system. The dynamic stress was quantified by the outage of Palo Verde (PV) generator units. There are three units at PV with each unit generating approximately 1370 MW. The methodology followed was to trip one or more of the units for each of the three scenarios one minute after the start of the simulation and to observe the resulting behavior of the system for the next eleven minutes or until the system collapsed. In all the simulations, the angle difference between Grand Coulee and Devers was monitored for assessment of system stress. The results obtained are shown in Figs. 6.5-6.13.

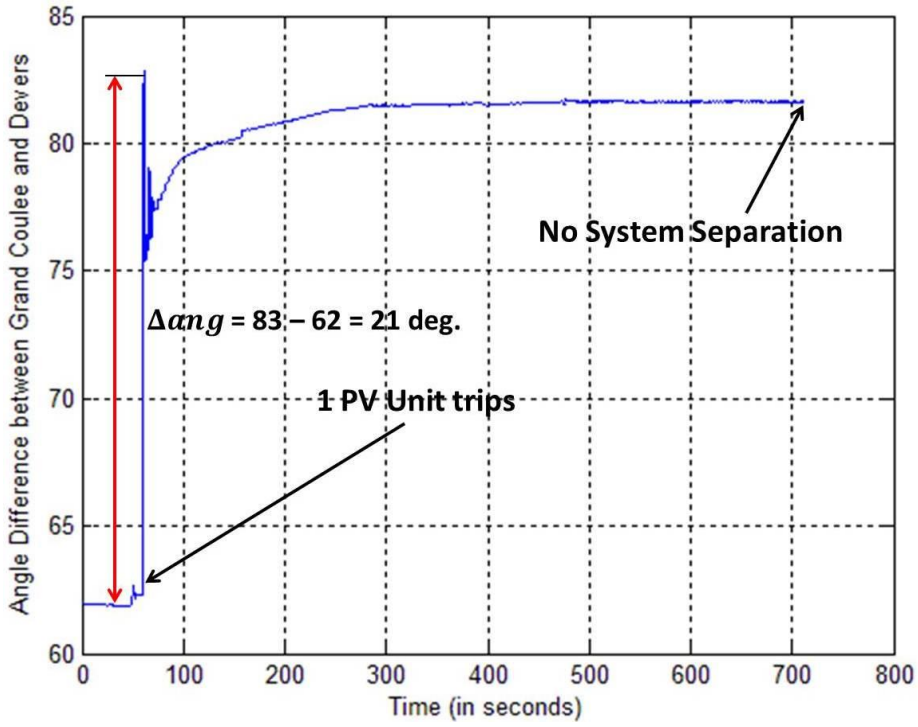

Fig. 6.5: Outage of one PV unit for a lightly loaded system

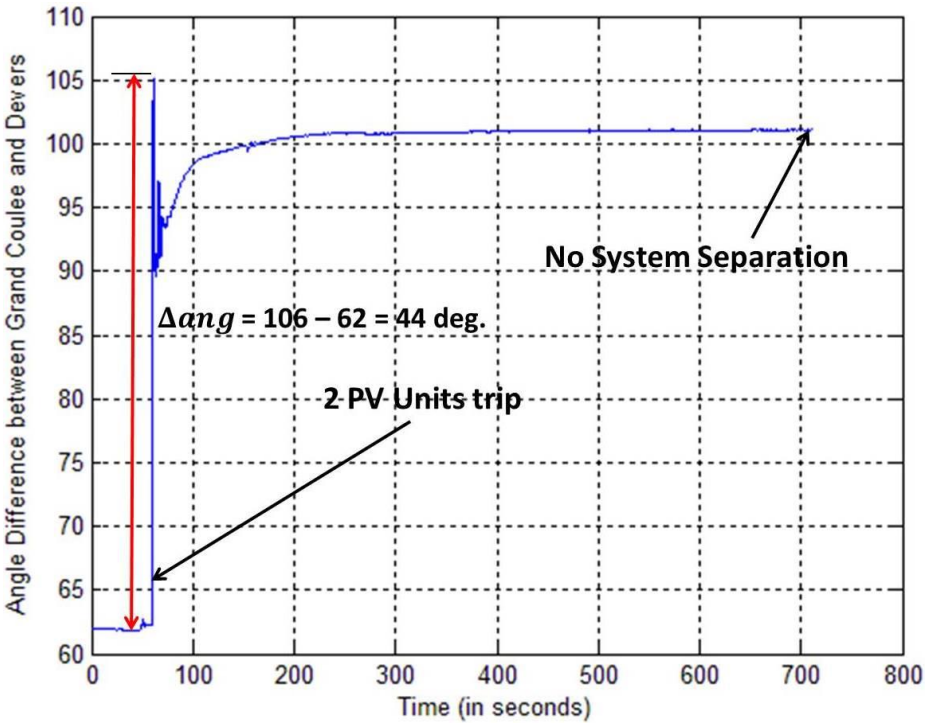

Fig. 6.6: Outage of two PV units for a lightly loaded system

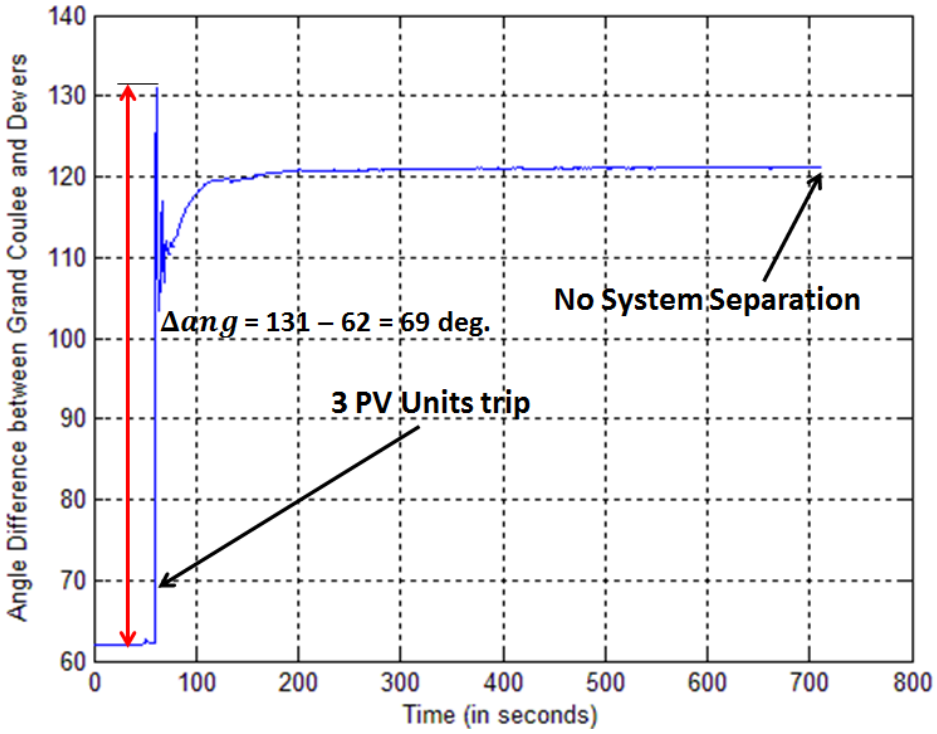

Fig. 6.7: Outage of three PV units for a lightly loaded system

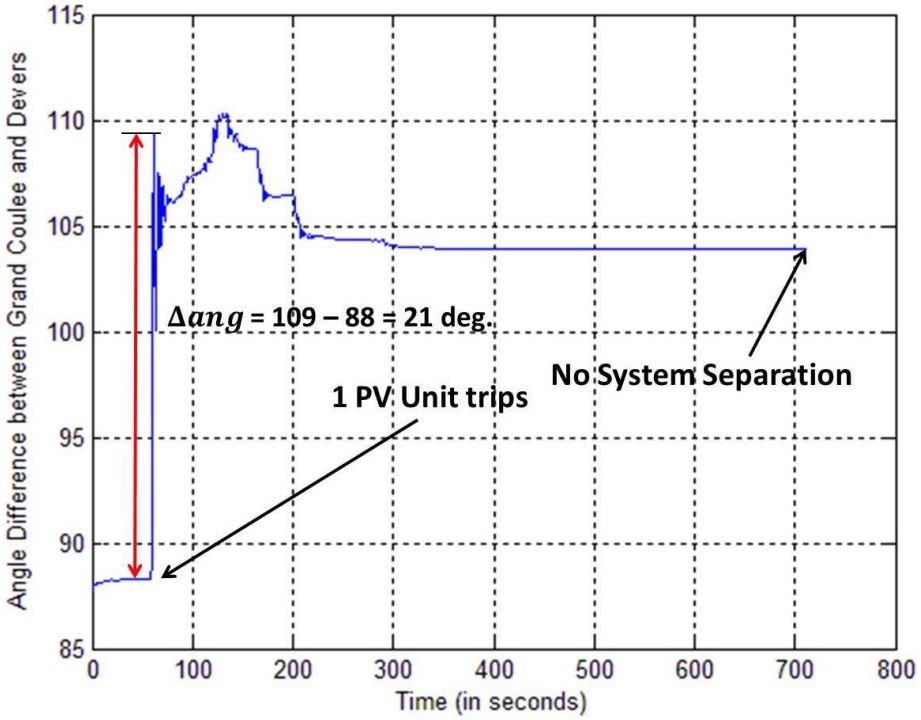

Fig. 6.8: Outage of one PV unit for a medium loaded system

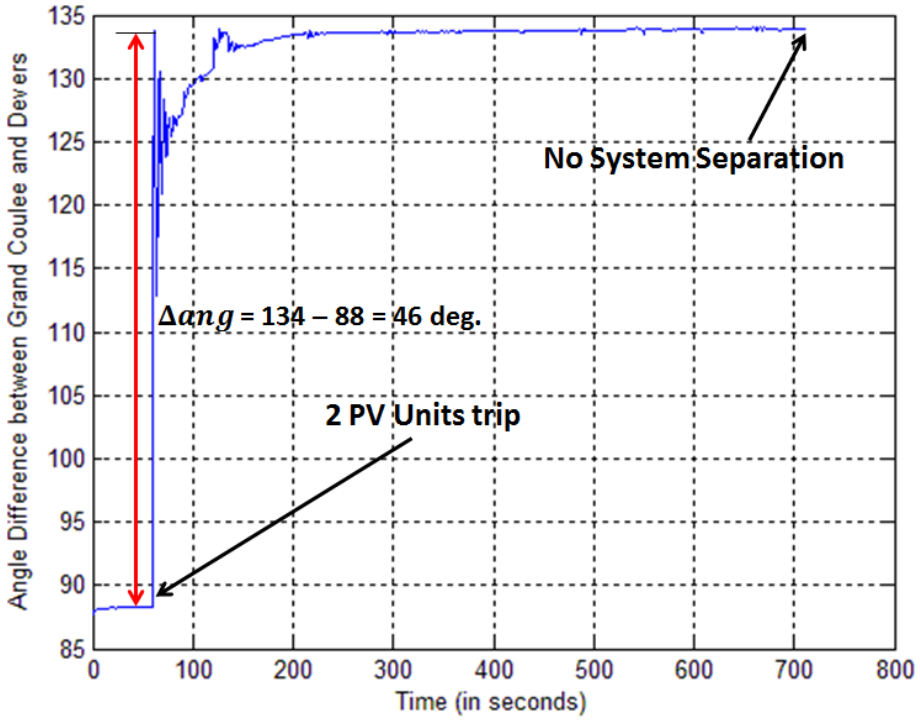

Fig. 6.9: Outage of two PV units for a medium loaded system

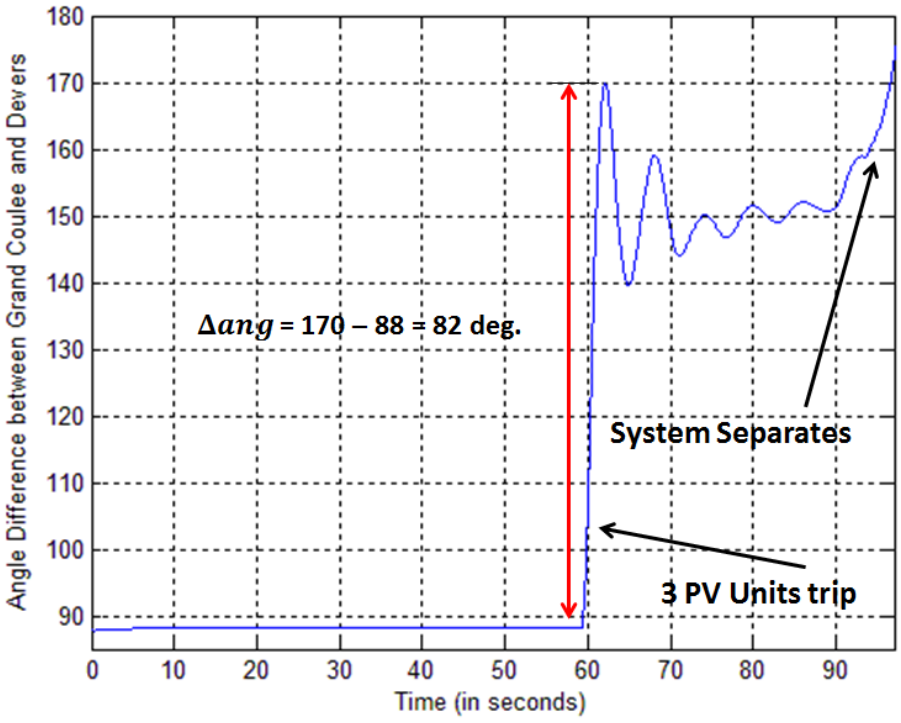

Fig. 6.10: Outage of three PV units for a medium loaded system

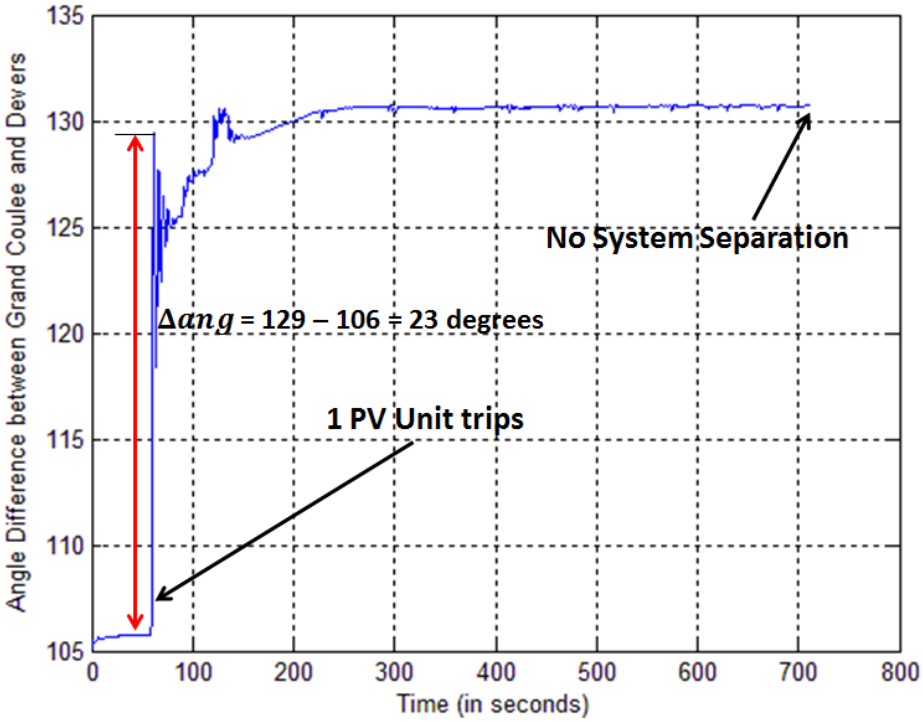

Fig. 6.11: Outage of one PV unit for a heavily loaded system

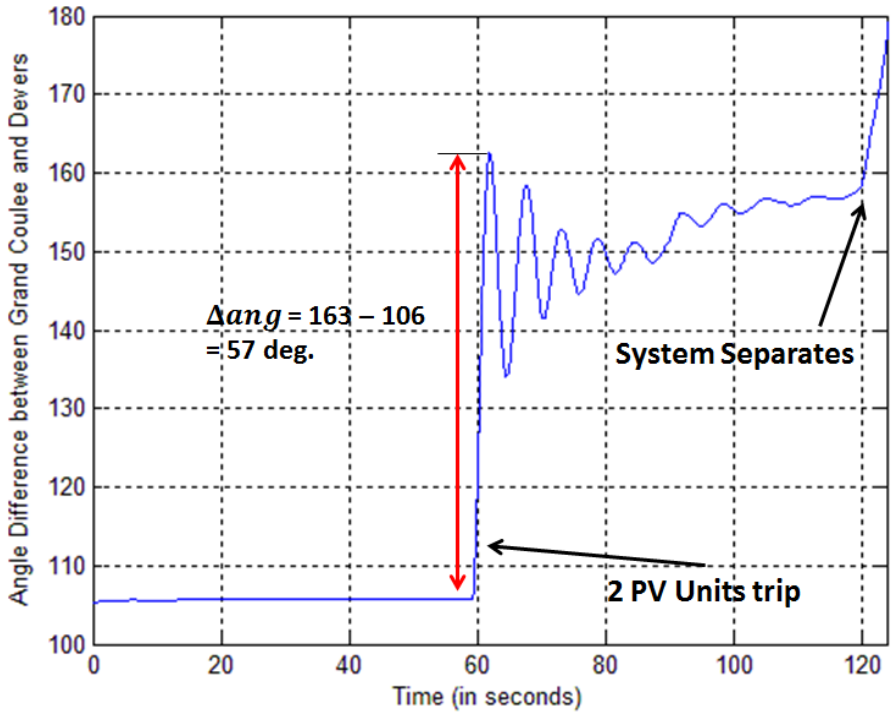

Fig. 6.12: Outage of two PV units for a heavily loaded system

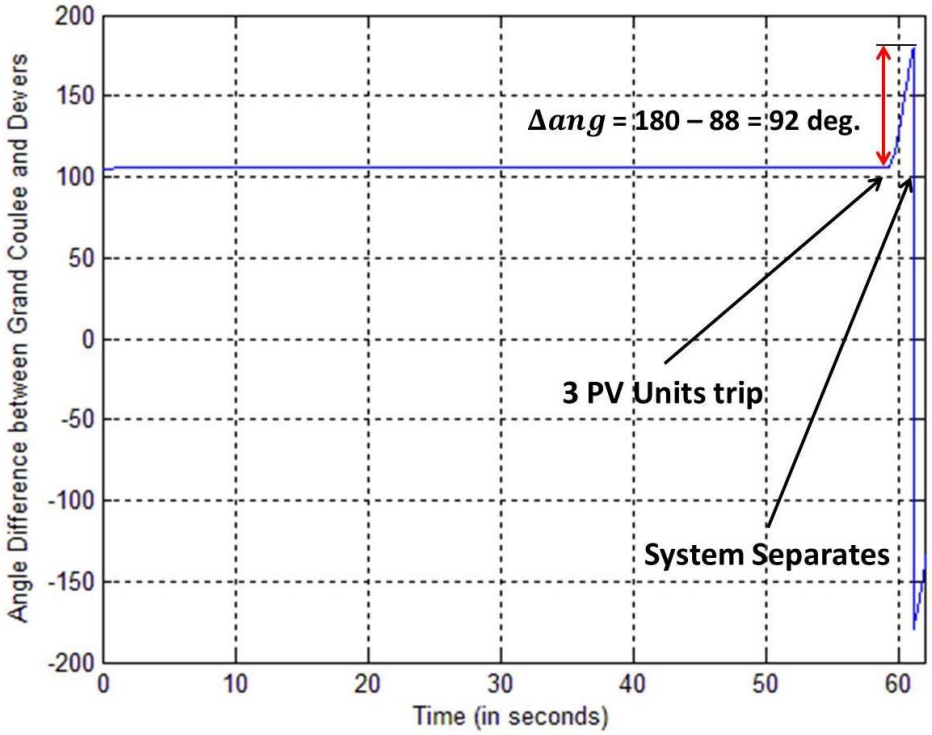

Fig. 6.13: Outage of three PV units for a heavily loaded system

Figs. 6.5-6.7 depict the outage of one, two and three units respectively for a lightly loaded condition; Figs. 6.8-6.10 depict the outage of one, two and three units respectively for a medium loaded condition; while Figs. 6.11-6.13 depict the outage of one, two and three units respectively for a heavily loaded condition. From Figs. 6.5-6.7 it is realized that a lightly loaded system (having an initial angle difference of 62°) is able to successfully withstand outage of three PV units. From Figs. 6.8-6.10 it is realized that a medium loaded system (having an initial angle difference of 88°) is able to withstand outage of two PV units but collapses when three units go out. From Figs. 6.11-6.13 it is realized that a heavily loaded system (having an initial angle difference of 105°) is able to withstand the outage of only one PV unit. From the plots given in Figs. 6.5-6.13, the following observations can be made:

- The model of the WECC system that had been used for the study is stable up to an initial angle difference of 135° between Grand Coulee and Devers
- The initial angle difference between 135° and 150° is the transition phase (vulnerable stage) and a clear demarcation between stability/instability cannot be made
- The model of the WECC system used for the study is likely to collapse if the initial angle difference between Grand Coulee and Devers exceeds 150°

In these observations, initial angle difference refers to the highest angle difference between Grand Coulee and Devers right after the dynamic event. From this analysis, it can be concluded that a high static stress limits a system's ability to handle high dynamic stress. For instance, if a system is operating at a static stress of x, where x is the pre-contingency angle difference between two critical node pairs, then it can successfully bear a dynamic stress of y, where y is angle by which the dynamic event affects their angle difference, such that $x + y \leq z$, where z is the angle difference limit between the critical node pairs that the system can bear. Therefore, for a given z, higher the value of x lesser will be the value of y, and vice-versa. Thus, by monitoring angle difference between different critical node pairs in real-time, one can capture a system's proximity to an unstable operation very quickly.

6.3.2 Sequential increase in loading of California-Oregon Inter-tie (COI)

The COI comprises of three 500kV transmission lines – two lines between Malin and Round-Mountain, and one line between Captain Jack and Olinda. The rated power flowing in these three lines is 4800 MW. For this set of simulation, this flow was increased from 4860 MW to 5680 MW and then to 6370 MW in two steps. This change in the loading was brought about by increasing generation in the North and loads in the South. Although for simulation purposes, this stress was artificially created, in reality, a very severe contingency *can* drive the COI flows to such high levels. Each of the loading "stressed" conditions lasted 5 min. resulting in a total simulation length of 15 min. Two different dynamic events were also applied to the system one min. after the start and their effects analyzed for the three loading conditions. The results obtained are as follows.

6.3.2.1 Load increase in the South

In this simulation, the loading of one bus in the South was increased by 100 MW independently for each of the three loading conditions. The resulting angle difference between Grand Coulee and Devers is shown in Fig. 6.14. From the figure it becomes clear that: (a) the damping of the oscillations decreased considerably as the loading on the system increased (red ovals); and (b) when the system is stressed, small changes in system conditions have much bigger impacts (black ovals). The Malin 500kV bus voltage was next monitored to test for its sensitivity with respect to change in COI flows. The results are shown in Fig. 6.15. The outer loops denote the transient swing following the changes in the COI loading whereas the solid red line depicts the best quadratic fit. The slope of the solid red line denotes the voltage sensitivity of Malin 500kV bus. From the figure it becomes clear that the slope would increase (become more negative) as the system moves closer to the nose-point. Therefore, by monitoring the

voltage sensitivity in real-time and setting alert/alarm thresholds based on its values, protective measures can be developed that will indicate system stress and possible collapse in advance.

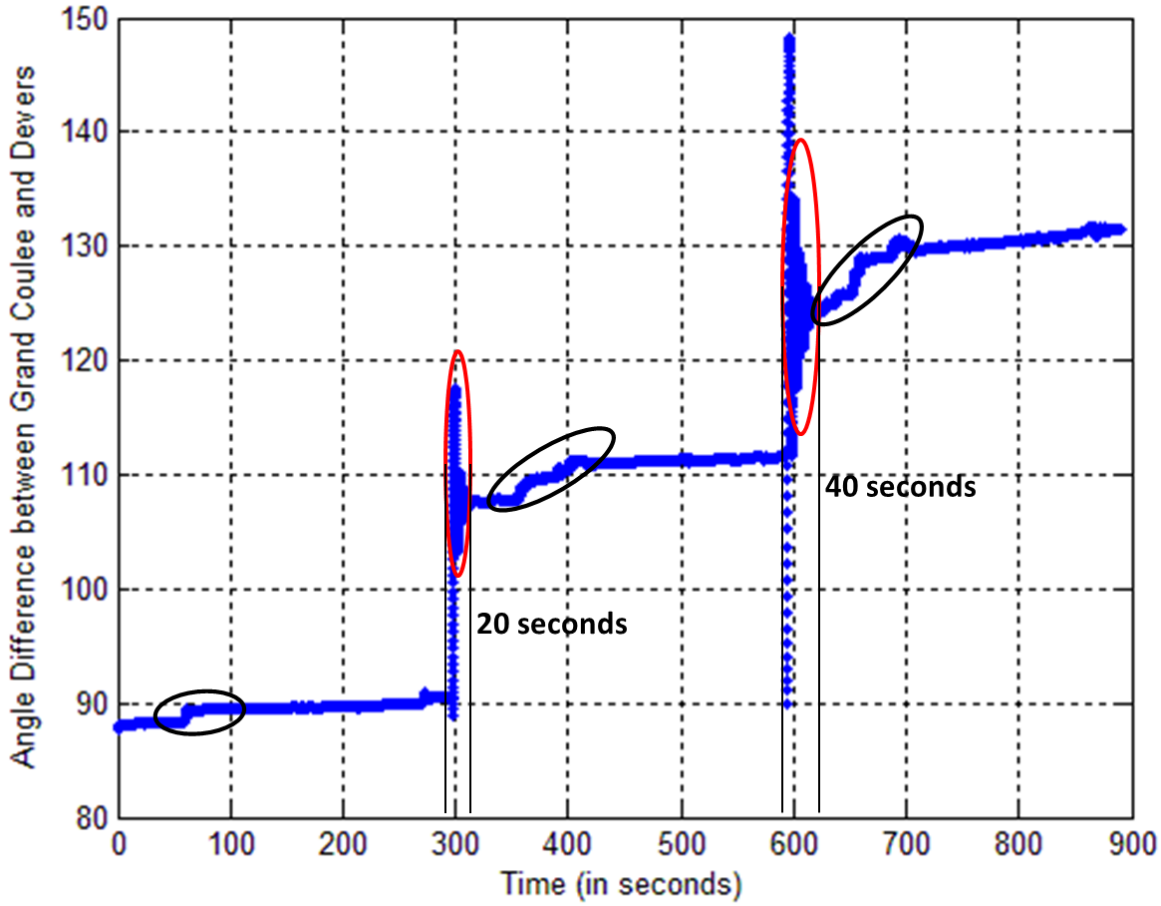

Fig. 6.14: Oscillations in angle difference between Grand Coulee and Devers for 100 MW load increase in the South

6.3.2.2 Load decrease in the North

In this simulation, 440 MW of load was dropped in the North and the resulting oscillations were analyzed for the three COI loading conditions. Fig. 6.16 shows the oscillations in the angle difference between Grand Coulee and Devers while Fig. 6.17 shows the variation in voltage magnitude of the 500kV Malin bus with respect to change in COI flow. From Fig. 6.16 it can be seen that the oscillations that resulted from the load drop take longer time to die out as the system becomes more and more stressed. The same fact is reflected in the voltage sensitivity plot of Fig. 6.17 which shows that the slope becomes increasingly negative with increase in stress. Thus, from these two simulations it can be

inferred that different types of stresses can be accurately analyzed by studying the angle difference and voltage sensitivity metrics in real-time.

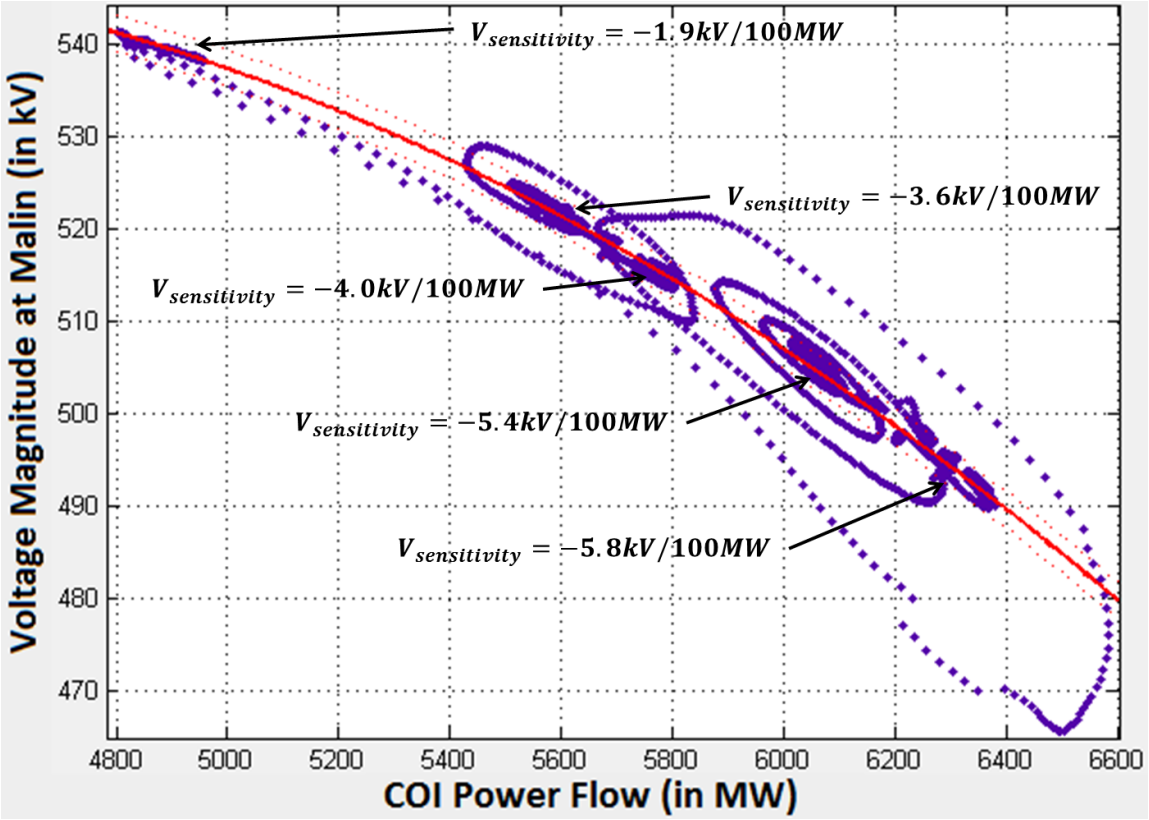

Fig. 6.15: Voltage sensitivity of 500 kV Malin bus as a function of the flow in the COI for a 100 MW load increase in the South

6.4 Integration with RTDMS

The simulations summarized in the previous section were created using PSLF software which is a power flow simulator developed by GE [116]. The primary advantages of using simulated data in comparison to real-world data are:

- Extreme events do not happen often enough to provide learning opportunities and hence simulations can be used to test contingency scenarios
- By using simulations, one can control the quality of the input data – there are no data drop-outs or stale/repeated values in a simulation, unless inserted knowingly

Since this study was done to analyze the performance of the proposed stress metrics, "good" data obtained from simulations was used. Moreover, simulated data also provided flexibility in terms of analysis and control (time and occurrence of event, region of study under test, etc.). However, since the ultimate goal is to test the utility of the proposed metrics with actual PMU data in real systems, an interface was built in MATLAB to integrate the simulations done in the previous section with RTDMS, which is an analytic and visualization platform developed by Electric Power Group (EPG). More details about RTDMS and the integration process are provided in the following sub-sections.

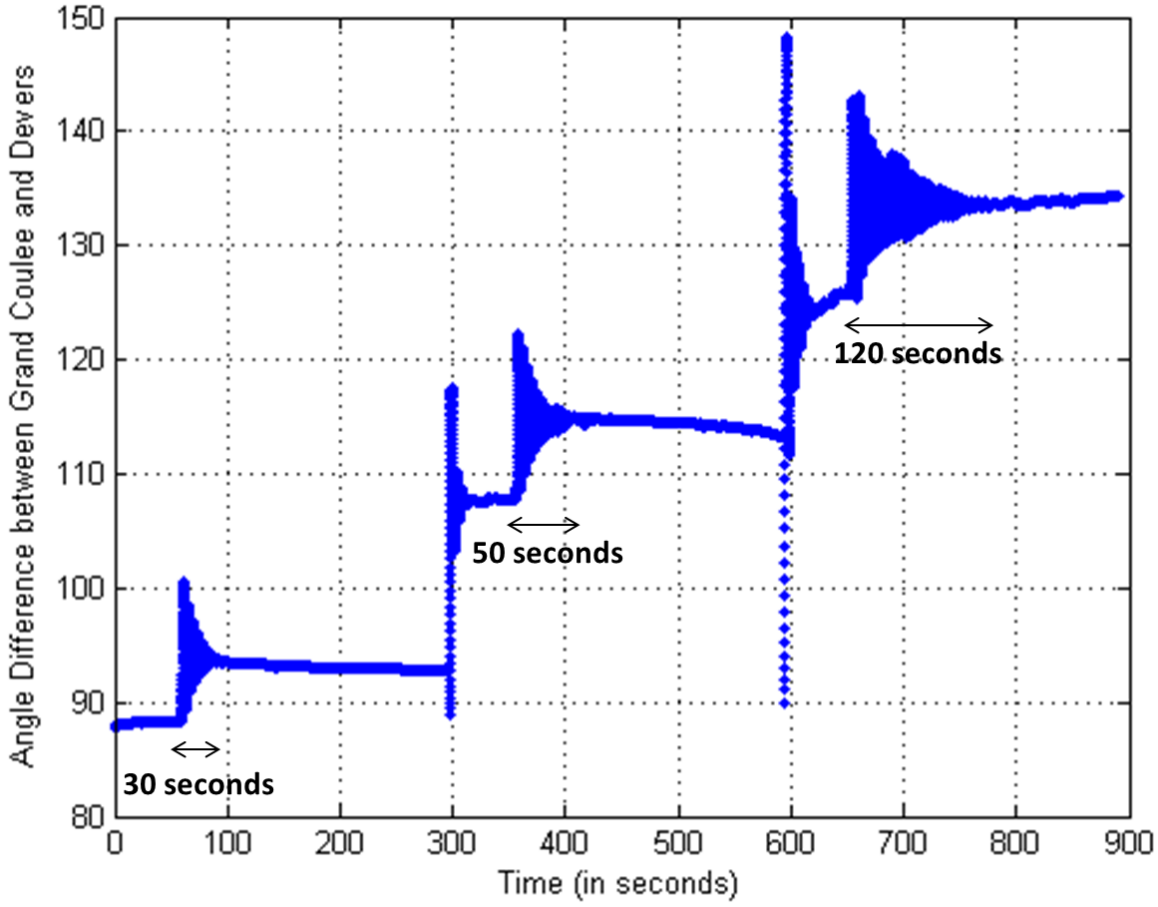

Fig. 6.16: Oscillations in angle difference between Grand Coulee and Devers for a load decrease of 440 MW in the North

6.4.1 Real Time Dynamics Monitoring System (RTDMS)

Investigations into major blackouts have concluded that the availability of real-time, wide area situational awareness is critical for reliability operations. Developed by EPG in early 2000, RTDMS is a synchrophasor based software application that addresses this critical need. It provides real-time, wide

area situational awareness to Operators, Reliability Coordinators, Planners and Operating Engineers and has been extensively used for monitoring and analysis of the power system [117]. RTDMS has been designed and built specifically for working with high resolution time synchronized data and has been upgraded over the years with new features and functionalities based on extensive industry feedback, research outcomes, and real world user experiences from field testing.

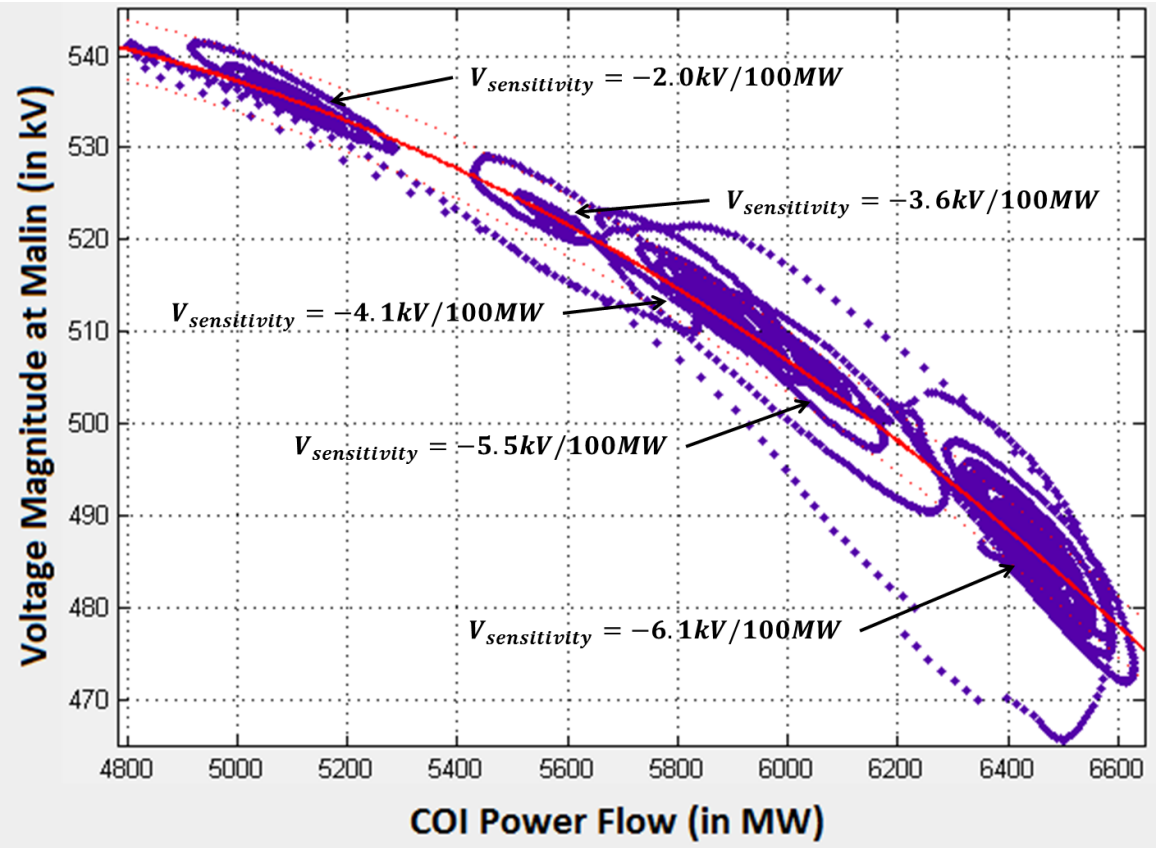

Fig. 6.17: Voltage Sensitivity of 500kV Malin bus as a function of the flow in the COI for a load decrease of 440 MW in the North

Some of the metrics that RTDMS has the capability to monitor and display are:

- Voltage Magnitude and Angles
- Angle differences between different buses
- Power flows (MW, MVARs)
- Oscillations (Frequency, damping and energy) and their detection
- Voltage and Angle sensitivities
- Alarms, etc.

Fig. 6.18 gives a snapshot of the RTDMS building blocks and functionalities [117]. RTDMS 2012 is the latest version of the software application and it has the following features:

- Multi-layer map giving quick access to different data metrics providing wide-area real-time visualization
- Providing clustering and de-clustering zoom in functionality
- Mouse over feature allowing operators to drill down to get more detailed information
- High-speed refresh rate trending charts
- Ability to use default displays or customize to meet operator preferences or situational circumstances
- RTDMS Event Analyzer providing a snapshot of critical location and information associated with an event via 'yellow pop ups' and drill down capability
- Display builder allowing users to create and save individual displays
- Integration with PI & EMS to exchange data and information between systems

Fig. 6.18: RTDMS building blocks and functionalities

6.4.2 Interfacing with RTDMS

As described in the previous sub-section, RTDMS has the ability to monitor angle differences and voltage sensitivities in real-time. Accordingly, an interface was built so as to integrate the simulations performed in section 6.3 with RTDMS. The role of the interface was to reorganize the data obtained from PSLF into a format that is compatible with RTDMS (IEEE C37.118). This post-processing of the data involved:

- Providing proper headers and time-stamps
- Computing df/dt
- Converting angles from radians to degrees
- Saving results in a comma separated value (CSV) file

Once the interface was built, the outputs of the PSLF simulations were fed into RTDMS. Identical results were obtained for all the test scenarios. The RTDMS snapshots depicting the more important results are provided in Figs. 6.19-6.33 with Tables 6.1 and 6.2 summarizing the effects. Figs. 6.19-6.28 correspond to the outage of PV unit/s for different levels of static stress (Section 6.3.1), while Figs. 6.29-6.32 depict the system state as the COI is progressively stressed along with a 100 MW load increase in the South (Section 6.3.2.1). Fig. 6.33 shows how the alarm panel in RTDMS will respond as the system conditions worsen for the scenario described in Figs. 6.29-6.32. Figs. 6.19 and 6.20 show the Grand Coulee-Devers angle difference and the 500kV Malin voltage, respectively, as three PV units trip in a lightly loaded condition. As can be seen from the plots, although there is a high angle difference between Grand Coulee and Devers and low voltage at Malin (indicating that the system is in a vulnerable state), there is no system separation or voltage collapse.

Figs. 6.21 and 6.22 show the Grand Coulee-Devers angle difference and the 500kV Malin voltage, respectively, as two PV units trip in a medium loaded condition. As can be seen from the plots, although there is a higher angle difference between Grand Coulee and Devers and lower voltage at Malin than the previous two figures (indicating that the system is in an even more vulnerable state), there is no system separation or voltage collapse. Fig. 6.23 and 6.24 show the Grand Coulee-Devers angle difference and the 500kV Malin voltage, respectively, as three PV units trip in a medium loaded condition. As can be seen from the plots, the 500kV Malin voltage collapses and the system separates. Moreover, it is also realized that since the system takes more than 30 seconds after the initiating dynamic event before the collapse occurs, if automatic load shedding schemes are put in place which will operate within that time frame (30 seconds), then the collapse can be avoided.

Figs. 6.25 and 6.26 show the Grand Coulee-Devers angle difference and the 500kV Malin voltage, respectively, as two PV units trip in a heavily loaded condition. As can be seen from the plots, the 500kV Malin voltage collapses and the system separates. However, in this scenario, the system took more than 60 seconds after the initiating dynamic event to collapse, indicating that if an automatic load shedding scheme is put in place that will operate within that time frame (60 seconds), then the collapse will be avoided. Figs. 6.27 and 6.28 show the Grand Coulee-Devers angle difference and the 500kV Malin voltage, respectively, as one PV unit trips in a heavily loaded condition. As can be seen from the plots, although there is a high angle difference between Grand Coulee and Devers and low voltage at Malin (indicating that the system is in a vulnerable state), there is no system separation or voltage collapse.

Figs. 6.29-6.32 show how the increase in COI power flow affect the Grand Coulee-Devers angle difference, the 500kV Malin voltage, as well as the voltage sensitivity of 500kV Malin bus w.r.t. COI. From the plots, it is observed that:

- As the COI flow is increased, the wide-area angle difference increases. This implies that the grid stress increases as the COI loading is increased.
- As the COI flow is increased, the 500kV voltage at Malin decreases. This implies that the system is developing a critical stress point at Malin.
- As the COI flow is increased, the voltage sensitivity of 500kV Malin bus w.r.t. COI becomes more negative. This implies that the increased stress is resulting in the system nearing the “nose point” of the PV curve.

Fig. 6.33 displays the alarm panel in RTDMS that will depict the state of the system corresponding to the events captured in Figs. 6.29-6.32. The rows of the alarm panel indicate the metric that is being monitored, while the columns indicate some of the large utilities/sub-regions present in the WECC. The color yellow denotes that a metric has exceeded its alert threshold, while the color red indicates that a metric has exceeded its alarm threshold. The threshold values are obtained from the base-line studies that have been previously performed on the system. As can be seen from Fig. 6.33, the base case condition has none of the indicators activated, thereby implying that the system is in normal condition. When the COI loading is increased to 118% (power flow increased to 5680 MW), the following indicators are activated:

- Indicator for the angle difference metric for Pacific Northwest is in red (alarm)
- Indicator for the angle difference metric for Southern California Edison (SCE) is in red (alarm)

- Indicators for MW and voltage sensitivity metrics for Pacific Northwest are in yellow (alert)
- Indicators for angle difference, MW, and voltage sensitivity metrics for Pacific Gas & Electric (PG&E) are in yellow (alert)

In the last panel, when the COI loading is increased to 133% (power flow increased to 6370 MW), the following indicators are activated:

- Indicators for angle difference, MW, MVAR, and voltage sensitivity metrics for Pacific Northwest are in red (alarm)
- Indicators for angle difference, MW, and voltage sensitivity metrics for Pacific Gas & Electric (PG&E) are in red (alarm)
- Indicator for the angle difference metric for Southern California Edison (SCE) is in red (alarm)
- Indicator for MW metric for Desert Southwest is in yellow (alert)
- Indicator for MW metric for Southern California Edison (SCE) is in yellow (alert)

Based on the above observations, it is realized that the number and severity of the metric state indicators (alerts/alarms) increase as the system stress increases (for this case, increase in loading of COI). Thus the alert/alarm panel of RTDMS is an excellent tool to visualize the state of a system in real-time. Table 6.1 summarizes the effect of Palo Verde unit trips on the WECC system (based on Figs. 6.19-6.28), while Table 6.2 summarizes the results depicted in Figs. 6.29-6.32. To conclude, the interface that was built for integrating the PSLF simulations with RTDMS was found to produce the desired results.

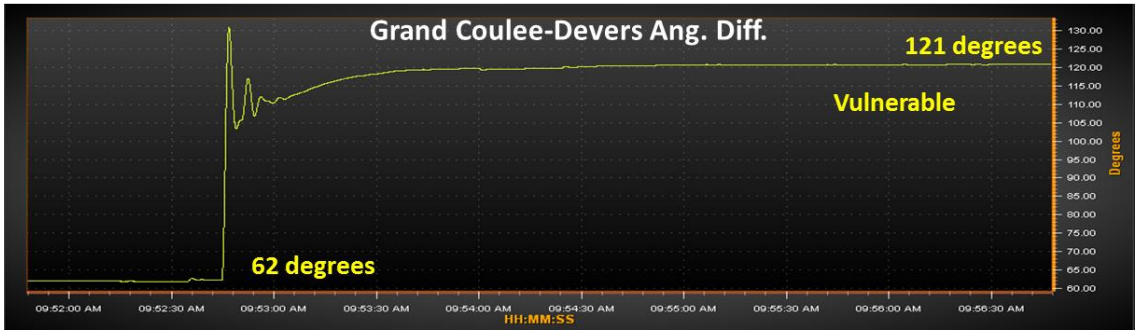

Fig. 6.19: RTDMS snapshot of Grand Coulee-Devers Angle Difference for outage of three PV units in a lightly loaded condition

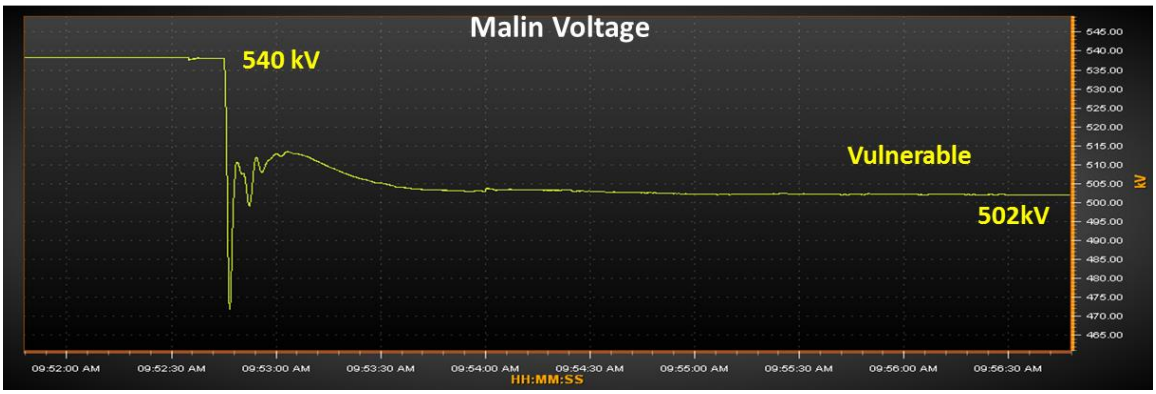

Fig. 6.20: RTDMS snapshot of 500kV Malin Voltage for outage of three PV units in a lightly loaded condition

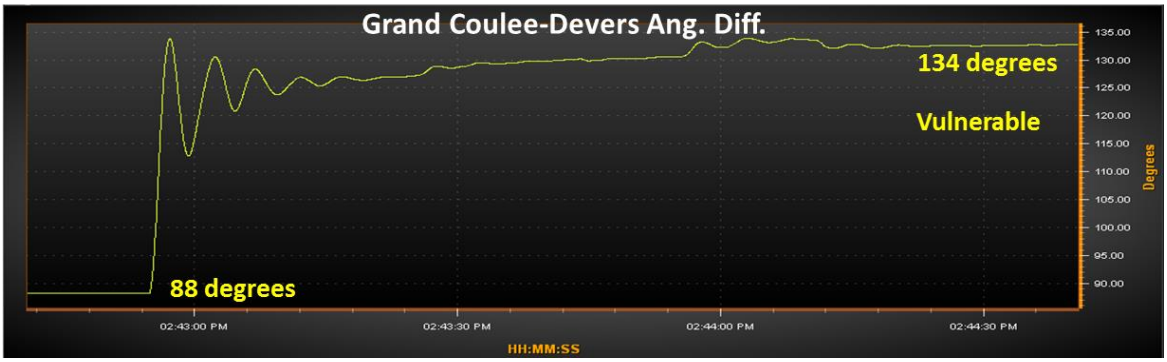

Fig. 6.21: RTDMS snapshot of Grand Coulee-Devers Angle Difference for outage of two PV units in a medium loaded condition

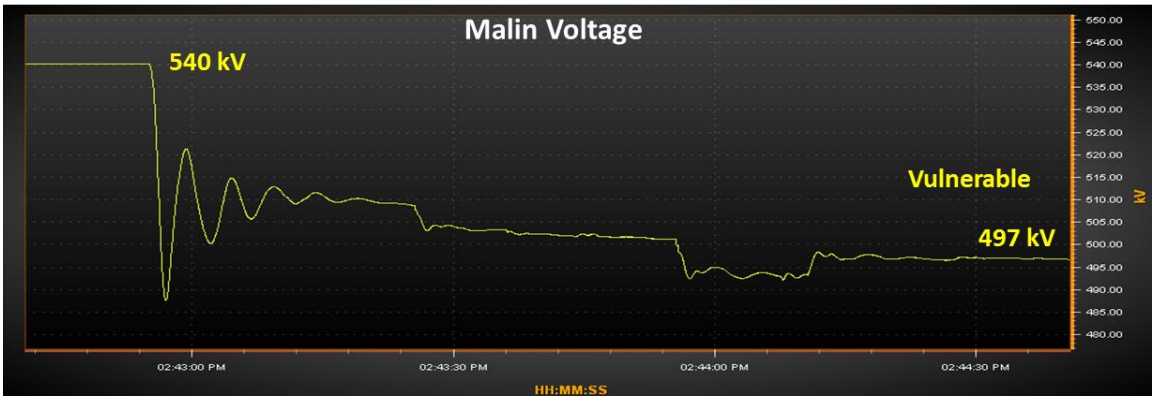

Fig. 6.22: RTDMS snapshot of 500kV Malin Voltage for outage of two PV units in a medium loaded condition

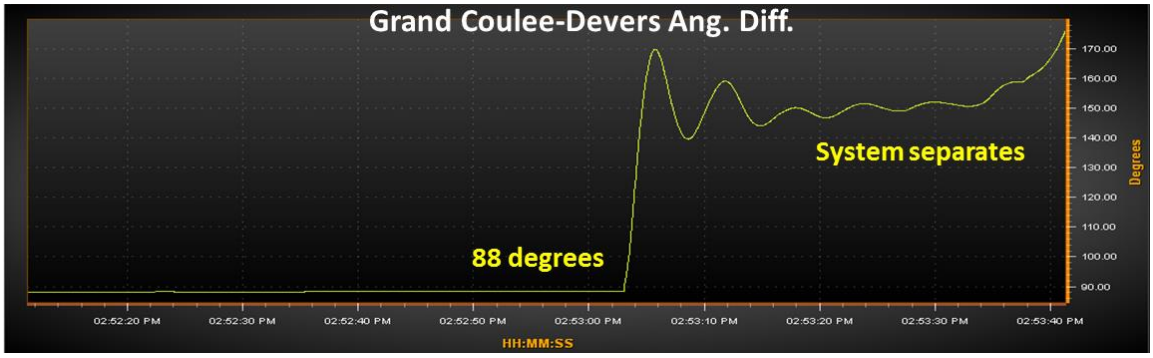

Fig. 6.23: RTDMS snapshot of Grand Coulee-Devers Angle Difference for outage of three PV units in a medium loaded condition

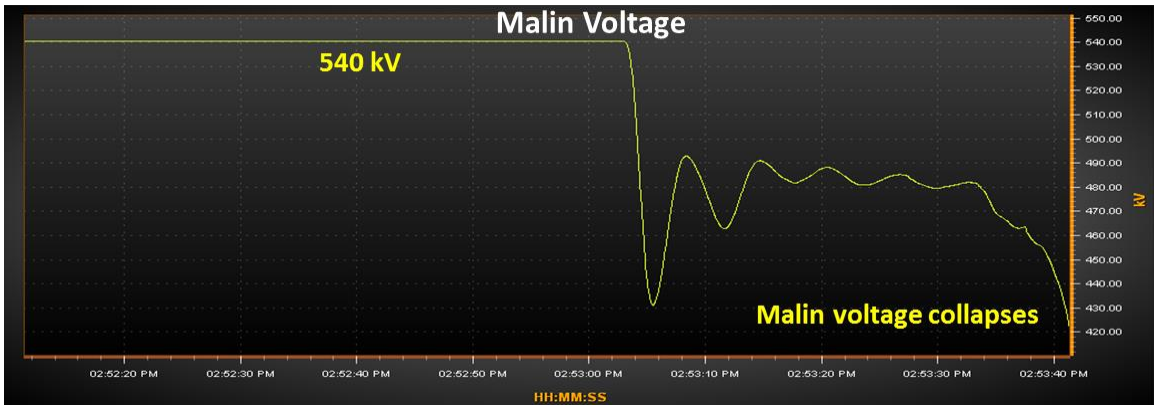

Fig. 6.24: RTDMS snapshot of 500kV Malin Voltage for outage of three PV units in a medium loaded condition

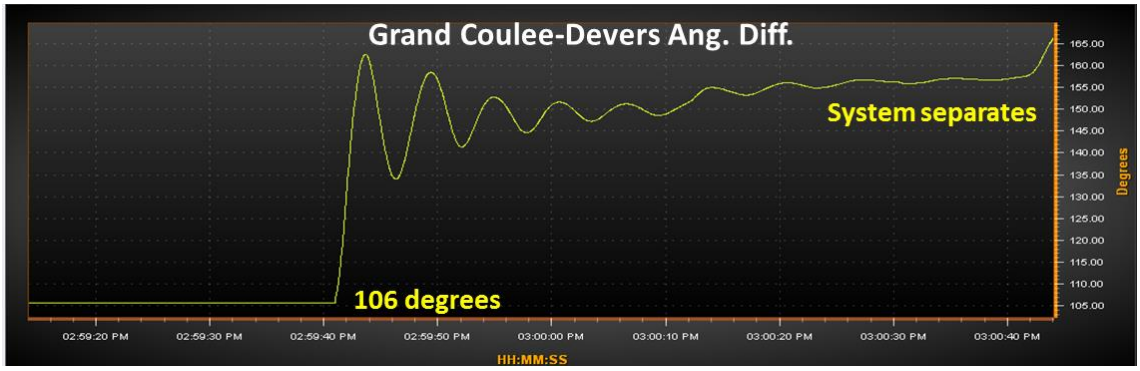

Fig. 6.25: RTDMS snapshot of Grand Coulee-Devers Angle Difference for outage of two PV units in a heavy loaded condition

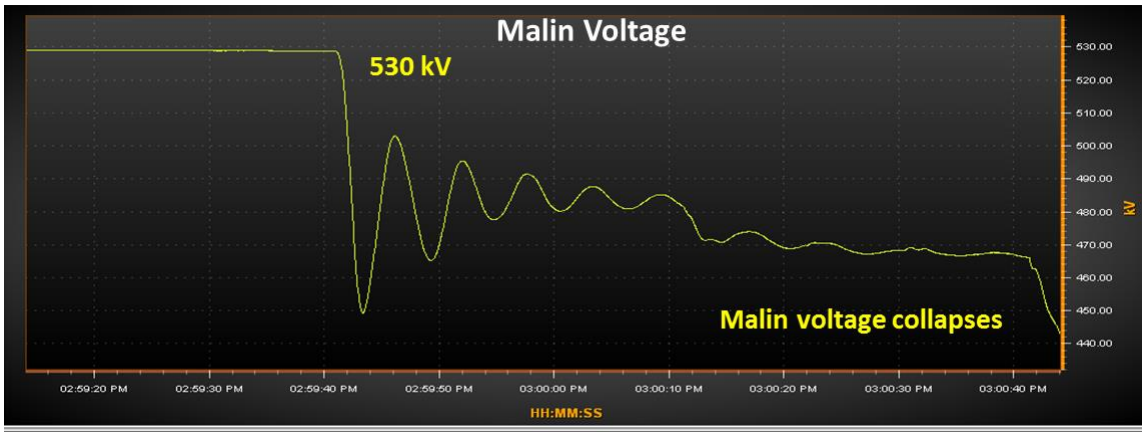

Fig. 6.26: RTDMS snapshot of 500kV Malin Voltage for outage of two PV units in a heavy loaded condition

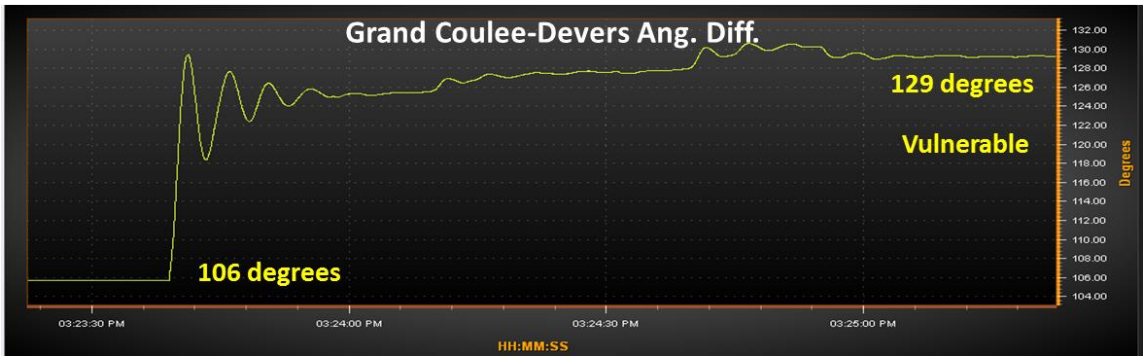

Fig. 6.27: RTDMS snapshot of Grand Coulee-Devers Angle Difference for outage of one PV unit in a heavy loaded condition

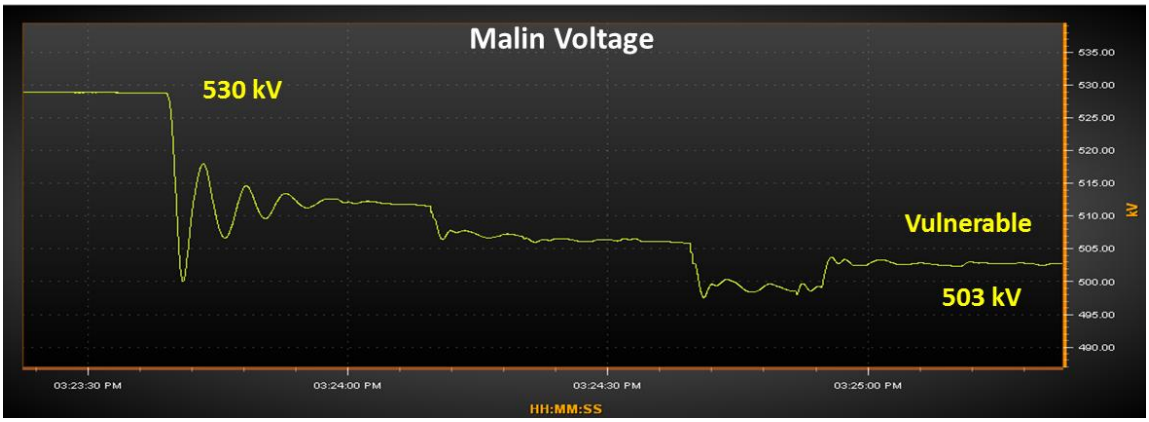

Fig. 6.28: RTDMS snapshot of 500kV Malin Voltage for outage of one PV unit in a heavy loaded condition

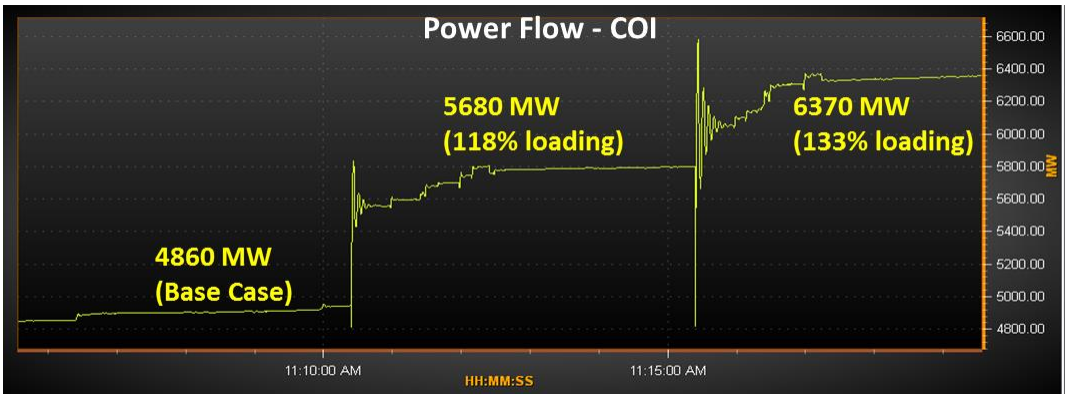

Fig. 6.29: RTDMS snapshot of Power flow in COI as the COI flow is increased along with a 100 MW load increase in the South

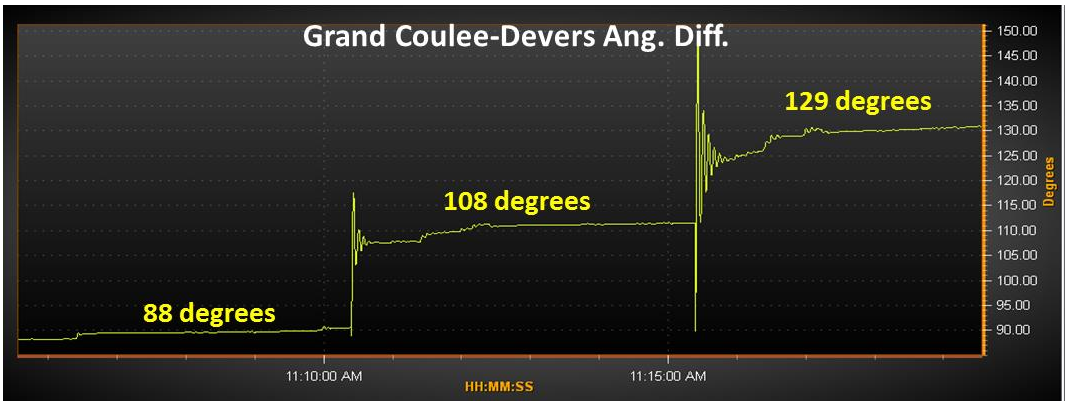

Fig. 6.30: RTDMS snapshot of Grand Coulee-Devers Angle Difference as the COI flow is increased along with a 100 MW load increase in the South

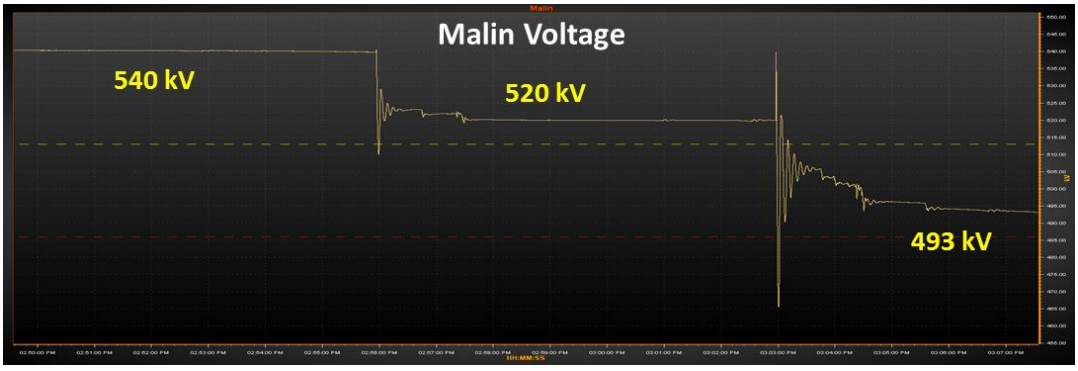

Fig. 6.31: RTDMS snapshot of 500kV Malin Voltage as the COI flow is increased along with a 100 MW load increase in the South

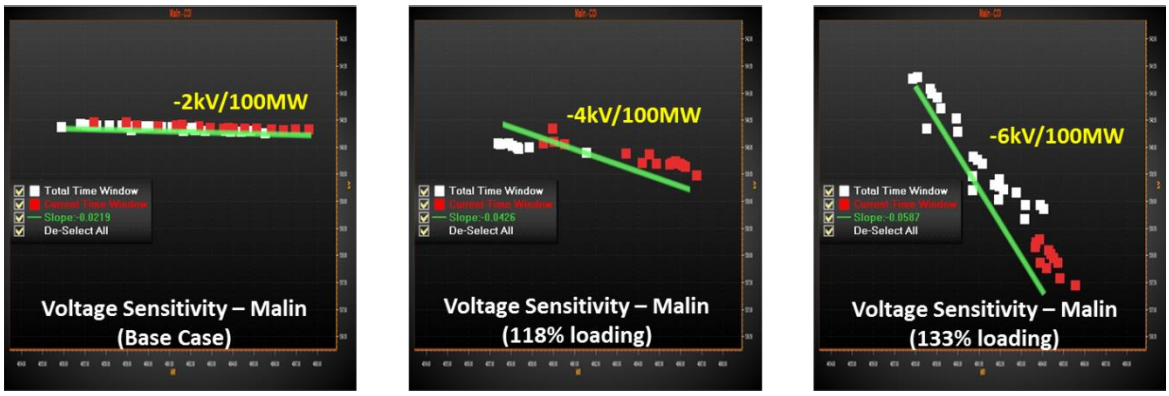

Fig. 6.32: Snapshots of the voltage sensitivity screen showing voltage sensitivity of 500kV Malin voltage with increase in COI flow

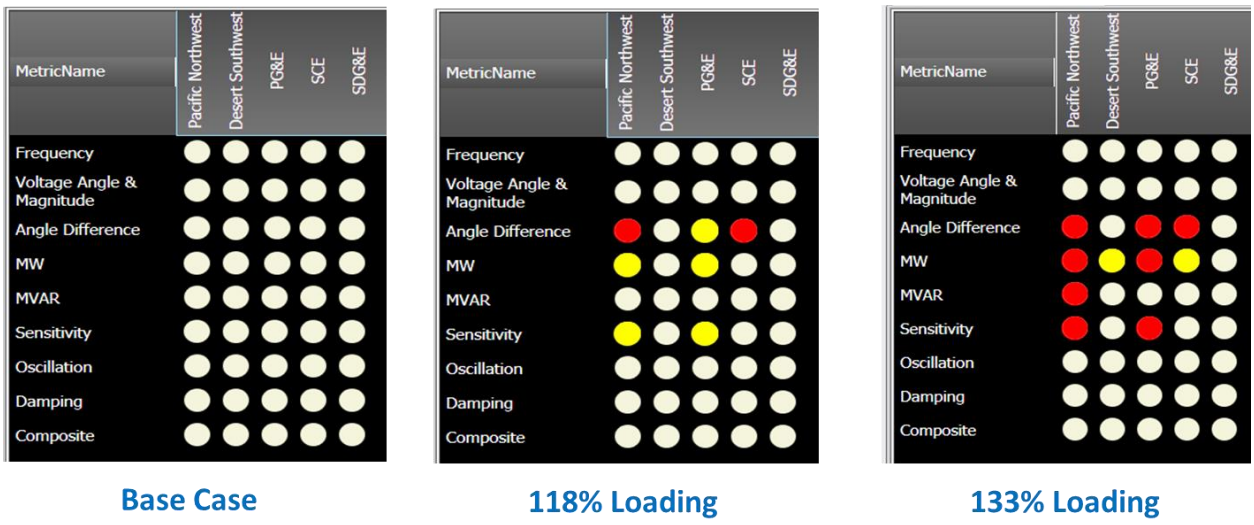

Fig. 6.33: Snapshots of the alarm panel showing worsening system condition

Table 6.1: Effect of Palo Verde Unit trips on the Grand Coulee-Devers Angle Difference

Static Stress Condition	Initial Angle Difference	Initial COI Loading	Final Angle Difference for different Dynamic Stress Conditions		
			1 Unit Trip	2 Units Trip	3 Units Trip
Light	62°	3213 MW	82° (Stable)	101° (Stable)	121° (Vulnerable)
Medium	88°	4800 MW	104° (Stable)	134° (Vulnerable)	>180° (Collapse)
Heavy	105°	5425 MW	131° (Vulnerable)	>180° (Collapse)	>180° (Collapse)

Table 6.2: Effect of increased COI flow on Malin 500kV bus's Voltage Sensitivity

Flow in COI	Loading Level	Angle Difference (static) between Grand Coulee and Devers	Voltage of Malin 500kV bus	Voltage Sensitivity of Malin 500kV bus w.r.t. COI flow
4860 MW	Base Case	88°	540kV	≈-2kV/100 MW
5680 MW	118% over load	108°	520kV	≈-4kV/100 MW
6370 MW	133% over load	129°	493kV	≈-6kV/100 MW

6.5 Conclusion

Two metrics are proposed in this chapter that use PMU data to monitor stress in a power system in real-time. Angle difference between substations located across the network and voltage sensitivity of buses lying in the middle are found to accurately reflect the static and dynamic stress of the system. The WECC system was used as the test system for this analysis. The simulations performed off-line were successfully integrated with RTDMS – a synchrophasor based software system developed by EPG for real-time wide-area visualization and situational awareness of the power system. The results indicate that by doing data mining on these two parameters and setting appropriate alerts/alarm limits, a more secure power system operation can be realized.

Chapter 7: Synchrophasor Data Conditioning and Validation and Possible Applications

All energy management systems (EMS) depend on algorithms that process raw power system data for computing the states of the system. The traditional non-linear state estimation techniques rely on supervisory control and data acquisition (SCADA) measurements for providing this raw data. The state estimator results in turn become the basis for other network applications such as real-time contingency analysis, system reliability studies, etc. As the electric utility industry becomes more and more familiar with synchrophasor technology, the transition of state estimation from a traditional non-linear formulation to one which is purely phasor based and linear becomes more and more realistic.

A purely PMU based state estimator has considerable advantages over a purely SCADA based or a mixed (SCADA-and-PMU based) state estimator [66], [67]. Firstly, being linear, the PMU only state estimator does not require any iteration. Secondly, it is free from the data scan that is required in conventional estimators. Thirdly, despite its formulation as a state estimation problem, the time-tagged data produces an estimate at such a fast enough rate that it can be considered to be truly dynamic. However, similar to the conventional state estimators, a PMU only state estimator also depends on a consistent, reliable stream of input data. Due to the streaming nature of the phasor data, downstream applications which use this data are vulnerable to network congestion, configuration errors, equipment failures, etc. Reference [118] highlights some of the data quality issues associated with PMU data, but does not provide any algorithm for its conditioning/validation. In [119] a computationally simple and efficient methodology for cleaning synchrophasor data was developed. In this chapter, the techniques developed in [119] will be elaborated upon and their possible use in solving other power system problems will be discussed.

7.1 Conceptual Design and Prototype Development at Dominion Virginia Power (DVP)

Both Virginia Tech (VT) and Dominion Virginia Power (DVP) have considerable experience in handling synchrophasor data. Virginia Tech has been a pioneer in the development of the PMU technology and DVP has a functioning three phase PMU-only state estimator. A PMU-based state estimator was first mentioned in [65] with details appearing in [66] and then in [120]. Such an estimator has been installed on DVP's 500kV network as part of a DOE demonstration project (DE-0E0000118) that has been led by Virginia Tech. The estimator and several applications have already been implemented in C# on the open-PDC platform. Since downstream applications will be affected by glitches in collected data, it becomes

necessary to develop techniques for conditioning and validating synchrophasor data in real-time. A methodology that can address this problem is described henceforth.

In order to detect bad data and switching operations that affect network topology, a technique to predict the next value of each voltage estimate from a history of previous estimates was developed in [27]. Fig. 7.1 shows this algorithm applied to a portion of a field data of samples and estimates of a complex voltage at 30 samples per second during a period of a low frequency oscillation at off-nominal frequency. In Fig. 7.1, the green line is actual synchrophasor data while the red circles are the estimates. The oscillation starts from the top right and moves to the bottom left. Since the estimate matches very well with the actual data, this three sample predictor model can be used to detect bad data by using an observation residual. It can also be used to smooth data by using subsequent measurements to obtain a better estimate which can be thought of as a technique for supplying missing data. Since this three-sample predictor model is very easy to implement, all measurements can be subjected to this same pre-processing, irrespective of the application for which it is used. Thus, it provides a simple and elegant solution to the synchrophasor data quality problem. Moreover, even if a linear state estimator is not desired, this data conditioning algorithm can be used independently for detecting bad data and finding the best estimate.

The objective of this research is to propose technical approaches to condition and validate synchrophasor data for real-time situational awareness applications. As such, the task approach and deliverables can be grouped under:

- System infrastructure design and maintenance
- Data checking algorithms
- Applications

The following sub-sections provide more details on the individual tasks.

7.1.1 System infrastructure design and maintenance

The goal is to make the synchrophasor infrastructure more robust with respect to component failures. This is done through substation level redundancy, measurement redundancy (with dual-use line relays), multiple fiber communication lines to control center, and machine redundancy in the central phasor data concentrator (PDC). Many of these problems can be avoided by taking precautionary measures during the commissioning process. The reason for this is that the root causes for most of these issues

are synchronization errors which are primarily due to errors in PDC delay settings. These errors can be prevented by being extra careful during the commissioning phase. Similarly, online determination of signal to noise ratio (SNR) of the PMU data can be used to observe the health of electrical equipments and detect potential problems in them in the early stages.

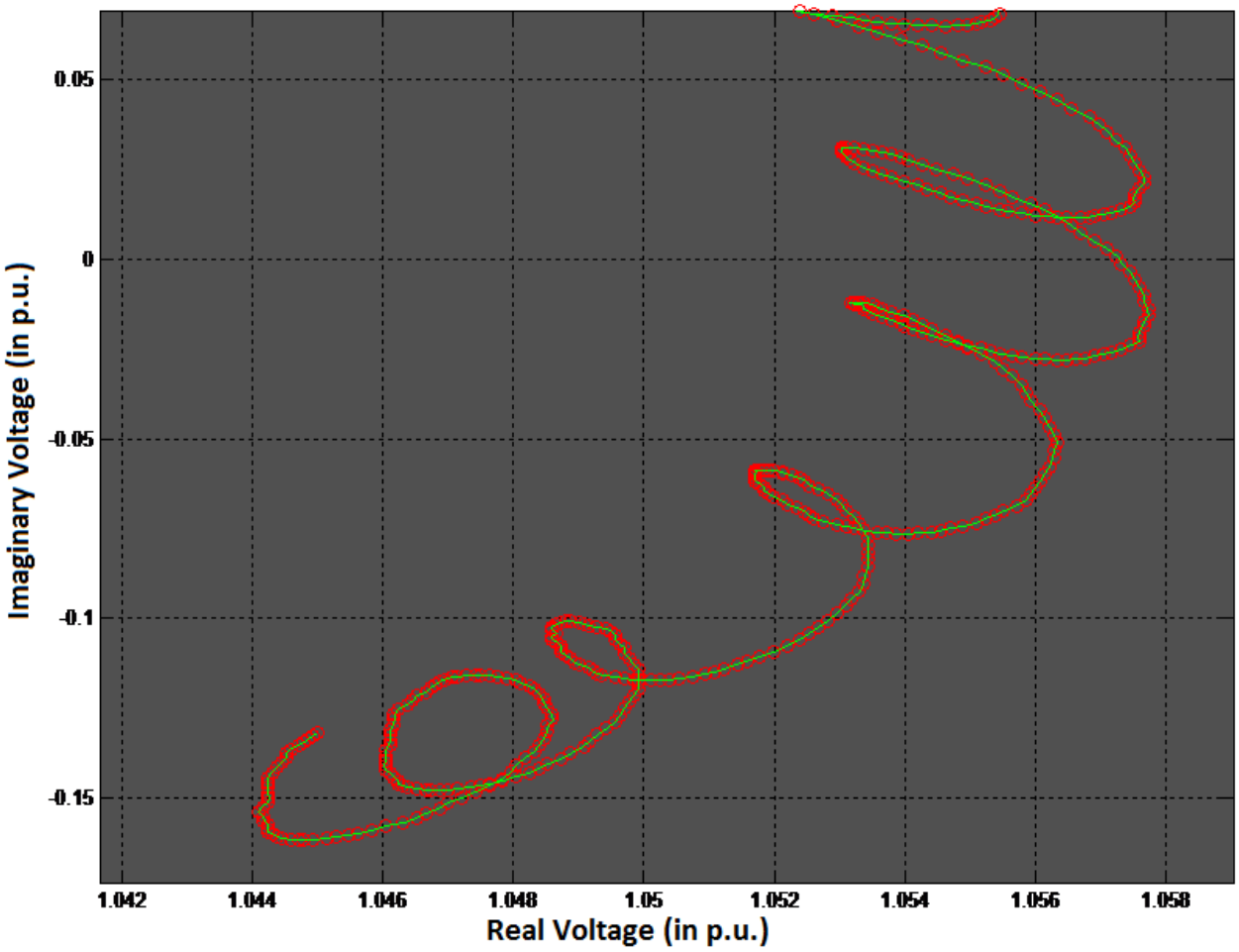

Fig. 7.1: Performance of the three sample predictor on real synchrophasor data

Dominion's central PDC architecture design and Emergency System Operation Center (ESOC) architecture design are found to be some of the best practices in the industry for ensuring high availability of data from the field to the control center. Data/measurement redundancy can also be realized by using dual-use line relays as PMUs so as to obtain multiple observations of voltages and breaker statuses. Moreover, the CBBBIO technique developed in Chapter 4 can be used for selecting relevant locations for placing the PMUs. By initially identifying buses critical to the network and by providing redundancy to their measurements, PMUs can be deployed efficiently and effectively.

7.1.2 Data checking algorithms

The aim is to provide algorithms for required data quality metrics and desired network monitoring approaches. To do this, the data is passed through two blocks before being fed into the linear state estimator. The cleaning block is responsible for conditioning the data when it is possible to do so. This will be accomplished with optimal filtering and smoothing techniques combined with knowledge from a quadratic prediction model [27]. The monitoring block is responsible for validating the quality of the incoming data and providing information when data cleaning is not possible/not sufficiently effective and manual intervention is required. The linear state estimator uses knowledge obtained from both of these blocks for performing bad data detection as well as for providing a best estimate when there is measurement redundancy. The block diagram describing the proposed data conditioning and validation process is shown in Fig. 7.2.

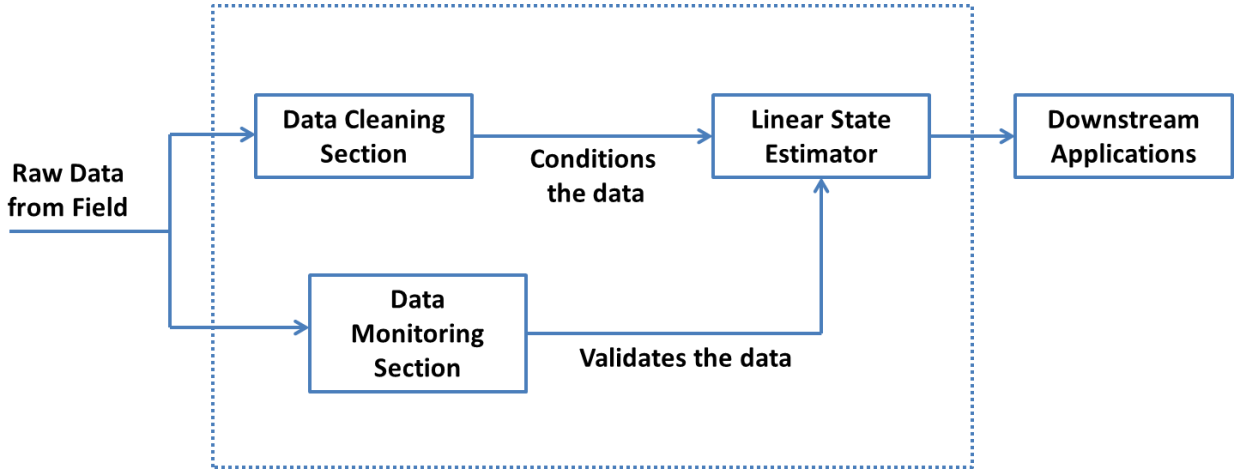

Fig. 7.2: Data Conditioning and Validation Module

7.1.3 Applications

The methodology for conditioning and validating synchrophasor data proposed in [119] is expected to address the following issues. It is to be noted here that many of the problems encountered below are specific to the Dominion system and therefore the solutions proposed are developed while taking that into account. At the same time, it can also be realized that some of the problems are more general in nature, for which case the solutions proposed will are also generic.

1. Loss of data from one or several PMUs: The existing linear state estimator that is in use in DVP is robust enough to reconfigure itself when there is loss of data from one or more PMUs [121].

This is done by removing those measurements from the estimation problem. However, if data loss is just intermittent (that is infrequent and with only a few adjacent points missing), the missing data can be provided by an optimal filtering algorithm in a pre-processing step, as will be seen in the next section. However, if a signal is completely lost and does not come back, even occasionally, then it is compromised and must be removed from the estimator.

2. Loss of signals in a PMU: Since its effect is similar to the previous item, the same logic applies. Missing measurements, if intermittent, are replaced using optimal filtering and smoothing algorithms, while if they are not, then they are dropped from the estimator altogether.
3. Stale (non-refreshing) data: Stale signals are continuously monitored but they are not included in the estimation process. By doing so, if the problem of stale data is found to persist, the data will continue to be ignored. However, when fresh data starts coming, it will be re-included in the estimation purposes.
4. Inconsistent data, data rates and latencies: Being primarily caused due to the improper settings of the PDC, this issue is addressed by modifying the PDC's settings. The root cause may be varied but properly regulating the lead and lag time settings of the PDC is expected to be the solution to the problem.
5. Off-sets in signal magnitude and phase: Offsets related to current transformer (CT) and potential transformer (PT) errors are constant for most loading conditions and can be solved by calibrating instrument transformers [122]. Temporary offsets have been observed in some of the older PMUs but for the current PMUs this should not be a problem as long as they satisfy the IEEE standard of having a total vector error (TVE) of less than one percent [2]-[4]. It will be shown later in this chapter that properly conditioned and validated synchrophasor data can also provide an insight into instrument transformer calibration.
6. Corrupted and drifting signals in a PMU: PMUs can detect this anomaly and report it via the Status Word in the C37.118 stream. If this is the case then measurements which have been compromised due to synchronization errors can be immediately removed from the state estimation process. This step can be performed online. However, if the PMU does not detect synchronization errors then each of the synchrophasors can be referenced to a single phasor. Then an algorithm must be developed that watches for changes in one or more reference angles with respect to the group. The algorithm must also be able to use multiple references to redundantly check if there is a drift in the reference itself. However, the development of such an algorithm is left as a future exercise.

7. Corrupted and drifting time reference in one or several PMUs: If a corrupt time stamp is detected online then the measurement is compromised and should be removed from the estimation process. This is also indicative of problems in the configuration of the PMU and not just loss of synchronization. If it is the latter case, then it can be identified during the commissioning phase itself. The last two issues have been observed by DVP when the PMU has not been configured correctly during installation. It has been fixed using proper settings and firmware updates.
8. Combination of several issues described above: If properly integrated into the synchrophasor estimator application, then all the issues described above can be properly dealt with in an online application. However, online handling of such issues should not be relied upon for dealing with *all* data quality issues. Data validation procedures should be created and executed upon installation of the PMU hardware in the substation so as to minimize problems from occurring in the future.
9. Loss of primary source and/or communication and transition to alternate source: DVP has addressed this issue by duplicating their synchrophasor architecture. In essence, the main PMU stream has been duplicated so that even if the fiber that connects to the control center is lost, the performance of the linear state estimator is not affected.
10. Failure of the topology processor and/or bad/incomplete topology information (where topology refers to the status of elements of the power system): This is mitigated by the state estimator reacting appropriately to missing data. Proper conditioning of synchrophasor data can provide assistance in mitigating incorrect impedance values in the network model. However, the logic that is to be followed for doing it is beyond the scope of this work.

7.2 Methodology for performing synchrophasor data conditioning and validation

A data conditioning algorithm for pre-processing synchrophasor data has been developed in [119]. A brief overview of the techniques proposed there is provided in this section. In [119], two methods for pre-screening the PMU data before it reached the linear estimator were introduced first. Next, it was followed by a Kalman filter [123] based filtering and smoothing technique that used a "quadratic prediction model" [27] as well as a resetting algorithm for data conditioning. It was observed that the approach proposed in [119] mitigated drop-outs, outliers, and other data quality issues that decreased the value of the phasor data at a downstream location, at the source itself.

7.2.1 Pre-screening of synchrophasor data

Similar to other algorithms that use SCADA data, purely synchrophasor data-based algorithms are also susceptible to data quality issues. Loss of GPS synchronization, incorrect PMU configuration, and communication network congestion are few of the problems commonly encountered in relation to phasor data. Two simple techniques for validating the quality of the incoming data even before it is received by the linear state estimator are:

- Plausibility Checks, and
- Signal-to-Noise Ratio (SNR)

Plausibility checks can be thought of as the first step for any data conditioning algorithm. It consists of a set of online filters which perform sanity checks on the incoming data. For instance, it is common practice at DVP to authenticate the PMU data after an installation before the stream is connected to the operations center. By doing so, issues resulting from an incorrect configuration of the PMU, problems with the GPS clock or an incorrectly connected signal wire can be captured and immediately resolved. In addition to preventing unworthy data from being consumed by the application, the online algorithm for plausibility checks also makes engineers aware of data quality problems that will require manual intervention. Different types of plausibility checks that would cause measurements to be eliminated before state estimation is performed are:

- In-service buses having zero, near zero or negative voltage magnitude measurement readings
- In-service lines having zero or near zero current magnitude measurement readings
- For three phase systems, phasor groups with improper phase relationships
- Bad, missing, or repeated time-stamps
- Frequency excursion of 0.1 Hz or more from the average nominal value (60 Hz)
- Rate of change of frequency excursion of 0.03 or more from the average nominal value (Zero)
- Measurements which have a C37.118 status word showing the *DataValid* bit asserted
- Measurements which have a C37.118 status word showing the *PMUSync* bit asserted
- Measurements which have a C37.118 status word showing the *PMUError* bit asserted
- Measurements which have other problems communicated via the C37.118 status word

Evaluating the Signal-to-Noise Ratio (SNR) of a signal is an efficient method to monitor the quality of that signal. Since reconstructing the original sinusoid would be difficult, the assumption made is that the

components of the phasor (magnitude and unwrapped referenced phase angle) are DC signals. Under such conditions, SNR is the mean of the signal divided by the standard deviation of the signal taken over a moving window [124] as shown in (7.1).

$$\mathrm{SNR_{DC}(in\ dB)} = 10\log\left(\frac{\mu}{\sigma}\right) = 10\log\left(\frac{\text{mean}}{\text{std. dev.}}\right) \tag{7.1}$$

SNR evaluation not only indicates loose connections or potential hardware problems, but also helps diagnose equipment issues much more accurately than the raw voltage measurement. An example of this is shown in Fig. 7.3. Fig. 7.3a depicts the SNR magnitude plot of a potential transformer (PT) of a 500kV bus few days prior to a fault. Fig 7.3b depicts the SNR angle plot for the same PT. It is clear from the figures that both the magnitude and the angle plots show a clear indication of a potential problem (identified by the wider spread of the C-phase data in comparison to the other phases). Moreover, since these types of devices fail slowly, by regularly monitoring the SNR, signs of failure can be identified days in advance. For instance, the SNR magnitude and angle plot shown in Fig. 7.3 captured the faulty C-phase data three days before the PT actually failed. Also, since SNR is a relative measure whereas the raw voltage measurement is an absolute one, SNR becomes a suitable candidate for setting alarm limits.

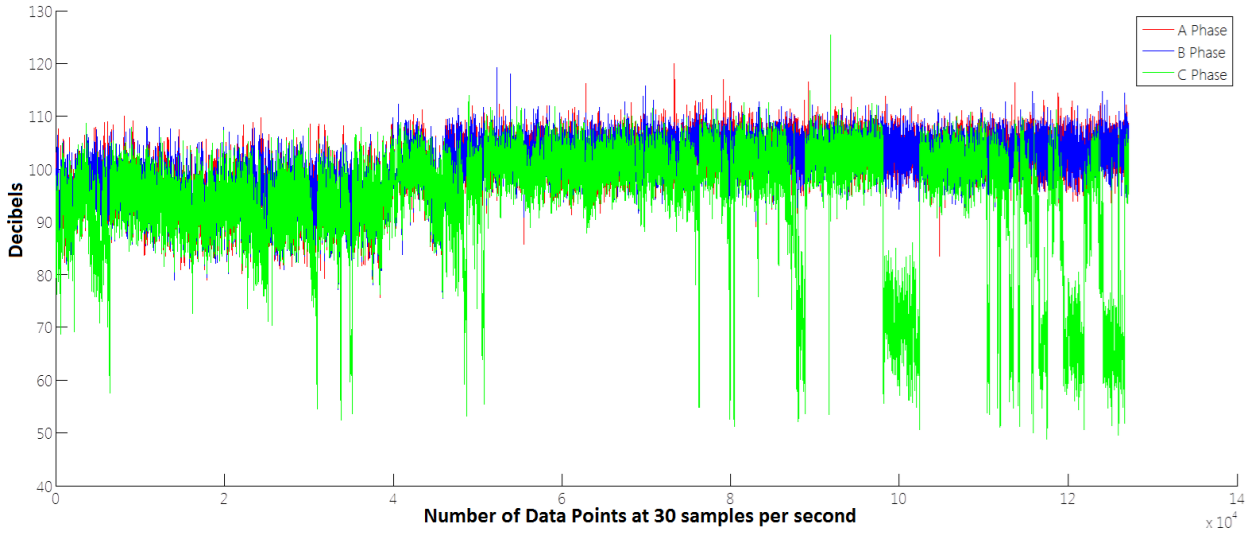

Fig. 7.3a: Signal-to-Noise Ratio of phase magnitude during C-phase PT failure

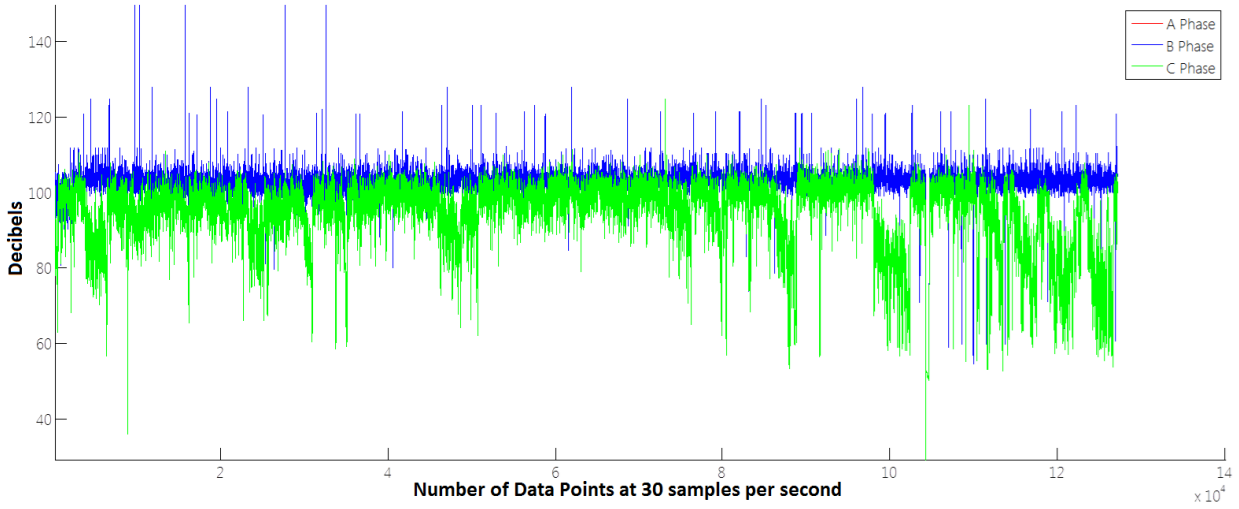

Fig. 7.3b: Signal-to-Noise Ratio of referenced phase angle during C-phase PT failure

A key assumption made during the computation of the SNR is the quasi-steady state operating condition of the power system. The size of the moving window used to calculate the mean and standard deviation components is critical for establishing a base-line criterion for alarming as it dictates the sensitivity of the calculation. Therefore, an intelligent alarming scheme would be necessary to prevent misinterpretation of the SNR during oscillations and when discrete changes occur in the network. The former can be avoided by using an oscillation detection algorithm while the latter can be circumvented by alarming only when the SNR is higher than a pre-defined threshold for a certain period of time.

7.2.2 Techniques developed for data conditioning and validation

The idea of a three phase linear state estimator using only synchrophasor data was originally proposed in [28]. However, the state estimator model developed in [28] was not a tracking state estimator because it considered each new frame as a separate problem. Therefore, it was impossible to detect/identify bad data using that model. An improvement to that model was made using [27] which identified the "quadratic" relationship between the past, present and future states. That relationships is given by,

$$\hat{x}(k+1|k) = 3\hat{x}(k|k) - 3\hat{x}(k-1|k-1) + \hat{x}(k-2|k-2) \tag{7.2}$$

In (7.2), x refers to the individual state, $\hat{x}$ (read as x-hat) denotes the estimated value of x, while the symbol | is the "given" operator. Therefore, $\hat{x}(k|j)$ reads as x-hat of k given j. Equation (7.2) is based on the logic that for a linear increase in load at constant power factor (true for a power system at 30 times

a second); the complex voltages (and currents, since currents are linear functions of voltage) will follow a quadratic trajectory with the next estimate depending on three previous estimates [27]. It is to be noted here that (7.2) is the same as (3.12) except that the individual state was represented by the letter y in (3.12) while it is denoted by x in (7.2). Using (7.2), two techniques for conditioning synchrophasor data via Kalman filtering are described below.

7.2.2.1 Kalman-filter based filtering

The classical model of a Kalman filter is given in (7.3). In the following equations, bold characters represent matrices.

$$\begin{aligned}\mathbf{x}(k+1) &= \mathbf{\Phi}(k+1,k)\mathbf{x}(k) + \mathbf{\Gamma}(k+1,k)\mathbf{w}(k)\\ \mathbf{z}(k+1) &= \mathbf{H}(k+1)\mathbf{x}(k+1) + \mathbf{v}(k+1)\end{aligned} \tag{7.3}$$

In (7.3), k is the discrete time step, $\mathbf{x}(k+1)$ is the system state at time $k+1$, $\mathbf{x}(k)$ is the system state at time k, $\mathbf{z}(k+1)$ is the actual measurement at time $k+1$, $\mathbf{w}(k)$ is the zero-mean Gaussian process noise at time k, $\mathbf{v}(k+1)$ is the zero-mean Gaussian measurement noise at time $k+1$, $\mathbf{\Phi}(k+1,k)$ is the state transition matrix relating the transition of the state from time k to time $k+1$, $\mathbf{\Gamma}(k+1,k)$ is the disturbance transition matrix relating the transition of the disturbance from time k to time $k+1$, and $\mathbf{H}(k+1)$ is the measurement matrix at time $k+1$. For optimal filtering we take the estimate of (7.3) and express it as a recursive relation in the Kalman filter notation as seen in (7.4a) and (7.4b).

$$\hat{\mathbf{x}}(k+1|k+1) = \mathbf{\Phi}(k+1,k)\hat{\mathbf{x}}(k|k) + \mathbf{K}(k+1)\big(\mathbf{z}(k+1) - \hat{\mathbf{z}}(k+1|k)\big) \tag{7.4a}$$

$$\hat{\mathbf{z}}(k+1|k) = \mathbf{H}(k+1)\hat{\mathbf{x}}(k+1|k) \tag{7.4b}$$

In (7.4a) $\mathbf{K}(k+1)$ is the Kalman gain. Equation (7.4a) and (7.4b) can be solved using the standard Kalman filtering technique [125]. However, when applied to synchrophasor data, it can be further simplified. Due to the nature of the quadratic prediction model, adjacent state vectors share two of the three state variables in common yielding an augmented state vector. This can be imagined as a moving window that contains three snapshots of the system at any given time and which moves forward only one snapshot at a time. Therefore, for predicting the next state based on (7.2), $\hat{\mathbf{x}}(k|k)$ and $\hat{\mathbf{x}}(k+1|k)$ can be expressed as,

$$\hat{\mathbf{x}}(k|k) = \begin{bmatrix} \hat{x}(k|k) \\ \hat{x}(k-1|k-1) \\ \hat{x}(k-2|k-2) \end{bmatrix} \tag{7.5a}$$

$$\hat{\mathbf{x}}(\mathrm{k}+1|\mathrm{k}) = \begin{bmatrix} \hat{\mathrm{x}}(\mathrm{k}+1|\mathrm{k}) \\ \hat{\mathrm{x}}(\mathrm{k}|\mathrm{k}) \\ \hat{\mathrm{x}}(\mathrm{k}-1|\mathrm{k}-1) \end{bmatrix} \tag{7.5b}$$

Since the estimate of the future state depends on the three previous state estimates, for filtering purposes, it makes sense to depict $\hat{\mathbf{x}}(\mathrm{k}|\mathrm{k})$ and $\hat{\mathbf{x}}(\mathrm{k}+1|\mathrm{k})$ as 3×1 matrices. Now, we know that $\mathbf{\Phi}(\mathrm{k}+1,\mathrm{k})$ relates the $\mathrm{k}+1$ state to the k state, i.e.

$$\hat{\mathbf{x}}(\mathrm{k}+1|\mathrm{k}) = \mathbf{\Phi}(\mathrm{k}+1,\mathrm{k})\hat{\mathbf{x}}(\mathrm{k}|\mathrm{k}) \tag{7.5c}$$

Therefore, based on (7.2), (7.5a), (7.5b) and (7.5c), $\mathbf{\Phi}(\mathrm{k}+1,\mathrm{k})$ can be formulated as a constant as shown in (7.5d).

$$\mathbf{\Phi}(\mathrm{k}+1,\mathrm{k}) = \begin{bmatrix} 3 & -3 & 1 \\ 1 & 0 & 0 \\ 0 & 1 & 0 \end{bmatrix} \tag{7.5d}$$

It is to be noted here that in (7.5a) and (7.5b), the states are the complex voltage and current measurements. Therefore, without any loss of generality, we can write (7.5e) and (7.5f).

$$\mathbf{z}(\mathrm{k}+1) = \mathrm{x}(\mathrm{k}+1) + \mathrm{v}(\mathrm{k}+1) \tag{7.5e}$$

$$\hat{\mathbf{z}}(\mathrm{k}+1|\mathrm{k}) = \hat{\mathrm{x}}(\mathrm{k}+1|\mathrm{k}) \tag{7.5f}$$

Using (7.5b) and (7.5f) in (7.4b), we get $\mathbf{H}(\mathrm{k}+1)$ as,

$$\mathbf{H}(\mathrm{k}+1) = [1 \quad 0 \quad 0] \tag{7.5g}$$

Thus, on substituting (7.5d) and (7.5g) in RHS of (7.4a) and (7.4b), respectively, a simplified model of the filtering technique will be developed as shown in (7.6a) and (7.6b).

$$\hat{\mathbf{x}}(\mathrm{k}+1|\mathrm{k}+1) = \begin{bmatrix} 3 & -3 & 1 \\ 1 & 0 & 0 \\ 0 & 1 & 0 \end{bmatrix} \hat{\mathbf{x}}(\mathrm{k}|\mathrm{k}) + \mathbf{K}(\mathrm{k}+1)\big(\mathrm{z}(\mathrm{k}+1) - \hat{\mathrm{z}}(\mathrm{k}+1|\mathrm{k})\big) \tag{7.6a}$$

$$\hat{\mathbf{z}}(\mathrm{k}+1|\mathrm{k}) = [1 \quad 0 \quad 0]\hat{\mathbf{x}}(\mathrm{k}+1|\mathrm{k}) \tag{7.6b}$$

The second term in RHS of (7.6a) corresponds to the steady state observation residual. Typical plots for the observation residuals obtained in case of actual data are shown in Fig. 7.4 and Fig. 7.5. Figs. 7.4a and 7.4b show the observation residual for the voltage magnitude and angle while, Figs. 7.5a and 7.5b show the observation residual for the current magnitude and angle. The mean that is observed in the

observation residuals corresponds to the ratio errors present in the measurements. Therefore, the mean of the residuals reflect the uncalibrated nature of the measurements [126].

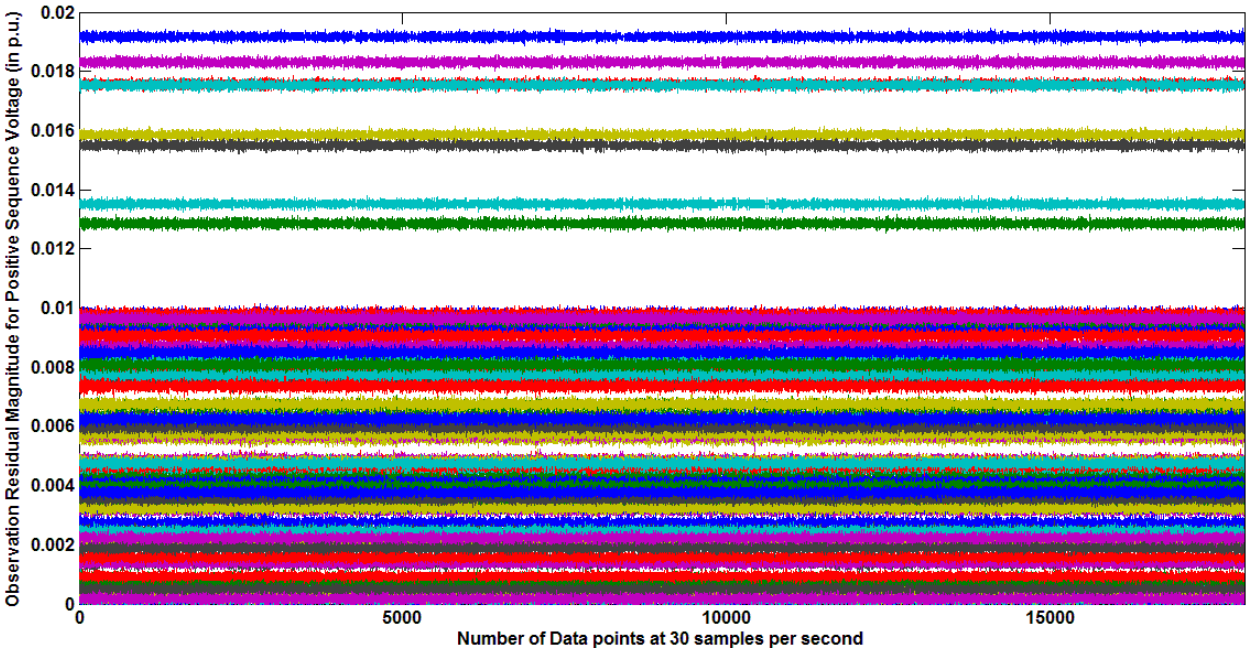

Fig. 7.4a: Observation residual for typical voltage magnitude measurements

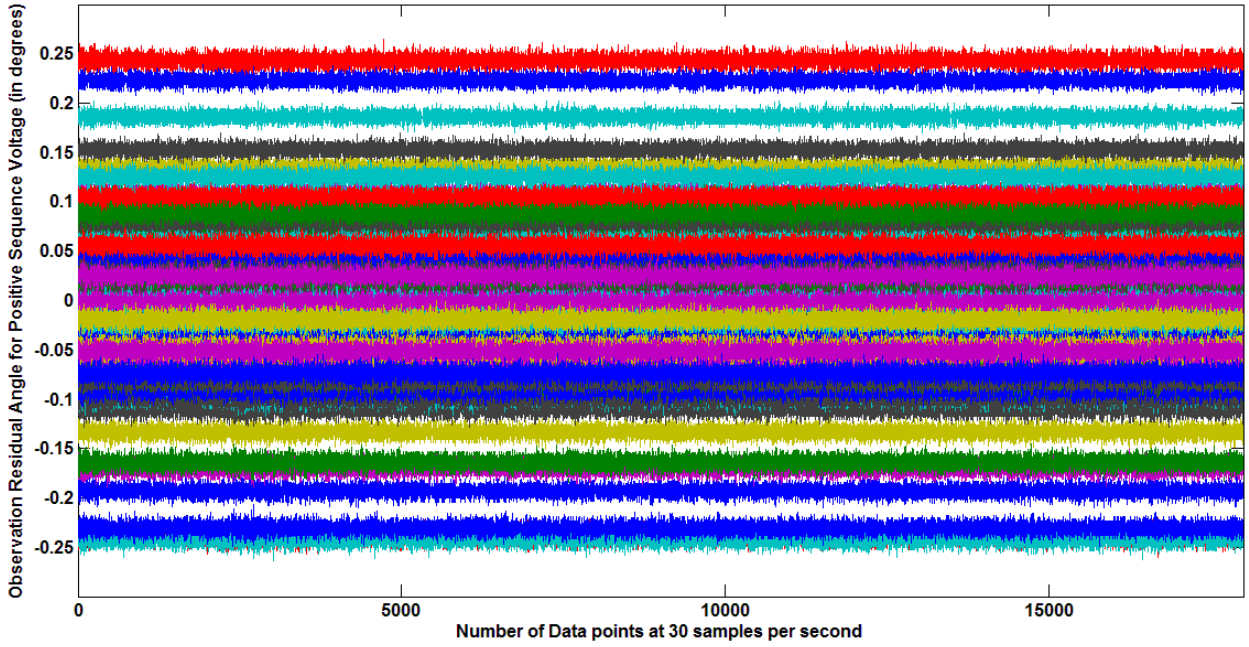

Fig. 7.4b: Observation residual for typical voltage angle measurements

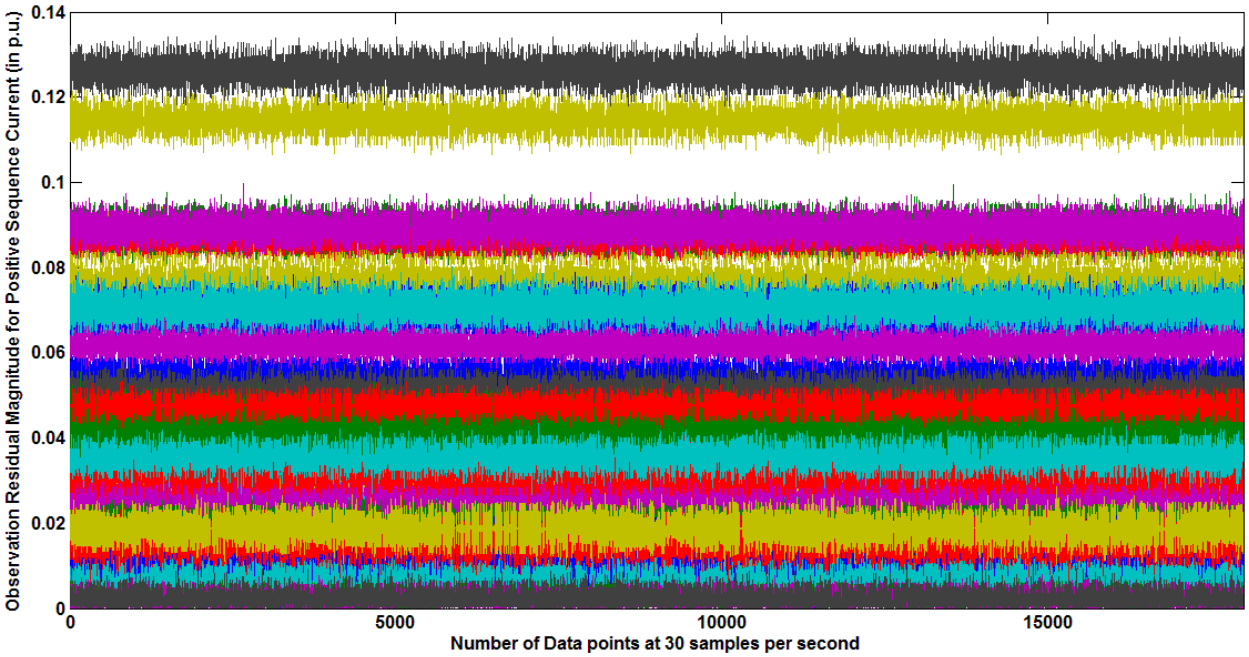

Fig. 7.5a: Observation residual for typical current magnitude measurements

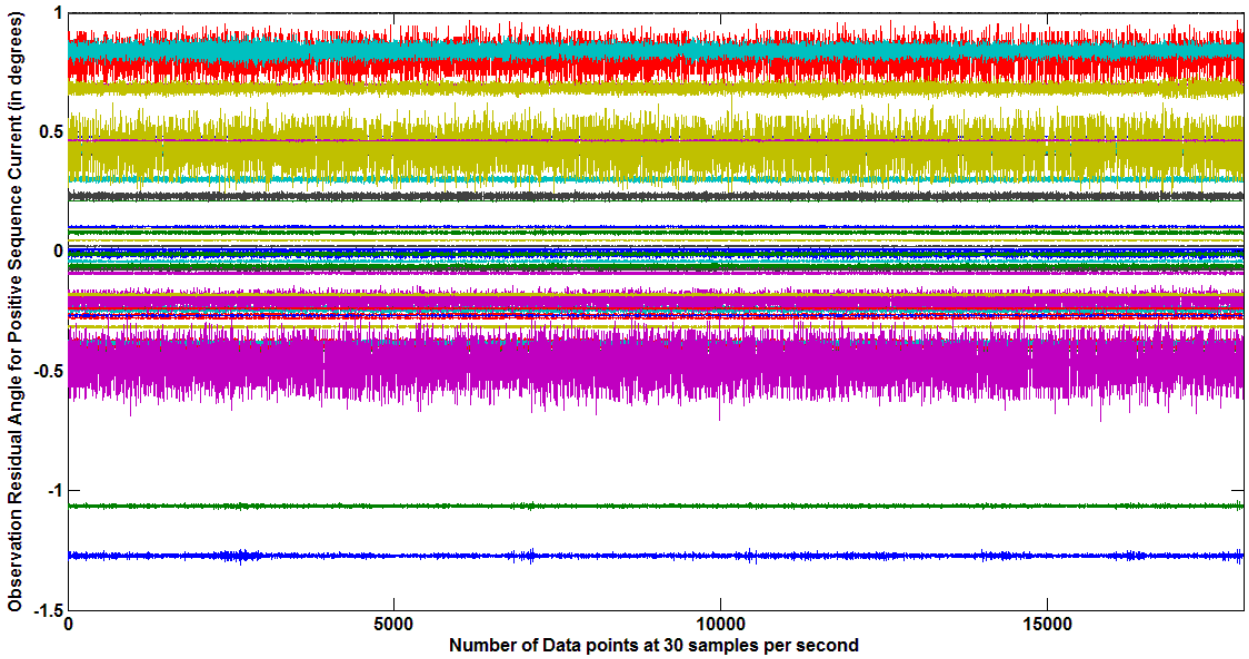

Fig. 7.5b: Observation residual for typical current angle measurements

7.2.2.2 Kalman-filter based smoothing

The smoothing algorithm estimates the previous states of the system using current measurements. Mathematically, this means solving for $\hat{\mathbf{x}}(\mathrm{k}|\mathrm{j})$ where $\mathrm{j} > \mathrm{k}$ [125]. The quadratic prediction model associated with synchrophasor data that had been used for filtering purposes also applies to the smoothing process. The model of the fixed-lag smoother that has been used was developed in [127]. It has a discrete time state equation in the form of a recursive Kalman filter with an augmented state vector, an associated augmented dynamical system, and an augmented measurement equation as seen in (7.7). More details about it can be found in [125] and [127]. In (7.7), N is the window length, while $\mathbf{K}(\mathrm{k}+1)$, $\mathbf{K}_1(\mathrm{k}+1)$ … $\mathbf{K}_{\mathrm{N}}(\mathrm{k}+1)$ are the gain matrices.

$$\begin{bmatrix} \hat{\mathbf{x}}(\mathrm{k}+1|\mathrm{k}+1) \\ \hat{\mathbf{x}}(\mathrm{k}|\mathrm{k}+1) \\ \hat{\mathbf{x}}(\mathrm{k}-1|\mathrm{k}+1) \\ \vdots \\ \hat{\mathbf{x}}(\mathrm{k}+1-\mathrm{N}|\mathrm{k}+1) \end{bmatrix}$$

$$= \begin{bmatrix} \boldsymbol{\Phi}(\mathrm{k}+1,\mathrm{k}) & \mathbf{0} & \mathbf{0} & \dots & \mathbf{0} \\ \mathbf{I} & \mathbf{0} & \mathbf{0} & \dots & \mathbf{0} \\ \mathbf{0} & \mathbf{I} & \mathbf{0} & \dots & \mathbf{0} \\ \vdots & \vdots & \vdots & \ddots & \vdots \\ \mathbf{0} & \mathbf{0} & \dots & \mathbf{I} & \mathbf{0} \end{bmatrix} \begin{bmatrix} \hat{\mathbf{x}}(\mathrm{k}|\mathrm{k}) \\ \hat{\mathbf{x}}(\mathrm{k}-1|\mathrm{k}) \\ \hat{\mathbf{x}}(\mathrm{k}-2|\mathrm{k}) \\ \vdots \\ \hat{\mathbf{x}}(\mathrm{k}-\mathrm{N}|\mathrm{k}) \end{bmatrix}$$

$$+ \begin{bmatrix} \mathbf{K}(\mathrm{k}+1) \\ \mathbf{K}_1(\mathrm{k}+1) \\ \mathbf{K}_2(\mathrm{k}+1) \\ \vdots \\ \mathbf{K}_{\mathrm{N}}(\mathrm{k}+1) \end{bmatrix} \left(\mathbf{z}(\mathrm{k}+1) - \mathbf{H}(\mathrm{k}+1)\hat{\mathbf{x}}(\mathrm{k}+1|\mathrm{k})\right) \tag{7.7}$$

Equation (7.7) can be solved recursively as shown in [127]. The matrices $\boldsymbol{\Phi}(\mathrm{k}+1,\mathrm{k})$ and $\mathbf{H}(\mathrm{k}+1)$ in (7.7) have same dimensions and values that were computed in the previous sub-section. A judicious choice of window length is important because although a higher value of N would introduce more delay between the received measurement and the smoothed state estimate, it will also improve the quality of the estimate by a significant amount. The reason for this being that an estimate obtained using $\hat{\mathbf{x}}(\mathrm{k}+1-\mathrm{N}|\mathrm{k}+1)$ will be intuitively better than one obtained using $\hat{\mathbf{x}}(\mathrm{k}+1-\mathrm{N}|\mathrm{k}+1-\mathrm{N})$ [125]. A suitable window length for the simulations done here was found at $N = 3$.

The smoothing technique works in the same way as the filtering technique with regards to time and measurement updates. Also, for both the filtering as well as the smoothing techniques, the initial conditions for all of the estimates and covariances can be zero without requiring an additional Kalman

filter to provide this information as long as it is acknowledged that the values for these will not be correct until the first window has been completely filled with data. Thus, in essence, the fixed lag smoothing algorithm is an extension of the filtering technique.

The relevance of a quadratic prediction model based Kalman filter is profound for the given application. Before the introduction of phasor measurements, the idea of tracking the state of the power system with a Kalman filter like process was suggested in [68]. The difficulty in the use of such a filter for the current application is that the number of measurements made using PMUs is inadequate to produce a successful estimate based on that approach. To elaborate, Dominion Virginia Power (DVP) has approximately 4,000 buses. Therefore, the traditional Kalman filter will require a state equation for the states of all the 4,000 buses. However, DVP has placed PMUs on only their high voltage network (500kV buses) which number about 30. In such a scenario, a traditional dynamic/tracking estimator will not work because all the states of the system will not be "observable". The proposed approach considers each state individually. Therefore, the predicted value of *a state* is based on the previous predicted values of the *same state*. Hence, the proposed methodology is independent of the network model/size. This also implies that the process and measurement noise associated with the proposed approach (commonly denoted by the process noise covariance, Q and the measurement noise covariance, R) are scalar quantities.

Another significance of the proposed approach is that it can detect bad data in the individual measurements based on the history of that measurement. The three-phase linear state estimator developed in [28] considered every measurement as a "fresh" measurement. Therefore, bad data detection was impossible using their approach. In the proposed approach, the quadratic prediction model developed in [27] is integrated with the linear state estimation formulation. By doing so, an observation residual is created (Eq. (7.6)) that detects anomalies in the individual measurements, thereby validating its quality. It is also important to point out here that the quadratic prediction model developed in [27] was meant for detecting bad data or exogenous events. It had not been used for "cleaning real synchrophasor data" which is the focus here. Moreover, the data used in [27] was simulated data (IEEE 118-bus system), whereas the data used here is real synchrophasor data obtained from the field. Therefore, they are two separate applications based on the same (quadratic) prediction model.

7.2.2.3 Resetting Function

The data conditioning algorithm based on Kalman-filter based filtering and smoothing algorithms was found to perform very well for data quality issues up to the 20% mark (probabilistically) [119], [126]. For higher percentages of bad data, it was observed that sustained dropouts were present in the incoming data. Consequently, as the probability of adjacent data point drops increased, the data conditioning algorithm lost its ability to make accurate predictions. Fig. 7.6 shows the phasor magnitude plot for a scenario where there is 50% likelihood (probabilistically) that each data point will be lost. Although the algorithm gives reasonable results for some time, it does not take long until so many adjacent data points are lost that the prediction diverges from the raw measurements. This is because if the observation residual remains high, the measurement will keep getting replaced by the optimal predicted estimate. Under such circumstances, even if after some time, the incoming data becomes good, the error in the optimal prediction would have compounded so many times that it would not be able to track the raw measurements anymore [126].

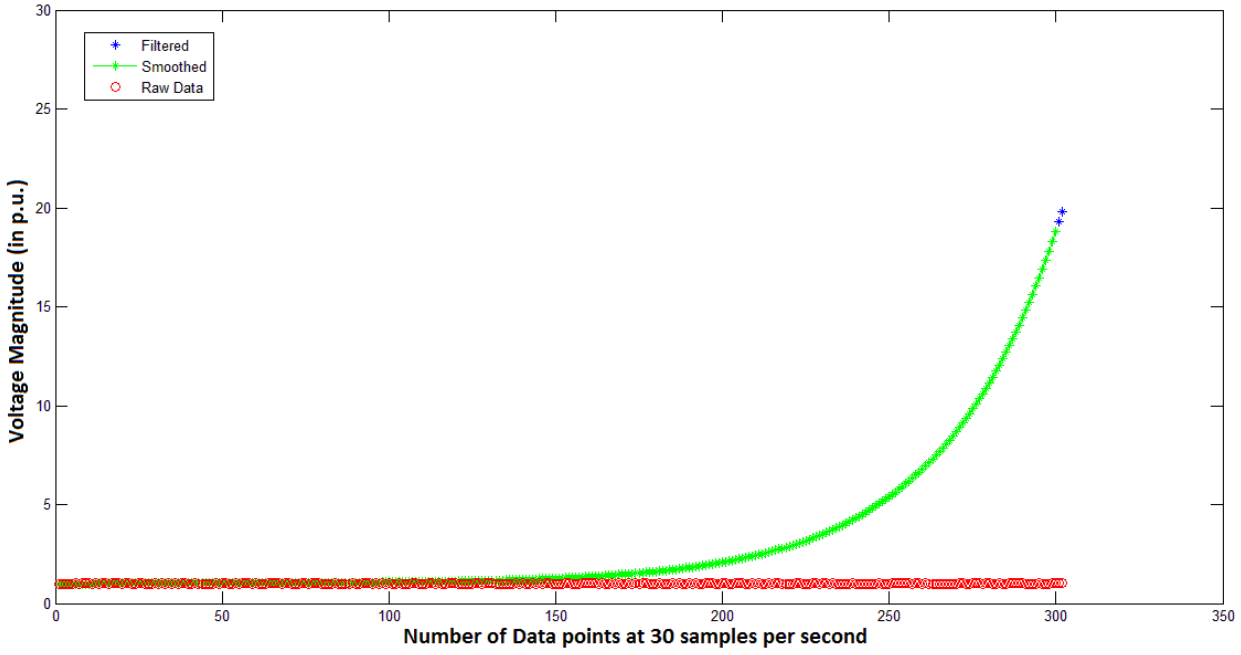

Fig. 7.6: Performance of data conditioning algorithm on phasor magnitude data having 50% drop-outs

In order to prevent the algorithm from becoming numerically unstable and diverging, a *reset* function is built-in to it that activates when the smoothing window is completely filled with estimated data. The pseudo-code for the algorithm's reset function is provided in Fig. 7.7. In Fig. 7.7, $N_{SubOptimalDataPoints}$

denotes the number of estimates. If the number of successive bad measurements received by the algorithm equals or exceeds the smoothing window length, then the algorithm will reset itself. It will start operating normally (afresh) once the smoothing window gets filled with raw data (and not estimates). Thus, for the quadratic prediction model used here, there will be a delay of at least three frames.

If $\begin{pmatrix} \text{Measurement fails SNR/Plausibility Checks } || \\ \text{ObservationResidual}_{\text{Measurement}} \geq \text{Predefined Threshold} \end{pmatrix}$
    $\text{Flag}_{\text{UnreliableQuality}} = 1$
else
    $\text{Flag}_{\text{UnreliableQuality}} = 0$
endif
If $\left(\text{Flag}_{\text{UnreliableQuality}} == 1\right)$
    Replace Measurement by Optimal Predicted Estimate
    $\text{N}_{\text{SubOptimalDataPoints}} = \text{N}_{\text{SubOptimalDataPoints}} + 1$
else
    $\text{N}_{\text{SubOptimalDataPoints}} = 0$
end if
If $\left(\text{N}_{\text{SubOptimalDataPoints}} \geq \text{SmoothingWindowLength}\right)$
    Reset Algorithm
    $\text{N}_{\text{SubOptimalDataPoints}} = 0$
end if

Fig. 7.7: Pseudo-code to depict data conditioning algorithm's reset functionality

However, proper selection of initial conditions can help the algorithm track the synchrophasor stream faster. For example, the steady state error covariance matrix and Kalman-filter gains can be saved and used to re-initialize the algorithm when required. The effect of the reset function on the same phasor magnitude plot that was described in Fig. 7.6 is shown in Fig. 7.8. The plot shows that although the output is mostly raw data (since there are not enough adjacent data points to support a quality prediction), there is no divergence even after the simulation has been run for more than twice the length of time that the first simulation (Fig. 7.6) was run for.

Another advantage of the reset functionality is that by using it, contingencies or discrete changes in the system can be properly conditioned. Since the quadratic prediction model developed in [27] cannot account for step changes, it takes several samples until the window has moved past the step change that occurred, before it can properly track the stream again. However, by resetting the algorithm at the right time, a discrete network change can be immediately acknowledged. Fig. 7.9 demonstrates the effectiveness of the algorithm's reset functionality during a loss of generation event simulated for the IEEE-118 bus system. In Fig. 7.9, the X-axis denotes the data points at 30 samples per second whereas

the Y-axis denotes the corresponding voltage magnitudes. From the figure it becomes clear that by resetting the algorithm at the correct instant, the optimal smoothed estimate (green star) is able to track the actual measurement (red circle) perfectly.

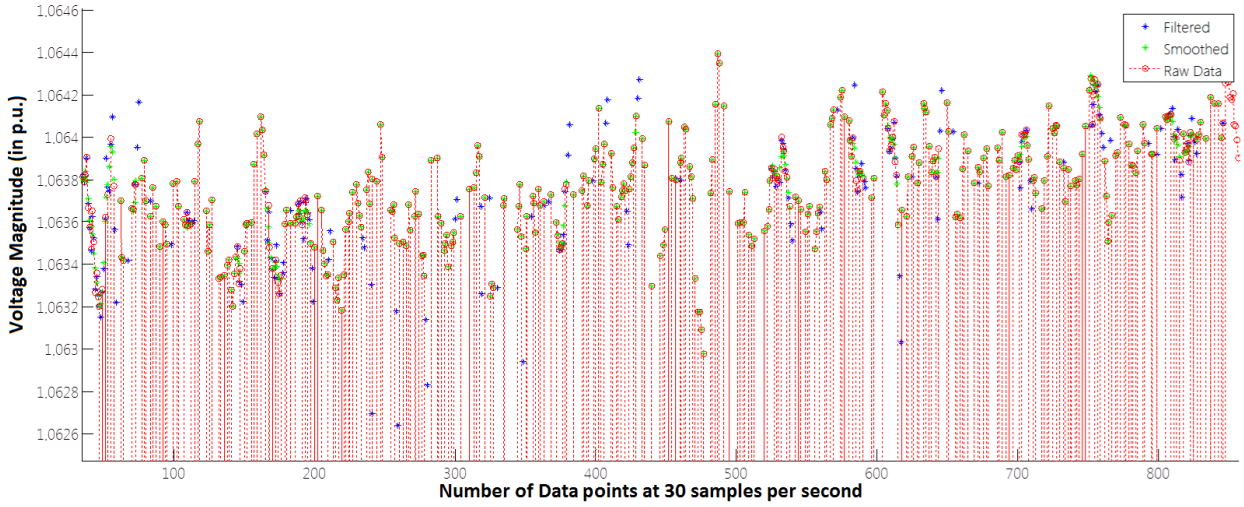

Fig. 7.8: Performance of data conditioning algorithm with reset functionality on phasor magnitude data having 50% drop-outs

To summarize, the following points can be considered to be the highlights of the proposed methodology:

- Provides optimal smoothed estimate under ideal conditions
- Uses optimal predicted estimate to replace bad/missing measurement
- Reset functionality prevents divergence when larger levels of bad/missing data is present
- Smoothed estimate tracks measurement accurately when discrete changes occur

The synchrophasor data conditioning and validation methodology described above provides a keener insight into the workings of a PMU-only linear state estimator. The ways in which this logic can aid in calibrating positive sequence instrument transformers forms the basis for the rest of this chapter.

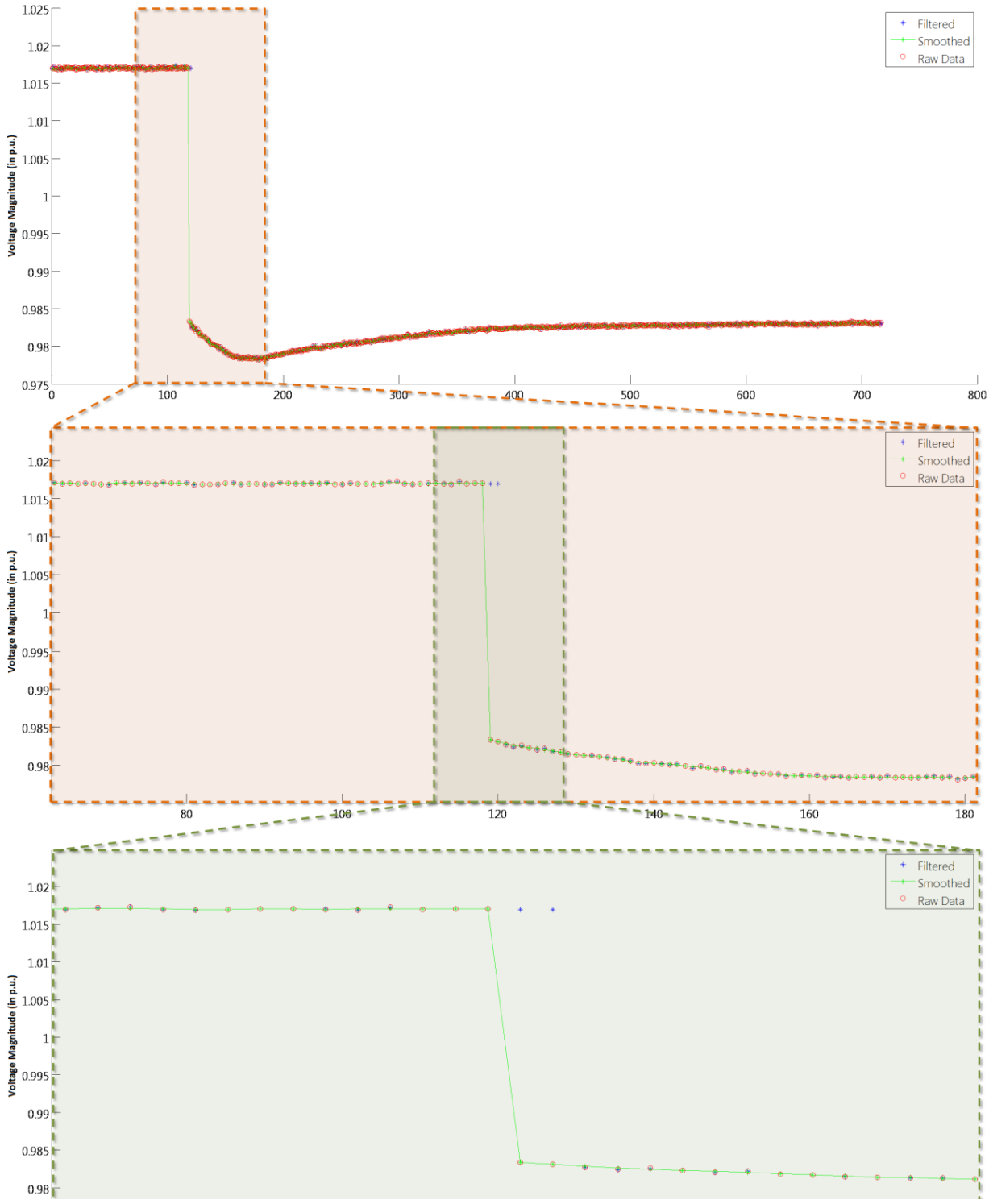

Fig. 7.9: Effect of data conditioning algorithm's reset functionality during a contingency (Loss of generation) in IEEE-118 bus system

7.3 Synchrophasor measurement based positive sequence transducer calibration

With the continued deployment of synchrophasor technology through utility investment and government grants, efforts across the industry are now beginning to shift to operationalizing the synchrophasor data in order to extract value from this investment in metering infrastructure. Ensuring the quality of the data set used for synchrophasor applications or any consumer of synchrophasor data is paramount for successful integration of this technology and a return on investment for the utilities. Historically, this same problem was solved in the context of SCADA/EMS by developing state estimation techniques to improve data quality. Fundamentally, the same type of solution is valid for PMU data. The solution proposed in the previous section shows how the linear state estimator can be used as a means to clean the synchrophasor data. In this section, conditioned and validated synchrophasor data will be used for positive sequence transducer calibration.

Our focus is on the high accuracy class relaying transducers. Relaying instrument transformers are installed throughout the transmission system to provide the necessary accurate voltage and current measurements for the protection system. Major control and measurement systems, such as SCADA/EMS also depend on the relaying instrument transformers for their proper functioning. PMU instrument transformers are assumed to have very high accuracy levels [2]-[4]. However, as the error values vary with the manufacturer and increase over time and usage (environmental conditions, prevailing burdens, etc.), the resulting biased measurements will become an inherent component of input data errors for both SCADA data as well as PMU data based applications [122]. Therefore, it becomes practically important to calibrate these instruments to account for their errors.

A lot of research has been done for developing effective ways to calibrate instrument transformers. Self-calibration of instrument transformers using zero-point test, artificial offset test and ratio meter test was proposed in [128]. However, that method required the calibrating instrument transformer to be taken off-line which would again cost time and labor. Impedance synthesis methods applicable in active, hybrid and phantom burdens for instrument transformer calibration were discussed in [129]. But as conducting onsite calibration tests are expensive and time-consuming, they are rarely performed on a system-wide basis. Calibration of current transformers (CTs) and voltage transformers (VTs) using PMUs was first proposed in [102] and later elaborated in [122] and [130]. In [122], three phase instrument transformer calibration was proposed using synchronized phasor measurements. It was found to be a labor-free calibration technique which could be performed as often as twice a day without taking the transducer off-line. More details about this method can be found in [130].

Since the methodology developed in [122] was to be implemented in the DVP system which has a three-phase linear state estimator running, it made sense to calibrate all three phases. However, most utilities of the world only have a positive sequence state estimator. Therefore it becomes necessary to realize if the logic proposed in [122] can be used for calibrating an "equivalent" positive sequence instrument transformer. This section addresses this concern. Furthermore, it is important to note here that the positive sequence that this "equivalent" instrument transformer will measure will be a function of the system frequency, the unbalance present in the individual phases, the ratio error of the individual "phase" transformers, as well as the PMU errors present in every measurement. The effect of these quantities on the net "positive sequence" is analyzed below.

The positive sequence voltage/current phasor is related to the corresponding phase quantity phasor by the relation given in (7.8).

$$P_{pos} = \frac{1}{3}(P_A + a \times P_B + a^2 \times P_C) \tag{7.8}$$

In (7.8), P denotes the phasor under test (which can be either voltage or current) and $a = \cos\left(\frac{2\times\pi}{3}\right) + j\sin\left(\frac{2\times\pi}{3}\right)$. Using (7.8), the equivalent positive sequence phasor can be computed for the following scenarios:

- Case 0: Under ideal conditions, the power system frequency is equal to its nominal value of 60 Hz and there is no PMU error, or ratio error, or unbalance. Therefore, the purely sinusoidal phase voltages/currents result in a constant positive sequence phasor as shown in Fig. 7.10. In Fig. 7.10, red color indicates phase A, blue color indicates phase B, green color indicates phase C, and black color indicates the positive sequence phasor. Fig. 7.10a shows the magnitude plot (in p.u.) while Fig. 7.10b shows the angle plot (in radians) for one day worth of data obtained at 30 samples per second and a sampling frequency of 2880 Hz. As can be observed from Fig. 7.10, under ideal conditions, the magnitude of all the phases as well as the positive sequence phasor is unity ($= 1\,p.u.$), while the angles of the three phases are 120° ($= 2 \times \frac{\pi}{3}\ radians$) apart with the positive sequence phasor angle superimposed on the phase A angle.

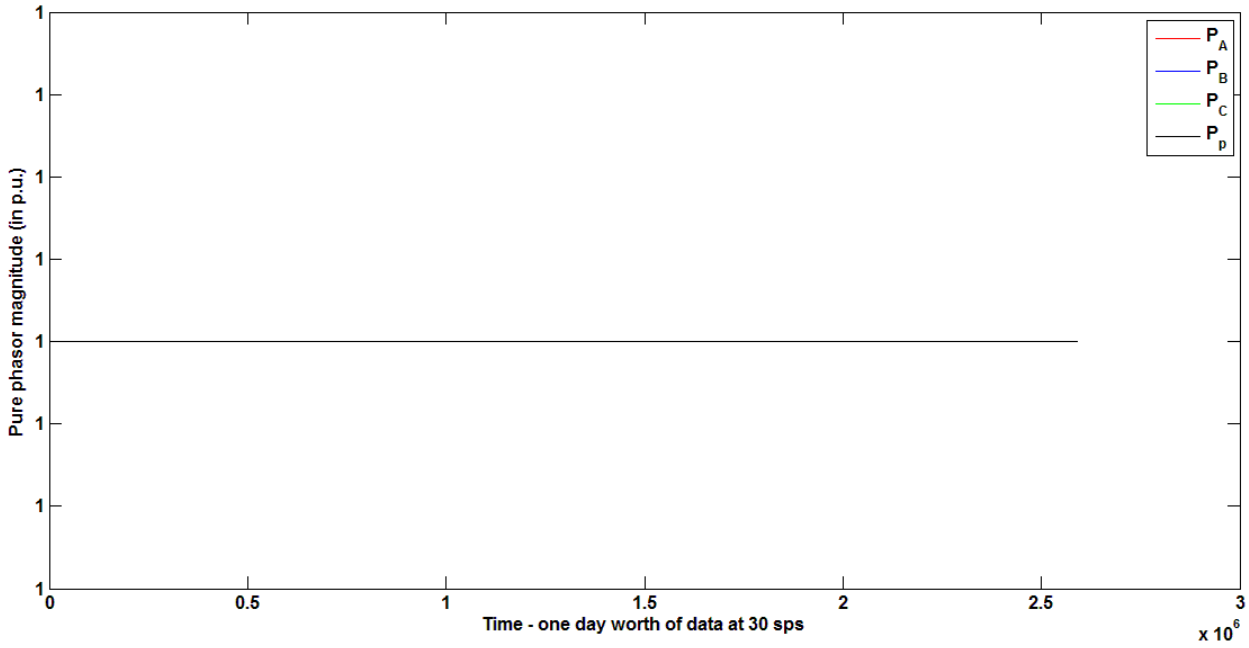

Fig. 7.10a: Phasor magnitude (in p.u.) under ideal conditions

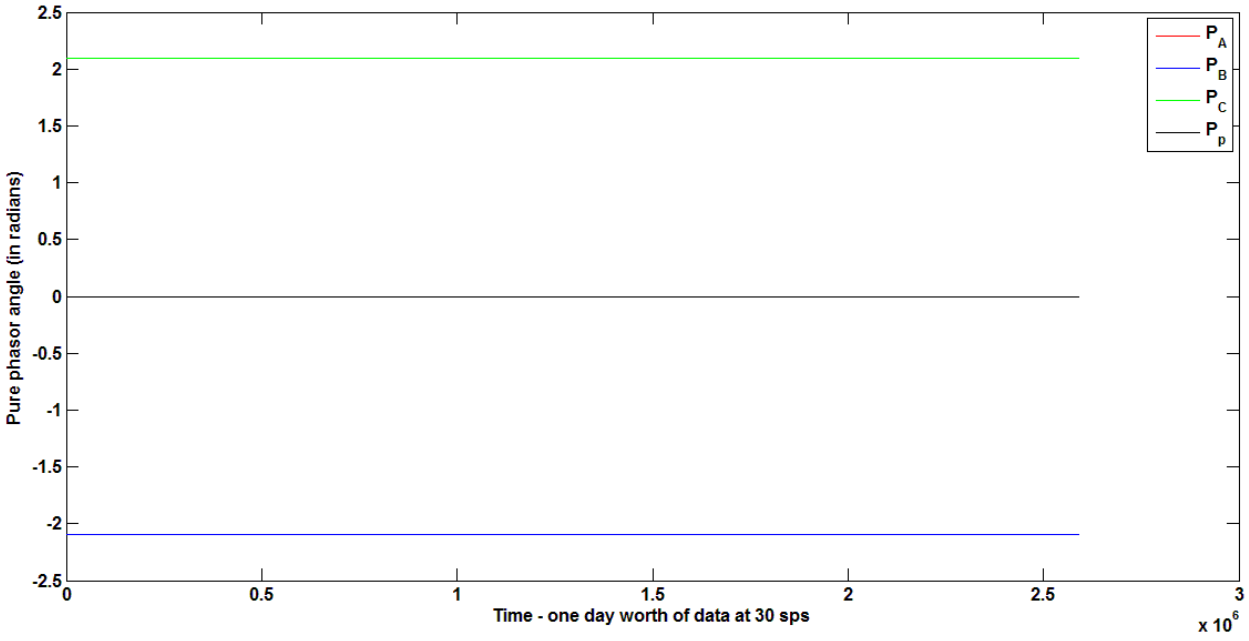

Fig. 7.10b: Phasor angle (in radians) under ideal conditions

- Case 1: In this case, only PMU errors are present, but the system is assumed to operate at 60 Hz. The PMU errors were assumed to be random variables having a zero-mean Gaussian distribution with an error of 0.2% in the magnitude and 0.104° in the angle (values provided by a PMU manufacturer). With all other conditions remaining the same as in the ideal case (no ratio error,

no unbalance, one day worth of data at 30 samples per second, etc.), a fuzz is observed on the positive sequence as seen in Fig. 7.11. Fig. 7.11a compares the positive sequence phasor magnitudes for the present case with the ideal condition while Fig. 7.11b gives a comparison of the same but for the positive sequence phasor angle. Since the mean of the PMU errors is zero, the mean of the non-ideal positive sequence phasor is almost the same as the constant ideal positive sequence phasor. Thus, the net effect of only PMU error at nominal frequency on the positive sequence phasor is negligible.

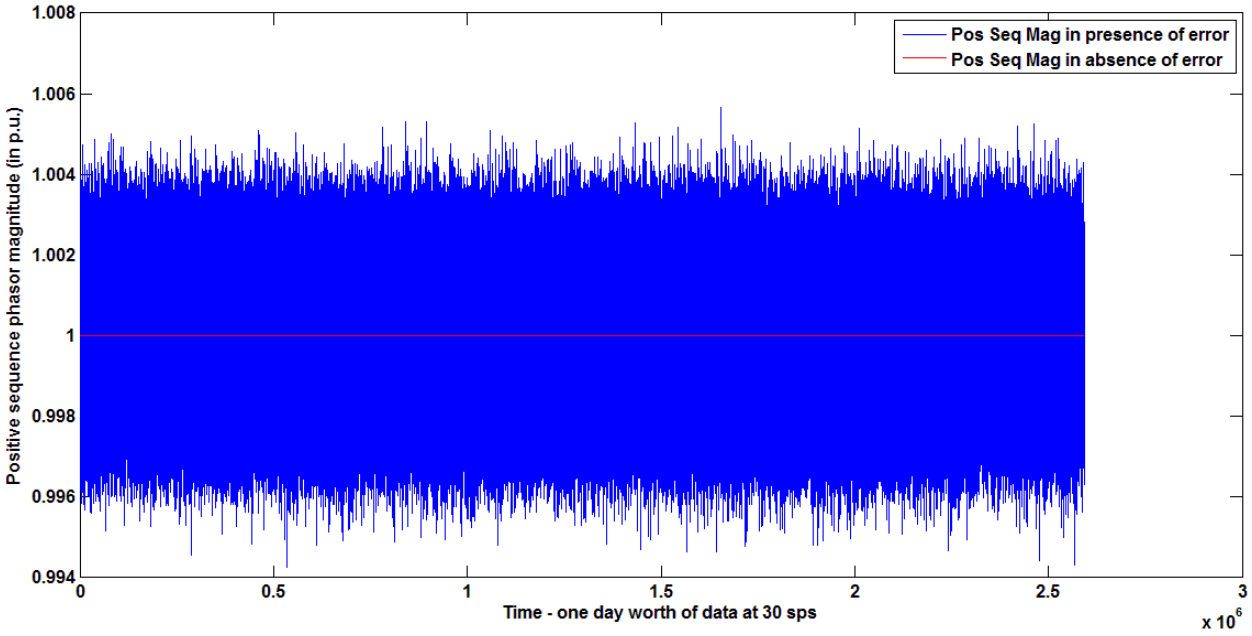

Fig. 7.11a: Comparison of positive sequence phasor magnitude (in p.u.) when only PMU error is present at nominal frequency

- Case 2: In this case, PMU errors as well as ratio errors are present, but the system is assumed to operate at 60 Hz. The ratio errors were assumed to be random variables chosen from a uniform distribution. For voltage transformers, the ratio errors lay between ±6% for the magnitude and ±4° for the angles. For current transformers, the ratio errors lay between ±3% for the magnitude and ±2° for the angles [130]. With all other conditions remaining the same as in the ideal case (no unbalance, one day worth of data at 30 samples per second, etc.), a mean is observed for the phasor error as shown in Fig. 7.12. This mean resembles the mean present in the observation residual plots of Figs. 7.4 and 7.5 and corresponds to the mean of the ratio errors of the individual phases.

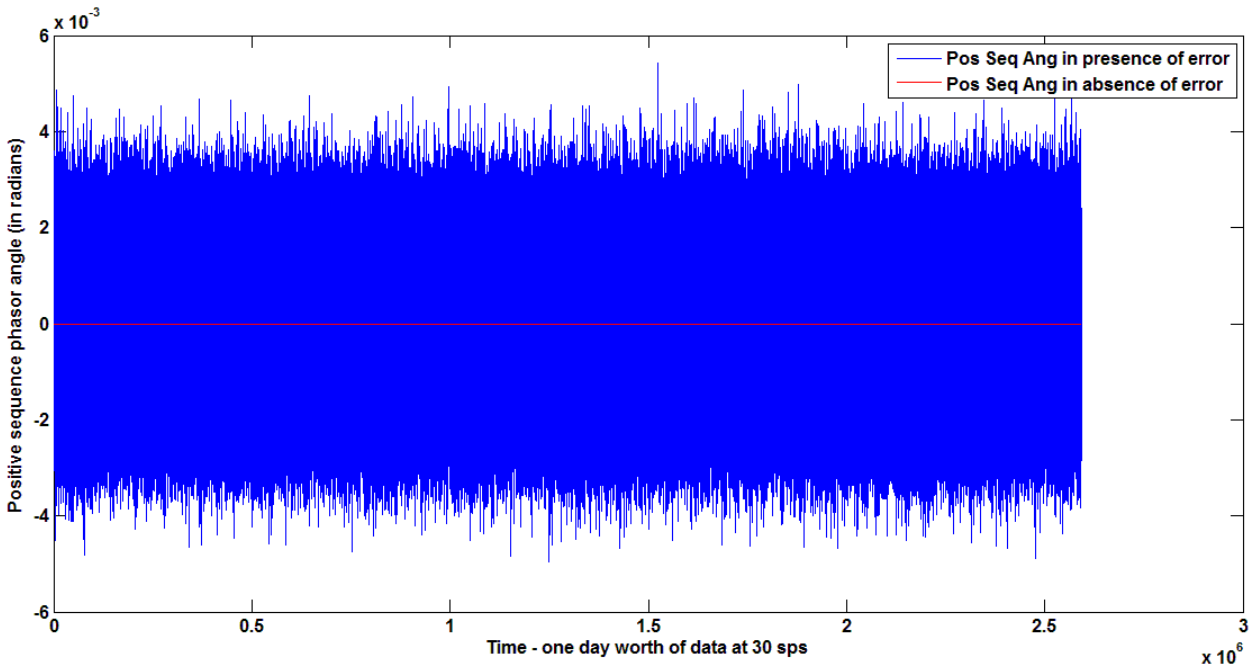

Fig. 7.11b: Comparison of positive sequence phasor angle (in radians) when only PMU error is present at nominal frequency

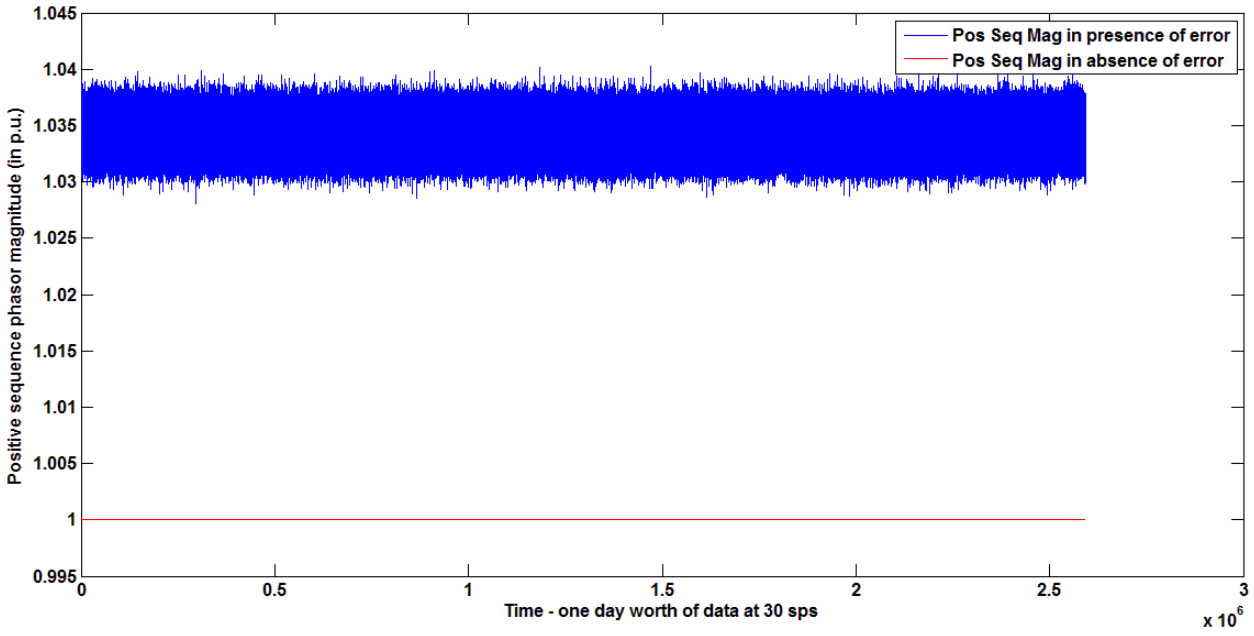

Fig. 7.12a: Comparison of positive sequence phasor magnitude (in p.u.) when PMU error and ratio error are present at nominal frequency

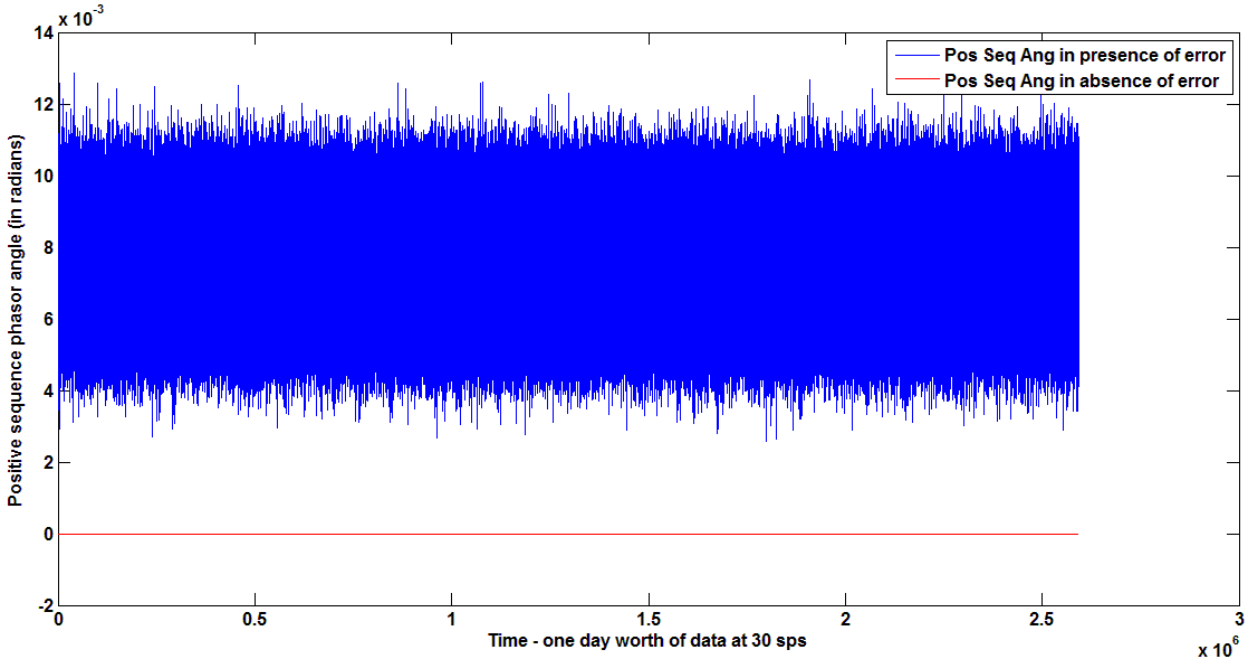

Fig. 7.12b: Comparison of positive sequence phasor angle (in radians) when PMU error and ratio error are present at nominal frequency

- Case 3: In this case, PMU errors, ratio errors as well as unbalance are present in the three phases, but the system continues to operate at 60 Hz. The unbalance in the three phases is primarily due to the absence of transposition of the transmission lines and is a significant quantity for the longer lines. Based on [120], the unbalance was assumed to be random variables chosen from a uniform distribution lying between ±5% for the magnitude and ±5° for the angles. The cumulative effect of unbalance, ratio errors, and PMU errors on the equivalent positive sequence phasor at the nominal frequency of 60 Hz is depicted in Fig. 7.13. The mean of the error observed in Fig. 7.13 was found to be the mean of the product of the ratio errors and the unbalances of the individual phases.

- Case 4: In this case, along with PMU errors, ratio errors and unbalance in the three phases, the system also operates at off-nominal frequencies. This is the most general case because the voltage and current signals have constantly changing fundamental frequency. The primary causes for the variations are load-generation imbalances, machine inertias, effects of controllers, etc. Thus, the power system frequency even under normal conditions will hover in a relatively narrow range around the nominal frequency, and will not be equal to the fundamental/nominal value all the time [13]. For simulation purposes, the frequency was varied

as a sinusoidal function between the range of 59.85 Hz and 60.15 Hz with a rate of change of frequency of 1.5 mHz/sec [131].

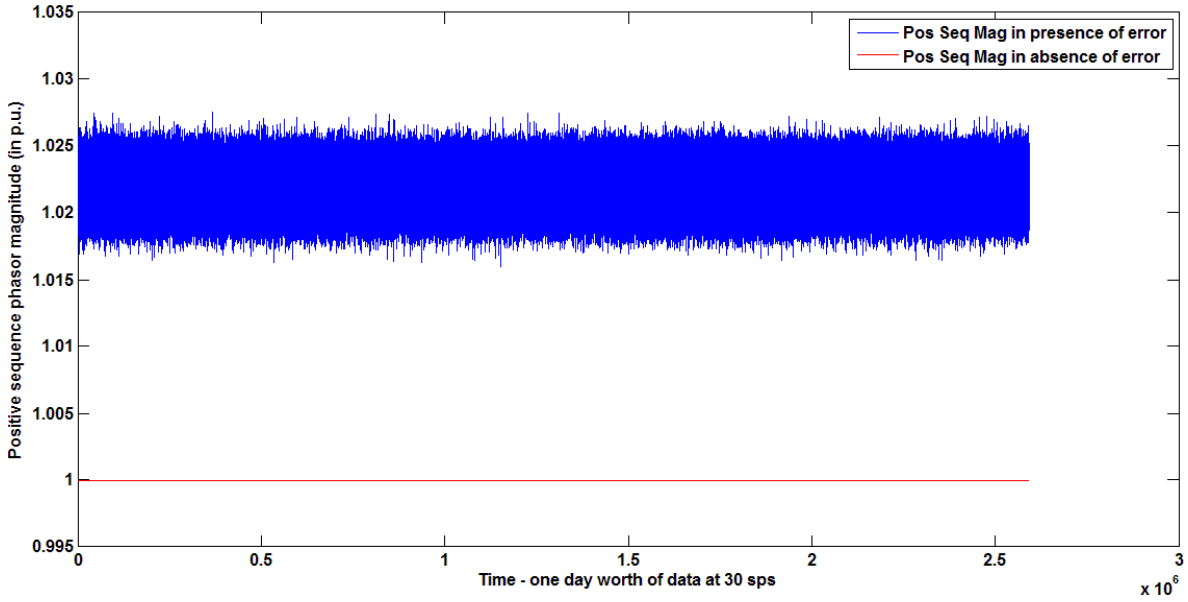

Fig. 7.13a: Comparison of positive sequence phasor magnitude (in p.u,) when PMU error, ratio error, and unbalance are present at nominal frequency

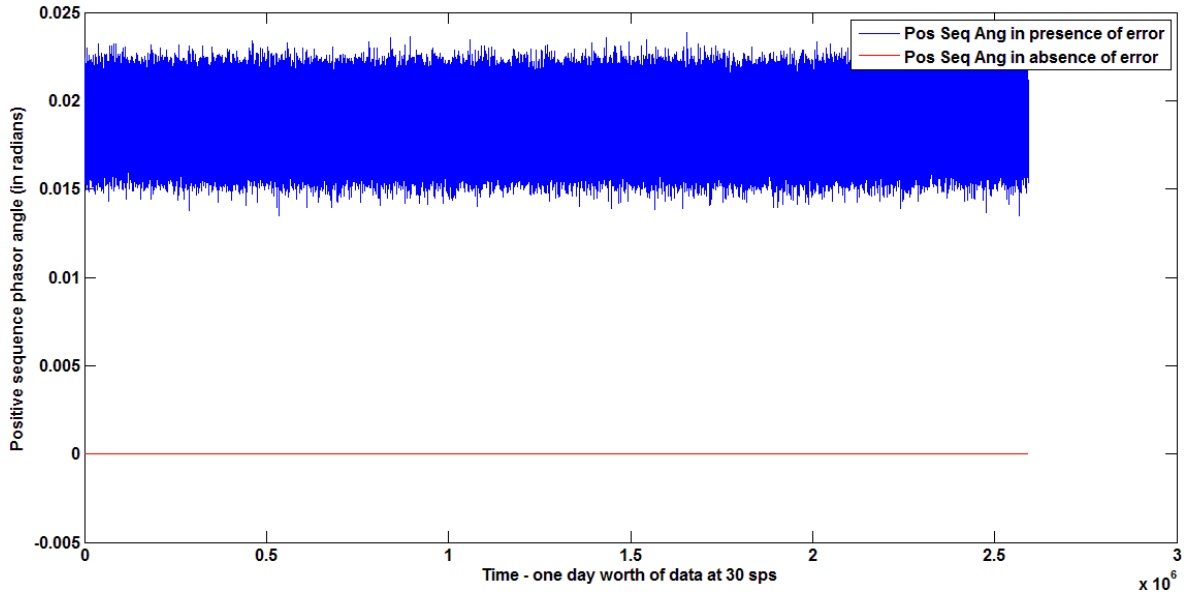

Fig. 7.13b: Comparison of positive sequence phasor angle (in radians) when PMU error, ratio error, and unbalance are present at nominal frequency

The current version of the standard [2]-[4] does not specify the methodology for computing phasors at variable off-nominal frequencies. For the simulations done here, the computation of the positive sequence phasor was done by re-sampling at a fixed interval and using a correction factor for the off-nominal frequency as proposed in [13]. The pseudo-code for doing this is given in Appendix D. The net effect on the equivalent positive sequence phasor is depicted in Fig. 7.14. In this case also, the mean of the error was found to be the mean of the product of the ratio errors and the unbalances of the individual phases. The plots depicted in Fig. 7.14 are truncated to one hour (instead of 24 hours) to better visualize the resulting waveforms (especially the waveform for the phasor angle). It is to be noted here that although PMUs built by different manufacturers will use different algorithms for computing phasors at variable off-nominal frequencies, the net effect on the positive sequence phasor error will be similar to what was observed here.

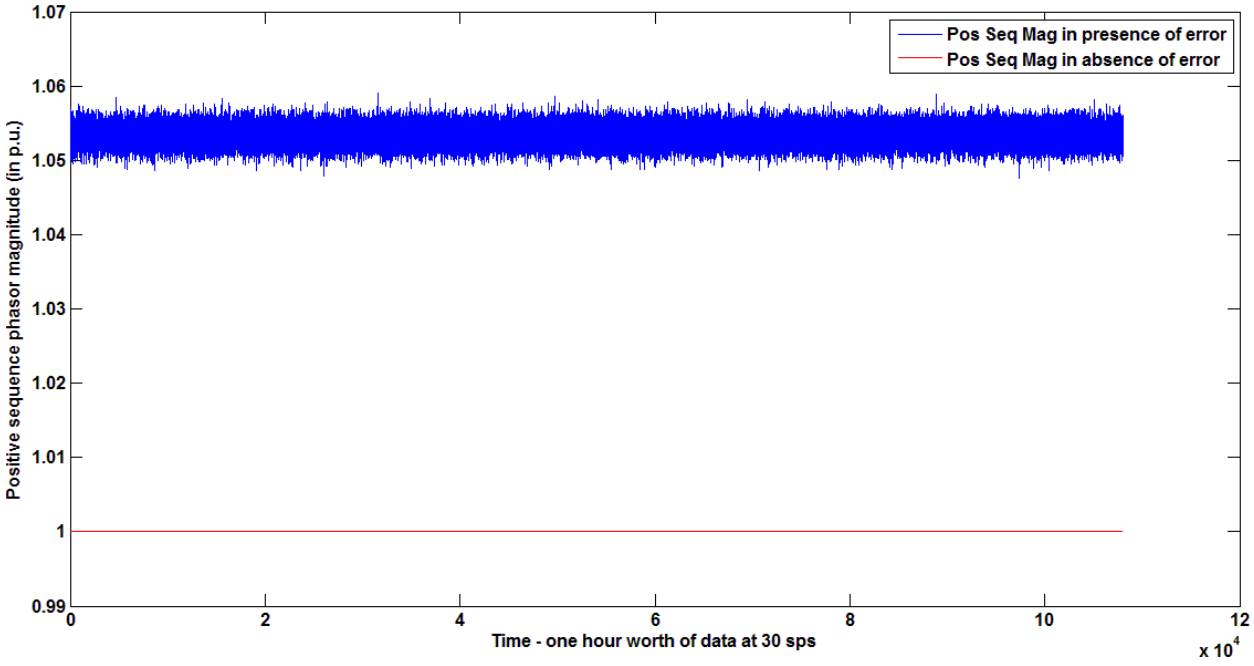

Fig. 7.14a: Comparison of positive sequence phasor magnitude (in p.u,) when PMU error, ratio error, and unbalance are present at off-nominal frequencies using resampling and post-processing

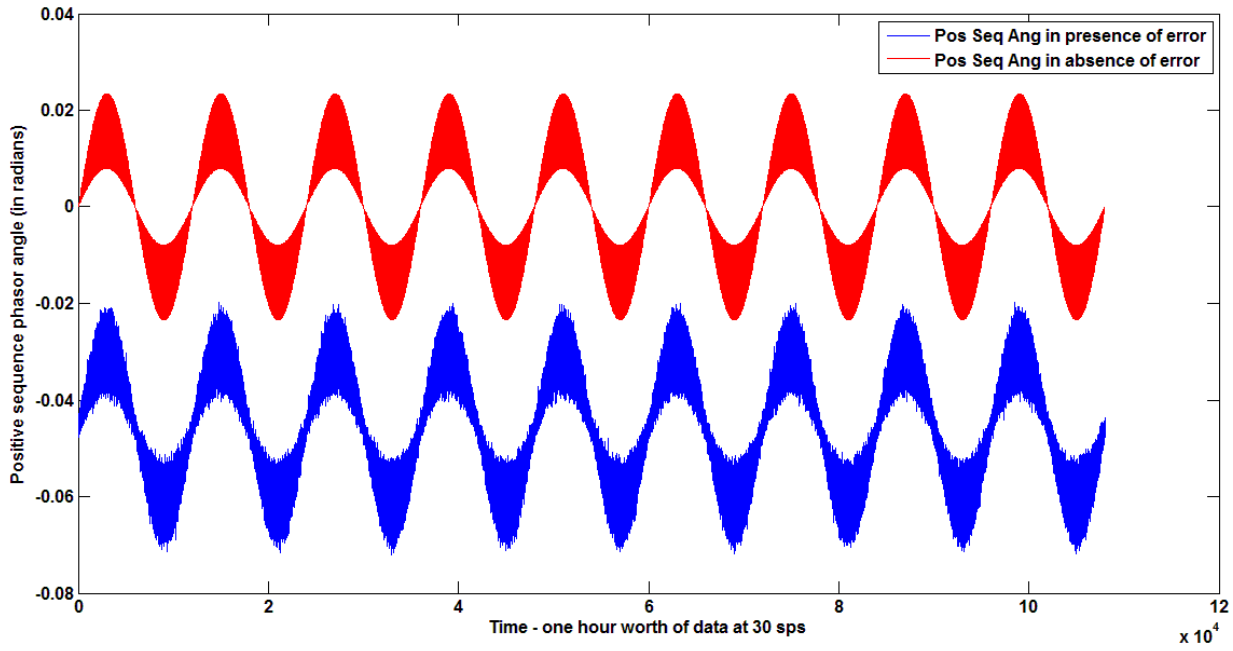

Fig. 7.14b: Comparison of positive sequence phasor angle (in radians) when PMU error, ratio error, and unbalance are present at off-nominal frequencies using resampling and post-processing

Table 7.1 summarizes the differences in the means of the magnitudes and angles of the ideal and the actual positive sequence phasors for the cases analyzed above. The difference in the magnitudes is defined as the ratio of the means of the magnitudes of the actual phasor to the ideal phasor. The difference in the angles is computed by subtracting the mean of the angle of the ideal phasor from the mean of the angle of the actual phasor. The mean of the error is the mean of the product of the ratio errors and the unbalances of the three phases. In the absence of unbalance, the mean of the error is the mean of the ratio errors of the three phases. Similarly, in the absence of both ratio errors and unbalances, the mean of the errors is a magnitude of unity and an angle of zero. From the table it becomes clear that in all the scenarios, the difference is equal to the product of the ratio error and the unbalance (whenever present). The conclusion that is drawn from this analysis is that the equivalent positive sequence will always reflect the anomalies present in the three-phase system. This is important because it implies that the logic proposed in [122] *can* be used for calibrating an "equivalent" positive sequence instrument transformer. In [130], after calibrating the relevant instrument transformers a methodology to compute line impedances using PMU data was also proposed. On the basis of the analysis done here, it can be hypothesized that estimation of positive sequence line parameters can also be done in a similar manner.

Table 7.1: Comparison of the means of the ideal and actual positive sequence phasors for different scenarios

Case Summary	Differences in the means		Mean Error	
	Magnitude (in p.u.)	Angle (in radians)	Magnitude (in p.u.)	Angle (in radians)
Only PMU error present with system operating at nominal frequency	0.99999892	1.711e-007	1	0
PMU error and Ratio error present with system operating at nominal frequency	1.03460739	0.00785021	1.03460971	0.0078003
PMU error, Ratio error, Unbalance present with system operating at nominal frequency	1.02357996	0.01961466	1.02358276	0.01961422
PMU error, Ratio error, Unbalance present with system operating at variable frequency using resampling and post-processing	1.05379542	-0.0480587	1.05337946	-0.0480611

7.4 Conclusion

This chapter presents an overview on synchrophasor data conditioning and validation. Plausibility checks and signal-to-noise ratios (SNRs) are presented as viable validation methods for preventing poor quality data from propagating downstream as well as for alerting engineers of problems which will require manual intervention. Then, by combining a quadratic prediction model with Kalman filter based filtering and smoothing techniques, conditioning of real synchrophasor data is demonstrated. The simulations indicate that the proposed methodology is guaranteed to provide a clean data stream to the linear estimator as well as to the downstream consumers and/or network applications that depend on it. The chapter concludes by describing how conditioned and validated synchrophasor data can be used in calibrating “equivalent” positive sequence instrument transformers under a variety of system conditions.

Chapter 8: Conclusion and Future Scope of Work

Monitoring and protection of modern power system networks is a challenging task. It requires an integration of efforts of many agencies – sub-station engineers, operators at the control center, etc. The ultimate objective of modern technology is to facilitate this integration to occur seamlessly. Phasor measurement units (PMUs) are a key component that modern technology has provided us. Its use in performing data mining, optimizing available resources, assessing system stress, and data conditioning is discussed in this dissertation. A synopsis of the work done is provided below.

8.1 Dissertation Summary

The most important function of any modern application is to aid in decision-making. Different applications are best compared based on their ability to make accurate and fast decisions. Since PMUs provide time synchronized measurements of the voltage phasor and the branch current phasors of all the branches emerging from the bus on which they are placed, there is an imminent need to enable decision-making based on PMU data that is both accurate and fast. In lieu with this thought, a methodology is developed in Chapters 2 and 3 in order to make multi-class decisions involving high-dimensional synchrophasor data.

In Chapter 2, Fisher's Linear Discriminant (FLD) is used as a pre-processing step before feeding the synchrophasor data into CART (which is a very popular decision tree learning technique). By computing the distance from an optimally selected hyperplane and using that one-dimensional entity (distance) as the deciding variable, splits are successfully performed even when the original data has many dimensions. By using simple examples, the superiority of the proposed approach to the traditional CART algorithm is demonstrated, both in terms of speed as well as accuracy.

In Chapter 3, the proposed Fisher's Linear Discriminant applied to Synchrophasor Data (FLDSD) technique is applied to solve two power system problems. In the first problem, it is applied to a detailed model of the California Power System, where it is used in the development of an adaptive protection scheme. The results indicate that by using the proposed methodology a smaller tree is able to provide higher classification accuracy. In the second problem, the FLDSD technique is applied to the IEEE 118-bus system, where it is used to classify dynamic events based on trajectories of voltage measurements obtained from PMUs. In this application also, the proposed technique was found to classify the events (faults, recloses, and Zone-II operations) with near-100% accuracy.

In order to attain maximum benefits from the placement of PMUs in the power grid, their locations must be selected judiciously. Accordingly, in Chapter 4, a PMU placement algorithm is developed that incorporates practical constraints. The Critical Bus Based Binary Integer Optimization (CBBBIO) technique initially identifies buses which are critical to the power system and provides them with redundancy in their measurement even at the highest depth of unobservability. Subsequently it adds more PMUs into the network to ensure complete system observability under the condition that the relevant portions of the system are protected at all times. In Chapter 5, the CBBBIO technique is combined with a community-based partitioning approach in order to reduce the computational burden of the optimization. The results indicate that a combination of the two techniques results in a PMU placement scheme that can be applied to power systems of any size.

Assessment of system stress is essential for effective monitoring and protection of a power system. In accordance with this logic, in Chapter 6, two synchrophasor-based metrics for assessing static and dynamic stresses in a power system were proposed. The base loading of the system constituted static stress. It referred to the normal/pre-contingency state of the system. Dynamic stress referred to the event/contingency that the system was subjected to. Angle difference between buses located across the network and voltage sensitivity of buses lying in the middle were the two metrics that were found to accurately reflect the static and dynamic stress of the system. With the aid of modern software tools, it is shown how metrics like these can be used for assessing the system's proximity to an insecure operation even for large systems (10,000+ buses) in real-time.

Since monitoring and protection functions rely heavily on the quality of input data, the dependability of PMU data needs to be verified before it can be used. In accordance with this thought, a methodology to perform synchrophasor data conditioning and validation that fits into the linear state estimation formulation was developed in Chapter 7. To do this, a two part module – conditioning and monitoring, was proposed. The conditioning module is responsible for cleaning the data whenever possible. This was accomplished with Kalman-filter based optimal filtering and smoothing techniques in combination with the quadratic prediction algorithm described previously in Chapter 3. The monitoring module was responsible for providing information when data cleaning is not possible and manual intervention is required. The linear state estimator was also considered part of the "cleaning" algorithm as is able to provide bad data detection, a best estimate when there is measurement redundancy, and an extension of observation with current measurements. The results indicate that the proposed technique provides a computationally simple, elegant solution to the synchrophasor data quality problem. Its ability to aid in

calibrating equivalent positive sequence transducers under different system conditions is also demonstrated.

The objectives of this dissertation were to address the issues of performing data mining, optimizing available resources, assessing system stress, and doing data conditioning with regards to monitoring and protection of power systems. Being very different natured-problems, each of the objectives required dedicated solutions. The techniques developed over the course of this study – the FLDSD technique, the CBBBIO technique and its integration with the community-based partitioning approach, etc., were found to successfully address each of the aforementioned concerns. Thus, this dissertation accomplished what it had set out to achieve.

8.2 Future avenues to be explored

As scholars and intellectuals from times immemorial have theorized, research is always a *work in progress*. That is, the ultimate purpose of any study made should be the paving of way for more studies to be made along similar lines. Since the research done in this dissertation was not an exception to this theory, it can be hypothesized that the work done here will pave the way for new research to be undertaken in the field of synchrophasor-based monitoring and protection of modern power system networks. Some key areas and applications that can be looked into are:

- Integration of FLDSD with BART
- Optimal substation coverage for PMU installations
- A partitioned state estimator

More details about these topics are described below:

Integration of FLDSD with BART: In the traditional CART algorithm, a binary tree is used to partition the predictor space recursively into distinct homogenous regions, where the terminal nodes of the tree correspond to the distinct regions. It has been found to effectively model non-linear or non-smooth relationships and can successfully interpret interactions among the predictor variables. Moreover, because of its binary structure, it can be easily implemented in practice. However, it has been found that CART has a tendency to over-fit the data. Additionally, since in CART one big tree is grown, it is hard to account for additive effects [132]. An improvement to the traditional CART algorithm was proposed by Chipman et al. called Bayesian Additive Regression Trees (BART). BART is a non-parametric Bayesian regression approach which uses dimensionally adaptive random basis elements for decision-making

[133]. The original model of BART was not designed for classification problems, but it has been subsequently improved upon and can now be applied to both regression, as well as classification problems [132], [134].

The Bayesian approach specifies a formal prior distribution for trees and other parameters and uses Markov Chain Monte Carlo (MCMC) methods to sample them from the posterior distribution. In the traditional BART algorithm, the mean of a continuous dependent variable is approximated by a "sum of trees" rather than a single tree. This "sum-of-trees" model is defined by a prior and a likelihood, and is fitted by an iterative MCMC algorithm. Each individual tree explains a different portion of the underlying mean function, but the sum of these trees turns out to be a flexible and adaptive model. In [132] and [134], this logic was extended to handle classification problems, albeit in different ways, and subsequently called Classification Bayesian Additive Regression Trees (CBART) and Bayesian Additive Classification Trees (BACT), respectively.

The advantages of the BART algorithm (applicable to both classification and regression problems) over CART are as follows [132]:

- Rather than using a single tree, BART uses a sum-of-trees model that accounts for additive effects
- BART can conduct automatic variable selection of inputs while searching for models with highest posterior probabilities during MCMC simulation
- Since it is based on Bayesian learning, BART can use newly coming data to update the current model instead of re-fitting the entire model

Moreover, since the binary tree structured is maintained in BART, the advantages of CART of effectively modelling non-linear and/or non-smooth relationships as well as ease of implementation are carried over to BART as well. However, the concern regarding the handling of complex numbers for decision making persists in BART as well. A pre-processing of the inputs to BART based on the FLDSD algorithm can be a possible solution to this problem. Future research done in this field might open-up possible ways of improving both the techniques.

Optimal substation coverage for PMU installations: In recent times, due to improvement in relaying technologies, digital relays can serve dual purposes - as a relay & as a PMU. In such a scenario, the cost of the PMU device itself is not the largest portion of the total cost, but rather the substation installation.

A recently completed large-scale deployment of PMUs on the extra high voltage (EHV) network of Dominion Virginia Power (DVP) has found this to be so. The assumption then becomes that if construction work is done in a substation, enough PMU devices should be placed such that everything at that substation is measured.

In most of the previous works, the terms “substation” and “bus” were used interchangeably. However, for a practical system, this is not appropriate because the different voltage levels in a substation might not be necessarily coupled through a transformer. Moreover, even if they are coupled, their tap settings might not always be known. In such a scenario, a utility may plan to estimate them using phasor measurements. As observability of one voltage level in a substation does not imply the observability of the whole substation, from an implementation point of view, it is not correct to treat a substation as a single bus. Therefore, in order to indirectly minimize the cost of synchrophasor deployment (by minimizing installation costs), a utility might choose to place the PMUs at minimum number of substations. The goal then becomes to deal with observability, bus-wise and with installation, substation-wise. Thus, buses belonging to the same voltage level inside a substation should be treated as a single bus but the whole substation should not be treated as one. This can also be a topic for further research.

A partitioned state estimator: The advances made in phasor technology have made it possible to integrate PMU measurements with traditional state estimators. The resulting estimator is faster and has significantly better quality [67]. However, one problem that still persists is the “seams issue” as identified in [13]. The “seams issue” is of identifying the simplest/best way of combining state estimates of two adjoining independent system operators (ISOs). This has to be done while considering the fact that the individual ISOs are large and have elaborate state estimation programs representing immense investment in people and equipments. Considering the size of the two systems, it’s a daunting task to start over and pool the data and models together to create a single estimator for the combined system. If a simpler solution that saves money, time, and frustration can be found it is definitely worth considering.

The community-based partitioning approach developed in Chapter 5 presents a way in which large systems can be partitioned into islands by removing the least number of branches. For a partitioned state estimator, these branches would be the tie-lines between the two ISOs. An example of a partitioned system is shown in Fig. 8.1, where the BEPP scheme identifies the tie-lines 1-2, 1-27, and 8-9 (highlighted in red) that must be removed in order to separate the New York and New England power

systems [135]. Then, if a separate state estimator is designed for the two sub-systems (New York system and New England system), the two state estimator results can be combined using (8.1) [13]:

$$\varphi = \frac{1}{NB}\sum_{i=1}^{i=NB}\left(\hat{\theta}_{1,i} - \hat{\theta}_{2,i}\right) \tag{8.1}$$

In (8.1), φ is the estimated difference between the two references denoted by $\hat{\theta}_1$ and $\hat{\theta}_2$ and NB is the number of boundary buses.

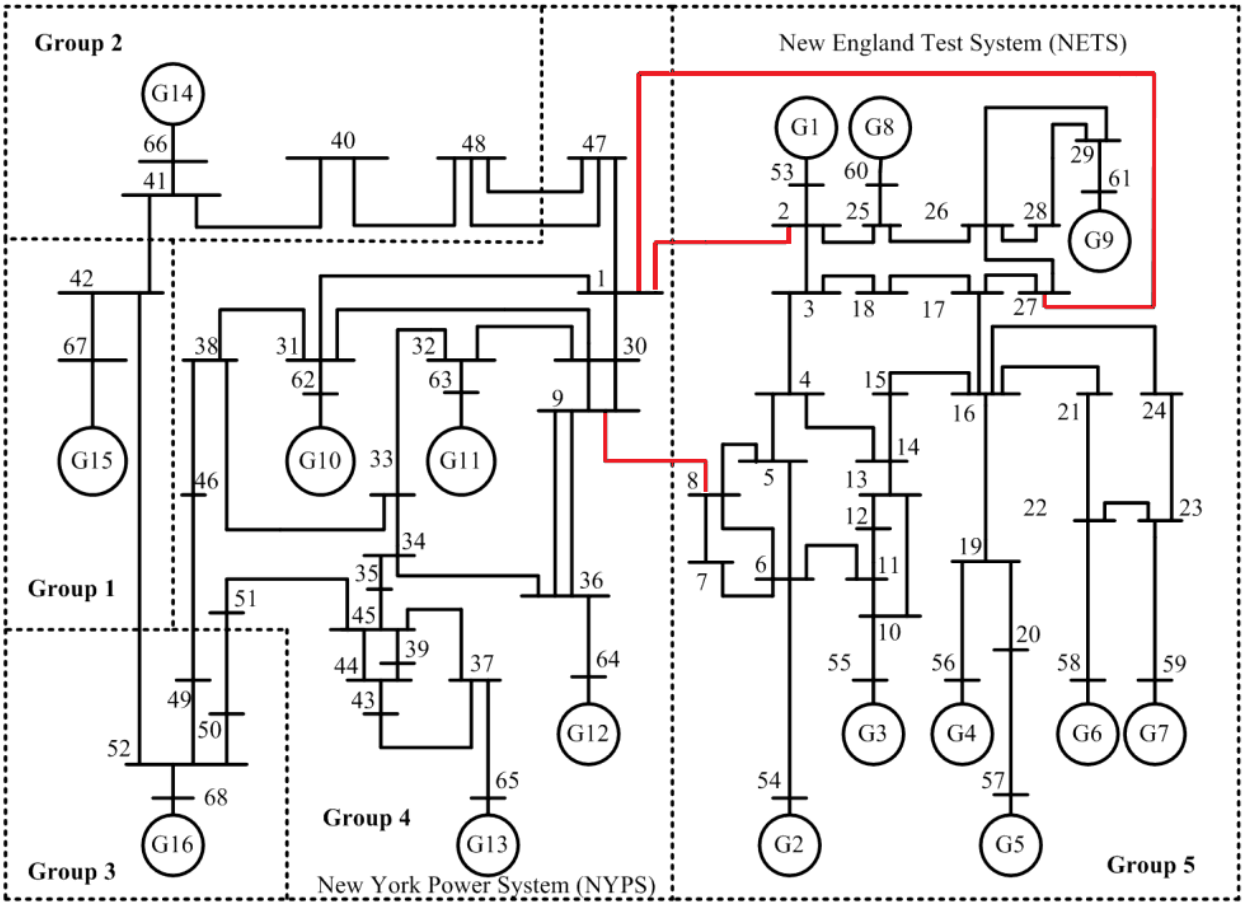

Fig. 8.1: A 16-machine, 68-bus model of the New York-New England interconnected power system

Since the estimators of the individual islands only differ in their references, one can estimate the differences between the two references by including the boundary buses in both the islands as done in (8.1). A simpler solution can be realized if the partitioned systems have linear estimators. In such a scenario, the estimator of the complete system can be obtained by a superposition of the individual

linear state estimators. Thus, creating partitioned state estimators for systems using the BEPP scheme (or a variant of it) is an exciting prospect and can be looked into in the future.

References

[1] J. De La Ree, V. A. Centeno, J. S. Thorp, and A. G. Phadke, "Synchronized phasor measurement applications in power systems," *IEEE Trans. Smart Grid*, vol. 1, no. 1, pp. 20-27, Jun. 2010.

[2] IEEE C37.118.1-2011 – IEEE Standard for synchrophasor measurements for power systems.

[3] IEEE C37.118.2-2011 – IEEE Standard for synchrophasor data transfer for power systems.

[4] IEC 61850 – Standard for design of electrical substation automation.

[5] Final Report on the August 14, 2003 Blackout in the United States and Canada: Causes and Recommendations, U.S.-Canada Power System Outage Task Force, Apr. 5, 2004. [Online]. Available: http://energy.gov/sites/prod/files/oeprod/DocumentsandMedia/BlackoutFinal-Web.pdf

[6] A. G. Phadke, "Synchronized phasor measurements in power systems," *IEEE Comput. Appl. Power*, vol. 6, no. 2, pp. 10-15, Apr. 1993.

[7] D. G. Hart, D. Uy, V. Gharpure, D. Novosel, D. Karlsson, and M. Kaba, "PMUs-A new approach to power network monitoring," [Online]. Available: http://www05.abb.com/global/scot/scot296.nsf/veritydisplay/2d4253f3c1bff3c0c12572430075caa7/$file/editorial_2001_04_en_pmus_-_a_new_approach_to_power_network_monitoring.pdf

[8] O. Faucon, and L. Dousset, "Coordinated defense plan protects against transient instabilities," *IEEE Comput. Appl. Power*, vol. 10, no. 3, pp. 22-26, Jul. 1997.

[9] J. S. Thorp, A. G. Phadke, S. H. Horowitz, and M. M. Begovic, "Some applications of phasor measurements to adaptive protection," *IEEE Trans. Power Syst.*, vol. 3, no. 2, pp. 791-798, May 1988.

[10] V. A. Centeno, J. De La Ree, A. G. Phadke, G. Michel, R. J. Murphy, and R. O. Burnett, Jr., "Adaptive out-of-step relaying using phasor measurement techniques," *IEEE Comput. Appl. Power*, vol. 6, no. 4, pp. 12-17, Oct. 1993.

[11] V. A. Centeno, A. G. Phadke, A. Edris, J. Benton, M. Gaudi, and G. Michel, "An adaptive out-of-step relay [for power system protection]," *IEEE Trans. Power Del.*, vol. 12, no. 1, pp. 61-71, Jan. 1997.

[12] E. E. Bernabeu, J. S. Thorp, and V. A. Centeno, "Methodology for a security/dependability adaptive protection scheme based on data mining," *IEEE Trans. Power Del.*, vol. 27, no. 1, pp. 104-111, Jan. 2012.

[13] A. G. Phadke, and J. S. Thorp, *Synchronized Phasor Measurements and Their Applications*, New York: Springer, 2008.

[14]A. Pal, “Co-ordinated control of inter-area oscillations using SMA and LMI,” M.S. Thesis, Electrical and Computer Engineering Department, Virginia Polytechnic Institute and State University, Blacksburg, Feb. 2012.

[15] A. Pal, and J. S. Thorp, “Co-ordinated control of inter-area oscillations using SMA and LMI,” in *Proc. IEEE Power Eng. Soc. Conf. Innovative Smart Grid Technol.*, Washington D.C., pp. 1-6, Jan. 2012.

[16]A. Pal, J. S. Thorp, S. S. Veda, and V. A. Centeno, “Applying a robust control technique to damp low frequency oscillations in the WECC,” *Int. J. Elect. Power Energy Syst.*, vol. 44, no. 1, pp. 638-645, Jan. 2013.

[17]A. Pal, and J. S. Thorp, Coordinated Control of Inter-area Oscillations using SMA and LMI: A Robust Control Technique for Damping Low Frequency Oscillations, *Lambert Academic Publishing*, Oct. 2012.

[18]G. T. Heydt, C. C. Liu, A. G. Phadke, and V. Vittal, “Solution for the crisis in electric power supply,” *IEEE Comput. Appl. Power*, vol. 14, no. 3, pp. 22-30, Jul. 2001.

[19]R. F. Nuqui, and A. G. Phadke, “Phasor measurement unit placement techniques for complete and incomplete observability,” *IEEE Trans. Power Del.*, vol. 20, no. 4, pp. 2381- 2388, Oct. 2005.

[20]G. A. Sanchez, A. Pal, V. A. Centeno, and W. C. Flores, “PMU placement for the Central American power network and its possible impacts,” in *Proc. IEEE Power Eng. Soc. Conf. Innovative Smart Grid Technol.*, Medellin, Colombia, pp. 1-7, 19-21 Oct. 2011.

[21]T. L. Baldwin, L. Mili, M. B. Boisen Jr., and R. Adapa, “Power system observability with minimal phasor measurement placement,” *IEEE Trans. Power Syst.*, vol. 8, no. 2, pp. 707-715, May 1993.

[22]D. J. Brueni, “Minimal PMU placement for graph observability: a decomposition approach,” M.S. Thesis, Computer Science and Applications, Virginia Polytechnic Institute and State University, Blacksburg, Dec. 1993.

[23]D. N. Kosterev, W. Taylor, and W. A. Mittelstadt, “Model validation for the August 10, 1996 WSCC system outage,” *IEEE Trans. Power Syst.*, vol. 14, no. 3, pp. 967-979, Aug. 1999.

[24]G. P. Liu, Z. Xu, Y. Huang, and W. L. Pan, “Analysis of inter-area oscillations in the South China interconnected power system,” *Elect. Power Syst. Research*, vol.70, pp. 38-45, Jun. 2004.

[25]M. Q. Dong, D. J. Yang, and Y. Huang, “Analysis on the low frequency oscillation incidents measured by WAMS of Central China power grid during the 2008 ice hazard,” *Central China Elect. Power*, vol. 21, vo. 5, pp. 22-25, 2008.

[26]F. Zhu, Z. H. Liu, and L. Chu, “Achievement and experience of improving power system stability by PSS/excitation control in China,” in *Proc. IEEE Power Eng. Soc. General Meeting*, Denver, CO, vol. 2, pp. 1767-1771, 10 Jun. 2004.

[27]F. Gao, J. S. Thorp, A. Pal, and S. Gao, “Dynamic state prediction based on Auto-Regressive (AR) model using PMU data,” in *Proc. IEEE Power and Energy Conference at Illinois (PECI)*, Champaign, IL, pp. 1-5, Feb. 2012.

[28]K. D. Jones, J. S. Thorp, and R. M. Gardner, “Three-phase linear state estimation using phasor measurements,” in *Proc. IEEE Power Eng. Soc. Gen. Meeting*, Vancouver, BC, Canada, pp. 1-5, 21-25 Jul. 2013.

[29]S. Rovnyak, C. W. Taylor, and Y. Sheng, “Decision trees using apparent resistance to detect impending loss of synchronism,” *IEEE Trans. Power Del.*, vol. 15, no. 4, pp. 1157-1162, Oct. 2000.

[30]R. Diao, V. Vittal, K. Sun, S. Kolluri, S. Mandal, and F. Galvan, “Decision tree assisted controlled separation for preventing cascading events,” in *Proc. IEEE Power Eng. Soc. Power Syst. Conf. Expo.*, Seattle, WA, pp. 1-8, 15-18 Mar. 2009.

[31]E. M. Voumvoulakis, A. E. Gavoyiannis, and N. D. Hatziargyriou, “Decision trees for dynamic security assessment and load shedding scheme,” in *Proc. IEEE Power Eng. Soc. Gen. Meeting*, Montreal, QC, Canada, pp. 1-7, 18-22 Jun. 2006.

[32]J. A. Huang, G. Vanier, A. Valette, S. Harrison, and L. Wehenkel, “Application of data mining techniques for automat settings in emergency control at Hydro-Quebec,” in *Proc. IEEE Power Eng. Soc. Gen. Meeting*, Toronto, Canada, vol. 4, pp. 2037-2044, 13-17 Jul. 2003.

[33]A. R. Khatib, R. F. Nuqui, M. R. Ingram, and A. G. Phadke, “Real-time estimation of security from voltage collapse using synchronized phasor measurements,” in *Proc. IEEE Power Eng. Soc. Gen. Meeting*, Denver, CO, vol. 1, pp. 582-588, 6-10 Jun. 2004.

[34]I. H. Mori, “State-of-the-art overview on data mining in power systems,” in *Proc. IEEE Power Eng. Soc. Gen. Meeting*, Montreal, QC, Canada, pp. 1-5, 18-22 Jun. 2006.

[35]S. Rovnyak, S. Kretsinger, J. S. Thorp, and D. Brown, “Decision trees for real-time transient stability prediction,” *IEEE Trans. Power Syst.*, vol. 9, no. 3, pp. 1417-1426, Aug. 1994.

[36]S. Rovnyak, and Y. Sheng, “Using measurements and decision tree processing for response-based discrete-event control,” in *Proc. IEEE Power Eng. Soc. Summer Meeting*, Edmonton, AB, Canada, pp. 10-15, 18-22 Jul. 1999.

[37]R. F. Nuqui, A. G. Phadke, R. P. Schulz, and N. Bhatt, "Fast on-line voltage security monitoring using synchronized phasor measurements and decision trees," in *Proc. IEEE Power Eng. Soc. Winter Meeting*, Columbus, OH, vol. 3, pp. 1347-1352, 28 Jan.-1 Feb. 2001.

[38]Z. Yi, and K. Tomsovic, "Real-time transient instability detection based on decision trees," in *Proc. Intell. Syst. Applicat. Power Syst.*, Curitiba, Brazil, pp. 1-6, Nov. 2009.

[39] Z. Li, and W. Wu, "Phasor measurements-aided decision trees for power system security assessment," in *Proc. IEEE Comput. Soc. 2nd Int. Conf. Inf. Comput. Sci.*, Manchester, vol. 1, pp. 358-361, 21-22 May 2009.

[40]G. Qun, and S. Rovnyak, "Decision trees using synchronized phasor measurements for wide-area response-based control," *IEEE Trans. Power Syst.*, vol. 26, no. 2, pp. 855-861, May 2011.

[41]R. Diao, K. Sun, V. Vittal, R. J. O' Keefe, M. R. Richardson, N. Bhatt, D. Stradford, and S. K. Sarawgi, "Decision tree-based online voltage security assessment using PMU measurements," *IEEE Trans. Power Syst.*, vol. 24, no. 2, pp. 832-839, May 2009.

[42]F. Mahmoodianfard, M. Mohammadi, G. B. Gharehpetian, and H. A. Abyaneh, "Optimal PMU placement for voltage security assessment using decision tree," in *Proc. IEEE PowerTech Conf.*, Bucharest, Romania, pp. 1-5, 28 Jun.-2 Jul. 2009.

[43]K. Sun, S. Likhate, V. Vittal, V. S. Kolluri, and S. Mandal, "An online dynamic security assessment scheme using phasor measurements and decision trees," *IEEE Trans. Power Syst.*, vol. 22, no. 4, pp. 1935-1943, Nov. 2007.

[44]D. H. Li, and Y. J. Cao, "SOFM based support vector regression model for prediction and its application in power system transient stability forecasting," in *Proc. 7th Int. Power Engg. Conf.*, Singapore, vol. 2, pp. 765-770, 29 Nov.-2 Dec. 2005.

[45]L. Breiman, J. H. Friedman, R. Olshen, and C. J. Stone, *Classification and Regression Tree*, Wadsworth & Brooks/Cole Advanced Books & Software, Pacific California, 1984.

[46]CART®. Tree-structured non-parametric data analysis. Classification and regression trees by Salford systems. <www.salford-systems.com>. [Online]. Available: http://www.salford-systems.com/cart.php.

[47]S. E. Kretsinger, S. M. Rovnyak, D. E. Brown, and J. S. Thorp, "Parallel decision trees for predicting groups of unstable generators from synchronized phasor measurements," in *Proc. Precise Measurements Power Syst. Conf.*, Arlington, VA, pp. 1-9, 25-29 Oct. 1993.

[48]A. Swarnkar, and K. R. Niazi, "CART for online security evaluation and preventive control of power systems," in *Proc. of the 5th WSEAS/IASME Int. Conf. on Elect. Power Syst., High Voltages, Elect. Mach.*, Tenerife, Spain, pp. 378-383, 16-18 Dec. 2005.

[49]R. J. Lewis, "An introduction to Classification & Regression Tree (CART) analysis," in *Proc. Annu. Meeting Soc. Academic Emergency Medicine*, San Francisco, CA, pp. 1-14, 2000.

[50]S. Garlapati, and J. S. Thorp, "Choice of reference in CART applications using PMU data," in *Proc. 17th Power Systems Computation Conf. (PSCC)*, Stockholm, Sweden, pp. 1-7, 22-26 Aug. 2011.

[51]S. K. Murthy, S. Kasif, and S. Salzberg, "A system for induction of oblique decision trees", *J. Artific. Intell. Res.*, vol. 2, no. 1, pp. 1 -32, 1994.

[52]R. Fisher, "The use of multiple measurements in taxonomic problems," *Ann. of Eugenics*, vol. 7, no. 2, pp. 179-188, Sept. 1936.

[53]Cholesky Decomposition. [Online]. Available: http://en.wikipedia.org/wiki/Cholesky_decomposition

[54]C. A. Jensen, M. A. El-Sharkawi, and R. J. Marks II, "Power system security assessment using neural networks: feature selection using Fisher discrimination," *IEEE Trans. Power Syst.*, vol. 16, no. 4, pp. 757-763, Nov. 2001.

[55]C. W. Liu, M. C. Su, S. S. Tsay, and Y. J. Wang, "Application of a novel fuzzy neural network to real-time transient stability swings prediction based on synchronized phasor measurements," *IEEE Trans. Power Syst.*, vol. 14, no. 2, pp. 685–692, May 1999.

[56]A. Karimi, "Power system transient stability margin estimation using neural networks," *Int. J. Elect. Power Energy Syst.*, vol. 33, no. 4, pp. 983-991, May 2011.

[57]A. Karimi, and S. Z. Esmaili, "Transient stability assessment of power systems described with detailed models using neural networks," *Int. J. Elect. Power Energy Syst.*, vol. 45, no. 1, pp. 279-292, Feb. 2013.

[58]D. You, K. Wang, L. Ye, J. Wu, and R. Huang, "Transient stability assessment of power system using support vector machine with generator combinatorial trajectories inputs," *Int. J. Elect. Power Energy Syst.*, vol. 44, no. 1, pp. 318-325, Jan. 2013.

[59]M. Li, A. Pal, A. G. Phadke, and J. S. Thorp, "Transient Stability Prediction Based on Apparent Impedance Trajectory Recorded by PMUs," *Int. J. Elect. Power Energy Syst.*, vol. 54, pp. 498-504, Jul. 2013.

[60]M. Li, "Transient stability prediction based on synchronized phasor measurements and controlled islanding," Ph.D. Dissertation, Electrical and Computer Engineering Department, Virginia Polytechnic Institute and State University, Blacksburg, Mar. 2013.

[61]R. Sun, “Wide area power system islanding detection, classification and state evaluation algorithm,” Ph.D. Dissertation, Electrical and Computer Engineering Department, Virginia Polytechnic Institute and State University, Blacksburg, Dec. 2012.

[62]IEEE Standard for relays and relay systems associated with electric power apparatus, 1989.

[63]S. H. Horowitz, and A. G. Phadke, *Power system relaying*. 2nd Ed. New York: Wiley, 1995.

[64]E. E. Bernabeu, “Methodology for a security-dependability adaptive protection scheme based on data mining,” Ph.D. Dissertation, Electrical and Computer Engineering Department, Virginia Polytechnic Institute and State University, Blacksburg, Dec. 2009.

[65]J. S. Thorp, A. G. Phadke, and K. J. Karimi, “Real time voltage-phasor measurement for static state estimation,” *IEEE Trans. Power App. Syst.*, vol. PAS-104, no. 11, pp. 3098-3106, Nov. 1985.

[66]A. G. Phadke, J. S. Thorp, and K. J. Karimi, “State Estimation with Phasor Measurements,” *IEEE Trans. Power Syst.*, vol. 1, no. 1, pp. 233-238, Feb. 1986.

[67]M. Zhou, V. A. Centeno, J. S. Thorp, and A. G. Phadke, “An alternative for including phasor measurements in state estimators,” *IEEE Trans. Power Syst.*, vol. 21, no. 4, pp. 1930-1937, Nov. 2006.

[68]A. S. Debs, and R. Larson, “A dynamic estimator for tracking the state of a power system,” *IEEE Trans. Power App. Syst.*, vol. PAS-89, no. 7, pp. 1670-1678, Sep. 1970.

[69]A. D. R. McQuarrie, and C. L. Tsai, *Regression and Time Series Model Selection*. World Scientific Publishing, 1998, pp. 89-91.

[70]M. Schatzman, *Numerical Analysis: A Mathematical Introduction*. Oxford: Clarendon Press, 2002.

[71]A. Eisinbergt, and P. Pugliese, “Exact inversion of a class of Vandermonde matrices,” in *Proc. Fifth SIAM Conf. on Appl. Linear Algebra*, pp. 239-243, Jun. 1994.

[72]A. W. F. Edwards, *Pascal's Arithmetical Triangle: The Story of a Mathematical Idea*, Johns Hopkins University Press, 2002, pp. 30-31.

[73]IEEE-118 Bus System. [Online]. Available: http://www.ee.washington.edu/research/pstca/pf118/pg_tca118bus.htm

[74]DSA Tools, Powertech Labs Inc., Surrey, British Columbia, Canada. http://www.DSATools.com/

[75]Responses Summary to Questionnaire on PMU Installation and Maintenance, Eastern Interconnection Phasor Project (EIPP) Performance Requirements Task Team (PRTT), May 2006.

[76]S. Chakrabarti, and E. Kyriakides, “Optimal placement of phasor measurement units for power system observability,” *IEEE Trans. Power Syst.*, vol. 23, no. 3, pp. 1433-1440, Aug. 2008.

[77] B. Gou, "Generalized integer linear programming formulation for optimal PMU placement," *IEEE Trans. Power Syst.*, vol. 23, no. 3, pp. 1099-1104, Aug. 2008.

[78] B. Xu, and A. Abur, "Observability analysis and measurement placement for systems with PMUs," in *Proc. IEEE Power Eng. Soc. Power Systems Conf. Expo.*, NY, vol. 2, pp. 943-946, 10-13 Oct. 2004.

[79] B. Xu, Y. J. Yoon, and A. Abur, "Optimal placement and utilization of phasor measurements for state estimation," in *Proc. 15th Power Systems Computation Conf. (PSCC)*, Liege, Belgium, pp. 1-6, 22-26 Aug. 2005.

[80] D. Dua, S. S. Dambhare, R. K. Gajbhiye, and S. A. Soman, "Optimal multistage scheduling of PMU placement: an ILP approach," *IEEE Trans. Power Del.*, vol. 23, no. 4, pp. 1812-1820, Oct. 2008.

[81] S. Chakrabarti, E. Kyriakides, and D. G. Eliades, "Placement of synchronized measurements for power system observability," *IEEE Trans. Power Del.*, vol. 24, no. 1, pp. 12-19, Jan. 2009.

[82] B. Milosevic, and M. Begovic, "Non-dominated sorting genetic algorithm for optimal phasor measurement placement," *IEEE Trans. Power Syst.*, vol. 18, no. 1, pp. 69- 75, Feb. 2003.

[83] N. H. Abbasy, and H. M. Ismail, "A unified approach for the optimal PMU location for power system state estimation," *IEEE Trans. Power Syst.*, vol. 24, no. 2, pp. 806-813, May 2009.

[84] F. Mahmoodianfard, M. Mohammadi, G. B. Gharehpetian, and H. A. Abyaneh, "Optimal PMU placement for voltage security assessment using decision tree," in *Proc. IEEE PowerTech Conf.*, Bucharest, Romania, pp. 1-5, 28 Jun.-2 Jul. 2009.

[85] L. Mili, T. Baldwin, and R. Adapa, "Phasor measurement placement for voltage stability analysis of power systems," in *Proc. 29th Conf. Decision and Control*, Honolulu, HI, vol. 6, pp. 3033-3038, 5-7 Dec. 1990.

[86] R. F. Nuqui, and A. G. Phadke, "Phasor measurement unit placement based on incomplete observability," in *Proc. IEEE Power Eng. Soc. Summer Meeting*, Chicago, IL, vol. 2, pp. 888-893, 21-25 Jul. 2002.

[87] J. R. Altman, "A practical comprehensive approach to PMU placement for full observability," M.S. Thesis, Electrical and Computer Engineering Department, Virginia Polytechnic Institute and State University, Blacksburg, Jan. 2007.

[88] B. Gou, and A. Abur, "An improved measurement placement algorithm for network observability," *IEEE Trans. Power Syst.*, vol. 16, no. 4, pp. 819-824, Nov. 2001.

[89] N. Korevaar, "Incidence is no coincidence," Univ. Utah Math Circle, Oct. 2002.

[90] D. Thukaram, B. Ravikumr, V. S. S. Kumar, Y. P. Rao, S. Surendra, and S. R. Kolla, "Real-time monitoring of critical nodes with minimal number of phasor measurement units," in *Proc. Int. Conf. Power Syst. (ICPS)*, Kharagpur, India, pp. 1-6, 27-29 Dec. 2009.

[91] A. Monticelli, *State Estimation in Electric Power Systems: A Generalized Approach*. Norwell, MA: Kluwer, 1999.

[92] A. Abur, and A. G. Exposito, *Power System State Estimation: Theory and Implementation*. New York: Marcel Dekker, 2004.

[93] Interconexión Eléctrica Colombia – Panamá (RS – T1241). Plan de Operaciones. Banco Interamericano de Desarrollo. Oct. 2006.

[94] Identificación de la Red de Transmisión Regional para el Año 2011. Ente Operador Regional. San Salvador, Dic. 2010.

[95] Informe de Evento del 13 de junio de 2010. Empresa Nacional de Energía Eléctrica. Tegucigalpa, Jun. 2010.

[96] Informe Preliminar del Evento del 9 de septiembre de 2010. Empresa Nacional de Energía Eléctrica. Tegucigalpa, Sep. 2010.

[97] J. Ma, S. Garlapati, and J. S. Thorp, "Robust WAMS based control of inter area oscillations," *Elect. Power Compon. Syst.*, vol. 39, no. 9, pp. 850-862, Jun. 2011.

[98] Informe de Máximas Transferencias de Potencia en el Sistema Eléctrico Regional. Época Seca 2007. Grupo Técnico de Seguridad Operativa – EOR. San Salvador, May 2007.

[99] Major Transmission Network of India. [Online]. Available: http://www.wbseb.gov.in/docs/1.MAJOR_TRANSMISSION_NETWORK_OF_INDIA.gif

[100] Power System Simulator for Engineering (PSS/E). Siemens PTI. [Online]. Available: http://www.energy.siemens.com/hq/en/services/power-transmission-distribution/power-technologies-international/software-solutions/pss-e.htm

[101] M. Zhou, V. Centeno, and A. G. Phadke, "Practical PMU placement for the North India power grid," Final Rep. EP-P23460/C11363, Virginia Tech-EPRI Project, Virginia Polytechnic Institute and State University, Blacksburg, USA, Dec. 2007.

[102] M. Zhou, "Advanced system monitoring with phasor measurements," Ph.D. Dissertation, Electrical and Computer Engineering Department, Virginia Polytechnic Institute and State University, Blacksburg, Apr. 2008.

[103] S. C. Srivastava, A. Velayutham, and A. S. Bakshi, "Report of the Enquiry Committee on Grid Disturbance in Northern Region on 30th July 2012 and in Northern, Eastern, & North-Eastern Region

on 31st July 2012," New Delhi, India. [Online]. Available: http://www.powermin.nic.in/pdf/GRID_ENQ_REP_16_8_12.pdf

[104] M. Rihan, M. Ahmad, and M. S. Beg, "Phasor measurements units in the Indian smart grid," in *Proc. IEEE Power Eng. Soc. Conf. Innovative Smart Grid Technol.*, Kollam, India, pp. 261–267, Dec. 1-3, 2011.

[105] S. S. Veda, "WAMS-based intelligent load shedding scheme for preventing cascading blackouts," Ph.D. Dissertation, Electrical and Computer Engineering Department, Virginia Polytechnic Institute and State University, Blacksburg, Dec. 2012.

[106] R. Sun, Z. Wu, and V. A. Centeno, "Power system islanding detection & identification using topology approach and decision tree," in *Proc. IEEE Power Eng. Soc. Gen. Meeting*, San Diego, CA, pp. 1-6, Jul. 24–29, 2011.

[107] Department Of Energy (DOE), U. S., "Smart grid investment grant program progress report," Jul. 2012. [Online]. Available: http://energy.gov/sites/prod/files/Smart%20Grid%20Investment%20Grant%20Program%20-%20Progress%20Report%20July%202012.pdf

[108] M. Patel, S. Aivaliotis, E. Ellen, et al., "Real-time application of synchrophasors for improving reliability," *North American Electricity Reliability Corporation*, Princeton, Princeton, NJ, Tech. Rep, Oct. 2010.

[109] M. E. J. Newman, and M. Girman, "Finding and evaluating community structure in networks," *Physical Review E*, vol. 69, no. 2, pp. 1-16, Feb. 2004.

[110] http://www.merriam-webster.com/dictionary/community

[111] M. Zhou, V. A. Centeno, A. G. Phadke, H. Yi, D. Novosel, and H. A. R. Volskis, "A preprocessing method for effective PMU placement studies," in *Proc. 3rd Int. Conf. Electric Utility Deregulation and Restructuring and Power Technologies (DRPT 2008)*, Nanjing, China, pp. 2862–2867, Apr. 6-9, 2008.

[112] M. Parashar, and M. Jianzhong, "Real time dynamics monitoring system (RTDMS): Phasor applications for the control room," in *Proc. 42nd Hawaii Int. Conf. Syst. Sci.*, Big Island, HI, pp. 1-11, 5-8 Jan. 2009.

[113] FERC/NERC Staff Report, "Arizona-Southern California outages on September 8, 2011: Causes and recommendations," Apr. 2012.

[114] B. Bhargava, "Monitoring voltage stability using real time dynamics monitoring system®," *Voltage Stability Panel Session, iPCGRID Meeting*, San Francisco, CA, 26 Mar. 2013. [Online]. Available:

https://www.cavs.msstate.edu/iPCGRID_Registration/presentations/2013/Voltage_Management_Panel_Bhargava_iPCGrid_2013.pdf

[115] Western Electricity Coordinating Council. [Online]. Available: http://www.wecc.biz/About/Pages/default.aspx

[116] Positive Sequence Load Flow. GE. [Online]. Available: http://site.ge-energy.com/prod_serv/products/utility_software/en/ge_pslf/training/index.htm

[117] Electric Power Group. Real time dynamics monitoring system (RTDMS). [Online]. Available: http://www.electricpowergroup.com/solutions/rtdms/index.html

[118] S. G. Ghiocel, J. H. Chow, G. Stefopoulos, B. Fardanesh, D. Maragal, B. Blanchard, M. Razanousky, and D. B. Bertagnolli, "Phasor-measurement-based state estimation for synchrophasor data quality improvement and power transfer interface monitoring," *IEEE Trans. Power Syst.*, vol. 29, no. 2, pp. 881-888, Mar. 2014.

[119] K. D. Jones, A. Pal, and J. S. Thorp, "Methodology for performing synchrophasor data conditioning and validation," submitted to *IEEE Trans. Power Syst.*

[120] A. G. Phadke, and J. S. Thorp, *Computer relaying for power systems*, Research Studies Press Ltd. 1988, Second Edition, John Wiley, 2009.

[121] K. D. Jones, "Three phase linear state estimation with phasor measurements," M.S. Thesis, Electrical and Computer Engineering Department, Virginia Polytechnic Institute and State University, Blacksburg, May, 2011.

[122] Z. Wu, K. Thomas, R. Sun, V. A. Centeno, and A. G. Phadke, "Three-phase instrument transformer calibration with synchronized phasor measurements," in *Proc. IEEE Power Eng. Soc. Conf. Innovative Smart Grid Technol.*, Washington D.C., pp. 1-6, Jan. 2012.

[123] R. E. Kalman, "A new approach to linear filtering and prediction problems," *J. Basic Eng. Trans. ASME*, Series D, vol. 82, pp. 35-45, Mar. 1960.

[124] D. J. Schroeder, "Astronomical Optics," *Academic Press (2nd Ed.)*, pp. 433, 1999.

[125] J. S. Meditch, *Stochastic Optimal Linear Estimation and Control*, McGraw-Hill Book Company, NY, 1969.

[126] K. D. Jones, "Synchrophasor-only dynamic state estimation & data conditioning," Ph.D. Dissertation, Electrical and Computer Engineering Department, Virginia Polytechnic Institute and State University, Blacksburg, May 2013.

[127] J. B. Moore, "Discrete-time fixed-lag smoothing algorithms," *IFAC-Automatica*, vol. 9, pp. 163-173, Mar. 1973.

[128] I. Zoltan, “A new self-calibrating instrument for voltage transformer calibration,” in *Proc. IEEE Conf. Precision Electromagnetic Measurements Digest*, Braunschweig, Germany, pp. 488-489, 17-21 Jun. 1996.

[129] I. Zoltan, “Impedance synthesis [instrument transformer calibration],” in *Proc. IEEE Instrum. Meas. Technol. Conf. (IMTC)*, vol. 3, Budapest, Hungary, pp. 1872-1874, 21-23 May, 2001.

[130] Z. Wu, “Synchronized phasor measurement applications in three-phase power systems,” Ph.D. Dissertation, Electrical and Computer Engineering Department, Virginia Polytechnic Institute and State University, Blacksburg, Mar. 2013.

[131] A joint EURELECTRIC – ENTSO-E response paper, “Deterministic frequency deviations - root causes and proposals for potential solutions,” Dec. 2011.

[132] S. Abu-Nimeh, D. Nappa, X. Wang, and S. Nair, “A distributed architecture for phishing detection using Bayesian additive regression trees,” in *Proc. IEEE e-Crime Researchers Summit*, Atlanta, GA, pp. 1-10, 15-16 Oct. 2008.

[133] H. A. Chipman, E. I. George, and R. E. McCulloch, “BART: Bayesian Additive Regression Trees,” *Ann. Appl. Stat.*, vol. 4, no. 1, pp. 266-298, Mar. 2010.

[134] J. L. Zhang, and W. K. Hardle, “The Bayesian additive classification tree applied to credit risk modelling,” *Comput. Stat. Data Anal.*, vol. 54, no. 5, pp. 1197-1205, May 2010.

[135] G. Rogers, *Power System Oscillations*, Norwell, MA: Kluwer, 2000.

Appendices

The appendix comprises of the pseudo-codes that were generated to execute the algorithms developed in this manuscript. Appendix A summarizes the steps that are to be followed for applying the FLDSD technique on line 38-65 of the IEEE 118-bus system. Appendix B computes incomplete observability using the CBBBIO Technique for the IEEE 118-bus system after considering the high voltage and the high connectivity buses as critical. Appendix C shows how the BEPP Scheme can be used to partition the IEEE 118-bus system and then compute for PMU placements in the created islands after considering the high voltage and high connectivity buses as critical. Appendix D describes the methodology that was followed for computing the positive sequence phasor for off-nominal frequencies in presence of different errors.

Appendix A: Pseudo-code for the FLDSD Technique

The following pseudo-code makes a 10-class classification of a 300-dimensional data. The data is obtained by computing the complex voltage measurements of buses on either ends of line 38-65 as well as the voltages of buses that lie one line away from the buses 38 and 65 (bus 30, bus 64, and bus 68, respectively) of the IEEE 118-bus system for different faults. Since there are 5 buses and the data is of one second duration at 30 samples per second, the dimensions of the data is 300, thereby implying that the number of columns is also 300 (See 3.2.2.1 for details). The 10-classes in which the data are classified are SLGNR (90 cases), SLGSHSR (90 cases), SLGUSHSR (90 cases), SLGZ2_38 (46 cases), SLGZ2_65 (45 cases), TPGNR (90 cases), TPGSHSR (90 cases), TPGUSHSR (90 cases), TPGZ2_38 (46 cases), TPGZ2_65 (45 cases), resulting in a total of 722 cases. Thus, the "$Data.mat$" file contains 722×300 matrix called D whose rows correspond to the number of cases and the columns correspond to the number of dimensions. Thus, the first 60 columns comprise of the real and imaginary voltages of bus 30, the second 60 columns comprising of the real and imaginary voltages of bus 38, and so on for buses 64, 65 and 68, respectively. The program which performs the classification based on this information is provided below.

```
%%%%%%%%%%%%%%%%%%%%%%%%%%%%%%%%%%%%%%%%%%%%%%%%%%%%%%%%%%%%%%%%%%%%%%%%%%%%%%%%
%                                                                                %
% Program Name: CART Tree Generator for Line 38-65 of IEEE 118-bus system       %
%                                                                                %
% Description: Generates CART Tree for performing 10-class classification       %
%              of 300 dimensional data                                           %
%                                                                                %
% Author: Anamitra Pal                                                           %
%         Virginia Tech.                                                         %
%                                                                                %
% Last Modified: 03/21/2014; 05:22 PM                                            %
%                                                                                %
%%%%%%%%%%%%%%%%%%%%%%%%%%%%%%%%%%%%%%%%%%%%%%%%%%%%%%%%%%%%%%%%%%%%%%%%%%%%%%%%

clc
clear

load Data % .MAT File containing the data in the correct format

[~,n] = size(D); % Dimensions of the Data
c = 10; % Number of classes
n1 = 90; % Number of cases in first class
n2 = 90; % Number of cases in second class
n3 = 90; % Number of cases in third class
n4 = 46; % Number of cases in fourth class
n5 = 45; % Number of cases in fifth class
n6 = 90; % Number of cases in sixth class
n7 = 90; % Number of cases in seventh class
n8 = 90; % Number of cases in eighth class
n9 = 46; % Number of cases in ninth class
n10 = 45; % Number of cases in tenth class

% Extracting data of different classes
x1(1:n1,:) = D(1:n1,:); % Class 1
x2(1:n2,:) = D(n1+1:n1+n2,:); % Class 2
x3(1:n3,:) = D(n1+n2+1:n1+n2+n3,:); % Class 3
x4(1:n4,:) = D(n1+n2+n3+1:n1+n2+n3+n4,:); % Class 4
x5(1:n5,:) = D(n1+n2+n3+n4+1:n1+n2+n3+n4+n5,:); % Class 5
x6(1:n6,:) = D(n1+n2+n3+n4+n5+1:n1+n2+n3+n4+n5+n6,:); % Class 6
x7(1:n7,:) = D(n1+n2+n3+n4+n5+n6+1:n1+n2+n3+n4+n5+n6+n7,:); % Class 7
x8(1:n8,:) = D(n1+n2+n3+n4+n5+n6+n7+1:n1+n2+n3+n4+n5+n6+n7+n8,:); % Class 8
x9(1:n9,:) = D(n1+n2+n3+n4+n5+n6+n7+n8+1:n1+n2+n3+n4+n5+n6+n7+n8+n9,:); %
Class 9
x10(1:n10,:) =
D(n1+n2+n3+n4+n5+n6+n7+n8+n9+1:n1+n2+n3+n4+n5+n6+n7+n8+n9+n10,:); % Class 10
% Computing the Means of the Distributions
xm(1,:) = mean(x1);
xm(2,:) = mean(x2);
xm(3,:) = mean(x3);
xm(4,:) = mean(x4);
xm(5,:) = mean(x5);
xm(6,:) = mean(x6);
xm(7,:) = mean(x7);
xm(8,:) = mean(x8);
xm(9,:) = mean(x9);
xm(10,:) = mean(x10);
```

```
% Computing the Covariances of the Distributions
S(1:n,:) = cov(x1);
S(n+1:2*n,:) = cov(x2);
S(2*n+1:3*n,:) = cov(x3);
S(3*n+1:4*n,:) = cov(x4);
S(4*n+1:5*n,:) = cov(x5);
S(5*n+1:6*n,:) = cov(x6);
S(6*n+1:7*n,:) = cov(x7);
S(7*n+1:8*n,:) = cov(x8);
S(8*n+1:9*n,:) = cov(x9);
S(9*n+1:10*n,:) = cov(x10);

% Computing for the Distance to the Hyper-plane
y = [ x1 ; x2 ; x3 ; x4 ; x5 ; x6 ; x7 ; x8 ; x9 ; x10 ];
testing = zeros(n1+n2+n3+n4+n5+n6+n7+n8+n9+n10,n);
ds = zeros(c-1,c);
d1 = zeros(c-1,c);
d = zeros(n1+n2+n3+n4+n5+n6+n7+n8+n9+n10,(c*(c-1)/2));
for i=1:(n1+n2+n3+n4+n5+n6+n7+n8+n9+n10)
    yy = y(i,:)';
    for j=1:c-1
        for k=j+1:c
            a = xm(j,:) - xm(k,:);
            J = S(((j-1)*n+1):(j*n),:)+S(((k-1)*n+1):(k*n),:); % Fisher's
Logic
            % Using QR Decomposition for performing the inverse
            [Q1,R] = qr(J);
            R1 = R';
            y1 = zeros(n,1);
            for l=1:n
                S1 = 0;
                for m=2:l
                    S1 = S1 + R1(l,m-1)*y1(m-1);
                end
                y1(l) = (a(l) - S1)/R1(l,l);
            end
            x = y1'*Q1';
            xh = 0.5*(xm(j,:) + xm(k,:));
            M = eye(n);
            M(:,n) = x';
            T1 = eye(n);
            T1(1:n-1,n) = -(x(1:n-1))';
            D = eye(n);
            D(n,n) = 1/x(n);
            G = T1*D;
            V = G(1:n-1,:)';
            W = eye(n) - V*((V'*V)\V');
            e = W*(yy - xh');
            testing(i,:) = e;
            ds(j,k) = sqrt(e'*e);
            d1(j,k) = ds(j,k)*sign(testing(i,:)*xm(j,:)');
        end
    end
```

```
    % Number of d's = c*(c-1)/2 where 'c' is the number of classes
    cnt = 1;
    for j=1:c
        for k=j+1:c
            d(i,cnt) = d1(j,k);
            cnt = cnt + 1;
        end
    end
end

% Naming the nodes
SS1 = ones(n1,1)*'SLGNR   ';
SS2 = ones(n2,1)*'SLGSHSR ';
SS3 = ones(n3,1)*'SLGUSHSR';
SS4 = ones(n4,1)*'SLGZ2_38';
SS5 = ones(n5,1)*'SLGZ2_65';
SS6 = ones(n6,1)*'TPGNR   ';
SS7 = ones(n7,1)*'TPGSHSR ';
SS8 = ones(n8,1)*'TPGUSHSR';
SS9 = ones(n9,1)*'TPGZ2_38';
SS10 = ones(n10,1)*'TPGZ2_65';
SS = [ SS1 ; SS2 ; SS3 ; SS4 ; SS5 ; SS6 ; SS7 ; SS8 ; SS9 ; SS10 ];

% Creating the tree
c = cellstr(char(SS));
t = classregtree(d,c,'names',{'d1-2 ' 'd1-3 ' 'd1-4 ' 'd1-5 ' 'd1-6 ' 'd1-7 '
'd1-8 ' 'd1-9 ' 'd1-10' 'd2-3 ' 'd2-4 ' 'd2-5 ' 'd2-6 ' 'd2-7 ' 'd2-8 ' 'd2-9
' 'd2-10' 'd3-4 ' 'd3-5 ' 'd3-6 ' 'd3-7 ' 'd3-8 ' 'd3-9 ' 'd3-10' 'd4-5 '
'd4-6 ' 'd4-7 ' 'd4-8 ' 'd4-9 ' 'd4-10' 'd5-6 ' 'd5-7 ' 'd5-8 ' 'd5-9 ' 'd5-
10' 'd6-7 ' 'd6-8 ' 'd6-9 ' 'd6-10' 'd7-8 ' 'd7-9 ' 'd7-10' 'd8-9 ' 'd8-10'
'd9-10' });
view(t)
sfit = eval(t,d);
pct = mean(strcmp(sfit,c));

% Testing the tree
cost = test(t,'crossvalidate',d,c);
[cn,s,n,best] = test(t,'cross',d,c);
tmin = prune(t,'level',best);
view(tmin)
[mincost,minloc] = min(cn);
plot(n,cn,'b-o',...
     n(best+1),cn(best+1),'bs',...
     n,(mincost+s(minloc))*ones(size(n)),'k--')
xlabel('Tree size (number of terminal nodes)')
ylabel('Cost')
grid
sfitn = eval(tmin,d);
pct2 = mean(strcmp(sfitn,c));
```

Appendix B: Pseudo-code for the CBBBIO Technique

The following pseudo-code computes for the optimal PMU placement for the IEEE 118-bus system based on the CBBBIO Technique. The buses of this system that are identified to be critical are: 8, 9, 10, 11, 12, 26, 30, 38, 49, 63, 64, 65, 66, 68, 80, 81, 92, and 100. Of these, buses 8, 9, 10, 26, 30, 38, 63, 64, 65, 68, and 81 are the high voltage buses, buses 12, 49, 80, and 100 are the high connectivity buses (≥ 7 connections), while the rest (buses 11, 66, and 92) provide redundancy in measurement to the critical buses and are hence also critical. The program which performs the optimization based on this information is provided below.

```
%%%%%%%%%%%%%%%%%%%%%%%%%%%%%%%%%%%%%%%%%%%%%%%%%%%%%%%%%%%%%%%%%%%%%%%%%%%%%%%%
%                                                                               %
% Program Name: PMU Placement for the IEEE 118-bus system using CBBBIO          %
%               Technique                                                       %
%                                                                               %
% Description: Computes optimal PMU placement for the IEEE 118-bus system       %
%              based on the CBBBIO Technique. High voltage buses and high       %
%              connectivity buses (≥ 7 connections) were considered             %
%              critical buses                                                   %
%                                                                               %
% Author: Anamitra Pal                                                          %
%         Virginia Tech.                                                        %
%                                                                               %
% Last Modified: 03/22/2014; 09:52 AM                                           %
%                                                                               %
%%%%%%%%%%%%%%%%%%%%%%%%%%%%%%%%%%%%%%%%%%%%%%%%%%%%%%%%%%%%%%%%%%%%%%%%%%%%%%%%

clc
clear

load A118 % A118 is the incidence matrix of the IEEE 118-bus system

N = length(A); % Number of buses present in the system

% Identifies critical buses present in the system
xi = zeros(N,1);
% List of critical high voltage buses
xi(8,1)=1;xi(9,1)=1;xi(10,1)=1;xi(26,1)=1;xi(30,1)=1;xi(38,1)=1;xi(63,1)=1;xi
(64,1)=1;xi(65,1)=1;xi(68,1)=1;xi(81,1)=1;
% List of critical high connectivity buses
xi(12,1)=1;xi(49,1)=1;xi(80,1)=1;xi(100,1)=1;
% List of extra buses that ensure redundancy of the critical buses
xi(11,1)=1;xi(66,1)=1;xi(92)=1;

% Defining parameters of the optimization
f = ones(N,1);
b = -1*ones(N,1);
beq = 0;
fi = f - 2*xi; % This gives priority during the minimization process to the
PMUs at critical buses
```

```
tic
% For Complete Observability
d = 0;
Aeq = xi'; % With this Aeq*x=beq=nnz(xi), we ensure that xi must be one for
the critical buses
AA = -A;
x0 = bintprog(fi,AA,b,Aeq,nnz(xi)); % Performs the optimization
d % Displays the depth of unobservability
NPMU = f'*x0 % Displays the number of PMUs required
c = 1;
for j=1:N
    if(x0(j)~=0)
        Loc(c) = j; %#ok<*SAGROW>
        c = c + 1;
    end
end
Loc % Displays the locations of the PMUs

% For different Depths of Unobservability
d = 1;
xold = x0;
cnt = 0;
AA = A;
while NPMU~=18
    Loc = 0;
    Aeq = (f - xold)';
    A1 = sign(AA);
    AA = sign(A*A1);
    xnew = bintprog(fi,-AA,b,Aeq,beq); % Performs the optimization
    d % Displays the depth of unobservability
    NPMU = f'*xnew % Displays the number of PMUs required
    c = 1;
    for j=1:N
        if(xnew(j)~=0)
            Loc(c) = j; %#ok<*SAGROW>
            c = c + 1;
        end
    end
    Loc % Displays the locations of the PMUs
    d = d + 1;
    if(xnew==xold)
        cnt = cnt + 1;
    end
    xold = xnew;
end
toc
```

Appendix C: Pseudo-code for the BEPP Scheme

The following pseudo-code performs community-based partitioning as well as computes for the optimal PMU placements in the created partitions in accordance with the BEPP scheme for the IEEE 118-bus system. The program is divided into two parts. The first section creates the partitions by eliminating branches with the highest weights and then clusters the buses together to form individual islands. The second section uses the results obtained in the first section to perform the optimization based on the CBBBIO technique for the created islands and then identifies the corresponding locations for PMU placement in the original, un-partitioned system. The link between the two sections is the $output.mat$ file which contains information about the number of islands formed, the branches removed, the final incidence matrix of the original system, as well as the buses present in the individual islands. The two programs are provided below.

```
%%%%%%%%%%%%%%%%%%%%%%%%%%%%%%%%%%%%%%%%%%%%%%%%%%%%%%%%%%%%%%%%%%%%%%%%%%%%%%%%
%                                                                                 %
% Program Name: Community based Island Identification for IEEE 118-bus           %
%               system                                                            %
%                                                                                 %
% Description: Identifies communities in the IEEE 118-bus system by              %
%              eliminating branches with highest weights and clusters the         %
%              buses together to form individual islands                          %
%                                                                                 %
% Author: Anamitra Pal                                                            %
%         Virginia Tech.                                                          %
%                                                                                 %
% Last Modified: 03/22/2014; 10:20 AM                                             %
%                                                                                 %
%%%%%%%%%%%%%%%%%%%%%%%%%%%%%%%%%%%%%%%%%%%%%%%%%%%%%%%%%%%%%%%%%%%%%%%%%%%%%%%%

clc
clear

load A118 % A118 is the incidence matrix of the IEEE 118-bus system

Num_island = input('Number of islands: '); % Enter number of islands in which
the system must be partitioned

tic
A_org = A;
n = length(A);
Brnch = zeros((nnz(A) - n)/2,2); % Computes for the number of branches
present in the system

% Defining constants used in the optimization
C = ones(n);
count = 1;
number = 0;
```

```
while number==0
    % Weight Computation Section
    % Forming the Depth Matrix
    Af = eye(n);
    Depth = zeros(n);
    i = 1;
    B = 0;
    cnt = 0;
    while cnt==0
        Ai = Af;
        if(isequal(Ai,C)==1)
            cnt = cnt + 1;
            B = 1;
        end
        Af = sign(A*Ai);
        for j=1:n
            for k=1:j
                if(Ai(j,k)==0 && Af(j,k)~=0)
                    Depth(j,k) = i;
                end
            end
        end
        if(isequal(Ai,Af)==1)
            if(B==0)
                cnt = cnt + 1;
            end
        end
        i = i + 1;
    end
    Depth = Depth + Depth';
    clear Ai Af
    % Forming the Vertex Number Matrix
    Vnum = zeros(n);
    for i=1:n
        cnt = 1;
        Vnum(i,i) = 1;
        while cnt<=max(Depth(:,i))
            for j=1:n
                if(j~=i)
                    for k=1:n
                        if(Depth(j,i)==cnt)
                            if(A(j,k)~=0)
                                if(Depth(j,i)>Depth(k,i))
                                    Vnum(j,i) = Vnum(j,i) + Vnum(k,i);
                                end
                            end
                        end
                    end
                end
            end
            cnt = cnt + 1;
        end
    end
```

```
    % Forming the Weight Matrix
    Wght = zeros(n);
    for i=1:n
        W = zeros(n);
        Anew = A;
        Anew = Anew - eye(n);
        for j=1:n
            for k=1:n
                if(Depth(j,i)==Depth(k,i))
                    Anew(j,k) = 0;
                    Anew(k,j) = 0;
                end
            end
        end
        for j=1:n
            for k=1:n
                if(Anew(j,k)~=0)
                    if(Depth(j,i)==max(Depth(:,i)))
                        W(k,j) = Vnum(k,i)/Vnum(j,i);
                    end
                end
            end
        end
        m = 1;
        while m<=max(Depth(:,i))
            for j=1:n
                if(Depth(j,i)==max(Depth(:,i))-m)
                    for k=1:n
                        if(Anew(j,k)~=0)
                            if(Depth(j,i)>Depth(k,i))
                                W(k,j) = (sum(W(j,:)) +
1)*(Vnum(k,i)/Vnum(j,i));
                            end
                        end
                    end
                end
            end
            m = m + 1;
        end
        Wght = Wght + W;
    end
    Weght = Wght + Wght';
    Weight = triu(Weght);
    [r c w] = find(Weight);
```

```
    % Clustering Section
    island_number = 0;
    length_A = length(A);
    Adjacency_A = A - eye(length_A);
    node_allocation_status = (1:length_A)';
    while sum(node_allocation_status)>0
        first_unallocated_node = find(node_allocation_status,1,'first');
        node_allocation_status(first_unallocated_node) = 0;
        Adjacency_A(:,first_unallocated_node) = 0;
        current_island(1)= first_unallocated_node;
        island_node_counter = 1;
        node_to_be_checked_counter = 2;
        adjacent_nodes = find(Adjacency_A(first_unallocated_node,:));
        check_more_nodes = length(adjacent_nodes);
        while check_more_nodes>0
            for i = 1:length(adjacent_nodes)
                Adjacency_A(:,adjacent_nodes(i)) = 0;
                current_island(island_node_counter+i) = adjacent_nodes(i);
%#ok<SAGROW>
                node_allocation_status(adjacent_nodes(i)) = 0;
            end
            island_node_counter = length(current_island);
            adjacent_nodes = find(Adjacency_A(...
                            current_island(node_to_be_checked_counter),:));
            check_more_nodes = check_more_nodes + length(adjacent_nodes) - 1;
            node_to_be_checked_counter = node_to_be_checked_counter + 1;
        end
        current_island = sort(current_island);
        island_number = island_number + 1;
        clear current_island
    end
    if(island_number>=Num_island)
        number = 1;
    end
    nmbr = 0;
    for i=1:length(w)
        if(w(i)==max(w) && number==0 && nmbr==0)
            Brnch(count,1) = r(i);
            Brnch(count,2) = c(i);
            A(r(i),c(i)) = 0; %#ok<SAGROW>
            A(c(i),r(i)) = 0; %#ok<SAGROW>
            count = count + 1;
            nmbr = nmbr + 1;
        end
    end
    Brnch(~any(Brnch,2),:) = [];
    clear Wght W Anew Depth Vnum Weght Weight
end
disp('Branches to be removed')
disp(Brnch)
```

```
% Saving final system configuration
[len,~] = size(Brnch);
A = A_org;
Island = zeros(Num_island,n);
for j=1:len
    A(Brnch(j,1),Brnch(j,2)) = 0;
    A(Brnch(j,2),Brnch(j,1)) = 0;
end
island_number = 0;
length_A = length(A);
Adjacency_A = A - eye(length_A);
node_allocation_status = (1:length_A)';
while sum(node_allocation_status)>0
    first_unallocated_node = find(node_allocation_status,1,'first');
    node_allocation_status(first_unallocated_node) = 0;
    Adjacency_A(:,first_unallocated_node) = 0;
    current_island(1)= first_unallocated_node;
    island_node_counter = 1;
    node_to_be_checked_counter = 2;
    adjacent_nodes = find(Adjacency_A(first_unallocated_node,:));
    check_more_nodes = length(adjacent_nodes);
    while check_more_nodes>0
        for i = 1:length(adjacent_nodes)
            Adjacency_A(:,adjacent_nodes(i)) = 0;
            current_island(island_node_counter+i) = adjacent_nodes(i);
            node_allocation_status(adjacent_nodes(i)) = 0;
        end
        island_node_counter = length(current_island);
        adjacent_nodes = find(Adjacency_A(...
                        current_island(node_to_be_checked_counter),:));
        check_more_nodes = check_more_nodes + length(adjacent_nodes) - 1;
        node_to_be_checked_counter = node_to_be_checked_counter + 1;
    end
    current_island = sort(current_island);
    island_number = island_number + 1;
    eval(['Island_' num2str(island_number) '= current_island']);
    for j=1:length(current_island)
        Island(island_number,j) = current_island(j);
    end
    clear current_island
end
toc

save output Num_island Brnch A Island
```

```
%%%%%%%%%%%%%%%%%%%%%%%%%%%%%%%%%%%%%%%%%%%%%%%%%%%%%%%%%%%%%%%%%%%%%%%%%%%%%%%%
%                                                                                %
% Program Name: PMU Placement in Islands created using Community-based           %
%               Partitioning for the IEEE 118-bus system                         %
%                                                                                %
% Description: Computes optimal number of PMUs in the created islands and        %
%              maps their locations on to the original system                    %
%                                                                                %
% Author: Anamitra Pal                                                           %
%         Virginia Tech.                                                         %
%                                                                                %
% Last Modified: 03/22/2014; 10:27 PM                                            %
%                                                                                %
%%%%%%%%%%%%%%%%%%%%%%%%%%%%%%%%%%%%%%%%%%%%%%%%%%%%%%%%%%%%%%%%%%%%%%%%%%%%%%%%

clc
clear

load output

% Critical buses of the original system
xi_org = [ 8 9 10 11 12 26 30 38 49 63 64 65 66 68 80 81 92 100 ];
% Identifying critical buses in the partitioned islands
c = 1;
xi_new = zeros(Num_island,length(Island));
for j=1:Num_island
    for k=1:length(xi_org)
        for l=1:length(Island)
            if(xi_org(k)==Island(j,l))
                xi_new(j,c) = l;
                c = c + 1;
            end
        end
    end
end
% Computing optimal PMU placement for the individual islands
tic
NPMUf = 0;
for j=1:Num_island
    num = nnz(Island(j,:));
    Atemp = eye(num);
    for k=1:num
        for l=1:num
            Atemp(k,l) = A(Island(j,k),Island(j,l));
        end
    end
    N = length(Atemp);
    f = ones(N,1);
    b = -f;
    beq = 0;
    xi = zeros(N,1);
    for k=1:length(xi_new)
        if(xi_new(j,k)~=0)
            xi(xi_new(j,k),1) = 1;
        end
    end
```

```
    fi = f - 2*xi; % This gives priority during the minimization process to
the PMUs at important buses
    % For Complete Observability
    Aeq = xi'; % With this Aeq*x=beq=nnz(xi), we ensure that xi must be one
for the important buses
    AA = -Atemp;
    x0 = bintprog(fi,AA,b,Aeq,nnz(xi)); % Performs the optimization
    NPMU = f'*x0;
    disp('Number of PMUs for Complete Observability')
    disp(NPMU) % Displays the number of PMUs required for the individual
system
    c = 1;
    Loc = zeros(1,N);
    for l=1:N
        if(x0(l)~=0)
            Loc(c) = l;
            c = c + 1;
        end
    end
    Loc(:,~any(Loc,1)) = [];
    Locf = zeros(1,length(Loc));
    for l=1:length(Loc)
        Locf(l) = Island(j,Loc(l));
    end
    disp('Location of PMUs in individual island')
    disp(Loc) % Displays the locations of PMUs in the individual island
    disp('Location of PMUs in original system')
    disp(Locf) % Displays the locations of PMUs in the original system
    NPMUf = NPMUf + NPMU;
end
toc
disp('Total number of PMUs required')
disp(NPMUf) % Displays the total number of PMUs required
```

Appendix D: Pseudo-codes for computing positive sequence phasor at off-nominal frequencies

The following pseudo-code shows how the positive sequence phasor can be computed at off-nominal frequencies. The frequency is first estimated using a suitable sample window. This is then used for re-sampling the correction factors as well as for transforming the nominal frequency phasors into off-nominal frequency phasors in accordance with the logic described in [13]. The program which does this is provided below.

```
%%%%%%%%%%%%%%%%%%%%%%%%%%%%%%%%%%%%%%%%%%%%%%%%%%%%%%%%%%%%%%%%%%%%%%%%%%%%%%%%
%                                                                                 %
% Program Name: Positive sequence phasor computation at off-nominal               %
%               frequencies using a correction factor and resampling              %
%                                                                                 %
% Description: Computes positive sequence phasors at off-nominal                  %
%              frequencies using a correction factor and resampling. The          %
%              variable off-nominal frequency is assumed to be a                  %
%              sinusoidal function.                                               %
%                                                                                 %
% Author: Anamitra Pal                                                            %
%         Virginia Tech.                                                          %
%                                                                                 %
% Last Modified: 03/22/2014; 10:55 PM                                             %
%                                                                                 %
%%%%%%%%%%%%%%%%%%%%%%%%%%%%%%%%%%%%%%%%%%%%%%%%%%%%%%%%%%%%%%%%%%%%%%%%%%%%%%%%

clc
clear
close all

% Input parameters
D = 0; % Angular starting point for the waveform in Degrees
fs = 2880; % Sampling Frequency
n = 30; % Number of samples per second
t  = 1:(3600*n); % One hour worth of data at n samples per second
t_len = length(t);
% Frequency is a sinusoidal signal lying between 59.85-60.15Hz and changing
by 1.5mHz/sec.
f = zeros(t_len,1);
T_f = 2*(0.3/0.0015);
for j=1:t_len
    f(j) = 60 + 0.15*sin(2*pi*j/(30*T_f));
end
N = fs/60; % Number of Samples of the Input Signal to compute first window
% Computing frequency using an N-sample window
c = N;
F = zeros(t_len,1);
F(1:N) = f(1);
```

```
while(c<=t_len-N)
    meanf = median(f(c:c+N-1));
    for j=1:N
        F(j+c) = meanf;
    end
    c = c + N;
end
f = F;
a = exp(1i*2*pi/3); % exp(j*120)
A = (1/3)*[ 1 1 1 ; 1 a a^2 ; 1 a^2 a ]; % Transformation matrix converting
three phase to symmetrical components
% Computing the correction factor for off-nominal frequencies by resampling
P = zeros(t_len,1);
Q = zeros(t_len,1);
for j=1:t_len
    P(j) = (sin(N*2*pi*(f(j)-60)/(2*fs))/(N*(sin(2*pi*(f(j)-
60)/(2*fs)))))*(exp((1i*(N-1)*2*pi*(f(j)-60))/(2*fs)));
    Q(j) =
(sin(N*2*pi*(f(j)+60)/(2*fs))/(N*(sin(2*pi*(f(j)+60)/(2*fs)))))*(exp((-1i*(N-
1)*2*pi*(f(j)+60))/(2*fs)));
    if(f(j)==60)
        P(j) = 1 + 1i*0;
        Q(j) = 0;
    end
end

% Pure Signal
VA = zeros(t_len,1);
VB = zeros(t_len,1);
VC = zeros(t_len,1);
for j=1:t_len
    VA(j) = exp(1i*D*pi/180);
    VB(j) = exp(1i*((D-120)*pi/180));
    VC(j) = exp(1i*((D+120)*pi/180));
end
VAold = VA;
VBold = VB;
VCold = VC;
% Transforming nominal frequency pure phasors into pure phasors at off-
nominal frequencies by resampling
cnt = 0;
while(cnt<=t_len-N)
    for j=1:N
        VA(j+cnt) = P(j+cnt)*VAold(j+cnt)*exp(1i*j*2*pi*(f(j+cnt)-60)/fs) +
Q(j+cnt)*conj(VAold(j+cnt))*exp(-1i*j*2*pi*(f(j+cnt)+60)/fs);
        VB(j+cnt) = P(j+cnt)*VBold(j+cnt)*exp(1i*j*2*pi*(f(j+cnt)-60)/fs) +
Q(j+cnt)*conj(VBold(j+cnt))*exp(-1i*j*2*pi*(f(j+cnt)+60)/fs);
        VC(j+cnt) = P(j+cnt)*VCold(j+cnt)*exp(1i*j*2*pi*(f(j+cnt)-60)/fs) +
Q(j+cnt)*conj(VCold(j+cnt))*exp(-1i*j*2*pi*(f(j+cnt)+60)/fs);
    end
    cnt = cnt + N;
end
Vpos = zeros(t_len,1);
for j=1:t_len
    Vpnz = A*[VA(j) ; VB(j) ; VC(j) ];
    Vpos(j) = Vpnz(2,1);
end
```

```
Vposmag = abs(Vpos);
Vposang = unwrap(angle(Vpos));

% Inserting Unbalance, Ratio errors and PMU errors in individual phases
% Adding unbalance
UB = zeros(3,1);
for j=1:3
    UB(j) = (1 + 0.05*rand)*exp(1i*10*(rand-0.5)*pi/180); % 0.95 to 1.05%
mag, +/-5 degree in angles
end
VAub = UB(1,1)*VAold;
VBub = UB(2,1)*VBold;
VCub = UB(3,1)*VCold;
% Adding ratio errors
RE = zeros(3,1);
for j=1:3
    RE(j) = (0.94 + 0.12*rand)*exp(1i*8*(rand-0.5)*pi/180); % 0.94 to 1.06%
mag, +/-4 degree in angles
end
VAreub = RE(1,1)*VAub;
VBreub = RE(2,1)*VBub;
VCreub = RE(3,1)*VCub;
% Adding PMU errors
s = 0.002; % Error in magnitude of 0.2%
an = 0.104; % Error in angle of 0.104 degree
PMU = zeros(t_len,3);
for j=1:t_len
    for k=1:3
        PMU(j,k) = (1 + s*randn)*exp((1i*an*randn)*pi/180);
    end
end
VAe = zeros(t_len,1);
VBe = zeros(t_len,1);
VCe = zeros(t_len,1);
for j=1:t_len
    VAe(j) = PMU(j,1)*VAreub(j);
    VBe(j) = PMU(j,2)*VBreub(j);
    VCe(j) = PMU(j,3)*VCreub(j);
end
VAeold = VAe;
VBeold = VBe;
VCeold = VCe;
% Transforming nominal frequency impure phasors into impure phasors at off-
nominal frequencies by resampling
cnt = 0;
while(cnt<=t_len-N)
    for j=1:N
        VAe(j+cnt) = P(j+cnt)*VAeold(j+cnt)*exp(1i*j*2*pi*(f(j+cnt)-60)/fs) +
Q(j+cnt)*conj(VAeold(j+cnt))*exp(-1i*j*2*pi*(f(j+cnt)+60)/fs);
        VBe(j+cnt) = P(j+cnt)*VBeold(j+cnt)*exp(1i*j*2*pi*(f(j+cnt)-60)/fs) +
Q(j+cnt)*conj(VBeold(j+cnt))*exp(-1i*j*2*pi*(f(j+cnt)+60)/fs);
        VCe(j+cnt) = P(j+cnt)*VCeold(j+cnt)*exp(1i*j*2*pi*(f(j+cnt)-60)/fs) +
Q(j+cnt)*conj(VCeold(j+cnt))*exp(-1i*j*2*pi*(f(j+cnt)+60)/fs);
    end
    cnt = cnt + N;
end
Vpos_e = zeros(t_len,1);
```

```
for j=1:t_len
    Vpnz_e = A*[VAe(j) ; VBe(j) ; VCe(j) ];
    Vpos_e(j) = Vpnz_e(2,1);
end
Vpos_e_mag = abs(Vpos_e);
Vpos_e_ang = unwrap(angle(Vpos_e));

% Plots
plot(t,Vpos_e_mag,'b')
hold on
% figure
plot(t,Vposmag,'r')
xlabel('Time - one hour worth of data at 30 sps')
ylabel('Positive sequence phasor magnitude (in p.u.)')
legend('Pos Seq Mag in presence of error','Pos Seq Mag in absence of error')
figureHandle = gcf;
set(findall(figureHandle,'type','text'),'fontSize',12,'fontWeight','bold')
figure
plot(t,angle(Vpos_e),'b')
hold on
% figure
plot(t,angle(Vpos),'r')
xlabel('Time - one hour worth of data at 30 sps')
ylabel('Positive sequence phasor angle (in radians)')
legend('Pos Seq Ang in presence of error','Pos Seq Ang in absence of error')
figureHandle = gcf;
set(findall(figureHandle,'type','text'),'fontSize',12,'fontWeight','bold')

% Comparison
abs_mean_E = abs(mean(RE.*UB));
angle_mean_E = angle(mean(RE.*UB));
mean_mag_Vpos = mean(Vposmag);
mean_mag_Vpos_e = mean(Vpos_e_mag);
mean_ang_Vpos = mean(Vposang);
mean_ang_Vpos_e = mean(Vpos_e_ang);
R_mag_Vpos = mean_mag_Vpos_e/mean_mag_Vpos;
R_ang_Vpos = mean_ang_Vpos_e - mean_ang_Vpos;
mag_error = abs_mean_E - R_mag_Vpos;
ang_error = angle_mean_E - R_ang_Vpos;
disp(mag_error)
disp(ang_error)
```